The use of Raman Spectroscopy for the Live Aseptic Monitoring of Stem Cell Differentiation

Adam James Mitchell

Submitted in accordance with the requirements for the degree of
Doctorate of Philosophy

The University of Leeds
Faculty of Engineering
School of Mechanical Engineering

December 2014

The candidate confirms that the work submitted is his/her own and that appropriate credit has been given where reference has been made to the work of others.

Acknowledgements

This has been a fantastic experience of highs and lows from start to finish. First off I would like to thank my three supervisors, Jennifer Kirkham, Xuebin Yang and Alastair Smith for their guidance, patience and understanding, particularly when things didn't always go to plan. I would like to thank all the staff in the Oral Biology department at the University of Leeds but especially Claire Godfrey for the administrative support necessary when working between two sites, El Mostafa Raif for support and advice in cell culture and Jackie Hudson for providing training in histology and scanning electron microscopy. Secondly, thanks to the people at Avacta Group plc for helping me to establish my own cell culture facilities in their labs and accommodating my every need. A particular thanks to Kurt Baldwin for training me how to use the Raman spectrometer and always being available whenever it had any problems. Finally I would like to thank Lorna Ashton and Roy Goodacre from the University of Manchester for the training in principal component analysis and the use of Matlab, possibly the singularly most complicated computer program I have ever used!

Publications and Presentations

Research Papers

- Raman Spectroscopy using an Aseptic Method can Detect Changes Associated with Osteogenic Differentiation in Dental Pulp Stromal Cells. *PLOS one* (under revision)

Oral Presentations

- Raman Spectroscopy in the Non-invasive Phenotyping of Human Dental Pulp Stem Cells (hDPSCs) – Identification of a Suitable Substrate for Cell Culture. *Leeds School of Dentistry postgraduate research day, July 2012*

- Raman spectroscopy can be used to non-invasively and aseptically characterise stem cell differentiation. *Leeds School of Dentistry postgraduate research day, July 2014* (1st place – oral presentation)

- Raman spectroscopy can be used to non-invasively and aseptically characterise stem cell differentiation. *Joint Doctoral Training Centre in Tissue Engineering and Regenerative Medicine conference, July 2014*

Poster Presentations

- Raman Spectroscopy in the Non-invasive Phenotyping of Human Dental Pulp Stem Cells (hDPSCs) – Identification of a Suitable Substrate for Cell Culture. *Joint Doctoral Training Centre in Tissue Engineering and Regenerative Medicine conference, July 2012*

- Development of a method for the non-invasive and non-destructive characterisation of human dental pulp stem cells. *Leeds School of Dentistry postgraduate research day, July 2013*

- Development of a method for the non-invasive and non-destructive characterisation of human dental pulp stem cells. *Joint Doctoral Training Centre in Tissue Engineering and Regenerative Medicine conference, July 2013*

- Development of a method for the non-invasive and non-destructive characterisation of human dental pulp stem cells. *Regener8 conference, Leeds, October 2013*

- Raman Spectroscopy Using an Aseptic Method can Characterise Osteo-induction in Dental Pulp Stromal Cells. *Termis EU, Genoa, Italy, June 2014*

- Raman Spectroscopy Using an Aseptic Method can Characterise Osteo-induction in Dental Pulp Stromal Cells. *International Association of Dental Research world congress, Cape Town, South Africa, June 2014*

Research papers and conference abstracts can be found in Appendix C.

Abstract

The characterisation of stem cell differentiation is currently performed using invasive/destructive methods, precluding cells from further use. There is an unmet need for techniques capable of characterising cells non-invasively in order to enhance the translation of stem cell-based therapies. Raman spectroscopy has previously been used to characterise cells and is non-invasive. However, almost all previous studies were not performed under aseptic conditions precluding any further use of those cells. The aim of this thesis was to determine whether Raman spectra could be acquired from the same stem cell cultures undergoing differentiation over time without compromising the sterility of these cell cultures and to identify aspects of the Raman spectra that may be used to predict eventual cell fate. Custom-built cell culture flasks with quartz windows (appropriate for acquiring Raman spectra) provided a platform for the maintenance of cell sterility whilst permitting the acquisition of Raman spectra comparable to those in the published literature. It was found that the osteogenic differentiation of dental pulp stem cells was associated with changes in protein content early in the process and prior to the end result being evident by the emergence of mineralised nodules. The adipogenic differentiation of adipose derived stem cells was found to be characterised by changes in lipid content throughout differentiation with the earliest detectable change after 3 days of differentiation. This is earlier than can typically be detected using currently established methods. Stem cell differentiation was also confirmed using conventional techniques including qRT-PCR and histology. Raman spectroscopy cannot provide the intricate detail of genetic/protein changes that occur as stem cells differentiate. However, this thesis demonstrates that stem cell fate can be monitored in an entirely non-invasive manner and could be applied to the scaled up production of differentiated stem cells for either clinical use or in a research setting.

Table of Contents

List of Tables

List of Figures

Chapter 1

Introduction

1.1 Overview of Tissue Engineering

An oft cited review in 1993 by Langer and Vacanti (1) marked the emergence of tissue engineering as a field in its own right. In this review the authors defined tissue engineering as "an interdisciplinary field that applies the principles of engineering and the life sciences toward the development of biological substitutes that restore, maintain, or improve tissue function". Current definitions have expanded upon this initial premise but the guiding principle remains the same. The current paradigm (Figure 1) in tissue engineering utilises one or more components drawn from cells, materials, chemical or physical cues to achieve a therapy capable of treating a given disease/condition. Researchers in the field are now taking this approach to repair or replace almost every tissue in the human body (2).

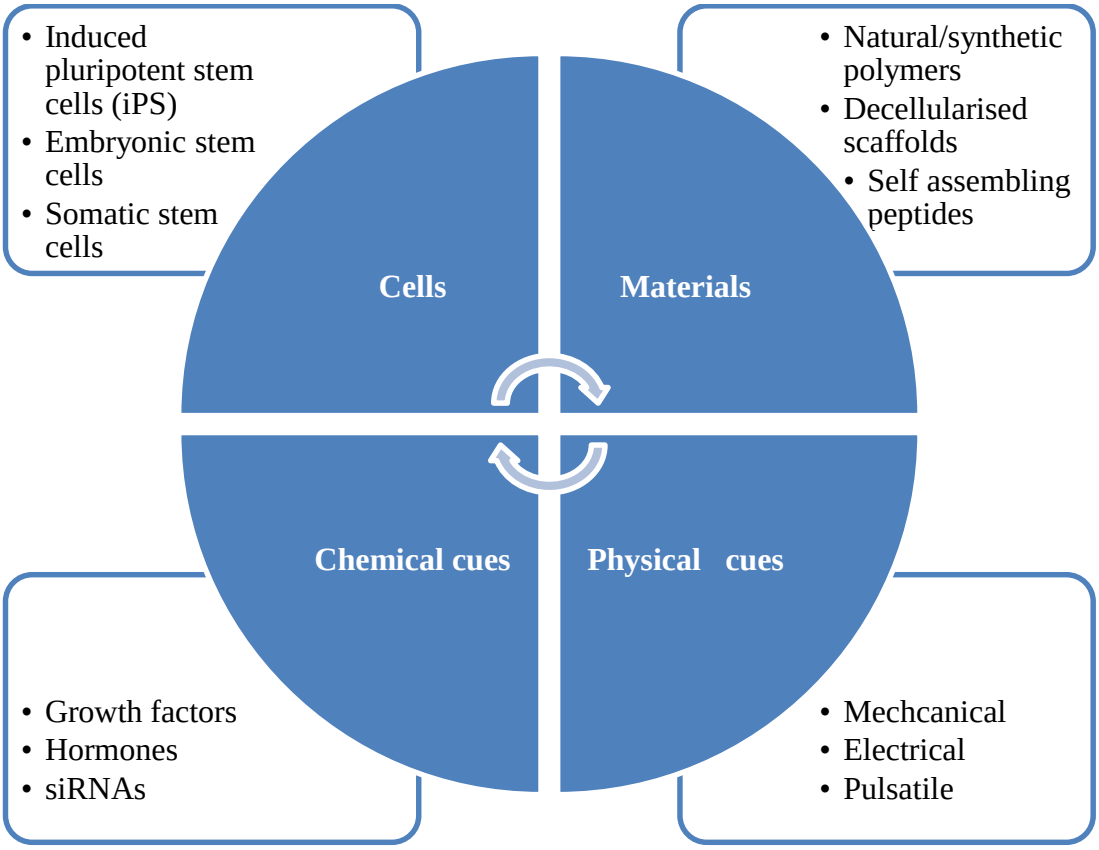

Figure 1. Schematic overview of tissue engineering and the factors involved.

1.1.1 Materials used in Tissue Engineering

Each tissue presents unique challenges in its repair or replacement, the cells and materials required to produce the desired architecture to replace bone are clearly different to those required to replace a blood vessel. There is a need to marry the structure and function of the tissue that is damaged/impaired to the design of the tissue engineering approach undertaken to replace/regenerate that tissue. Table 1 outlines some of these approaches.

Table 1. A selection of body tissues, their structure and function and biomaterials designed for their replacement/regeneration.

Tissue	Structure	Function	Biomaterials
Bone	Porous biological (primarily type I collagen) and mineral (hydroxyapatite) composite imparting flexibility and strength respectively	Primarily to withstand and evenly distribute compressive forces	Glass ceramic/polymer composites that mimic strength and flexibility (3, 4)
Intervertebral disc	Gelatinous collagen matrix with high proteoglycan content creating a high swelling pressure	Acts as a shock absorber in the spine able to resist high compressive forces and permits 3D rotational movement	Hydrogels that mimic high swelling pressure (5)
Skin	Highly cellular and vascular tissue with a porous elastic proteinaceous membrane	Primarily to act a barrier capable of rapid healing	Porous polymer meshes that can encourage cellular migration and vascularisation (6, 7)
Tendon/ligament	Primarily type I collagen arranged in uniaxial fibres with a “crimp-like” structure permitting elongation and tensile resistance	Stabilise joints by constraining their range of motion	Aligned polymer fibres with a high tensile strength (8, 9)
Vasculature	Layers of circumferential and axial aligned collagen and elastic fibres with high tensile strength and resistance to sheer stress	To transport blood at a wide range of pressures	Ordered polymer scaffolds primed by mechanical strains (10, 11)

1.1.1.1 Glass/ceramics in Tissue Engineering

Glass/ceramics represent a class of inorganic materials that are typically used in bone tissue engineering. Perhaps one of the oldest materials is Bioglass® which is composed of SiO_2, Na_2O, CaO and P_2O_5, the weights of which vary according to the specific formulation. Bioglass® has been shown to bind to both the soft tissue and bone were it is implanted promoting osteogenesis and has been in clinical use since 1985 (12). There have since been many attempts toward attenuating glass/ceramic scaffolds through manipulation of their composition, in order to better match their mechanical properties and porous architecture to those of native bone, with mixed results (3). Native bone contains both an inorganic mineral phase and an organic polymer phase that impart both its strength and flexibility. This has led to the development of composite glass/ceramic/polymer scaffolds in order to produce a scaffold that is mechanically strong yet flexible and permits enhanced attachment and proliferation of cells (4). There are a small number of composite scaffolds commercially available such as Actifuse, a silicon substituted hydroxyapatite mixed with a resorbable polymer, marketed by Baxter.

1.1.1.2 Synthetic Polymers in Tissue Engineering

Synthetic polymers based on poly(α-hydroxyesters), such as poly-glycolic acid, poly-lactic acid, their co polymer, poly(lactic-co-glycolic) acid (PLGA) and poly-capralactone are widely used materials in tissue engineering (13). Such materials are already approved for medical uses by the U.S. Food and Drug Administration (FDA), initially for use as biodegradable sutures (14). Their uses are now vast, from musculoskeletal (15, 16) to nerve (17) and vascular tissue engineering (18). However, one of the drawbacks of such synthetic polymers is a lack of compatibility with cells, particularly, a lack of cell binding sites. This has led to increasingly complex methods of synthesis to improve their bioactivity, such as the incorporation of RGD cell binding motifs (19) or the tuneable release of bioactive compounds, such as transforming growth factors or bone morphogenetic proteins (20). Despite this several products based on synthetic polymers have reached the market including InQu®, a PLGA bone void filler marketed by Integra LifeSciences and X-repair, a woven PLLA mesh, used for soft tissue reinforcement during surgery marketed by Synthasome (14).

1.1.1.3 Natural Polymers in Tissue Engineering

Natural bio-polymers do not suffer the same issues, such as a lack of bioactivity or cell binding sites, as synthetic polymers and are usually based on extracellular matrix proteins (ECM) and other macromolecules such as collagen, fibrin or hyaluronic acid (21). Collagens, primarily types I and II, are perhaps the most widely used natural polymers in tissue engineering applications as they are structural proteins found in the ECM of most tissues. Collagens can be processed into many formats including membranes (22), sponges (23) and hydrogels (24) and have been used in a number of different contexts including as nerve conduits for peripheral nerve repair (25), bladder reconstruction (26) and as skin substitutes (27). Natural scaffolds tend to mechanically inferior than the native tissue they are intended to replace due to difficulties in synthesis and processing (28). As with synthetic polymers some natural polymers are already available within the marketplace, including Excellagen®, used to treat diabetic foot ulcers, marketed by Cardium Therapeutics and Endoform™, a wound dressing marketed by Mesynthes (14).

1.1.1.4 Decellularised Biological Scaffolds in Tissue Engineering

In order to retain gross tissue architecture and the intrinsic mechanical properties of tissues, researchers have decellularised natural tissues leaving the native ECM as a "biological scaffold". The decellularisation process involves the use of detergents, chemicals and enzymes and may also require mechanical forces, though the exact parameters are generally dependent on the size and structure of the tissue/organ being decellularised (29). Ultimately the goal is to remove all immunogenic material from the tissue to prevent rejection whilst retaining as much of the native ECM and glycosaminoglycan's (GAGs) as possible. A range of tissues, skin (30), tendon (31), bone (32) and organs, lung (33), liver (34) and kidney (35) have been decellularised and assessed. Whilst much of this research is still confined to animal models, a few decellularised products have made it to market including CryoValve® SG for pulmonary heart valve replacement marketed by CyroLife and Vascu-Guard®, a peripheral vascular patch marketed by Synovis (14). However, such products do not contain a cellular component which has made their regulatory approval more expedient. Research into decellularised scaffolds may envision a second stage where the scaffold is repopulated by the patient's own stem cells prior to implantation.

1.2 Stem Cells and Stem Cell Based Therapies

"Regenerative medicine" whilst frequently synonymous/combined with tissue engineering often puts greater emphasis on the use of stem cells to achieve the same goals. Stem cells have been known to science since the early 20th century with one of the earliest references being to what is now known as the haematopoietic stem cell (HSC) (36). Now widely studied, stem cells are considered to possess many potential applications in regenerative medicine. Intrinsic to this perception are the characteristics that define stem cells, namely their capacity for self-renewal and the potential to differentiate into one or more specialised adult cell(s) (37). Whilst it is true that stem cells exhibit extensive self-renewal *in vitro* (38), several groups have shown that stem cells *in vivo* undergo limited self-renewal, instead they maintain a quiescent state for the majority of normal tissue homeostasis (39, 40). Nevertheless, the capacity for rapid expansion *ex vivo* is one of the key driving forces behind stem cell research in regenerative medicine.

1.2.1 Stem Cell Classification

The mechanisms underpinning stem cell self-renewal vary widely between different stem cell populations. Self-renewal is regulated by the complex interplay between signalling pathways controlling the cell cycle and through interactions with the local microenvironment, such as the ECM and soluble growth factors and hormones (41). Much of this variation is linked to the developmental potential of a given stem cell, described as "stem cell potency" or "stemness". Potency is a hierarchical classification beginning with totipotent, through pluripotent, multipotent and unipotent into which the majority of stem cells can be classified (Figure 2).

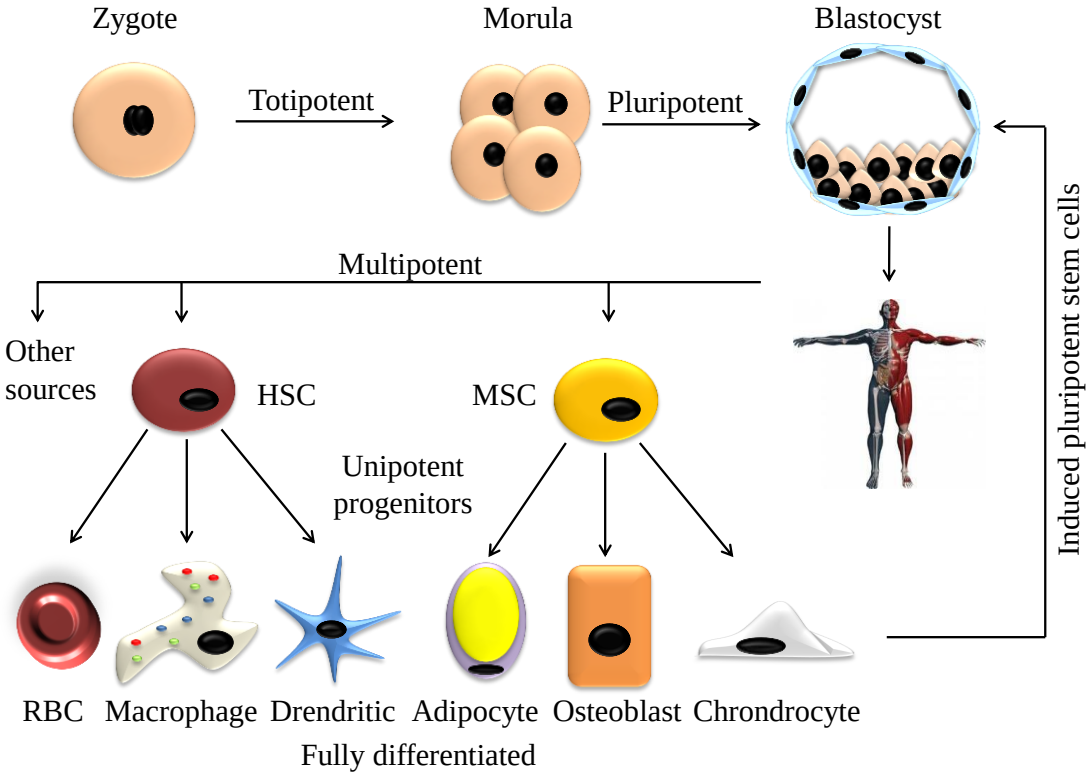

Figure 2. Overview of stem cell hierarchy with examples of cells. HSC – haematopoietic stem cell, MSC mesenchymal stem cell, RBC – red blood cell

In nature only the zygote, formed after the fusion of the gametes, can be considered a truly totipotent cell. Totipotency therefore refers to the fact that a cell is capable of generating an entire organism including all of its cells and those of the extra-embryonic tissues. However, a study by Mitalipov *et al* 2002 (42) suggested that cells of the morula at the 2 and 4 cell stage following the division of the zygote may also be considered to be totipotent as they were found to be capable of establishing fully developed Rhesus monkeys upon isolation and *in vitro* fertilisation transplantation.

Approximately one week into human embryonic development, the blastocyst forms. The cells of the blastocyst inner mass are considered as embryonic stem cells (ESCs) and were first described in mice by Evans and Kaufman in 1981 (43) and in humans by Thomson *et al* in 1998 (44). Embryonic stem cells are pluripotent as they cannot alone give rise to a whole organism but they are capable of differentiating

into any of the three primary germ layers; the ectoderm, endoderm or mesoderm and therefore any cell within the developed organism (45, 46). This property has resulted in extensive research into embryonic stem cells and their potential application in regenerative medicine. However, research with ESCs has been stifled to an extent due primarily to an ethical debate regarding their isolation, the main points of which have been extensively reviewed by several authors (47-49). In 2006, Takahashi and Yamanika (50) demonstrated an ethically sound method for the production of pluripotent stem cells by reprogramming somatic fibroblasts using a cocktail of factors including Oct3/4, Sox2, c-Myc, and Klf4. The resultant cells were termed "induced pluripotent stem (iPS) cells".

Of particular interest to this thesis are multipotent stem cells, of which there are many types residing in almost all the tissues of the adult body. These include mesenchymal stem cells (MSCs) found in a range of tissues including bone marrow (51), adipose tissue (52) and dental pulp (53); HSCs, also found in the bone marrow (36) and neural stem cells (54). The term multipotent indicates that a stem cell may become any of the specialised cell types within its parent tissue. The MSC (from the mesodermal germ layer) is a notable exception to this rule as transdifferentiation to cells of the ectodermal (neural cells) and endodermal (hepatocytes) germ layers has been demonstrated (55, 56). Stem cell research is extensive and cell based therapies, in various stages of development, have been suggested for a range diseases/conditions.

1.2.2 Stem Cell Based Therapies

Research into stem cell based therapies ranges from basic *in vitro* lab based studies through to preclinical *in vivo* animal studies and the various phases of in human trials. Much of the early research with stem cells focused on the production of differentiated cell types that may have a clinical utility such as cardiomyocytes (57), chondrocytes (58) and hepatocytes (59) from many of the stem cell sources highlighted. Methods to characterise this process and to isolate and produce quantities of clinically relevant stem cells also featured prominently. However, many initial preclinical studies reported poor results when stem cells produced *in vitro* based on these early studies were used (60). It has since been demonstrated that

such simple *in vitro* studies poorly recapitulate the intricacies of stem cell mediated tissue repair *in vivo* (61). Potential reasons for this include the heterogeneity of stem cell populations isolated by such simple means as adherence to tissue culture plastic (62), inconsistent definitions regarding the characterisation of undifferentiated stem cells (63) and the loss of the trophic support stem cells receive from their niche *in vivo* (64). Consequently many lab based stem cell studies now seek to address these issues.

The stem cell surface antigen profile has been extensively studied with the aim of improving the isolation and enrichment of therapeutically relevant stem cell populations. Methods such as flow cytometry have been used to isolate MSC subpopulations based on the expression of markers such as STRO-1, CD146 and SSEA-4 without any prior cell culture and have been shown to enhance colony forming unit – fibroblast potential resulting in a more homogenous population (65). Microfluidic chip systems have also been used to measure the expression of up to 96 genes from single cells and found that the negative selection of CD105 improved the osteogenic potential of adipose derived MSCs (66). However, such studies serve to highlight the inherent heterogeneity in stem cell populations and the need for methods that are not reliant on such changeable markers. Furthermore, *in vivo* stem cell phenotype is maintained through the interaction between the ECM, other cells and the associated paracrine/autocrine signalling and mechanical forces (67-69). In recognition of this there is growing interest in the co-culture of stem cells with other ‘supportive’ cell populations (70) as opposed to stem cell enrichment strategies.

Greater control over the stem cell microenvironment can include many factors such as oxygen tension, medium perfusion, multicellular cultures and substrate stiffness, topography and epitope presentation. Oxygen tension is known to have a significant impact on cellular biology. Tissues in the body, from cartilage to circulating blood, are exposed to a range of oxygen concentrations (2-13%) and this has led to attempts to optimise oxygen supplementation *in vitro* to affect stem cell proliferation and differentiation (71-73). Similarly medium perfusion has been shown to affect both stem cell proliferation and differentiation down multiple lineages including neural and cardiac (74-76). Cells *in vivo* are rarely in a homogenous environment and the

co-culture of two or more cells types aims to recapitulate the cross-talk found between cells of different types. The co-culture of stem cells with endothelial cells has been widely studied and shows promise in stimulating angiogenesis and neovascularisation (77). Finally, the substrate on which cells are cultured possess many characteristics that influence cell fate including stiffness, topography and biochemistry and have been extensively reviewed (60, 78, 79)

Regardless of the many unanswered questions, in 2011 Trounson *et al* (80) recorded that there were 123 clinical trials using MSCs listed on clinicaltrials.gov; as of July 2014 that number stood at 411 MSC based therapies at various stages of development. Significant progress with stem cell based therapies has clearly been made in the last 20 years. However, to enhance the clinical translation of stem cell based therapies and facilitate their scale up, non-invasive methods that are not perturbed by the myriad factors governing stem cell differentiation are highly desirable. There are many techniques that could be applied to the non-invasive characterisation of stem cells, some of which are listed in Table 2; of particular interest to this thesis is Raman spectroscopy which is more comprehensively described in the following sections.

Table 2. List of techniques that are or could be used for the non-invasive characterisation of stem cells, their mode of action and some of their current uses.

Technique	Mode of action	Current uses
Dielectric/impedance spectroscopy	Measures the interaction of a sample with a range of radio-frequency alternating current fields	Combined with fluidics can be used to separate cells in suspension based on their electric impedance (81, 82)
Light scattering spectroscopy	Measures elastic light scattering at visible wavelengths	Measurement of the size of intracellular organelles such as the nucleus which can be enlarged in conditions such as cancer (83)
Optical coherence tomography	Analogous to ultrasound, uses light reflected from within 3D samples to construct an internal image	Mapping the movements and formation of cellular structures within tissue engineered constructs (84, 85)
Photoacoustic microscopy	Based on the detection sound waves, induced by the absorbance of near infrared pulses supplied to a sample	Similar to optical coherence tomography, can be used to map tissue engineered constructs (85)
Raman spectroscopy	Discussed in section 1.3.2	Discussed in section 1.5

1.3 Principles of Spectroscopy, Particularly Raman Spectroscopy

1.3.1 Basics of Spectroscopy

In the most basic sense, spectroscopy can be described as the study of matter using electromagnetic radiation (86). The electromagnetic (EM) spectrum (Figure 3) describes light as a function of its wavelength from sub nanometre gamma rays to radio waves in the order of metres.

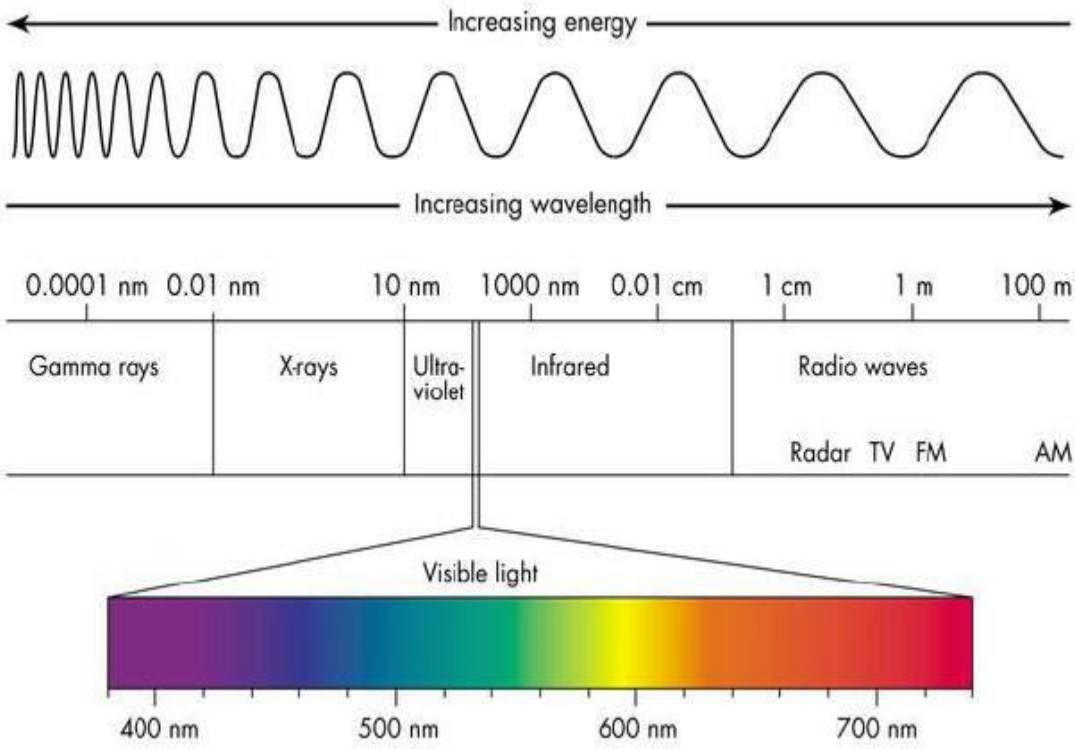

Figure 3. Depiction of the electromagnetic spectrum (87).

In its most basic iteration a spectroscope contains a light source which is focused on to a sample, the light from which is split by a prism and collected on a screen (Figure 4). In such a spectroscope the sample will absorb photons (or emit if heated) of a certain wavelength of light according to its chemical composition creating a unique spectrum of light on the collecting screen. Every element generates a unique spectrum in this manner and several elements including rubidium and caesium were first discovered by spectroscopy.

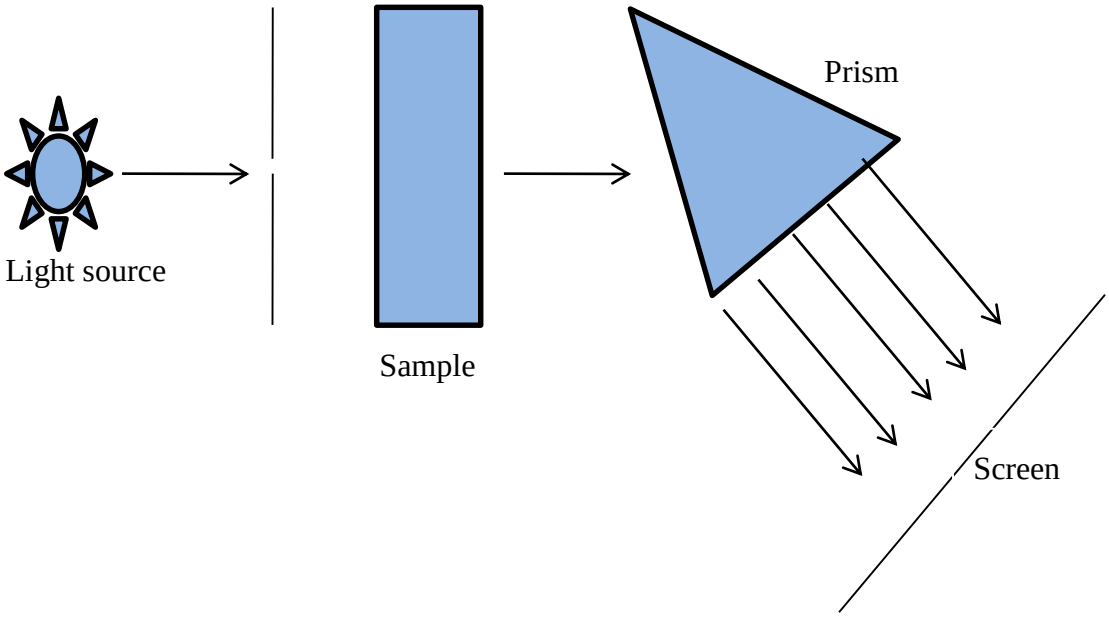

Figure 4. A simplified schematic of the first spectroscope created by created by Bunsen and Kirchhoff in 1860, adapted from (86).

Modern spectroscopes are far more complicated than this simplistic model but have been developed to utilise a light source drawn from almost every part of the electromagnetic spectrum with each describing different properties of the sample analysed. Some of the most common forms of spectroscopy with potential applications in biomedical research are listed in Table 3, many of which can be used in a non-invasive and non-destructive manner.

Table 3. Brief summary of spectroscopic techniques with biomedical applications

EM Region	Spectroscopic Technique	Process Involved	Biological Applications
Radiowave	Nuclear magnetic resonance (NMR)	Changing nuclear spin orientation	*In vivo* imaging and quantification of metabolites in the brain and tumour identification (88, 89)
Microwave	Electron spin resonance (ESR)	Changing electron spin orientation	*In vivo* measurement of tissue pO_2 and redox status (90, 91)
Infrared	Fourier transform (FTIR), Raman	Changing molecular vibrational state	Molecular characterisation of cells, tissues and tumours (92-94)
Visible/Ultraviolet (UV)	Steady state reflectance/fluorescence spectroscopy	Changing atomic or molecular electronic state	*In vivo* cancer biomarker detection, reviewed in (95)

1.3.2 Raman Spectroscopy and its Derivatives

Raman as with other forms of spectroscopy, measures the interaction between certain wavelengths of electromagnetic radiation with matter. However, it is unique amongst other forms of spectroscopy in that it measures a difference in the energy of incident and emitted photons as opposed to the energy of the photons themselves (96). This is due to a process known as the Raman Effect, or the inelastic scattering of light. Briefly, during inelastic scattering, incident light interacts with the nuclei of a molecule, which results in their displacement with respect to their electron clouds. Such displacements represent distinct energy levels different to the non-excited/ground state and are referred to as vibrational energy states. Hence a shift occurs in the energy level of emitted photons with respect to the incident photons due to their differing energy levels, known as a Raman shift, essentially inelastic light scattering, (Figure 5). Detection of Raman shifts yields information as to the vibrational state of the molecule under investigation and by extension its molecular bonds and composition as many molecular bonds possess a unique Raman shift. For a thorough review of biological Raman peak assignments please refer to (97). A plot of all the Raman shifts observed in a sample produces a spectrum where shifts are characterised in wavenumbers (inverse of wavelength in cm^{-1}) from the incident frequency.

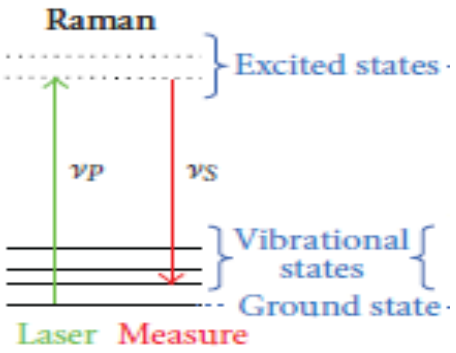

Figure 5. Schematic energy level diagram of Raman spectroscopy, where *vp* is the frequency of the incident/absorbed photon and *vs* is the frequency of the emitted photon, the difference between the two equalling the vibrational energy state of the molecular species being characterised, (98).

There are several key parts to a basic Raman apparatus, an EM source, typically a monochromatic laser, a focusing lens, dichroic mirror, a spectrometer, and a detector, typically a cooled silicon charge coupled device (CCD), (Figure 6). Raman spectra may also be mapped to an image if a microscope is incorporated (98). The most common lasers currently used in the acquisition of spectra from live cells operate in the near infra-red region of the EM spectrum at wavelengths of 633 nm (HeNe laser) and 785 nm (AlGaAs diode) (99-104). The wavelengths selected are in part predetermined by limitations in the silicon CCDs that detect the Raman shift (they rapidly lose response at wavelengths >1000 nm) (92) but the selection of wavelength can also be seen as a compromise. Shorter wavelengths improve inelastic scattering efficiency and the spatial resolution of images that are captured, whilst longer wavelengths reduce the amount of background signal due to their greater power (105); though there is evidence that higher powered lasers can induce photodamage, a light induced reduction in cell viability (106). A lens is used to focus the incident light on to the sample. Emitted light is then directed to a dichroic mirror which separates light of an identical wavelength to the incident light, i.e. elastically scattered light, from the Raman shifted light which is directed to a spectrometer. The spectrometer splits the Raman shifted light into a spectrum which is recorded by a cooled silicon CCD (98). When a microscope is incorporated the image emitted by the sample through the microscope is channelled in the same way to the CCD but the spectral data is mapped to the image localising the intensity of the Raman shifts to the image (107).

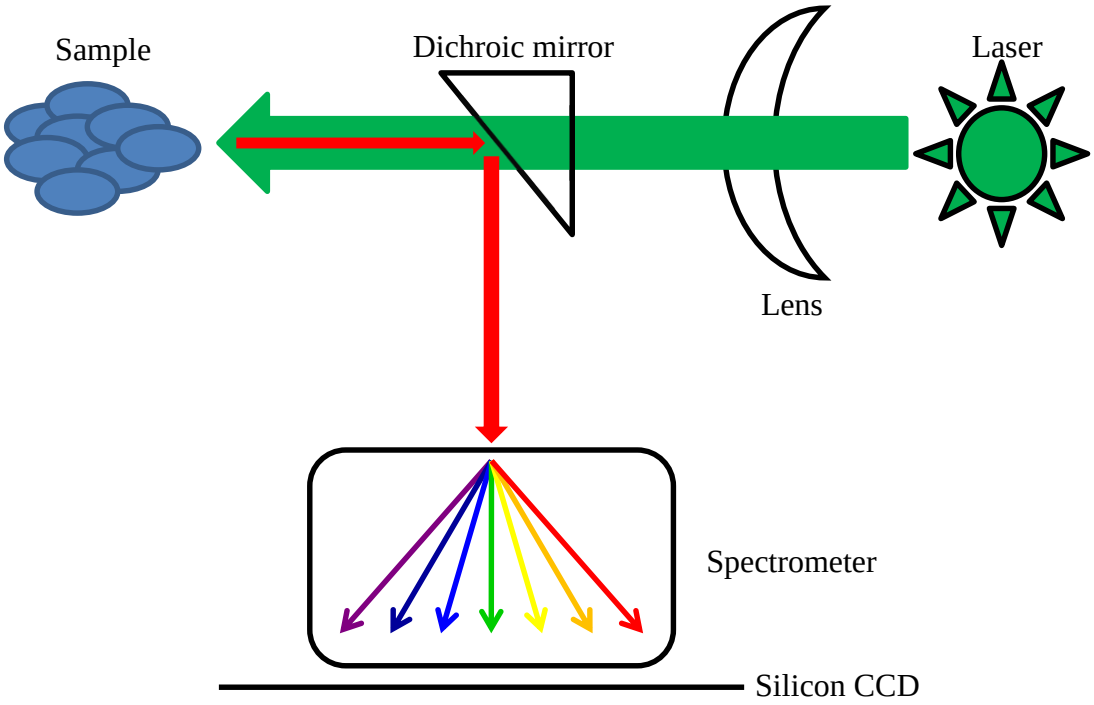

Figure 6. Schematic representation of the components in a basic Raman experiment, additional or more specialised components can be included according to the application.

Raman scattering is a highly inefficient process. It is estimated that between $1x10^{6}$-$1x10^{8}$ (108) or $1x10^{10}$ (109) photons will shift in wavelength upon interaction with a sample. Due to this, several derivatives of the basic Raman technique have been developed, including resonance Raman spectroscopy (RRS), surface and tip enhanced Raman spectroscopy (SERS and TERS), and coherent anti-stokes Raman spectroscopy (CARS). RRS uses lasers that excite the sample in the UV range (<270 nm). It is termed resonance Raman spectroscopy as the excitation wavelength of the laser is matched to the absorption maximum of the molecule of interest. The key advantage to RRS is that by using UV lasers the Raman shifts occur in an area of the spectrum far from the background noise, vastly improving the resolution of the spectral data of interest (110). However, the technique is unsuitable for live cell imaging due to the potential for photo-induced mutagenicity through the use of UV lasers (111). SERS and TERS operate through the same principle, using metal ions - most often gold - to improve the resolution of images acquired by microscopes attached to a Raman spectrometer. In SERS, gold nanoparticles, generally coated in surfactant to prevent aggregation, are added to the sample. This has dual effects, first amplifying the power of the incident light thereby reducing the background noise with respect to the Raman signal, and second enhancing the Raman shifted signal

itself by several orders of magnitude (98). TERS works by the same principles as SERS, however gold is coated on the tip of an atomic force microscope in order to produce similar effects (112). However, neither approach is suitable for the non-invasive imaging of live cells due to the introduction of exogenous metal ions. In CARS two lasers are shone on the sample, the difference in excitation wavelength between which corresponds to the vibrational frequency of a molecule of interest. As with SERS and TERS, CARS improves the resolution of Raman spectral images by approximately a factor of 5, producing highly detailed maps in much shorter timescales than with normal Raman. However, excitation of a sample at only one vibrational frequency greatly reduces the amount of spectral information generated and whilst it is possible to perform excitation at sequential frequencies, the propensity for live cells and their organelles to move could greatly reduce the accuracy of results (92, 98).

1.4 Analysis and Interpretation of Raman Spectra

1.4.1 Pre-processing of Spectra

Aside from containing chemically relevant data from a sample, Raman spectra also contain several extraneous components that should be removed prior to any further meaningful analysis. This can include fluorescence background, CCD noise, Gaussian noise and cosmic noise. The Raman signal from materials in the vicinity of the sample must also be removed (113). The method by which this is carried out is termed “pre-processing” and there are many approaches available to execute this. The aim of pre-processing is to improve the robustness and interpretability of the data whilst removing outliers and irrelevant data (114). Some of these techniques including smoothing, baseline correction, normalisation and the differentiation of spectra are extensively reviewed elsewhere (114, 115).

Smoothing of spectra can be reasonably simple and generally involves some averaging of data points (116). Baseline corrections can be achieved most simply by an offset correction, that is, reducing the lowest point on the spectrum to zero and reducing all other points by the appropriate amount. A more accurate baseline correction involves fitting a polynomial line to the spectrum and this is particularly useful in removing the fluorescence background from Raman spectra (117). Derivative methods such as the first or second derivative are also particularly useful at removing the fluorescence background from Raman spectra (118). One commonly used smoothing filter which is also a derivative method and can be used to correct a baseline is the Savitzky-Golay filter (119). Here a polynomial line is drawn beneath the spectrum to remove the baseline and a number of points are selected for the averaging and smoothing of the remaining spectrum. Figure 7 illustrates a baseline correction by fitting a polynomial line with smoothing.

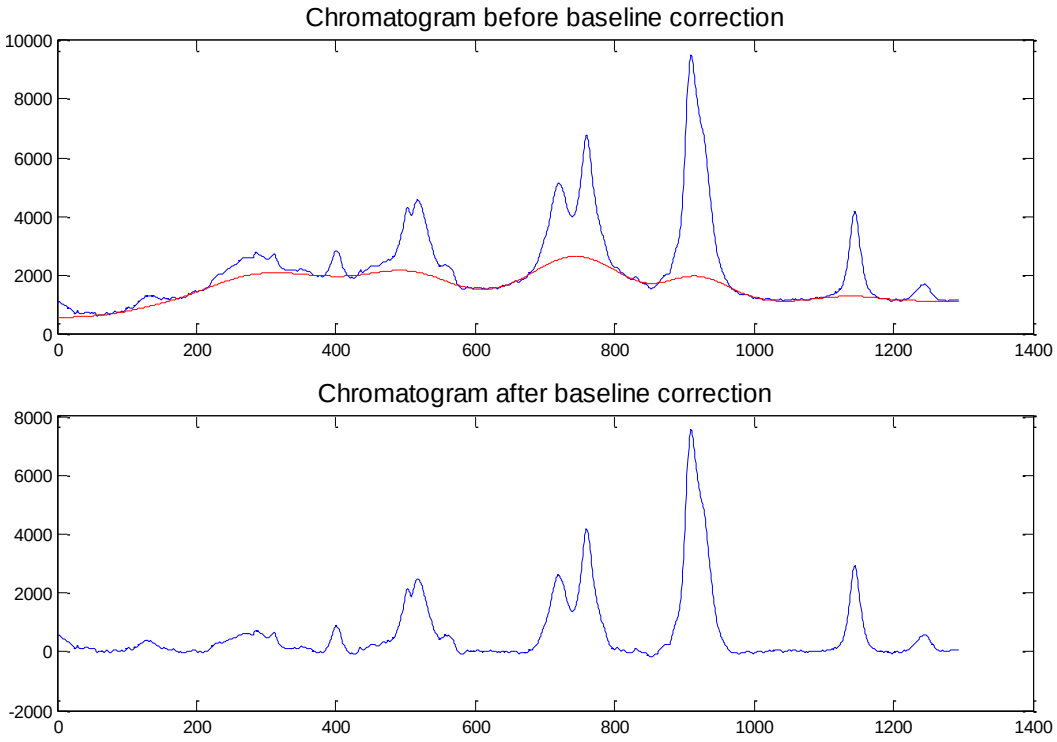

Figure 7. An illustration of a baseline correction to a Raman spectrum by fitting and subtracting a polynomial line (drawn in red).

The selection of which pre-processing technique is to be used on a given data set is very much dependant on the individual data and the severity of the extraneous influences within it. Further, poor pre-processing can influence the quality of any subsequent analysis and even produce false positives. In order to prevent this most researchers conduct a "grid search", in essence conducting all possible combinations of pre-processing in order to find the appropriate combination. This can be a highly time consuming process but a study by Bocklitz *et al* 2011 (113) demonstrated that the process could be performed and optimised using a genetic algorithm to find the best possible combination of available techniques using several different data sets.

1.4.2 Multivariate Analysis of Spectra

Raman spectra typically have many data points most of which represent biochemically important data, all of which have the potential to be associated with one another. As such there is a need for techniques capable of uncovering and describing this inherent complexity. Multivariate analysis techniques achieve this by simplifying a data set and so aiding its visualisation and may also permit

classification or prediction of outcome (120). There are many techniques and some of the most commonly used to visualise spectral data include principal component analysis (PCA), partial least squares (PLS), multiple linear regression (MLR), artificial neural networks (ANN) and genetic algorithms (GA).

PCA, perhaps the most commonly used method, takes a data matrix (tabulated spectral data) and reduces it into principal components (PCs). PCs describe the variance of the data set where PC1 contains the most variation, PC2 the second most variation and so on. In the case of spectral data, this means that the wavenumbers (peaks that relate to particular molecular species) that vary most are grouped in PC1 and so on. In order to visualise the data, each spectrum in the data matrix is assigned a score and each wavenumber a loading for each PC. Scores and loadings can both be plotted and provide complementary results. The scores for two principal components can be plotted against one another in a scatter plot and this reveals how the spectra in the original data matrix cluster according to the variables contained within the two selected PCs. As such the scores plot can be used to classify the original spectra according to selected variables. The variables within a PC can be visualised with a loadings plot. The loadings for a single PC can be presented as a line graph revealing which wavenumbers vary most within that PC. The loadings for two PCs can also be presented as a scatter plot and when taken with scores plot from the same two PCs can be used to visualise upon which clusters of spectra the wavenumbers which constitute those loadings vary the most. All of this means that PCA can be used to identify trends, clusters and outliers within a data set and then relate this back to the biochemical nature of the sample investigated (120-123).

Figure 8 contains an example of this description of PCA from a tutorial review of PCA by Bro and Smilde 2014 (121). In this example 44 different wines produced in 4 regions (Argentina, Australia, Chile and South Africa) were compared on the basis of 14 different variables (ethanol, total acid, volatileA, malic acid, pH, lactic acid, sugar, citric acid, CO_2, density, folinC, glycerol, methanol and tartaricA). The first aim of this analysis was to ascertain if wines produced in the same region were similar to one another. Figure 8A is the PCA scores plot for the data using PC1 and PC2; it shows that wines from each region tended to cluster together according to the variables measured/their composition. In order to determine which variables

were most important in the wines from each region, the loadings for PC1 and PC2 were plotted against one another (Figure 8B). Chilean wines were found in the lower left quadrant of the scores plot and citric acid and CO_2 were found in the same quadrant of the loadings plot, indicating that Chilean wine is best described by its citric acid and CO_2 content. Similarly, Australian wines were found in the upper right quadrant of the scores plot and ethanol, methanol and glycerol are found in the same quadrant of the loadings plot, indicating that Australian wine is best described by its ethanol, methanol and glycerol content. Due to the absence of any wines in the lower right quadrant of the scores plot, malic acid found in the same quadrant of the loadings plot is a poor variable for describing any of the wines, at least as far as PCs 1 and 2 are concerned. Figure 8C shows bar charts of the loadings for each individual PC. In this case, bar charts are the best representation as these variables are discrete data. In the case of spectra, which are continuous data, these loadings would be best drawn as line graphs.

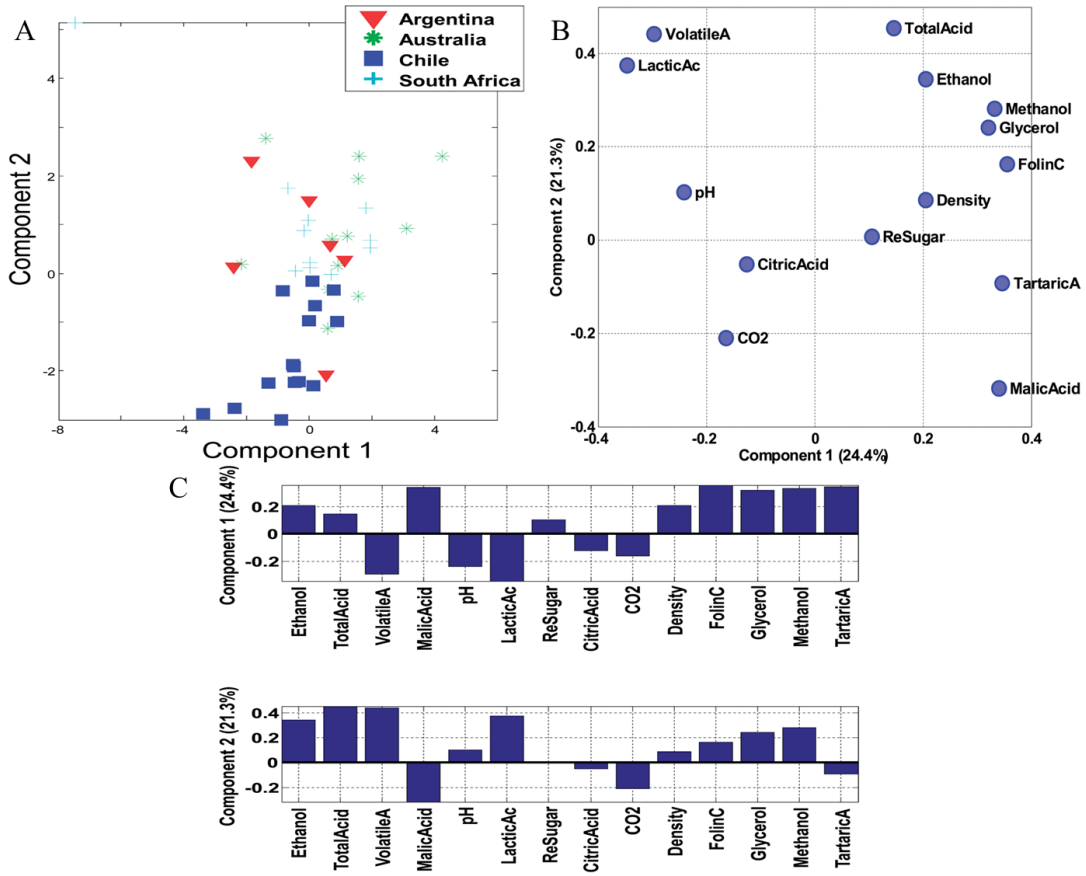

Figure 8. An illustrated example of how PCA data can be represented. The analysis was performed on 44 different wines produced in 4 different regions using 14 different variables to characterise them. A) PCA scores plot for PCs 1 and 2, B) Loadings for PC1 vs PC2, C) individual loadings for PC1 and PC2. Figures reproduced from (121).

PLS like PCA is a method to reduce the dimensionality of a data set producing scores and loadings plots that can be used to derive similar visualisation of the data. Where they differ is in the method for the calculation of scores and loadings (120).

ANNs and GAs are techniques that are also used to solve prediction and classification problems and are beginning to be more widely used to analyse spectral data. ANNs are a computational algorithm that attempts to simulate the interconnectedness of biological neural networks. They contain inputs, (in the case of spectra wavenumbers) one or more hidden layers of neurons also termed processing elements, and outputs, (Figure 9). Using an iterative process of changing the weightings of the inputs, the network is able to 'learn' which features best describe the inputs. If a network is first trained with a data set with a known classification, it can then be subsequently used to predict the classification of any further data (124, 125). GA algorithms attempt to simulate the processes of meiosis and reproduction, which, in the biological sense, after many generations might be termed "evolution", in that only the most fit recombination's of genetic information survive. For GAs the input, in this case spectral, goes through an iterative process of division and recombination in an effort to identify those features which best approximate the input where the best approximations are retained whilst the poorest are discarded. As with ANNs this process can be used to classify and predict new data (126). Both ANNs and GAs have found a wide variety of applications from accounting and finance, health and medical, engineering, manufacturing and marketing (125).

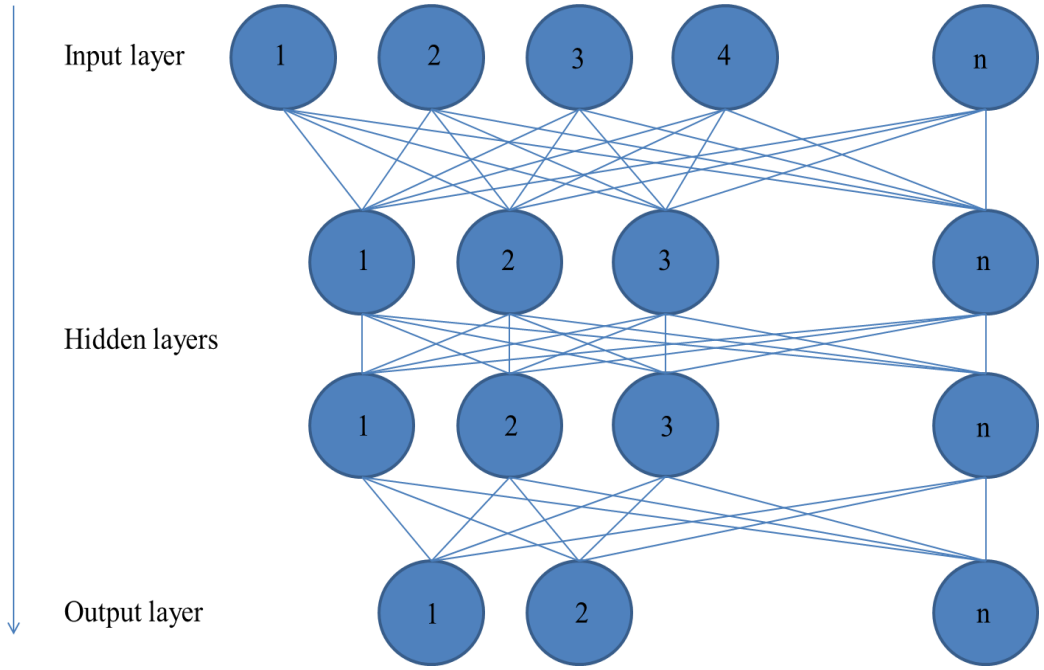

Figure 9. Basic architecture of an ANN. Circled are the nodes or processing elements (PE). Each PE is connected to all PEs in the layer beneath. In the case of spectra the input layer contains the intensity of each wavenumber of the spectra. The nodes in the hidden layer contain a function that transforms the data and the output layer is the result. Through an iterative process of communication between the layers, the ANN 'learns' which of those inputs best describe the data as a whole. Figure adapted from (127).

1.5 Raman Spectroscopy and Stem Cells

There are several examples where Raman spectroscopy has been/is being used as an adjunct to stem cell research. For example, Raman spectroscopy has been used to determine cell viability (99, 128, 129), to discriminate between various different cell types (102, 130), to identify general markers of stem cell differentiation (104, 128, 131), to track stem cell differentiation to an osteoblastic phenotype (132), and to elucidate changes in ECM crystallinity with osteoblastic differentiation (101, 133, 134).

1.5.1 Raman Spectroscopy to Determine Cellular Viability

Bai *et al* 2011 (99) took Raman spectra of undifferentiated umbilical cord-derived MSCs whose viability was either high (>90%) or low ((<20%), induced by starvation in PBS), predetermined by a Trypan blue assay. After statistical analysis they found that there was significant variation ($p<0.001$) in the intensity of three peaks at 744 cm^{-1} (C=O bending in tryptophan), 877 cm^{-1} (C-C symmetrical stretching in lipids) and 1342 cm^{-1} (CH deformation in proteins), the two former being 2x greater in intensity in low viability MSCs and the latter 30% lower in low viability MSCs. The change in intensity of the three bands was attributed to the generation of reactive oxygen species (ROS) caused by the reduction in viability. ROS are known to attack nucleic acid bases and lipids, hence the increased intensity of bands at 744 cm^{-1} and 877 cm^{-1}. However, no further data were presented to support an increase in ROS, the quantification of which can be detected by several commercially available assays. The band at 1342 cm^{-1} was said to have been indicative of α-helical protein. ROS are known to attack di-sulphide and hydrogen bonds important in maintaining α-helical conformation hence a reduction in this band at low viability. Again however, no further data was presented to support this conclusion.

Pully *et al* 2010 (128) investigated the effect on cell viability of culturing bone marrow derived MSCs in medium perfused microbioreactors. They identified and assigned peaks in their spectra at 788 cm^{-1} (DNA), 1004 cm^{-1} (phenylalanine), 1032 cm^{-1} (phenylalanine), 1094 cm^{-1} (nucleotide backbone), 1126 cm^{-1} (protein),

1304 cm^{-1} (adenine), 1339cm^{-1} (adenine) and 1660 cm^{-1} (amide I) and found no significant variation over the course of 21 days. Whilst their spectra were not compared with MSCs grown in static culture (therefore not precluding the possibility that the presence of these bands may have been an effect of perfusion), their band assignments are consistent with the results of others where undifferentiated MSCs have been grown in static culture (99, 132, 134), indicating that they may be potential markers of healthy undifferentiated MSCs. They also noted the absence of bands at 1578 cm^{-1} and 1607 cm^{-1} which are considered to be indicative of necrotic cells (135). Finally, an earlier paper by Pully *et al* 2009 (129) investigated the presence of a peak at 1602 cm^{-1} in MSCs as well as other cell types. Through imaging and cluster analysis of the spectra, the band was found to be at its greatest intensity in the membrane of mitochondria. Though no band assignment was given, further evidence for a mitochondrial role/origin through the manipulation of Ca^{2+} levels (mitochondria play a key role in intracellular calcium storage and signalling) in the culture medium and concomitantly manipulation of the band at 1602 cm^{-1} was presented. This peak, the authors argue, could therefore be considered a marker of healthy, metabolically active cells.

1.5.2 Discriminating Between Different Cell Types Using Raman Spectroscopy

One of the earliest studies involving cells and Raman spectroscopy utilised it to distinguish between differing cell types. The study by Notingher *et al* 2004 (102) looked at three different types of bone cell, primary osteoblast, SV40 large T antigen immortalised alveolar bone cells and the osteosarcoma cell line MG63 with the aim of ascertaining if Raman spectroscopy could be used to detect differences in phenotypically similar cell types. Using PCA and linear discriminant analysis they found that the two non-cancerous cell types (primary osteoblasts and SV40 alveolar bone cells) were clearly grouped apart for the cancerous MG63 cells with a high degree of prediction (96.66%). This was found to be due to differing protein and nuclei acid content between the two groups. A more recent study by Ilan and Kraft (130) sought to demonstrate that different cells, even when co-cultured, could be distinguished using Raman spectroscopy. In their study they took individual spectra from four different cell types: MDCK (Madin-Darby canine kidney cells), CHO (Chinese hamster ovary cells), NIH 3T3 (mouse fibroblasts), and Clone 15

(transfected NIH 3T3 mouse fibroblasts), using these as reference spectra to predict cell type with a high degree of accuracy when co-cultured. The capacity to accurately predict cell phenotype within a multi-cellular environment has many potential applications perhaps most notably in identifying cancers, another widely studied application for Raman spectroscopy (136-138).

1.5.3 Characterising General Indicators of Stem Cell Differentiation Using Raman Spectroscopy

Schulze *et al* 2010 (104) investigated whether Raman spectroscopy could uncover any general changes in cellular composition through differentiation though without using MSCs. They highlighted 6 bands whose intensity changed as the cells (human embryonic stem cell line CA1) differentiated to neural, gut, fibroblast and adipocyte like cells: 782 cm^{-1} (cysteine, uracil, thymine ring), 788 cm^{-1} (O-P-O stretching in DNA), 811 cm^{-1} (O-P-O stretching in RNA), nucleic acid bands, 757 cm^{-1} (tryptophan ring), 937 cm^{-1} (C-C stretching), and 1003 cm^{-1} (phenylalanine ring), protein bands. They found a correlation in that in undifferentiated cells the nucleic acid band intensities were high and protein band intensities were low and that throughout differentiation nucleic acid band intensity decreased whilst protein band intensity increased. The authors' interpretation was that undifferentiated cells are actively proliferating, therefore regularly doubling their DNA for mitosis, whilst differentiated cells are performing their function, which likely involves the production and secretion of proteins for numerous applications. Their conclusions were further confirmed through biochemical assays of cell lysates from differentiated and undifferentiated cells, demonstrating similar DNA/protein ratios to those seen using spectroscopy. A recent study by Ichimura *et al* 2014 (131) also investigated differentiation markers in embryonic stem cells using Raman Spectroscopy. Working at the individual cell level and using PCA to analyse the data, they found a clear separation between the spectra acquired from the nuclei of differentiated and undifferentiated ESCs. The authors did not put much emphasis on the band assignments of their spectra or the underlying biological meaning of the data, stressing that this was unnecessary if one's aim is to remove undifferentiated cells from ESC cultures, cells which could ultimately be cancerous if implanted. However, they did speculate that epigenetic events occurring during differentiation may have been the cause.

1.5.4 Specific Indicators of Osteogenic Differentiation Determined Using Raman Spectroscopy

Chiang *et al* 2009 (132) investigated if Raman spectroscopy could be used to specifically assess the differentiation of bone marrow derived MSCs to osteoblasts. They identified 3 bands in their MSCs following differentiation, the most prominent in intensity being at 960 cm^{-1} (PO_4^{3-} symmetric stretch in hydroxyapatite), with lesser bands at 1030 cm^{-1} (PO_4^{3-} asymmetrical stretching) and 1072 cm^{-1} (C-O vibration in plane stretching of CO_3^{2-}). However, further analysis and interpretation of these results was lacking. In addition, there were several other issues with this paper. Osteogenic induction of MSCs is generally considered to take up to 28 days with the onset of matrix mineralisation taking place after approximately 14 days (139). The MSCs in this paper were only induced for 14 days. The authors state that prior to Raman analysis, cell were trypsinised from tissue culture plastic and resuspended on quartz but this could have been highly detrimental to their analysis as the trypsinisation process will likely remove much of the ECM produced by the cells which is an integral part of their phenotype. Compared with other papers, a relatively low number of spectra (five) were taken at each time point during differentiation (days 7, 11, 14 18 and 21), undermining the potential accuracy of the results. Finally, the authors state that they had subtracted out the contribution to their spectra from the biological matrix, though how and why they did this was not explained. Given the importance of the biological matrix in bone providing a nucleation site for the inorganic phase, this appears somewhat illogical. Perhaps the first paper to use Raman spectroscopy to demonstrate MSC differentiation to osteoblasts and the only paper where dental pulp-derived MSCs have been investigated was published by Liu *et al* 2005 (133). However, this was not the key aim of the paper, which was to characterise the expression of matrix extracellular phosphoglycoprotein (MEPE) with MSC differentiation. Raman spectroscopy in this instance was used as a tool in the end point analysis of differentiation. Peaks at 960 cm^{-1} (PO_4^{3-} stretching) and 1070 cm^{-1} (CO_3^{2-}) were prominent with lesser peaks at 1300 cm^{-1}, 1450 cm^{-1} and 2800 cm^{-1} said to be protein remnants. No further analysis was performed as the data were presented as complementary with their Alizarin red staining and confirmation of an inorganic matrix.

Two studies, one by Gentleman *et al* 2009 (101) and one by McManus *et al* 2011 (134) have most thoroughly investigated MSC differentiation to an osteoblast phenotype and particularly the changes in ECM crystallinity that occur. Gentleman *et al* investigated three cell types in all, ESCs, MSCs and osteoblasts, all murine, each of which underwent osteo-induction and were assessed by a range of techniques including Raman spectroscopy, qRT-PCR, energy dispersive X-ray spectroscopy, SEM and TEM, immunohistochemistry, Alizarin red staining and alkaline phosphatase activity. The key finding of the paper was that ESCs produce an inorganic matrix inferior to that of MSCs and native osetoblasts. Raman spectroscopy was used to assess putative mineralised nodules prior to mineralisation at day 14 and mature mineralised nodules post mineralisation at day 28. Pre-mineralisation Raman measurements demonstrated peaks at 815 cm^{-1} (C-C backbone stretching), 936 cm^{-1} (C-C skeletal vibrations), 1246, 1269 cm^{-1} amide I (protein bands), and 853 cm^{-1} (tyrosine), 872 cm^{-1} (hydroxyproline), and 921 cm^{-1} (proline). Further, peaks at 1003 cm^{-1} and 1665 cm^{-1} were demonstrated to have a 0.96 correlation co-efficient with a type II collagen standard, indicating its abundance pre-mineralisation. The presence of type II collagen was confirmed with immunohistochemistry and qRT-PCR demonstrated the expression of the transcription factors SOX9, a regulator of type II collagen expression in chondrogenesis. This led the authors to hypothesise that MSC osteogenesis is mediated by endochondral ossification, an embryonic bone formation process where osteoblast like cells first create a cartilaginous type II collagen ECM and undergo hypertrophy before the onset of matrix mineralisation and maturation to type I collagen. Post mineralisation Raman measurements demonstrated a distinctly different spectroscopic profile with high intensity peaks at 960 cm^{-1} (PO_4^{3-} symmetric stretching) and 1070 cm^{-1} (C-O vibration in plane stretching of CO_3^{2-}) and lower intensity peaks at 1020-1100 cm^{-1} (PO_4^{3-} asymmetric stretching), 1595-1720 cm^{-1} (amide I), and 1243-1269 cm^{-1} (amide III). This was calculated as having a correlation co-efficient of >0.99 compared with data derived from native bone. The bands attributed to type II collagen pre-mineralisation were no longer present whilst amide I and III bands indicative of type I collagen were now detected, the presence of which was confirmed with immunohistochemistry, lending further credence to their hypothesis. Finally, multivariate principal component and factor analysis was performed on MSC bone nodules. This demonstrated that the band at

960 cm^{-1} was an amalgam of three distinct inorganic species, all found in native bone, amorphous phosphate species at 945-950 cm^{-1}, B-type carbonate substituted apatite at 955-959 cm^{-1}, and crystalline non-substituted hydroxyapatite at 962-964 cm^{-1}, leading the authors to conclude that MSCs had produced mature mineralised nodules of similar composition to native bone.

The study by McManus *et al* (134) was largely in agreement with Gentleman *et al*, however, human MSCs were used and they also explored changes in matrix crystallinity with differentiation. Univariate analysis of the peaks at 960 cm^{-1} (PO_4^{3-} symmetric stretch) and 1070 cm^{-1} (CO_3^{2-} in plane vibration) revealed increasing carbonate to phosphate ratio between days 14 and 21 followed by decreasing matrix crystallinity between days 21 and 28 and an increase in the mineral to matrix ratio throughout when comparing the peaks at 960 cm^{-1} (PO_4^{3-} symmetric stretch) and 850 cm^{-1} (hydroxyproline). Factor analysis of the peak at 960 cm^{-1} at days 14, 21 and 28 revealed the same three inorganic species as Gentleman *et al*, however, they varied over time. At day 14 only crystalline non-substituted hydroxyapatite at 962-964 cm^{-1} was evident. At days 21 and 28 only amorphous phosphate at 945-950 cm^{-1} and B-type carbonate substituted apatite at 955-959 cm^{-1} were detected. This is in contrast with Gentleman *et al* but in support of the univariate analysis demonstrating increasing carbonate to phosphate ratios and decreasing matrix crystallinity. However, the two are not directly comparable as species differences may be responsible for the differing results.

The studies discussed in this section clearly demonstrate the utility of Raman spectroscopy for the non-invasive characterisation of stem cells. In order to further advance the utility of this technique, experiments need to be performed repeatedly in real time under aseptic conditions leaving cell cultures intact and suitable for further use.

1.6 Aims and Objectives

The aim of this thesis was to determine whether Raman spectra could be acquired from the same stem cell cultures undergoing differentiation over time without compromising the sterility of these cell cultures. The following objectives were identified in order to achieve this goal:

1. To identify cell culture substrates that are suitable for Raman spectroscopy but do not affect the differentiation potential of DPSCs.
2. To develop a method for the reproducible, aseptic acquisition of Raman spectra from DPSCs across their differentiation pathway.
3. To validate the newly developed aseptic methodology by characterising DPSC osteogenic differentiation using Raman spectroscopy and comparing this with conventional phenotyping methods and the results of previously published material.
4. To use the new methodology to characterise differentiation down a previously sparsely published cell lineage; adipogenic differentiation using adipose-derived stem cells (ADSCs).

Chapter 2

General Materials and Methods

2.1 Dental Pulp Stromal Cell (DPSC) Isolation

Human molars were obtained from the University of Leeds School of Dentistry Research Tissue Bank (DREC 07/H1306/93+5) with full ethical consent. Teeth from one male and two female donors, aged 9-35, mean age 22 years were used. No later than 24 hours after extraction, dental pulp stromal cells (DPSC) were isolated as follows. Teeth were immersed in 70% ethanol for several minutes after which a sterilised scalpel was used to remove any extraneous tissue. The teeth were then cracked open in a vice to expose the dental pulp. The pulp was removed from the tooth ensuring no fragments of dentine and enamel remained and placed in Alpha Modified Essential Medium (α-MEM) (Invitrogen, Paisley, UK), where it was finely diced with a sterile scalpel. A cell suspension was obtained by enzymatic digestion of the diced pulp, using 4 mg/mL dispase II (Roche, Welwyn Garden City, UK) and 3 mg/mL collagenase I (Invitrogen, Paisley, UK), dissolved in α-MEM. Digests were incubated at 37°C, 5% CO_2, and agitated by pipetting every 15 minutes until no pulp fragments remained. Cell suspensions were incubated in 25cm^2 cell culture flasks at 37°C in basal medium, α-MEM containing 10% foetal calf serum (FCS) (Biosera, Ringmer, UK), 1% penicillin (10000 units), streptomycin (10 mg/mL) solution (Sigma-Aldrich, Gillingham, UK) and 1% 200 mM L-glutamine (Sigma-Aldrich, Gillingham, UK).

2.2 Expansion and Storage of DPSCs

Adherent DPSCs were cultured and passaged as follows. The culture medium was replaced twice weekly until cultures were ~80% confluent, at which point they were passaged. DPSCs were washed twice with 1x phosphate buffered saline (PBS) (Sigma-Aldrich, Gillingham, UK) then incubated with trypsin (0.5 g/L), EDTA (0.2 g/L) solution (Sigma-Aldrich, Gillingham, UK) at 37°C for several minutes. Complete cell detachment was encouraged by gentle agitation of the cell culture flask and confirmed under a microscope. Trypsin activity was neutralised with an

equal volume of medium containing 10% FCS and the cell suspensions centrifuged at 1500 rpm for 5 minutes. The cell pellet was resuspended in culture medium and split into three 175 cm^2 cell culture flasks. At the end of the second passage this process was repeated, however, the DPSCs were counted on a haemocytometer using trypan blue (Sigma-Aldrich, Gillingham, UK) to discriminate dead cells. DPSCs were then cryopreserved in liquid nitrogen in vials of approximately 1 x 10^7 cells suspended in α-MEM containing 40% FCS and 10% dimethylsulphoxide (Sigma-Aldrich, Gillingham, UK) for use in all future experiments.

2.3 RNA Isolation and Reverse Transcription

Prior to qRT-PCR, RNA must be isolated from cell culture lysates and reverse transcribed in to cDNA. Cell lysis was performed by incubation with Trizol® (Invitrogen, Paisley, UK) for 20 minutes at room temperature. RNA was extracted from cell lysates using an RNeasy mini kit with additional DNase digestion (Qiagen, Crawley, UK) following the manufacturers recommendations. RNA concentrations were quantified using a NanoDrop spectrophotometer (Thermo Scientific, Wilmington, USA). A High Capacity RNA-to-cDNA Kit (Applied Biosystems, Carlsbad, USA) was used to prepare 200 ng of cDNA in 20 µL reaction volumes as per the manufacturer's instructions. Reactions were run on a MJ Research PTC-100 Thermo Cycler, at 37°C for 1 hour and 95°C for 5 minutes.

2.4 Quartz Customised Flask Preparation

Cell culture flasks with quartz windows suitable for Raman spectroscopy were prepared as follows. Holes, 1cm in diameter, were drilled in 25 cm^2 cell culture flasks. Flasks were washed several times with sterile pure water to remove debris and finally sterilised with 70% ethanol. Heat sterilised quartz discs (Global Optics, Bournemouth, UK), 14 mm diameter x 0.15 mm thickness, were glued to the outside of the flasks using a UV cured methacrylate glue (Loctite, Hempstead, UK) and cured for 5 minutes under UV light. To ensure complete sterilisation, flasks were

placed under a UV lamp for 90 minutes and periodically rotated to ensure penetration to all surfaces.

2.5 Optimised Raman Spectroscopy and Sample Preparation

2.5.1 Raman Spectrometer

Raman spectra were acquired using a Renishaw RM series 1000 with attached Leica LMDM microscope (Leica Microsystems, Milton Keynes, UK). Excitation to the sample was provided by a 785 nm diode laser with an output power of 250 mW delivering 66 mW to the sample. Holographic notch filters were used to discard Rayleigh scattered light. Raman scattering was detected by a thermoelectrically cooled CCD camera. The microscope was equipped with a motorised XYZ stage and a camera to visualise samples under transmitted and reflected light. The system was controlled using Renishaw WiRE software and processed in Grams/32 (Thermo Scientific, Waltham, USA).

2.5.2 Raman Spectrometer Calibration

Each day prior to collection of Raman spectra from the cells, the system was calibrated as follows. The absorbance of a neon light was measured for peaks at 10930.5, 13255.5 and 13802.8 all within ±1 any deviations from which were corrected. Secondly, the Raman shift of the laser was measured at 0 cm^{-1}±1 and corrected if necessary. Finally, a spectrum of a silicon wafer was taken which has a known wavenumber shift at 520 cm^{-1} again within a ±1 tolerance and with a minimum intensity value of 60000 arbitrary units.

2.5.3 Sample Preparation and Spectrum Acquisition

Once optimised, as described in Chapter 4, DPSC sample preparation and Raman spectrum acquisition were performed as follows. DPSCs were isolated and expanded as described in sections 2.1 and 2.2 . Quartz customised flasks were prepared as described in section 2.4. Prior to the seeding of DPSCs on the flasks, poly-L-lysine was used to coat the quartz surface to enhance cell adhesion. Flasks were washed

twice with de-ionised water then 100 µL aliquots of poly-L-lysine solution (0.1 mg/mL, molecular weight, 70000-150000) (Sigma-Aldrich, Gillingham, UK) were incubated on the quartz surface for 10 minutes at room temperature. The solution was then aspirated and the flask placed in an incubator at 37°C overnight to dry. It has been shown previously that poly-L-lysine coatings have little/no effect on Raman spectra (140). DPSCs, 1 x 10^5 cells/cm^2, were pipetted directly on to the quartz surface and the flasks were incubated overnight at 37°C to permit cell adherence. The following day, flasks were topped up with fresh osteogenic or adipogenic medium as described in the appropriate sections (5.2.1.1 and 6.2.1.1 respectively). Prior to Raman analysis, the cell culture medium was aspirated and the flasks filled with Hanks balanced salt solution (HBSS) with 0.45% added glucose. Flasks were placed on the microscope stage inverted toward the objective. A 40x/0.8NA water immersion objective was immersed in a small drop of HBSS placed on the quartz surface. Spectra were then acquired for the region 600-1800 cm^{-1} wavenumbers, the number of samples, time points, number of spectra acquired and exposure time are given in the appropriate sections (5.2.1.2 and 6.2.1.2). Cell free areas were used to acquire background spectra. Following analysis the HBSS was aspirated and replaced with osteogenic or adipogenic medium and placed back in the incubator.

2.6 Processing of Raman Spectra

Raman spectra were pre-processed in Grams/32 and further processed and analysed in Matlab version R2013b. A complete description of the process can be found in Appendix A.

Chapter 3
Osteogenic Differentiation of DPSCs Cultured on Various Substrates Appropriate for Raman Spectroscopy

This chapter addresses the first of the project's objectives, the determination of a cell culture substrate that is suitable for Raman spectroscopy but is also compatible with DPSC osteogenic differentiation.

3.1 Introduction

The differentiation of stem cells into specialised cell types is a common theme in regenerative medicine. *In vivo* stem cell fate is tightly controlled through a combination of soluble chemical factors, cell-cell interactions, cell-extracellular matrix interactions and physical/mechanical forces in regions termed the "stem cell niche" (Figure 10) (67-69). *In vitro* differentiation of stem cells can be achieved by mimicking one or more of these parameters, most simply through chemical induction of cell monolayers (52, 55, 141). However, there is growing interest in more closely mimicking the stem cell niche through the guided differentiation of stem cells using rationally designed, highly specific scaffolds (142). Such scaffolds guide differentiation by the presentation of particular chemical motifs and/or by their reaction to mechanical stimuli, their gross architecture, nano-scale topography and charge. Some examples are presented in Table 4. Such studies demonstrate the complex nature of stem cell differentiation and the myriad factors that can enhance or diminish their potential to differentiate into a given lineage.

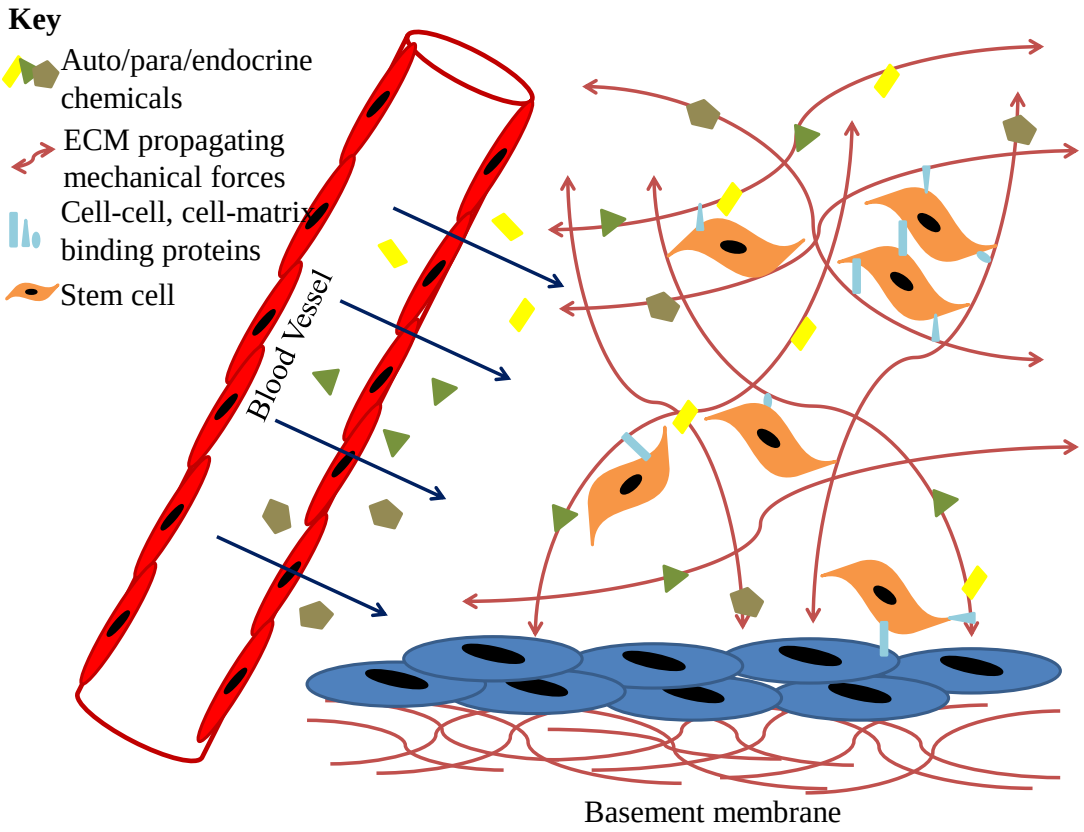

Figure 10. Representation of a generalised stem cell niche depicting the many factors that determine stem cell fate.

One of the most enduring and common methods for culturing and differentiating stem cells involves their growth on treated plastic surfaces as 2D monolayers and traditional methods for phenotyping have stained cells *in situ* or researchers have detached the cells for their further characterisation. Raman spectroscopic analysis of the cultures offers the potential for repeated measurements of the same cell population to characterise cells in 2D culture but the technique brings with it inherent problems. Raman spectroscopy can provide a 'fingerprint' of a sample based on the frequency with which the molecular bonds contained within occur. However, as plastic is created from organic substances it shares many of the molecular bonds in common with a sample of cells and at much higher frequencies, effectively obscuring and confounding the resulting spectra that might be obtained for cells cultured in monolayers on tissue culture plastic. An ideal substrate to use in Raman spectroscopy would therefore be inorganic, possessing minimal Raman shift in the region of interest for the cells, 600-1800 cm^{-1}, termed the "biological fingerprint region" (135). Several studies have used Raman spectroscopy to

interrogate stem cells and have used a range of inorganic materials as substrates to culture their cells on, including, MgF_2 (101, 102), CaF_2 (128), quartz/fused silica (100, 132, 134) and glass (143, 144).

The differentiation of stem cells can be influenced by the properties of a material used as a growth substrate as outlined in Table 4. Osteogenic differentiation of MSCs, from a wide variety of sources, cultured as a monolayer on tissue culture plastic is well characterised (52, 53, 145-148). This process takes up to 28 days and requires supplementation of the cell culture medium with dexamethasone, β-glycerophosphate and ascorbic acid. However, the growth and differentiation of stem cells on Raman appropriate materials such as MgF_2 and quartz is much less well characterised. The surface chemistry of such materials is clearly different to that of tissue culture plastic. In order to encourage cell adhesion to Raman appropriate substrates, such materials are usually coated in various solutions such as poly-L-lysine (128, 135), fibronectin (144) and matrigel (103, 144). Whilst osteogenic differentiation has been demonstrated and assessed by Raman spectroscopy (101, 134) it is unclear whether the results are comparable to more common methods of cell culture or whether the unusual substrates are in any way modifying or influencing cell behaviour.

Table 4. Examples of biomaterials, their properties, and their effects on stem cell differentiation.

Material property	*Description*
Surface chemistry	Silane modified surfaces with -SH or $–NH_2$ functional groups promoted osteogenesis in bone marrow derived MSCs whilst –OH and –COOH groups promoted chondrogenesis (149)
	Fibronectin coated on a $–NH_2$ modified surface promoted osteogenesis and adipogenesis in bone marrow derived MSCs whilst fibronectin coated on a –OH modified surface promoted osteogenesis alone (150)
Macro/micro architecture	Polycaprolactone scaffolds with an average pore size of 370-400 μm promoted chondrogenesis in adipose derived MSCs whilst 90-105 μm pores inhibited chondrogenesis (151)
	Silk fibroin scaffolds with a pore size of 100-300 μm promoted osteogenesis in bone marrow derived MSCs (152)
Nano topography	Polymethylmethacrylate patterned with randomly positioned nanoscale circles promoted osteogenesis in bone marrow derived MSCs whilst an ordered pattern did not (153)
	Titanium with 15 nm pillars enhanced osteogenesis in bone marrow derived MSCs over flat titanium surfaces (154)
Mechanical properties	Polyacrylamide gels of increasing stiffness promoted neurogenesis, myogenesis and osteogenesis in bone marrow derived MSCs (155)
	Poly(ethylene glycol)-diacrylate with an ‘intermediate stiffness’ (55 kPa) combined with 10 μg ml^{-1} fibronectin increased adipose derived MSC osteogenesis (156)

The aim of this study was to assess DPSC osteogenesis on two commonly used Raman appropriate substrates, MgF_2 and quartz, and to compare this to DPSC osteogenesis when cultured on tissue culture plastic.

3.2 Materials and Methods

3.2.1 DPSC Adherence and Proliferation on MgF_2 and Quartz

Prior to the osteo-induction of DPSCs, their adherence to and proliferation on MgF_2 and quartz was assessed and compared with their behaviour on tissue culture plastic. Isolation and expansion of DPSCs was performed as previously described in the general methods (section 2.1). Cryopreserved DPSCs were resurrected in complete cell culture medium and expanded *in vitro* to ~80% confluence. Following this DPSCs were trypsinised and counted as previously described in the general methods (section 2.2). DPSCs were used at passage 3 for this experiment. Discs of magnesium fluoride (MgF_2) and quartz (Qz) (Global Optics, Bournemouth, UK), 14 mm diameter x 0.15 mm thickness, were sterilised in 70% ethanol and preconditioned in basal medium overnight. The preconditioned discs were then placed into a 24 well cell culture plate and seeded with DPSCs (5×10^3 cells/cm^2). DPSCs were seeded into tissue culture well plates at the same density to provide a control. Cell cultures were maintained for 1, 3, 5 and 7 days and the medium replaced once after 3 days. Cell proliferation was quantified at each time point by cell counting as previously described in the general methods (section 2.2). Adherence of the DPSCs on the different substrates was assessed by scanning electron microscopy (SEM). Samples were washed twice in PBS then fixed in 10% neutral buffered formalin (NBF) (Sigma-Aldrich, Gillingham, UK) for two hours at room temperature. Following this, samples were dehydrated in graded alcohols for 30 minutes each at room temperature and allowed to air dry overnight. MgF_2 and Qz discs were placed directly on to aluminium SEM stubs. Tissue culture plastic wells were freed using a hot scalpel and then placed on to SEM stubs. A 4 nm gold coating was applied to samples using an Agar Auto Sputter Coater and the samples imaged using a Hitachi S-3400N SEM.

3.2.2 The Effect of Culturing on MgF_2 and Quartz on DPSC Osteogenesis

Preconditioned MgF_2 and quartz discs were placed into a 24 well cell culture plate, seeded with DPSCs (5×10^4 cells/cm^2) and cultured in basal medium for three days to permit adhesion to their substrates. DPSCs were seeded into tissue culture plates at the same density to provide a control. Then, osteogenic differentiation was

induced by supplementing basal medium with 0.25 mM ascorbic acid, 10 mM β-glycerophosphate and 100 nM dexamethasone (all Sigma-Aldrich, Gillingham, UK) in half of the wells (n=3), the other half remained in basal medium as controls (n=3). Cultures were maintained for 7 and 28 days and the culture medium was replaced twice weekly. At each time point osteogenic differentiation was assessed by Alizarin red staining and quantitative real-time polymerase chain reaction (qRT-PCR) for osteogenic marker genes, type 1 collagen (*COL1A1*), runt related transcription factor 2 (*RUNX2*), alkaline phosphatase (*ALP*), and osteocalcin (*OC*).

3.2.3 Osteogenic Marker Gene Expression of DPSCs Cultured on MgF_2 and Quartz Determined by qRT-PCR

RNA isolation and reverse transcription was performed as previously described in the general methods (section 2.3). qRT-PCR was performed using TaqMan gene expression assays (Applied Biosystems, Carlsbad, USA) for *COL1A1*, *RUNX2*, *ALP* and *OC*: assay numbers Hs00164004-m1, Hs00231692-m1, Hs01029144-m1 and Hs00609452-g1 respectively. Reactions were carried out in 96 well plates as per the manufacturer's instructions on a Roche LightCycler® 480 system. Optimal cDNA concentration was determined as 5 ng/reaction by plotting standard curves with known cDNA concentrations. Data was normalised to *GAPDH* or *YWHAZ* (assay numbers Hs99999905-m1 and Hs00237047_m1), and analysed using the comparative cycle threshold method (ΔCT). *GAPDH* is increasingly thought to be an unreliable housekeeping gene. A study by Ragni *et al* 2013 (157) demonstrated this and suggested *YWHAZ* as an alternative. To investigate this for the present study two patient samples were analysed both in biological triplicate and each with 3 technical repeats for a total n=18 for each time point/substrate. Graphs of the mean ± SE were plotted in Microsoft Excel and statistical significance was determined by a Mann-Whitney test using GraphPad Instat 3 software.

3.2.4 Extracellular Matrix Calcification of DPSCs Cultured on MgF_2 and Quartz Determined by Alizarin Red Staining

For DPSCs following 28 days in culture the cell culture medium was removed and cultures washed twice with PBS. DPSCs were fixed in NBF for 1 hour at room temperature and washed twice in de-ionised water. A 1% Alizarin red solution

(Sigma-Aldrich, Gillingham, UK) was prepared, adjusted to pH 4.2, and incubated on DPSCs for 20 minutes at room temperature. The Alizarin red solution was then removed and excess stain washed away with repeated washes with de-ionised water. DPSCs were then imaged using an Olympus BX50 microscope with accompanying Nikon DS-Fi1 camera.

3.2.5 Determination of F^- in Cell Culture Medium using Energy Dispersive X-ray Spectroscopy (EDX)

Samples of cell culture medium from day 7 and 28 cell cultures were analysed using EDX to detect the presence of fluoride ions. Samples were loaded on to the cool stage (set to -15°C) of a Hitachi S-3400N scanning electron microscope. EDX acquisition time was set to 60 seconds and the atomic percentage of fluoride recorded. Known concentrations of NaF dissolved in de-ionised water were used to plot a standard curve. Sample fluoride concentration was derived from this and converted to parts per million.

3.3 Results

Tissue culture plastic is an unsuitable cell culture substrate for Raman spectroscopy applications due to its strong Raman signal. Quartz and MgF_2 are both routinely used in Raman spectroscopy and therefore their suitability for DPSC culture was compared with tissue culture plastic.

3.3.1 The Effect of Substrate Choice on Adherence and Proliferation of DPSCs

DPSCs successfully adhered to all three substrates after 1 day assuming a characteristic flattened morphology and had proliferated to confluence within 5 days (Figure 11).

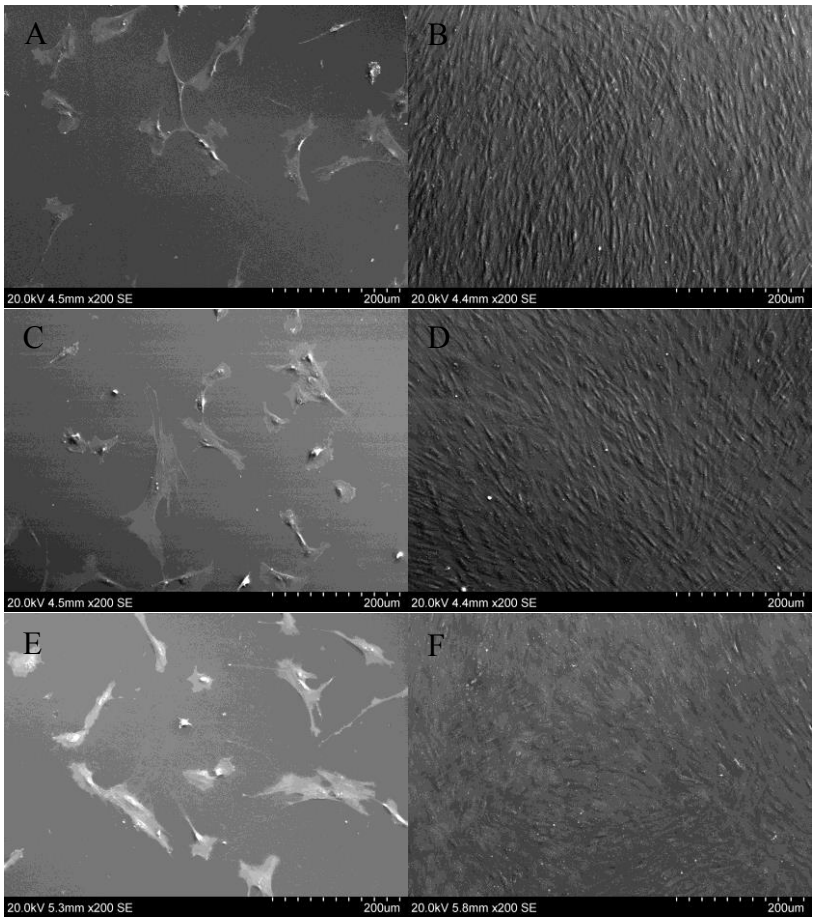

Figure 11. Scanning electron micrographs of DPSCs cultured on (A-B) MgF_2, (C-D) quartz and (E-F) tissue culture plastic after 1 (A, C, E) and 5 (B, D, F) days. No discernible differences were observed between substrates at either time point. Scale bars = 200 µm.

Proliferation of DPSCs on all three substrates was similar over the course of 7 days and no significant differences in cell numbers were observed (Figure 12). Negligible dead cells were recorded on all three substrates. Population doubling times were 41.6 hours on MgF_2, 36.8 hours on quartz and 36.1 hours on tissue culture plastic.

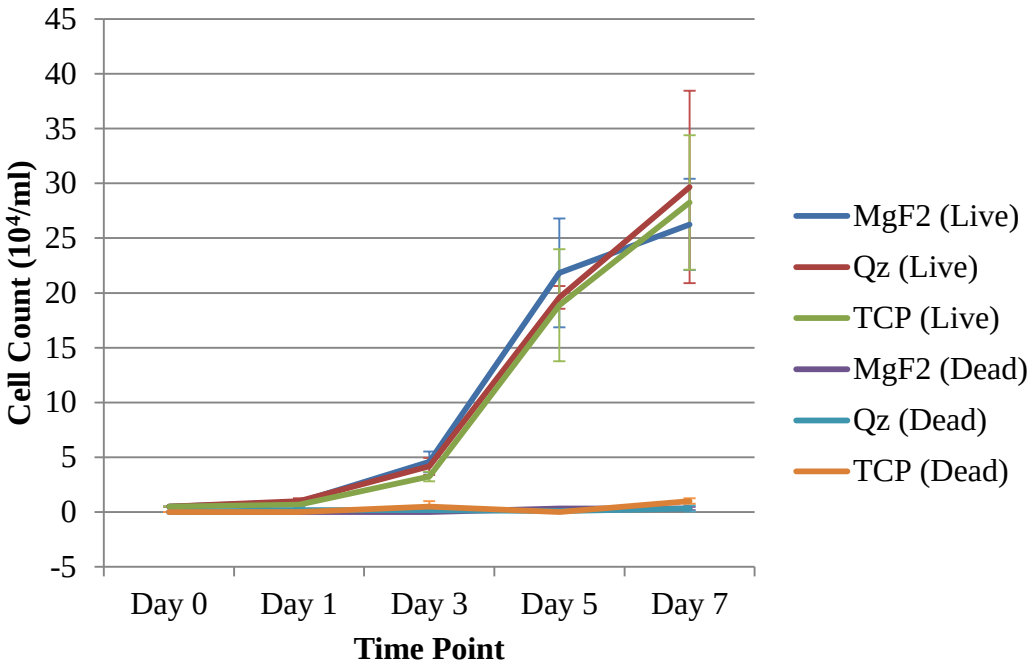

Figure 12. Line graph charting DPSC proliferation over 7 days for cells cultured on MgF_2, quartz (QZ) and tissue culture plastic (TCP). The values represent mean ± SD. No significant differences in the numbers of live or dead cells were observed between cells cultured on each substrate at any time point.

3.3.3 The Effect of Substrate Choice on the Expression of Osteogenic Marker Genes

Prior to the commencement of qRT-PCR, probe efficacy and optimal cDNA concentration were determined by plotting standard curves of known cDNA concentration for each probe (Figure 13).

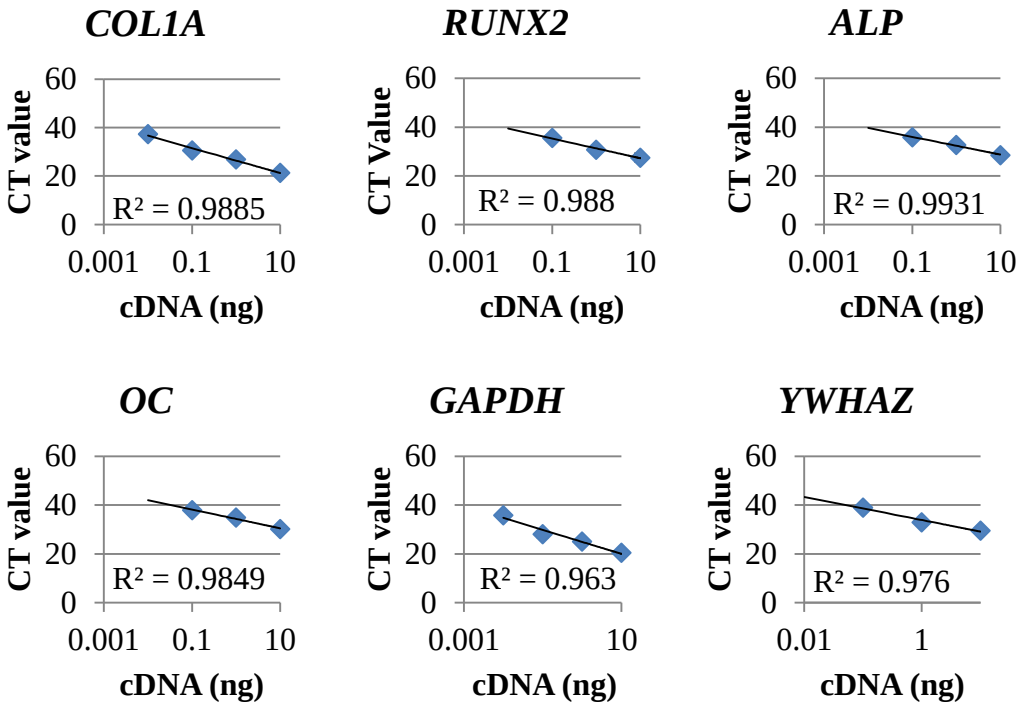

Figure 13. Standard curves using known concentrations of cDNA from naïve DPSCs and probes for the four osteogenic marker genes: type 1 collagen (*COL1A*), runt related transcription factor 2 (*RUNX2*), alkaline phosphatase (*ALP*) and osteocalcin (*OC*) and the housekeeping genes glyceraldehyde-3-phosphate dehydrogenase (*GAPDH*) and tyrosine 3-monooxygenase/tryptophan 5-monooxygenase (*YWHAZ*).

Probe efficacy for all genes of interest was good as demonstrated by R^2 values nearing 1. Optimal cDNA concentration was determined to be 5 ng/reaction yielding a mid-range CT value ~20-25 which would permit increases or decreases in gene expression to be detected throughout the experiment.

Housing keeping genes are used to normalise the expression of target genes in qRT-PCR analysis. For this to be meaningful the expression of the house keeping gene should vary little throughout an experiment. Figure 14 shows the expression of *GAPDH* and Figure 15, *YWHAZ* by DPSCs cultured on all three substrates over the course of 28 days of osteogenic induction.

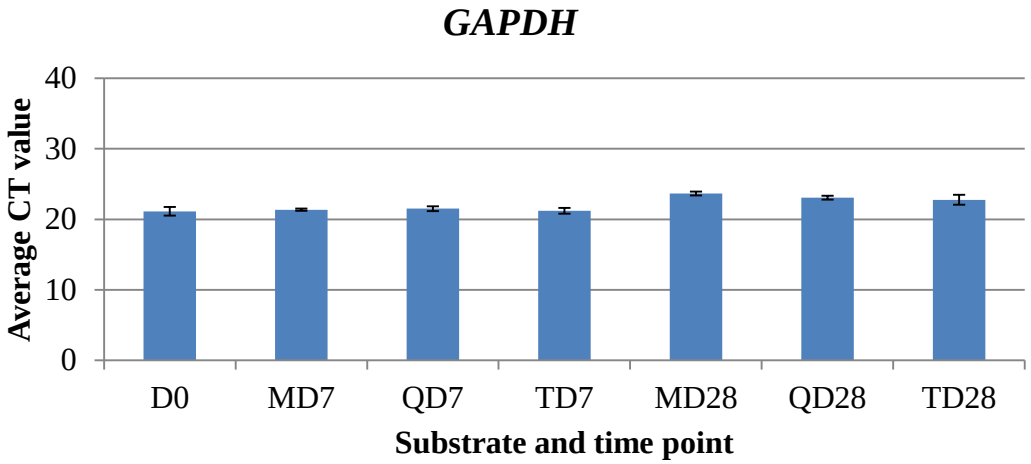

Figure 14. CT value of *GAPDH*, derived from 3 biological replicates each with 3 technical replicates, from DPSCs cultured on MgF_2 (M), quartz (Q) and tissue culture plastic (T) over 28 days of osteo-induction. Results show mean ± SD. $p<0.01$ for QD28 vs D0, MD7, QD7, TD7 and QD28, $p<0.001$ for TD28 vs D0, MD7, QD7, TD7 and MD28.

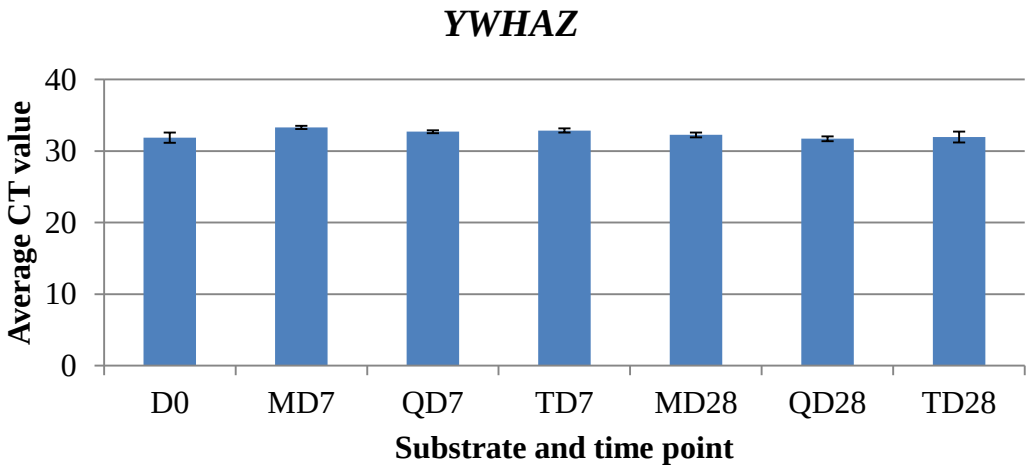

Figure 15. CT value of *YWHAZ*, derived from 3 biological replicates each with 3 technical replicates, from DPSCs cultured on MgF_2 (M), quartz (Q) and tissue culture plastic (T) over 28 days of osteo-induction. Results show mean ± SD. $p<0.05$ for QD7 vs D0 and TD28, $p<0.01$ for D0 vs TD7, MD7 vs MD28 and QD7 vs QD28, $p<0.001$ for MD7 vs D0, QD28 and TD28 and TD7 vs QD28.

Statistically significant variation can be observed in the expression of both housekeeping genes using a one-way ANOVA with Bonferroni post-test. For *GAPDH*: $p<0.01$ for QD28 vs D0, MD7, QD7, TD7 and QD28, $p<0.001$ for TD28 vs D0, MD7, QD7, TD7 and MD28. For *YWHAZ*: $p<0.05$ for QD7 vs D0 and TD28, $p<0.01$ for D0 vs TD7, MD7 vs MD28 and QD7 vs QD28, $p<0.001$ for MD7 vs D0, QD28 and TD28 and TD7 vs QD28. However, whilst expressed at lower levels than *GAPDH*, the expression of *YWHAZ* was the more consistent of the two and therefore was used to normalise all subsequent data.

qRT-PCR was used to determine the expression of osteogenic markers at early (day 7), and late (day 28), stages of cell culture, (Figure 16). At day 7, the only significant difference between cells cultured on the two Raman-appropriate substrates and those cultured on tissue culture plastic was a higher level of *RUNX2* expression for DPSCs cultured on quartz, ($p=0.0083$). At day 28, there was highly significant lower expression for *COL1A* and *OC* in DPSCs cultured on MgF_2, ($p<0.0001$). There were also significantly lower levels of *COL1A*, *RUNX2*, *ALP* and *OC* expression in DPSCs cultured on quartz, ($p=0.0191$, $p=0.0401$, $p=0.0011$ and $p=0.0367$ respectively).

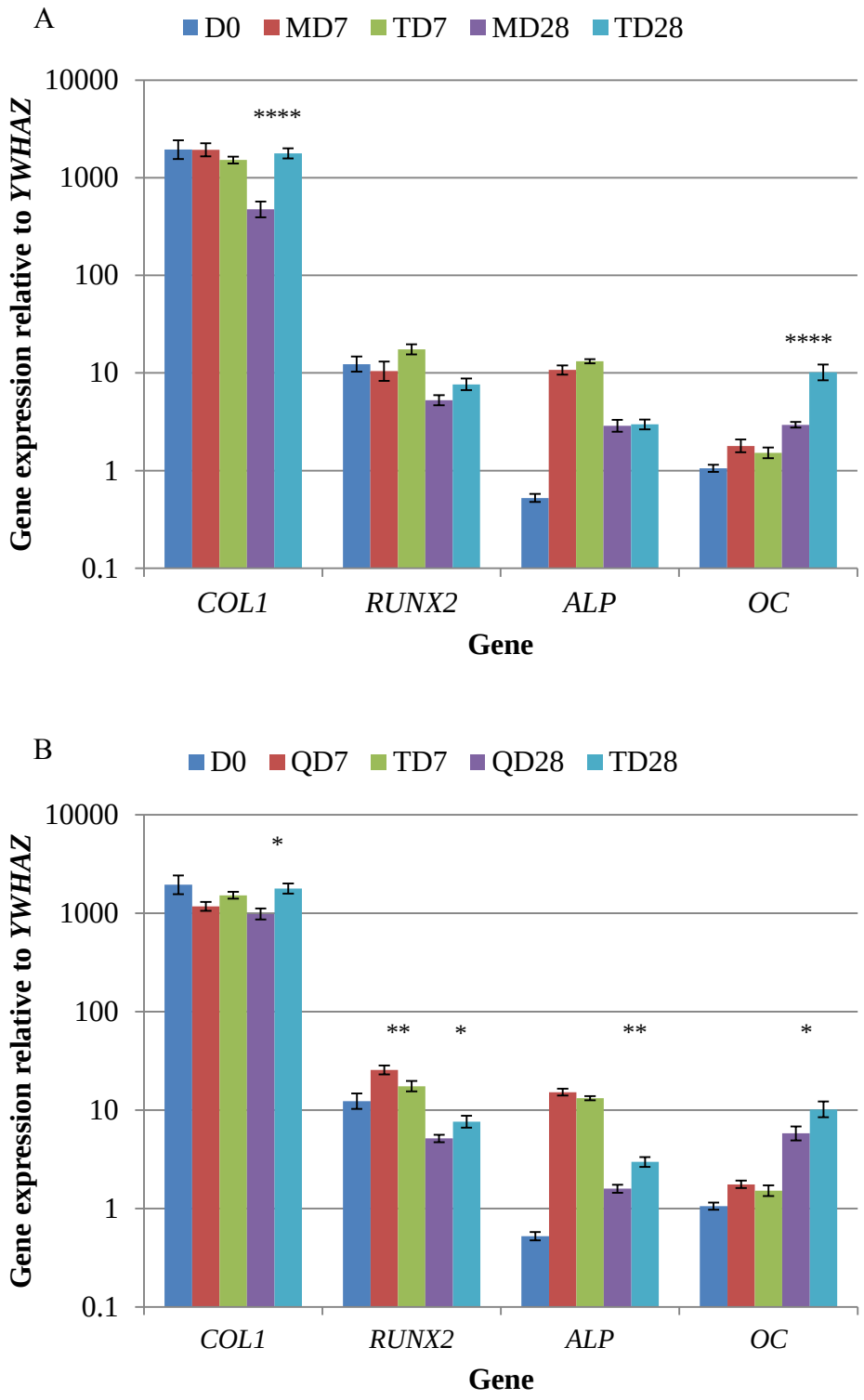

Figure 16. A comparison of DPSC osteogenic gene expression after 7 and 28 days of induction after culturing on A) MgF_2 (M) and tissue culture plastic (T) and B) quartz (Q) and tissue culture plastic (T). Statistical significance only displayed for direct comparisons, i.e. expression levels at the same time points on different substrates, *, p<0.05, **, p<0.01, ****, p<0.0001. Results show mean ± SE, n=18. The expression of early osteogenic markers at day 7 is broadly similar between substrates but the expression of late markers at day 28 is much lower on MgF_2.

3.3.4 DPSC Extracellular Matrix Calcification as Determined by Alizarin Red Staining

Alizarin red staining was used to indicate extracellular matrix calcification after 28 days of osteogenic induction (Figure 17). Uniform positive staining was observed for DPSCs cultured on quartz and tissue culture plastic but not for those cultured on MgF_2.

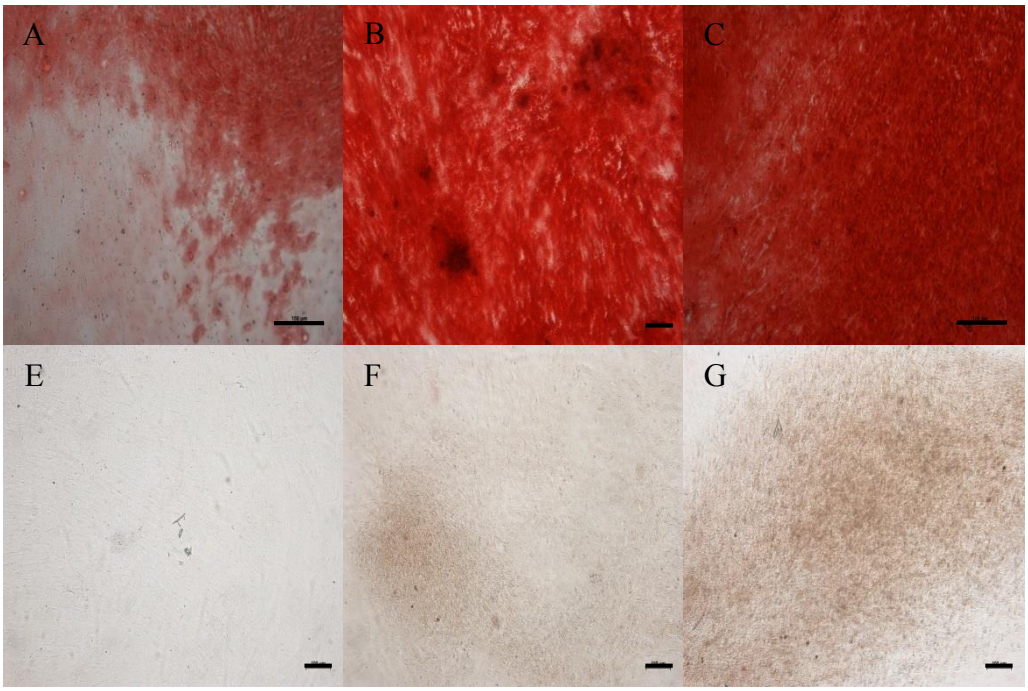

Figure 17. Alizarin red staining of DPSCs cultured on (A) MgF_2, (B) quartz and (C) tissue culture plastic after 28 days of osteogenic induction. Below (E-G) respective controls with no osteo-induction. Scale bars = 100 µm. Alizarin red staining whilst positive for DPSCs cultured on MgF_2 was weaker than those cultured on quartz and tissue culture plastic.

3.3.5 Fluoride Ion Levels in Cell Culture Medium Detected by Energy Dispersive X-ray Spectroscopy

EDX was used to determine the presence of F^- in the cell culture medium of DPSCs cultured on MgF_2 as a possible cause for the observed lack of late stage osteogenic differentiation in these cultures (Figure 18). The presence of Mg^{++} was not investigated as cells will naturally absorb Mg^{++} from culture medium. There was no significant difference found in F^- levels in cultures ± MgF_2 discs at both 7 and 28 days. F^- concentrations were consistent at approximately 1 ppm.

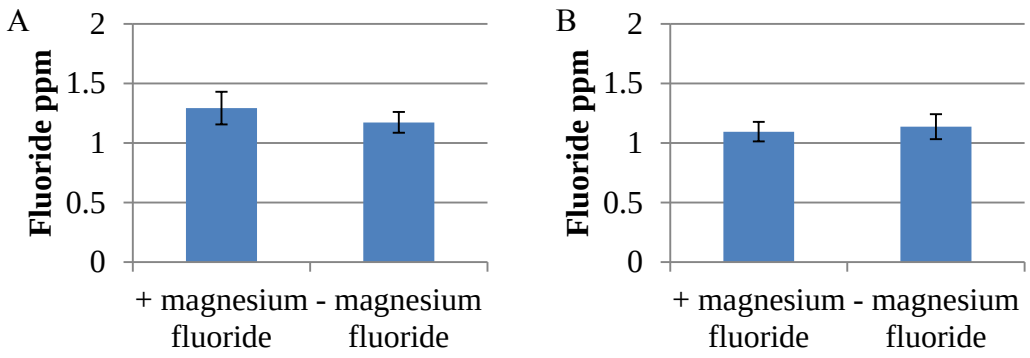

Figure 18. Fluoride concentration in cell culture medium samples with and without magnesium fluoride discs at (A) day 7 and (B) day 28 as determined by EDX. Results show mean ± SD, n=6. No significant differences were observed.

3.4 Discussion

Prior to the commencement of studies attempting to utilise Raman spectroscopy to predict/characterise stem cell differentiation, it was essential to determine whether potential Raman appropriate cell culture substrates had any effect on the osteogenic differentiation of DPSCs. MgF_2 and quartz were chosen as the Raman appropriate substrates, being two of the more commonly used substrates for such applications (100-102, 132, 134). Osteogenic differentiation of DPSCs on the two substrates was assessed by the expression of four markers genes, *COL1A, RUNX2, ALP,* and *OC,* at early and late stages of differentiation and by Alizarin red staining. The data was then compared with DPSCs cultured on tissue culture plastic under the same conditions.

Differentiation of DPSCs on all three substrates was confirmed by a significant increase in the expression of the early marker genes *RUNX2* and *ALP* after 7 days of induction relative to undifferentiated DPSCs, followed by a decrease in their expression after 28 days of induction. Further, DPSCs cultured on all three substrates exhibited a significant increase in the expression of the late marker *OC* after 28 days of induction. This is a gene expression profile that is typical for the osteogenic differentiation of DPSCs, and MSCs more generally, and is consistent with the findings of many authors reported previously (141, 158-162). Alizarin red staining demonstrates the presence of calcium and as such can be used as a marker of extracellular matrix calcification (163). Positive Alizarin red staining after 28 days of osteogenic induction was observed for DPSCs cultured on all three substrates. When combined with the gene expression analysis this indicates the differentiation of DPSCs towards a mature osteoblast-like phenotype over the course of the experiment. However, the aim of this study was not to demonstrate the osteogenic differentiation of DPSCs on MgF_2 and quartz but to ascertain if differentiation on these substrates was comparable with the more common format on tissue culture plastic.

Lower expression levels of osteogenic marker genes by DPSCs on both MgF_2 and quartz suggested weaker/delayed osteogenic differentiation compared with DPSCs

cultured on tissue culture plastic. However, of the two substrates MgF_2 was associated with the most significant reduction in gene expression. DPSCs cultured on MgF_2 demonstrated significantly lower expression levels of the late differentiation marker *OC*, indicating weaker progression of osteogenic differentiation. This was further confirmed by weaker Alizarin red staining indicating lower degrees of extracellular matrix calcification. Fluoride is known to be toxic to cells at millimolar concentrations (164) impairing mitochondrial function leading to ATP depletion (165). Magnesium ion, Mg^{2+}, is known to compete with Ca^{2+} for protein binding sites potentially impairing cellular functions (166) and may also inhibit osteogenic differentiation (167). EDX was therefore used to determine if higher F^- concentrations were present in the cell culture medium of DPSCs cultured on MgF_2 as a potential explanation for the weaker osteogenic differentiation. Mg^{2+} levels were not checked as cells naturally deplete Mg^{2+} from culture medium. However, there was no significant increase in F^- detected at either early or late time points of the culture period. This is consistent with the findings of Notinger *et al* 2004 (102) who also concluded, indirectly through a MTT metabolic assay, that there was negligible F^- release from MgF_2 discs. Therefore a different factor such as surface chemistry or nano-topography must be the cause of the weaker osteogenic differentiation on both MgF_2 and quartz.

There is little published data regarding the surface chemistry and nano-topography of MgF_2, however, more data is available regarding quartz. A study by Weder *et al* 2010 (168) demonstrated that fibroblasts adhered most strongly to flat quartz surfaces compared with quartz with nanopillars. However, when quartz nanopillars were functionalised with streptavidin they increased cell spreading and proliferation (169). In this study, flat, polished quartz surfaces were used and no differences in the adhesion or proliferation of DPSCs was found when compared with DPSCs cultured on tissue culture plastic, however, without further experimentation nano-topography cannot be ruled out as influencing DPSC differentiation. Koehler *et al* 2013 (170) demonstrated that various proteins adsorbed to quartz to varying degrees dependent upon the pH of their solution. The authors attributed this to differences in the electrostatic potential of pure SiO_2 (quartz) and of their proteins under various pH values. Fears *et al* 2013 (171) have shown that certain proteins undergo conformational changes when adsorbed to quartz. Again this was attributed to the

interplay of electrostatic charge between substrate and protein. As previously discussed, stem cell differentiation is known to be guided by the presence of particular proteins presented in the correct conformation, such as might be found in their extracellular matrix. These studies suggest that the potential for such proteins to be absent or changed by their interaction with quartz or possibly MgF_2 may result in the weaker osteogenic differentiation of DPSCs cultured on these surfaces. However, further work would be required to test this hypothesis. Although DPSCs exhibited weaker osteogenic differentiation on both MgF_2 and quartz, the effects were less dramatic with quartz and as a result quartz was chosen as the cell culture substrate for all future experiments. This was a conclusion also reached by Draux *et al* 2009 (172) when comparing the morphology and proliferation of cancer cells cultured on quartz, calcium fluoride and zinc selenide.

Chapter 4
Development of a Method for the Phenotypic Characterisation of DPSCs by Raman Spectroscopy Under Sterile Conditions

Previous studies investigating the use of Raman spectroscopy in the characterisation of cells have used either fixed cells or live cells in a non-sterile environment. The aim of this study was to develop a method to permit the repeated acquisition of Raman spectra from live cells under aseptic conditions with time. This is a pre-requisite if Raman spectroscopy is to be used in an entirely non-invasive and non-destructive manner.

4.1 Introduction

Raman spectroscopy as a technique shows promise both as a research tool and in clinical diagnostics as it has the capacity to be entirely non-invasive (93, 110, 173). It achieves this by exploiting a natural phenomenon in the interaction between light and matter, namely the Raman effect, and as such does not require the use of any exogenous labels. Upon interaction with a molecule, a small number of photons from a monochromatic light source (light of a single wavelength) will undergo a transfer of energy resulting in a small shift in their wavelength relative to the incident light (Figure 19). The Raman shift can be defined as the amount of energy transferred that is required to bring about a change in the vibrational motion of the interacting molecule. This transfer of energy is different and unique for every molecular species/bond. Therefore a sum of all the various shifts in wavelength, expressed in wavenumbers, and the frequency with which they occur provides a biochemical fingerprint of a sample. Raman spectroscopy can be performed with a wide variety of wavelengths of light from ultra violet (UV) to infra-red and with a wide range of power. Typically high powered lasers using shorter wavelengths in the UV region increase the efficiency of Raman scattering and therefore the quality of the resulting spectra (174). However, in the interrogation of living biological samples a compromise must be made as UV light can damage DNA and the heat generated by high powered lasers could induce a heat shock response (106, 175).

Many previous studies have used a 785 nm (near infra-red) light source and it has been shown that 115 mW laser power applied to a live sample for 40 minutes does not cause damage to the sample (135).

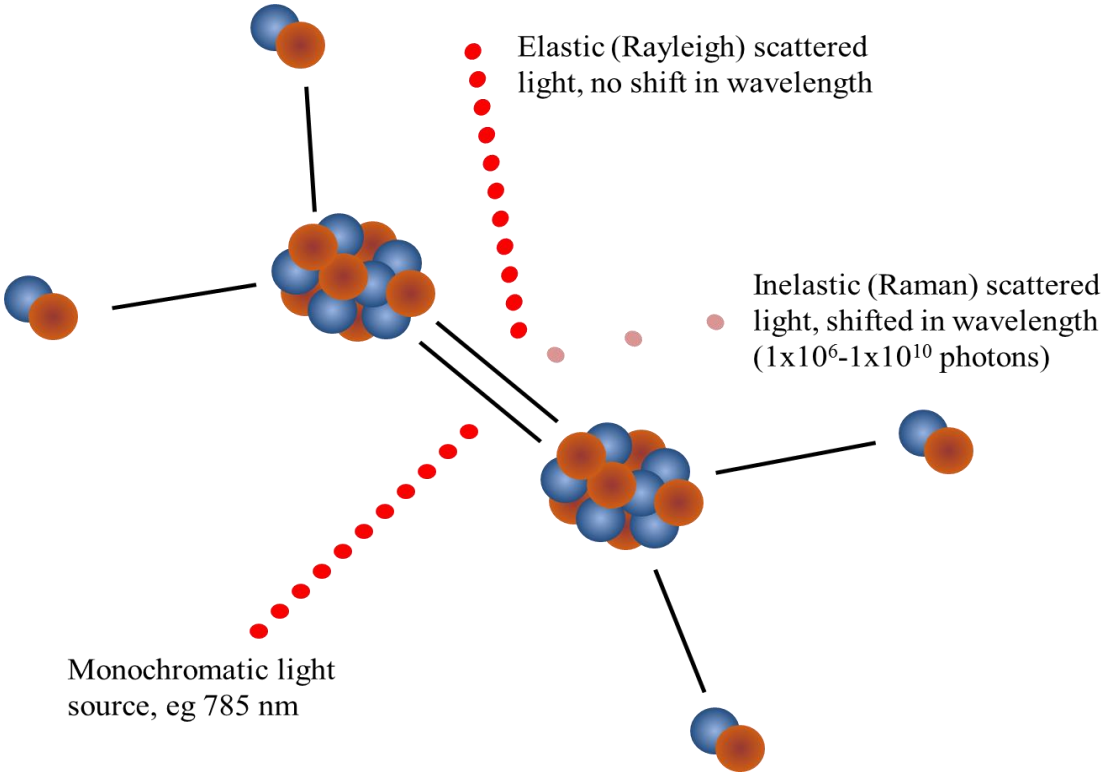

Figure 19. Diagram of light interaction with ethylene, illustrating Raman scattering.

Perhaps the simplest and most efficient method to analyse cells using Raman spectroscopy is to fix them prior to analysis. The primary goal of fixation is to preserve a sample in as close to a physiological state as possible. In order to achieve this metabolism has to be arrested to prevent autolytic degradation and cellular organelles and molecules must be immobilised in order to stabilise the sample for further examination (176). There are many techniques available for cellular and tissue fixation including chemical, such as aldehydes or alcohols and temperature both heating or freezing. All have their advantages and disadvantages and the choice of fixation method is generally determined by the data the investigator wishes to obtain from a given sample. Listed in Table 5 are some of the known issues with various fixation methods.

Table 5. Various fixation methods and some of the known artefacts they can induce

Fixation method	Known issues
Aldehydes	Crosslinking of protein amino acid residues by methylene bridges (177, 178)
	Molecular changes in nucleic acids, carbohydrates and phospholipids (178-180)
Alcohols	Antigen loss through protein coagulation (178, 181)
Heating	Protein coagulation, nucleic acid breakdown and leakage of low molecular weight proteins (140)

Despite the artefacts fixing a sample can introduce there have been studies investigating fixed cells with Raman spectroscopy. In two recent studies Ali *et al* 2013 (182, 183) found Raman spectroscopy coupled with *K*-means cluster analysis was able to differentiate between the different layers in formalin fixed, paraffin embedded and de-waxed skin samples. However, Raman bands indicative of lipids were significantly perturbed compared with non-fixed samples. Meade *et al* 2010 (184) investigated the effect of two chemical fixatives, formalin and Carnoy's fixative, on various cell lines using Raman spectroscopy coupled with principal component analysis (PCA). Whilst it was reported that formalin was the better fixative when spectra were compared with those from live cells, neither were an adequate match with nucleic acid degradation, protein denaturation and lipid leeching all observed in the spectra. When comparing the effect of ethanol, formaldehyde and heat fixation on spectra acquired from *Rhodobacter sphaeroides*, Kniggendorf *et al* 2011 (140) reported similarly poor spectra when compared with non-fixed samples. Regardless of the merits and issues with sample fixation it is clear that a study whose aim is to repeatedly measure spectra from live cells cannot use any form of cell fixation.

Many more studies have used Raman spectroscopy to investigate live cells. One approach is to suspend the cell sample prior to analysis (185-187) negating the need to culture the sample on substrates appropriate for Raman spectroscopy but rarely used in cell culture. This approach may also have clear uses as demonstrated by

Pascut *et al* 2011 (185). If the cells are passed though the laser beam and a spectrum can be acquired fast enough (~5 seconds) this opens up the possibility for Raman cell sorting analogous to fluorescence-activated cell sorting (FACS) or it could permit the discrimination of differing cell types in a heterogeneous cell sample. However, such an approach when monitoring the course of stem cell differentiation would probably be detrimental as regular disruption of the sample and the associated extracellular matrix would likely inhibit differentiation given that the deposited matrix helps guide the process (67-69). Several others have used Raman spectroscopy to investigate adherent cell samples (101, 132, 134). However, these studies were investigating specific differentiation events, such as extracellular matrix calcification, so neither the maintenance of sterility or repeated measurements were required.

The aim of this study was to develop a method that would permit the long term aseptic culture of DPSCs whilst at the same time allowing the acquisition of high quality reproducible Raman spectra.

4.2 Materials and Methods

4.2.1 Quantifying the Metabolic Activity of DPSCs Immersed in Various Solutions using an Alamar Blue Assay

Quartz disc preparation and DPSC culture was performed as previously described in section 3.2.1. DPSCs were seeded at a density of 5 x 10^4/cm^2 in 24 well plates and allowed to proliferate to confluence. At this point DPSCs were washed twice with PBS and then incubated with 1 mL of either PBS, HBSS (Invitrogen, Paisley, UK) with 0.1% or 0.45% added glucose (described as "low" and "high" concentrations respectively by Invitrogen cell culture medium formulations), Hibernate® medium (Invitrogen, Paisley, UK) or α-MEM. Hibernate® medium is designed for the storage and transport of live cells in ambient conditions. Into triplicate wells containing DPSCs, 100 µL Alamar Blue reagent (Sigma-Aldrich, Gillingham, UK) was added. Wells without cells were used as controls. Assays were incubated at ambient temperature for four hours to simulate the conditions of Raman spectra acquisition. Absorbance at 570 nm and 600 nm was measured using a Thermo Scientific Varioskan Flash Multimode Reader every 30 minutes. The percentage of the Alamar Blue dye that had been reduced was calculated at each time point with the following equation (Figure 20):

$$\% \text{ Reduction} = ((\varepsilon_{ox}\lambda_2 * A\lambda_1) - (\varepsilon_{ox}\lambda_1 * A\lambda_2)/(\varepsilon_{red}\lambda 1 * A'\lambda_2) - (\varepsilon_{red}\lambda_2 * A'\lambda_1)) * 100$$

Figure 20. Calculation for the % reduction of Alamar Blue dye. $\varepsilon\lambda_1$ and $\varepsilon\lambda_2$ are constants representing the molar extinction coefficient of Alamar Blue at 570 and 600 nm, respectively, in the oxidised (ε_{ox}) and reduced (ε_{red}) forms. $A\lambda_1$ and $A\lambda_2$ represent the absorbance of the test wells at 570 and 600 nm respectively, $A'\lambda_1$ and $A'\lambda_2$ represent their negative controls. Adapted from (188)

4.2.2 Cell Culture

4.2.2.1 Culture of DPSCs in Petri Dishes for Raman Spectroscopy

DPSCs were cultured on quartz discs as previously described in section 3.2.1. When confluent the DPSCs were transferred to a sterile petri dish containing a quartz platform. HBSS was added until the DPSCs were covered and the lid replaced (Figure 21). The Raman spectrometer was calibrated as previously described in the

general methods (section 2.5.2). A 785 nm diode laser with an output power of 250 mW, delivering 66 mW power to the sample, provided excitation. A 50x/0.75NA dry objective was used to visualise the DPSCs and collect spectra. Raman refracted light was collected back through the objective and passed through a 40 µm slit into the spectrometer. Ten spectra were acquired with a 60 second integration time over the wavenumber range 600-1800 cm^{-1}. A cell-free replica was used to determine the background. Spectra were pre-processed as described on Appendix A and graphs drawn in Microsoft Excel.

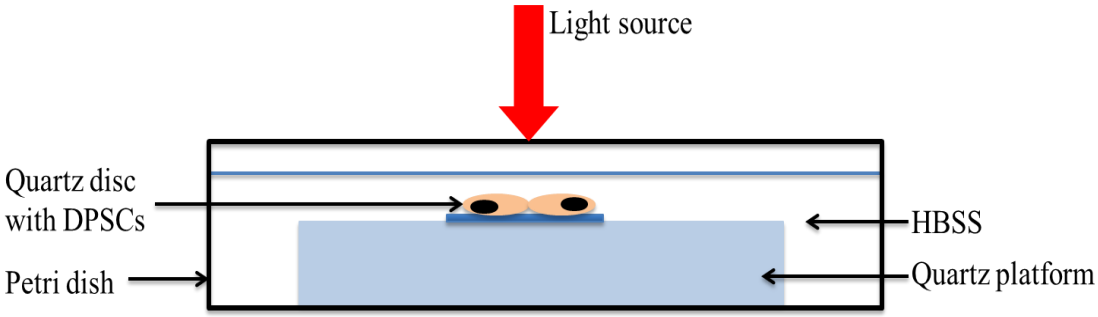

Figure 21. Diagrammatic representation of Raman spectroscopy using a petri dish.

4.2.2.2 Culture of DPSCs in Quartz Cuvettes for Raman Spectroscopy

DPSCs were cultured as previously described in the general methods (section 2.2). A Raman grade quartz cuvette with 1 mm thick walls and screw top (Sigma-Aldrich, Gillingham, UK) was sterilised in ethanol and left in cell culture medium overnight. The following day one side of the cuvette was seeded with 5 x 10^4 DPSCs/cm^2 and cultured to confluence (Figure 22). Prior to analysis, the cell culture medium was aspirated and cuvettes filled with HBSS with 0.45% added glucose. The Raman spectrometer was calibrated and set up as previously described in the general methods, with one exception, a 5x microscope objective was used. This was because as the thickness of a material increases high numerical aperture objectives suffer from increasing spherical aberration and thus reduced collection efficiency of the Raman refracted light (189). Ten spectra were acquired with a 60 second integration time and one of the other quartz walls used to acquire the cell free background. Spectra were pre-processed as described in Appendix A and graphs drawn in Microsoft Excel.

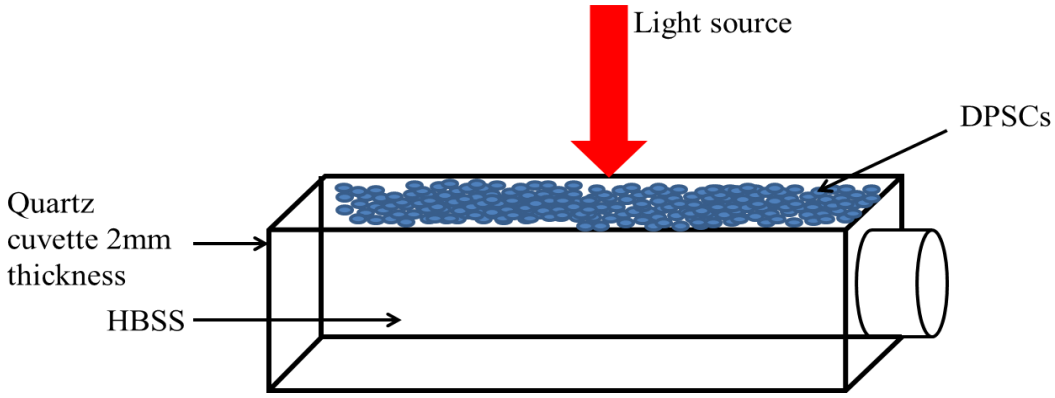

Figure 22. Diagrammatic representation of Raman spectroscopy using a quartz cuvette.

4.2.2.3 Culture of DPSCs in Quartz Customised Cell Culture Flasks for Raman Spectroscopy

DPSCs were prepared and quartz customised cell culture flasks (Figure 23) produced as previously described in the general methods, sections 2.2 and 2.4. Quartz windows were coated in 0.01% poly-L-lysine (molecular weight 70,000-150,000) solution and DPSCs seeded at 4 x 10^5/cm^2. Prior to Raman analysis, cell culture medium was aspirated and flasks filled with HBSS containing 0.45% added glucose. The Raman spectrometer was calibrated and set up as previously described (section 2.5.2) and the 50x/0.75NA objective attached. Ten spectra were acquired with a 60 second integration time and a cell free flask used to acquire background. Spectra were pre-processed as described in Appendix A and graphs drawn in Microsoft Excel.

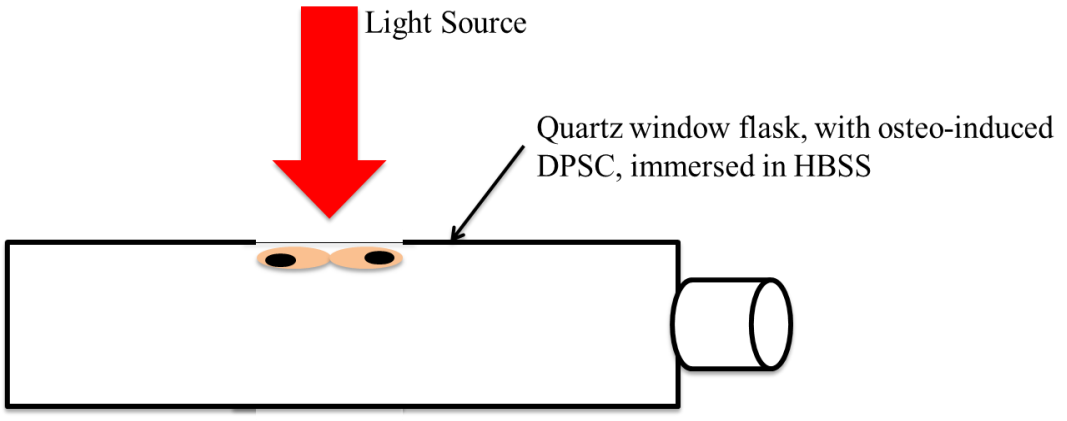

Figure 23. Diagrammatic representation of Raman spectroscopy using a quartz window modified cell culture flask.

4.2.3 Optimisation of Optics for Raman Spectroscopy

DPSC culture in quartz customised flasks and the calibration and set up of the Raman spectrometer were performed as previously described in the general methods, sections 2.4 and 2.5 (Figure 24). It has previously been shown that the quality of images acquired through coverslips using a laser confocal system can be improved by the use of water immersion lenses (190). The Raman spectrometer also employs a confocal system so several water immersion objectives were tested to investigate if the quality of the spectra acquired could be further improved. A range of objectives were selected, 20x/0.95NA, 40x/0.8NA, 63x/0.9NA and 63x/1.2NA. Lower magnifications generate a larger spot size and therefore sample a greater number of cells, whilst higher numerical apertures possess a greater Raman collection efficiency through a thin substrate. The effect of Raman acquisition time was also investigated within the confines of the cells being in ambient conditions for no more than 4 hours. Fifty spectra were acquired with a 30 second integration time and compared with the acquisition of 15 spectra with a 120 second integration time. In each instance the signal:noise was calculated as the peak intensity of phenylalanine at 997 cm^{-1} divided by the standard deviation of all the intensity values in the range of 1700-40 cm^{-1}, which was designated as noise due to the absence of any Raman peaks produced by the sample. All spectra were processed and graphs plotted as described in Appendix A.

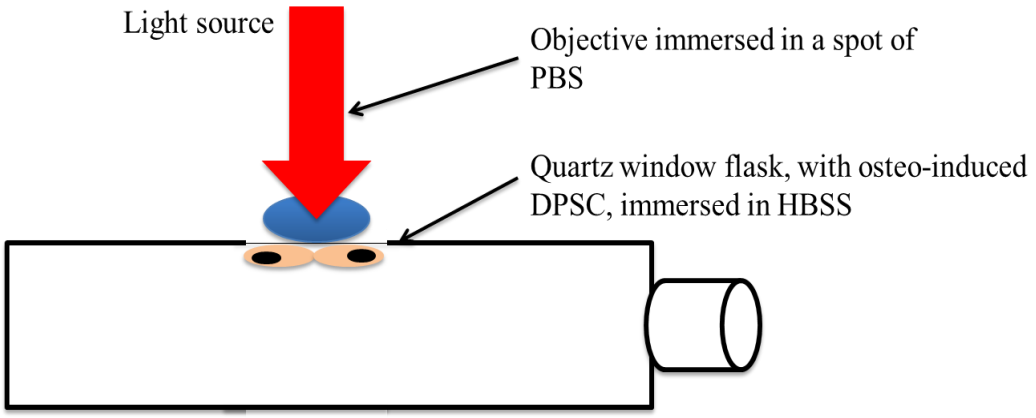

Figure 24. Diagrammatic representation of Raman spectroscopy using a quartz window modified cell culture flask and a water immersion objective.

4.3 Results

4.3.1 Metabolic Activity of DPSCs in Solutions Appropriate for Raman Spectroscopy

An ideal solution in which to immerse cells for Raman spectroscopy would have a minimal number of constituents and be chemically well defined so as to possess little background signal. However, optimal maintenance of living cells generally requires complex solutions. An Alamar Blue assay was performed on DPSCs immersed in various solutions to ascertain the best compromise. The percentage of the Alamar Blue dye reduced by DPSCs was calculated over the course of 4 hours at regular 30 minute intervals (Figure 25). As one might expect DPSCs in the more chemically complex solutions reduced a greater amount of the Alamar Blue indicating that they were more metabolically active. However, the lower R^2 value from the DPSCs in α-MEM indicated that their metabolism began to slow after ~3 hours. The 3 test solutions (HBSS with 0.1% or 0.45% glucose and Hibernate®) all maintained cells such that a steady rate of Alamar Blue reduction was observed over the 4 hour period. The HBSS with 0.45% added glucose was selected for future experiments, as it is better chemically defined than Hibernate® medium whilst still being able to maintain DPSC metabolic activity in ambient conditions.

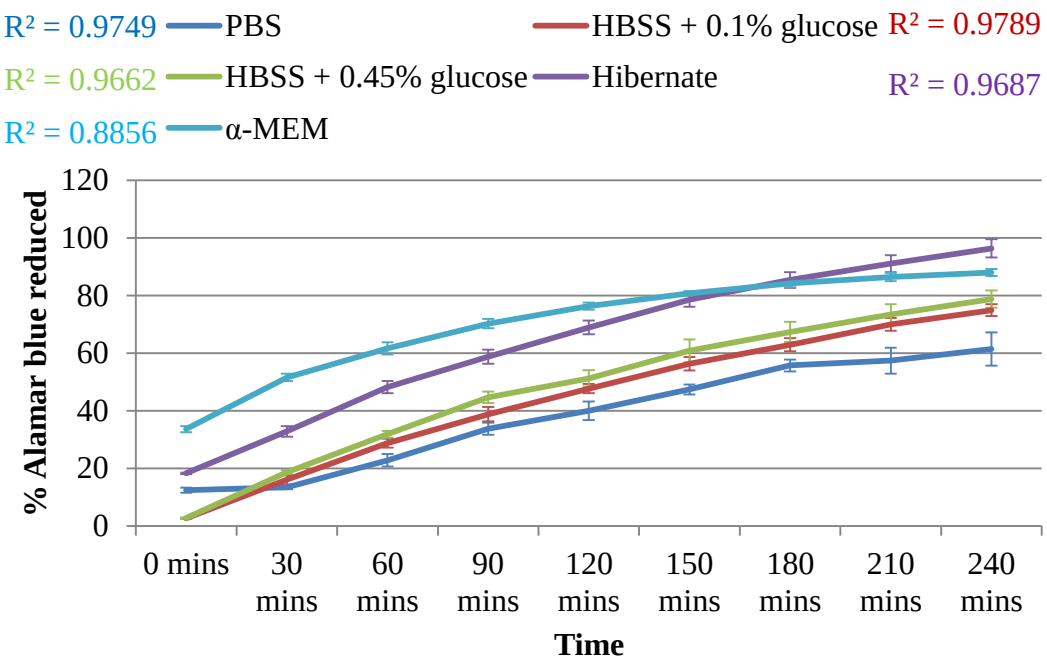

Figure 25. Alamar Blue reduction by DPSCs in various solutions. R^2 values displayed indicate linearity. DPSCs reduced Alamar Blue in a linear fashion over four hours. DPSCs in the more complex solutions (α-MEM and Hibernate) reduced more Alamar Blue than those in simpler solutions (HBSS and PBS)

4.3.2 Raman Spectroscopy of DPSCs in Different Sterile Cell Culture Conditions

4.3.2.1 Raman Spectroscopy of DPSCs Cultured in Petri Dishes

The first cell culture method investigated was to culture DPSCs on quartz discs, performing Raman spectroscopy within a closed petri dish in order to maintain sterility. Figure 26c shows a spectrum acquired from DPSCs minus the background. Several peaks were evident, including, 999 cm^{-1}, 1027 cm^{-1} and 1599 cm^{-1}. However, these peaks are likely to have been contributed by the polystyrene from the petri dish (Figure 27). This method was therefore discounted due to the potential for the Raman signal from the petri dish to obscure the result.

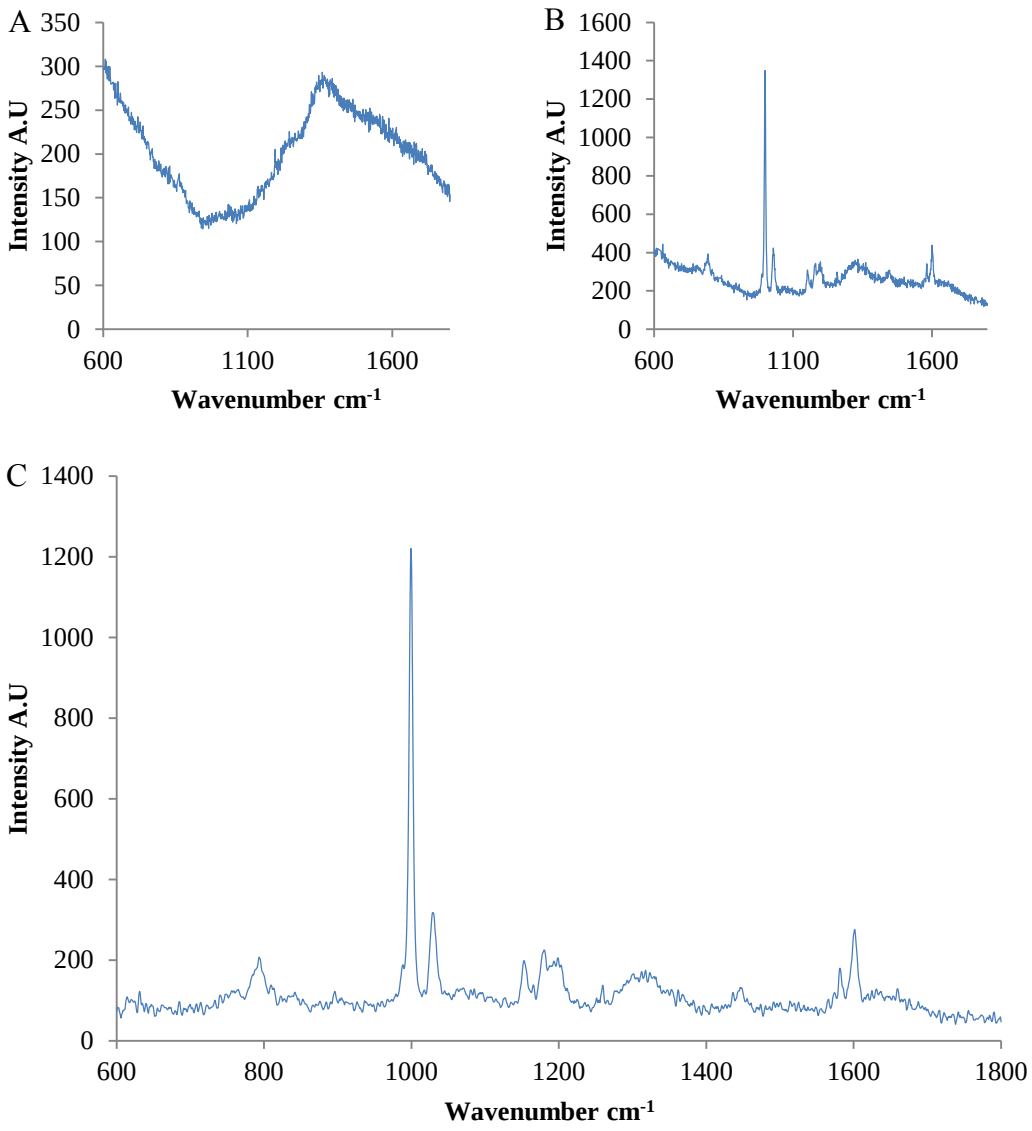

Figure 26. Raman spectra of DPSCs cultured on quartz in a closed petri dish. A) raw control spectrum, B) raw test spectrum, C) processed difference spectrum.

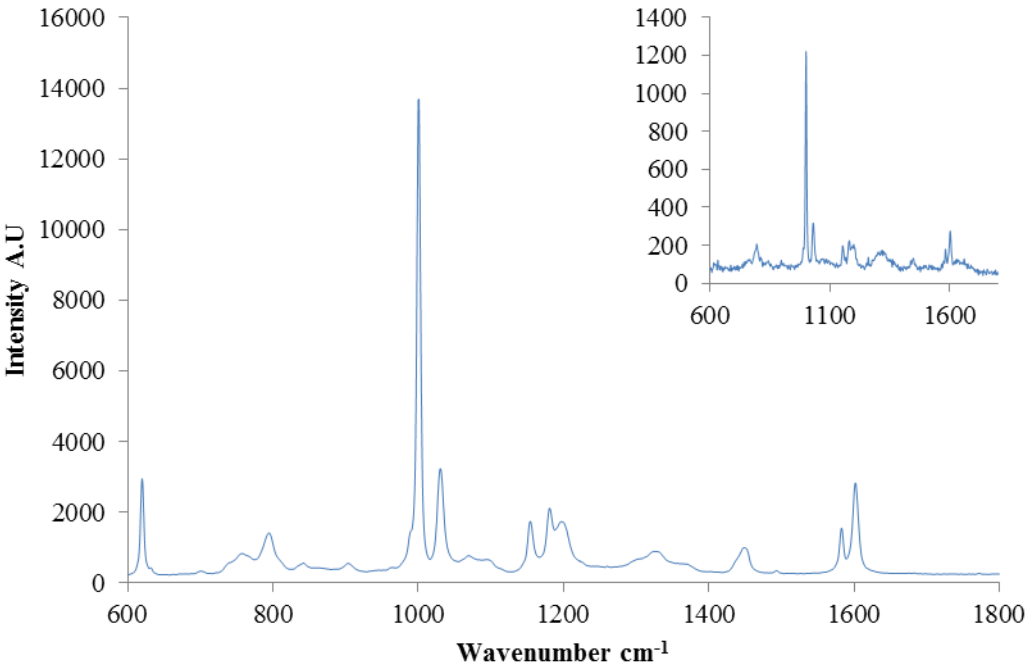

Figure 27. Raman spectrum of a petri dish. Inset is the previous spectrum acquired from DPSCs for comparison. The Raman peaks from the polystyrene petri dish are clearly evident in the spectrum of the DPSCs.

4.3.2.2 Raman Spectroscopy of DPSCs Cultured in Quartz Cuvettes

The second method investigated was to culture DPSCs in quartz cuvettes designed for use in bench top spectrophotometers. Figure 28c shows a spectrum acquired from DPSCs minus the background. Some peaks indicative of cells were evident at 1000 cm^{-1}, 1032 cm^{-1}, 1186 cm^{-1} and 1637 cm^{-1}. However, there were clearly issues with high signal to noise ratios and the result was still far removed from a typical cell spectrum in the published literature (102, 135).

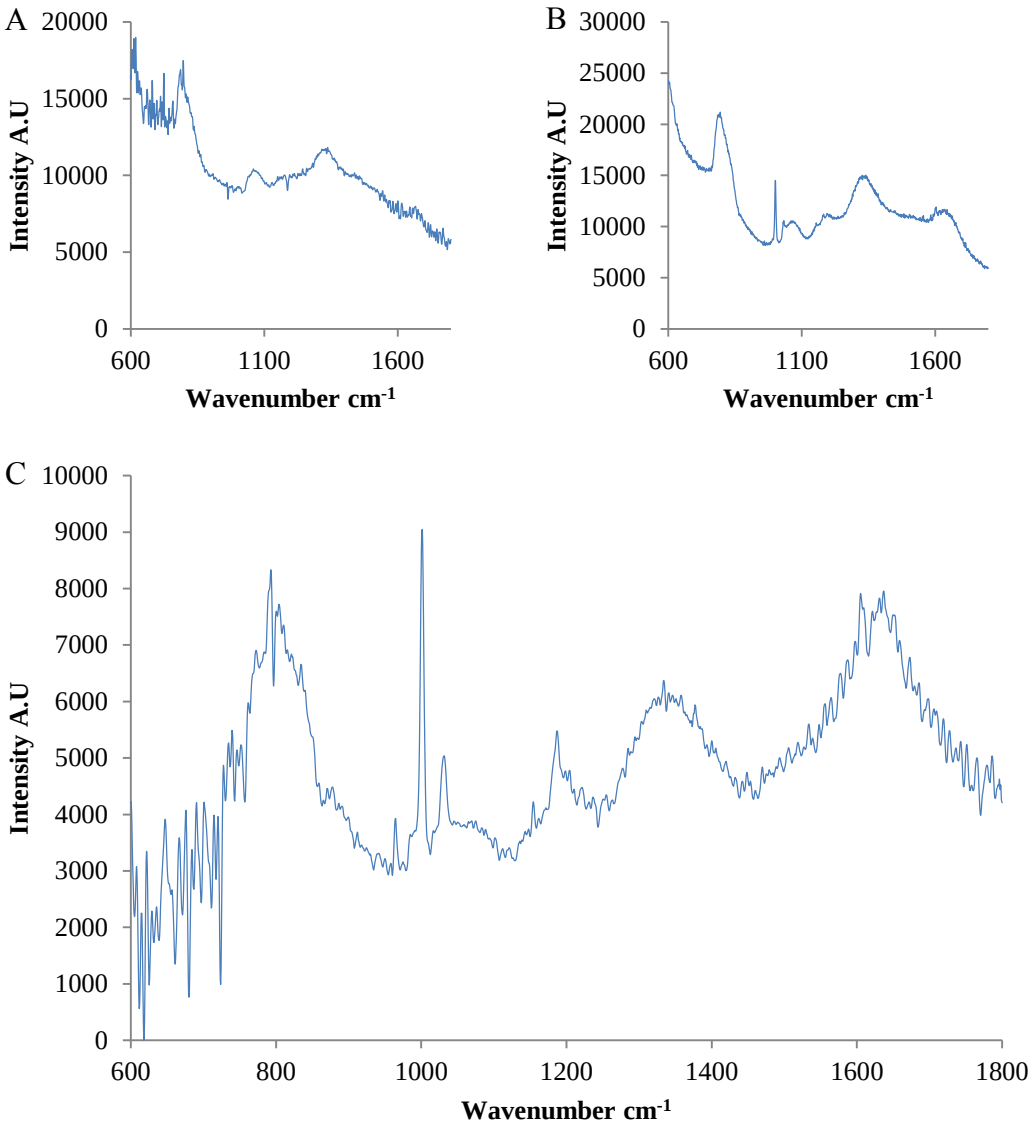

Figure 28. Raman spectra of DPSCs cultured in a quartz cuvette. A) raw control spectrum, B) raw test spectrum, C) processed difference spectrum.

4.3.2.3 Raman Spectroscopy of DPSCs Cultured in Quartz Customised Cell Culture Flasks

The final method tested was to culture DPSCs on quartz windows attached to standard cell culture flasks. Figure 29c shows a spectrum acquired from DPSCs following subtraction of the background. Several peaks indicative of cells were again evident at wavenumbers 998 cm^{-1}, 1260 cm^{-1}, 1332 cm^{-1}, 1445 cm^{-1} and 1648 cm^{-1}. Whilst clearly in need of further optimisation this result was the most consistent with the published literature (102, 135) so quartz window modified flasks were taken forward as the cell culture method of choice.

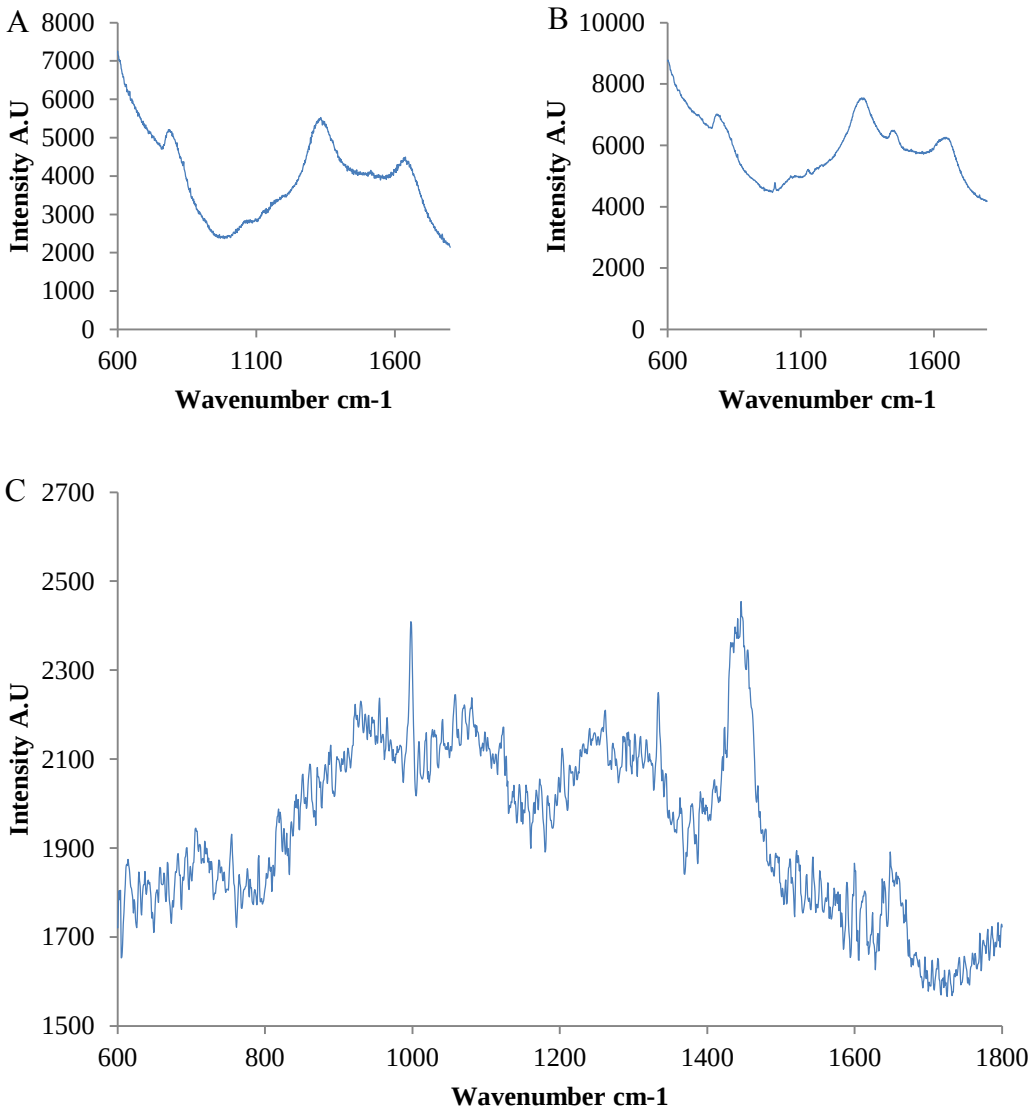

Figure 29. Raman spectra of DPSCs cultured in quartz customised flasks. A) raw control spectrum, B) raw test spectrum, C) processed difference spectrum.

4.3.3 Raman Spectroscopy of DPSCs using Various Optical Configurations

To better match the refractive index of the light path from objective to sample several water immersion objectives were tested, where the objective was immersed in an aliquot of HBSS atop the quartz window of the modified flasks. Figure 30 shows the processed Raman spectra of DPSCs acquired with several different objectives. The results were very similar to previously published data (102, 135), with many peaks evident, particularly those acquired with the 40x/0.8NA and 63x/1.2NA objectives.

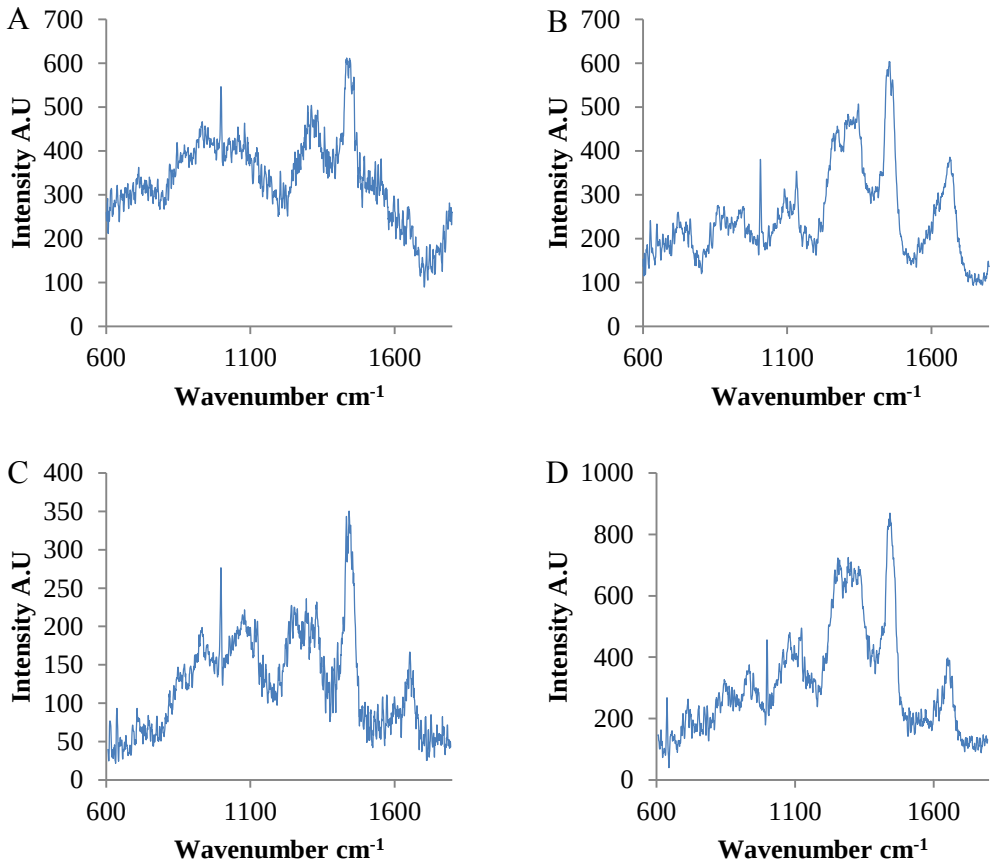

Figure 30. Representative processed spectra acquired using A) 25x/0.95NA water immersion objective, B) 40x/0.8NA water immersion objective, C) 63x/0.9NA water immersion objective and D) 63x/1.2NA water immersion objective. Sample n=50, control n=10, 30 seconds acquisition time. The 40x/0.8NA and 63x/1.2NA (B and D) objectives appear to produce the least noisy spectra.

To quantify the results, the signal to noise ratio was calculated using the peak at 997 cm^{-1} and the region 1700-40 cm^{-1} which was designated as noise due to the absence of any Raman peaks in this region given off by the cells (Table 6). This confirmed the superior performance of the 40x/0.8NA and 63x/1.2NA objectives compared with the others based on the higher signal:noise in spectra acquired using those objectives.

Table 6. Average signal to noise ratio of Raman spectra acquired from DPSCs over 30 seconds using various water immersion objectives. The 40x/0.8NA and 63x/1.2NA objectives outperformed the other two as indicated by the higher signal:noise ratio of spectra acquired using them.

Microscope objective	Signal intensity of peak at 997 cm^{-1}	Noise at 1700-40 cm^{-1}	Average S:N
25x/0.95NA	157.25	24.64	6.37
40x/0.8NA	174.58	8.19	21.32
63x/0.9NA	174.82	15.83	11.04
63x/1.2NA	251.37	11.99	20.97

The results of the Alamar Blue assay, described in section 4.3.1, suggested that the metabolic activity of DPSCs may begin to slow after 3-4 hours in ambient conditions. Within this time constraint, the effect of acquiring multiple spectra (50) with a short (30 seconds) exposure time, (Figure 30), was compared with acquiring fewer spectra (15) with a longer (120 seconds) exposure time (Figure 31). The same peaks were clearly evident in all spectra from the various microscope objectives.

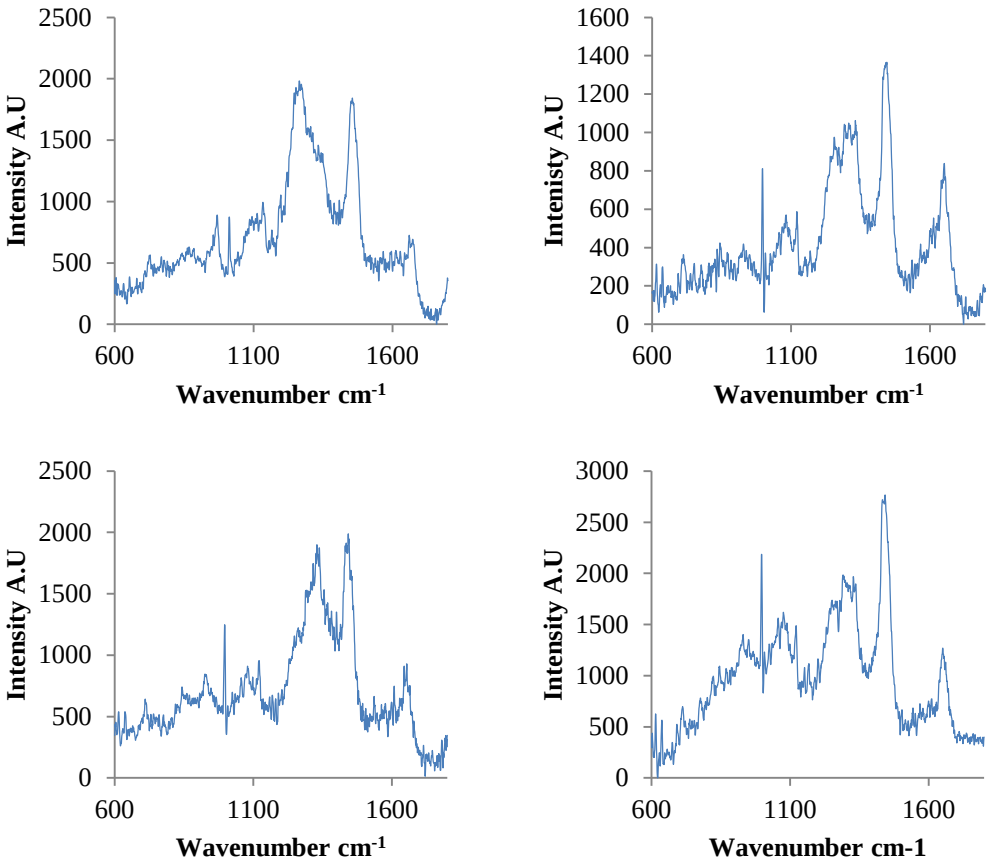

Figure 31. Representative processed spectra acquired using A) 25x/0.95NA water immersion objective, B) 40x/0.8NA water immersion objective, C) 63x/0.9NA water immersion objective and D) 63x/1.2NA water immersion objective. Sample n=15, control n=3, 120 seconds acquisition time. All 4 objectives appear to produce less noisy spectra when fewer are acquired over longer exposure times *vs* many over shorter exposure times (Figure 30).

The signal to noise ratios of the spectra derived using each of the objectives were calculated again using the same method as previously described (Table 7). This demonstrated an approximate doubling of signal to noise ratio when using fewer, longer exposures. The 40x/0.8NA and 63x/1.2NA objectives performed the best again in this respect.

Table 7. Average signal to noise ratio of Raman spectra acquired from DPSCs over 120 seconds using various water immersion objectives. Superior performance using the 40x/0.8NA and 63x/1.2NA objectives was repeated as indicated by the higher signal:noise ratios of spectra acquired with them.

Microscope objective	Signal intensity of peak at 997cm^{-1}	Noise at 1700-40 cm^{-1}	Average S:N
25x/0.95NA	858.65	37.54	22.87
40x/0.8NA	941.64	21.49	43.81
63x/0.9NA	810.45	51.53	15.78
63x/1.2NA	1222.85	25.07	48.76

The results of these experiments indicate that the optimal conditions for the acquisition of Raman spectra from living DPSCs were obtained when using a cell culture flask modified with a quartz window and using a 40x/0.8NA water immersion objective sampling 15 separate loci with a 120 second exposure.

4.4 Discussion

In order to use Raman spectroscopy to non-invasively characterise the course of DPSC differentiation using one continuous sample taking repeated measurements over time, a new method was required that could permit both long term aseptic cell culture and the acquisition of high quality, reproducible Raman spectra.

To develop such a methodology, the testing of several possibilities was required in order to refine an optimal method. Two initial approaches were discounted at an early stage: the use of enclosed petri dishes and quartz cuvettes. Acquiring spectra using petri dishes presented several problems not least that the petri dish itself was detected by the spectrometer despite the distance from the focal point. Maintaining sample sterility for a prolonged period would also likely have been an issue requiring regular transiting of the cell sample to the petri dish.

Quartz cuvettes provided a much simpler cell culture modality, eliminating the need to transfer the cell sample from one culture environment to another for the purpose of acquiring spectra. However, the thick walls of these cuvettes at ~2 mm, precluded the acquisition of high quality spectra. This was due to the need to use low magnification microscope objectives with a longer working distance to the sample reducing the amount of Raman signal collected.

Finally, conventional cell culture flasks that had been modified with quartz windows for sampling were tested. This method provided the first clear detection of several peaks, commonly seen in cell samples, such as phenylalanine at ~998 cm^{-1} and CH_3, CH_2 at 1445 cm^{-1}. However, the spectra acquired had a poor signal:noise ratio and were likely unusable in further analysis. Work by Hasselhoff *et al* 1999 (190) demonstrated that the resolution of images acquired using confocal laser systems could be improved by using a water immersion lens if the sample itself was immersed in a mounting solution beneath a glass coverslip. Based on this observation, several water immersion lenses were tested with the customised cell culture flask in order to improve the quality of the Raman spectra acquired. This approach yielded a significant improvement in the quality of the spectra. Figure 32

shows a representative spectrum acquired using a 40x/0.8NA from DPSCs cultured in a quartz customised cell culture flask.

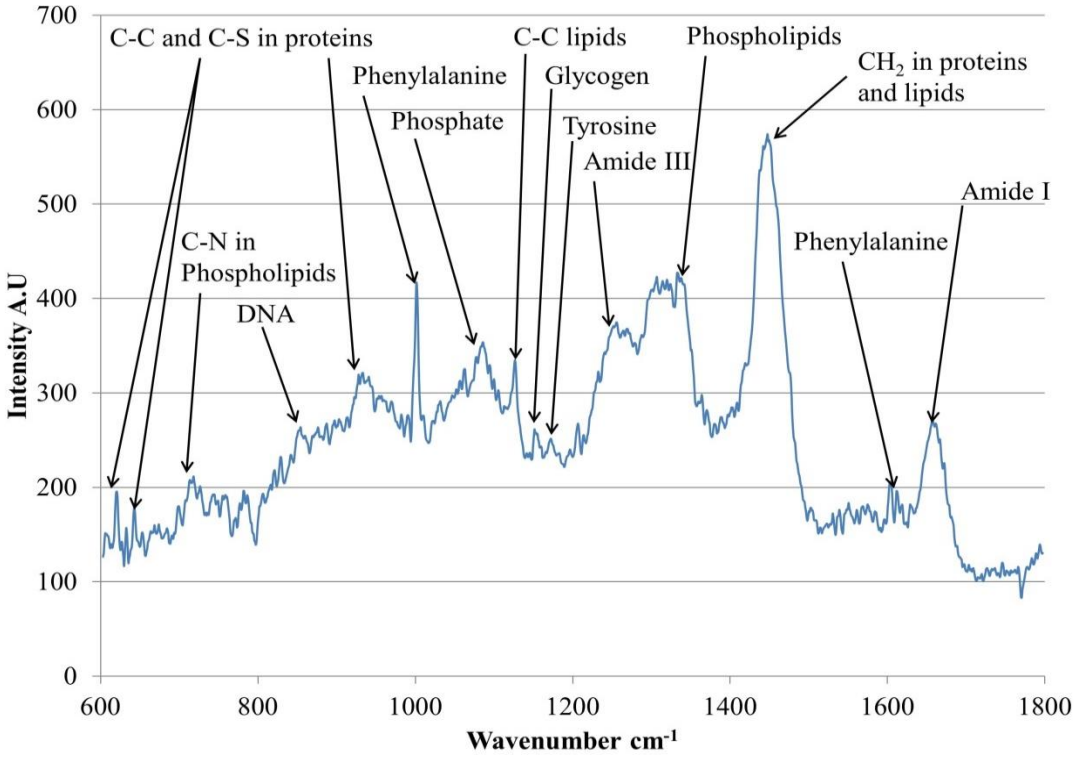

Figure 32. Representative Raman spectrum of DPSCs after optimisation of cell culture technique, Raman optical and system configuration and processing of spectra. Major peak assignments are marked based on (97)

The three cell culture modalities used this this study underline an important consideration when attempting to acquire Raman spectra from DPSCs or indeed any cell. In the published literature non-sterile approaches are used to acquire spectra from cells. This permits the use of high powered microscope objectives with very short working distances between the cells and objective. A short working distance allows the capture of a greater proportion of the Raman refracted light from the cells thereby increasing the signal:noise ratio of the spectra acquired. The first two cell culture modalities assessed in this study (petri dishes and cuvettes) both required a long working distance between the cells and objective due to their design and so the spectra acquired had a poor signal:noise ratio. The final method tested (quartz window customised flasks) had a much smaller working distance between the cells and objective and so the spectra acquired had a better signal:noise ratio. This underlines that when attempting to acquire spectra from cells in an aseptic manner

there is tension between the need to maintain an enclosed sterile culture environment and capturing as much Raman signal from the cells as possible by reducing the working distance. This may reflect why previous studies have not used an aseptic method as the primary aims were to demonstrate that Raman spectra could be acquired from, and used to, characterise cells.

Whilst using quartz window customised flasks meets the criteria of being able to maintain DPSCs in aseptic conditions over long periods and permits the acquisition of high quality, reproducible spectra there are still potential issues. The lack of control over temperature and O_2/CO_2 concentrations means that sampling must be performed in ambient conditions. Additionally the culture flasks must be filled with fluid to prevent desiccation when presenting the samples to the microscope objective which may hinder efficient gas diffusion. DPSC metabolism was shown to remain constant over four hours under ambient conditions. However, this does not preclude the induction of a heat shock or hypoxic response. This will be addressed in the following chapter.

Chapter 5
Characterisation of DPSC Osteogenic Differentiation using Raman Spectroscopy

The aim of this study was to use the aseptic methodology developed in Chapter 4 to characterise osteogenic differentiation of DPSCs using Raman spectroscopy and to validate this using traditional phenotyping techniques. The osteogenic lineage was chosen for this work as there have been previous studies where Raman spectroscopy has been used to characterise osteogenesis (though not maintaining culture sterility), the data from which could be used to inform as to the validity of the method.

5.1 Introduction

Raman spectroscopy has the capacity to be both non-invasive and non-destructive and utilises a monochromatic light source to determine sample chemistry. Upon interaction with the sample a small fraction of the light, approximately 1 in 10^6 to 10^8 photons (108), is shifted in wavelength with respect to the incident laser. Many chemical bonds in the sample cause unique Raman shifts such that the resultant spectrum can be considered to be a 'molecular fingerprint' that is unique to the sample under analysis. As described in section 1.6 there are many active areas of research with Raman spectroscopy and stem cells a number of which have specifically addressed the osteogenic differentiation process. These studies have identified a spectroscopic signature for the differentiation of stem cells down the osteogenic lineage based on the emergence and relative ratios of peaks in their Raman spectra as illustrated in Figure 33. Whilst these data have highlighted the potential usefulness of Raman spectroscopy in stem cell phenotyping, to date studies taking multiple longitudinal measurements of the *same* cell population have been limited due to the need to maintain sterility of the cell cultures. One recent study by Ghita *et al* 2014 (191) acquired spectra from aseptic osteo-induced MSCs over a 28 day time period and their data agreed with the findings of previous studies. However, their focus was on acquiring spectra later in the differentiation process from putative and developed mineralised nodules at which point Raman

spectroscopy is not strictly required to determine differentiation status (mineralised nodules can be seen easily under a light microscope without the need for staining). The early stages of osteogenesis - and the potential to use Raman spectroscopy as a predictive indicator of the process - remain to be addressed.

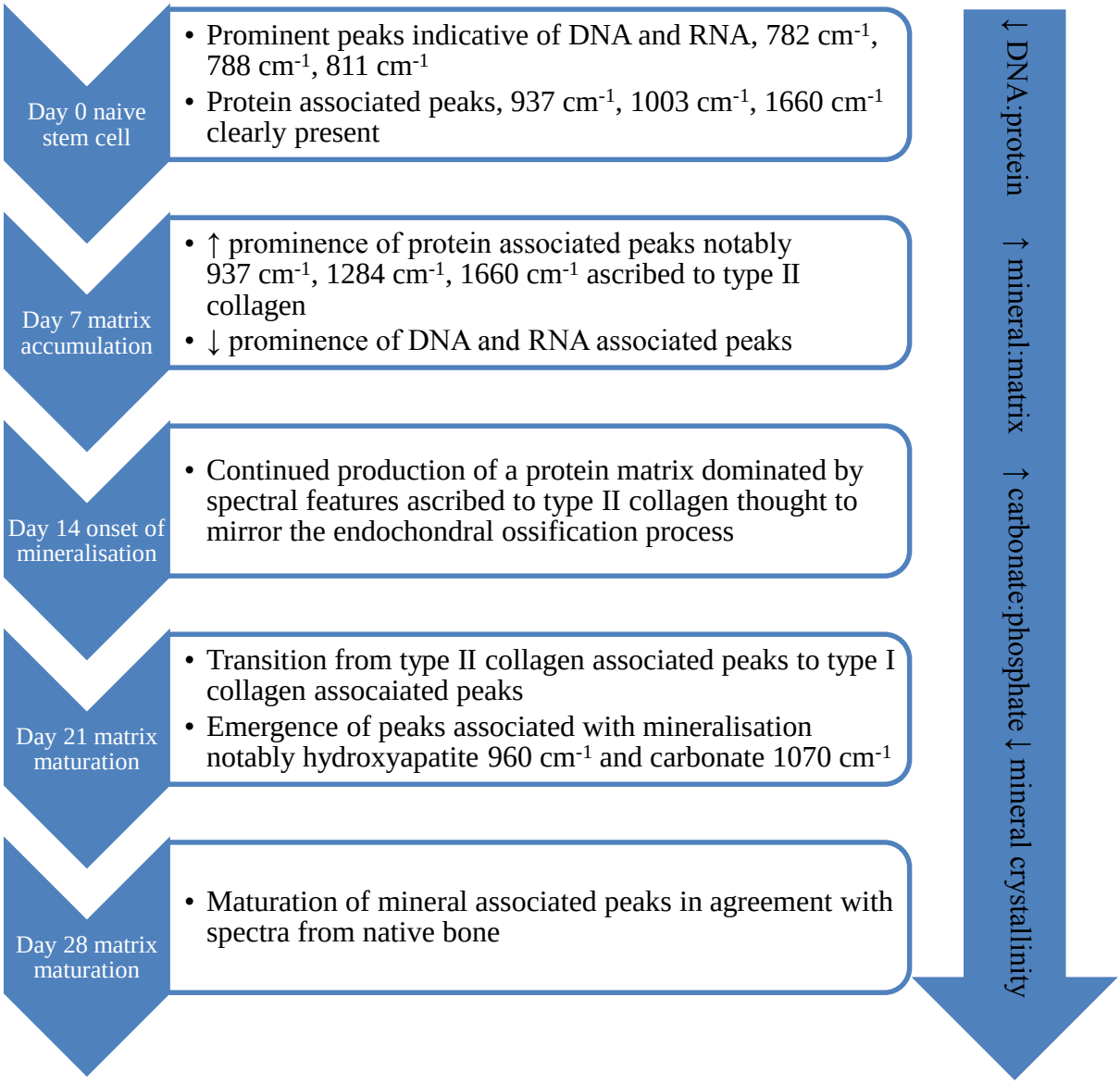

Figure 33. Proposed timeline of events outlining the osteogenic differentiation process of stem cells using Raman spectroscopy, based on data from (101, 104, 129, 132-134).

Raman scattering efficiency is very poor and the distance between the sample and the microscope objective needs to be as small as possible to combat this. In order to maximise the potential of Raman spectroscopy as a tool for *non-invasive* stem cell

characterisation, studies need to be conducted under aseptic conditions while maintaining the strength of the Raman signal. This would then ultimately permit early/predictive identification of differentiation such that stem cells may be used in further downstream applications. In this study, having developed the aseptic method in Chapter 4, the aim was to validate this using the osteogenic differentiation of DPSCs as an exemplar. DPSCs are one of several cell sources that are more broadly classed as MSCs. They were chosen specifically for this study as they have a proven predisposition toward the osteogenic/dentinogenic lineage (192), presenting a reliable and well documented sample for evaluating the newly developed method. Furthermore, the findings outlined in Figure 33 provided *a priori* knowledge as to which spectral features to expect. Therefore DPSCs were osteo-induced and Raman spectra acquired at regular time intervals throughout the osteogenic pathway both to determine technical feasibility and identify whether changes in the Raman spectra might be indicative/predictive of the differentiation process. The majority of spectra were acquired during the earlier stages of differentiation to ascertain if there were any features that were predictive of eventual cell fate. Finally, qRT-PCR for the osteogenic markers genes *ALP* and *OC* as well as Alizarin red staining were performed to confirm that DPSCs had successfully undergone osteogenic differentiation.

5.2 Materials and Methods

5.2.1 Analysis of DPSC Osteogenic Differentiation using Raman Spectroscopy

5.2.1.1 Cell Culture

Triplicate samples of DPSCs, taken from each of three donors, were isolated, expanded and prepared for Raman spectroscopy as described in the general methods (sections 2.1, 2.2 and 2.5.3). When samples reached confluence, after approximately 3 days of culture in basal medium, osteogenesis was induced by supplementation of basal medium with 0.25 mM ascorbic acid, 10 mM β-glycerophosphate and 100 nM dexamethasone (all Sigma-Aldrich, Gillingham, UK). This time point was designated as day 0. To assess the effects of Raman spectroscopy and the sampling process on DPSCs, an equal number of samples were maintained in osteogenic conditions but did not undergo Raman analysis. The total culture period for both sample groups was 28 days.

5.2.1.2 Raman Spectroscopy

Raman spectroscopy was performed using a Renishaw RM series 1000 microscope as described in the general methods (section 2.5.3). Spectra were acquired at days 0, 3, 7, 10, 14 and 28. At each time point, 15 spectra were acquired over the wavenumber range 600-1800 cm^{-1} with an exposure time of 120 seconds for a total of 135 spectra at each time point. To obtain a spectrum, the DPSC monolayer was first focused under transmitted white light then over-focused by 5 µm and switched to 785 nm light to acquire the spectrum. All spectra were acquired from the DPSC monolayer, even at later time points, despite the presence of mineralised nodules, for consistency. Cell free sections of quartz, identical to that used in the experiments, were used to acquire background spectra.

5.2.1.3 Processing and Analysis of Spectra

Pre-processing of spectra was performed in Grams/32 with further processing and validation carried out using principal component analysis (PCA) performed in Matlab version R2013b. A full description of this process can be found in Appendix A. Briefly, in Grams, the background was subtracted from each individual spectrum,

the x-axis normalised to the peak at ~1000 cm^{-1}, the baseline flattened and smoothed using a 7 point Savitzky-Golay filter and the lowest point on the y-axis offset to 0. All spectra were then exported to Microsoft Excel for further processing in Matlab. PCA was performed on all spectra from each individual donor and used to remove outlying spectra from each time point. The data was then averaged using one spectrum from each donor per time point. Following this 2nd derivative spectra were calculated and further smoothing performed.

5.2.2 The Effect of Raman Spectroscopy on Osteogenic and Cell Stress Marker Gene Expression using qRT-PCR

RNA isolation and reverse transcription were performed as previously described in the general methods (section 2.3). qRT-PCR was performed using TaqMan gene expression assays (Applied Biosystems, Carlsbad, USA) for *ALP* and *OC*: assay numbers Hs01029144-m1 and Hs00609452-g1 respectively, to investigate osteogenic marker expression and, heat shock transcription factor 1 (*HSF1*), hypoxia inducible factor 1 (*HIF1A*) and lactate dehydrogenase (*LDH*): assay numbers Hs00232134-m1, Hs00153153-m1 and Hs00929956 respectively, to investigate cell stress marker expression. Reactions were carried out in 96 well plates as per the manufacturer's instructions on a Roche LightCycler® 480 system. Optimal cDNA concentration was determined as 5 ng/reaction by plotting standard curves with known cDNA concentrations. Data was normalised to *YWHAZ* assay number Hs00237047_m1, and analysed using the comparative cycle threshold method (ΔCT). DPSC samples from three patients, one in duplicate (total number of samples = 4), were analysed ± Raman spectroscopy after 28 days of osteo-induction. Each sample was analysed in triplicate giving a total n=12 for each group. A sample from day 0 was used to provide a baseline. Graphs of the mean ± SE were plotted in Microsoft Excel and statistical significance was determined by one-way ANOVA using GraphPad Instat 3 software.

5.2.3 The Effect of Raman Spectroscopy on Extracellular Matrix Calcification using Alizarin Red Staining

Alizarin red staining was performed on DPSCs at day 28 ± Raman spectroscopy (n=2 for each) as described in section 3.3.4.

5.3 Results

5.3.1 Characterisation of Osteogenic Differentiation of DPSCs by Raman Spectroscopy

Raman spectroscopy has previously been used to demonstrate late stage osteogenic differentiation of stem cells by analysing putative mineralised nodules (101, 134). In this study DPSCs were analysed by Raman spectroscopy with a focus on earlier time points, prior to the emergence of mineralised nodules, to ascertain if the spectra were indicative/predictive of or associated with the osteogenic differentiation process. Figure 34 depicts the average spectra for each time point (day 0 to day 28) following subtraction of the signal from the (quartz) background. Many peaks typical of biological samples were clearly evident such as phenylalanine at 1003 cm^{-1}, CH_3, CH_2 found in collagen at 1453 cm^{-1} and amide I at 1660 cm^{-1}.

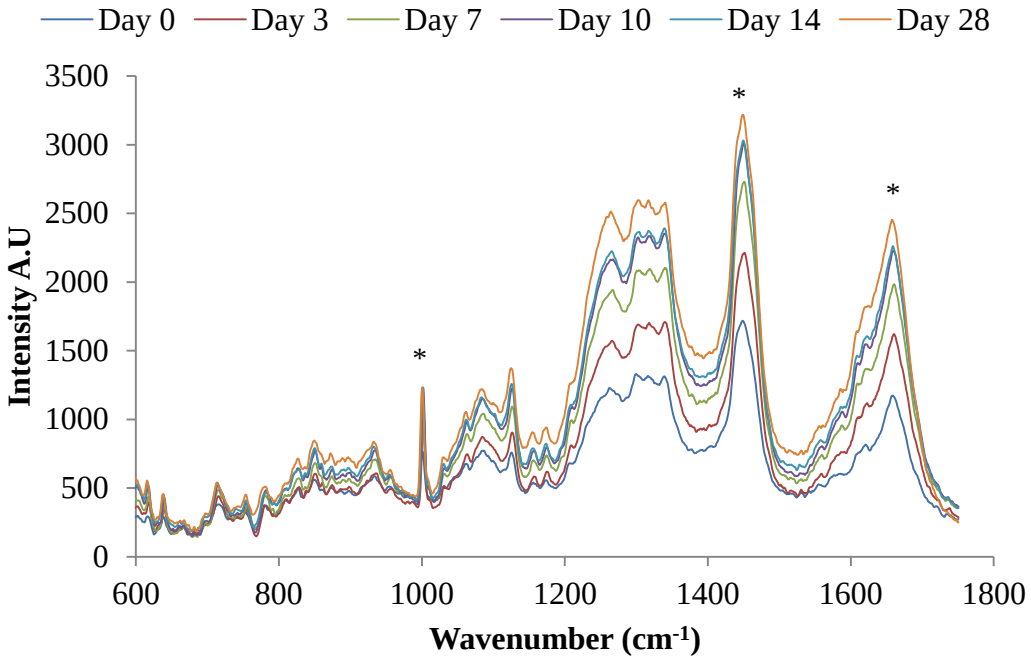

Figure 34.Average background subtracted spectra of osteo-induced DPSCs at days 0, 3, 7, 10, 14 and 28, n=135 spectra per time point from three separate donors. A selection of peaks typical of spectra from biological samples are marked *

Principal component analysis (PCA) was performed on spectra obtained from DPSCs from three donor samples, analysed in triplicate, which had been averaged,

n=135 spectra at each time point. Figure 35 is a 2D scatter plot of PC1 and PC2 scores accounting for 54.2% and 12.4% of the variation in the data set respectively.

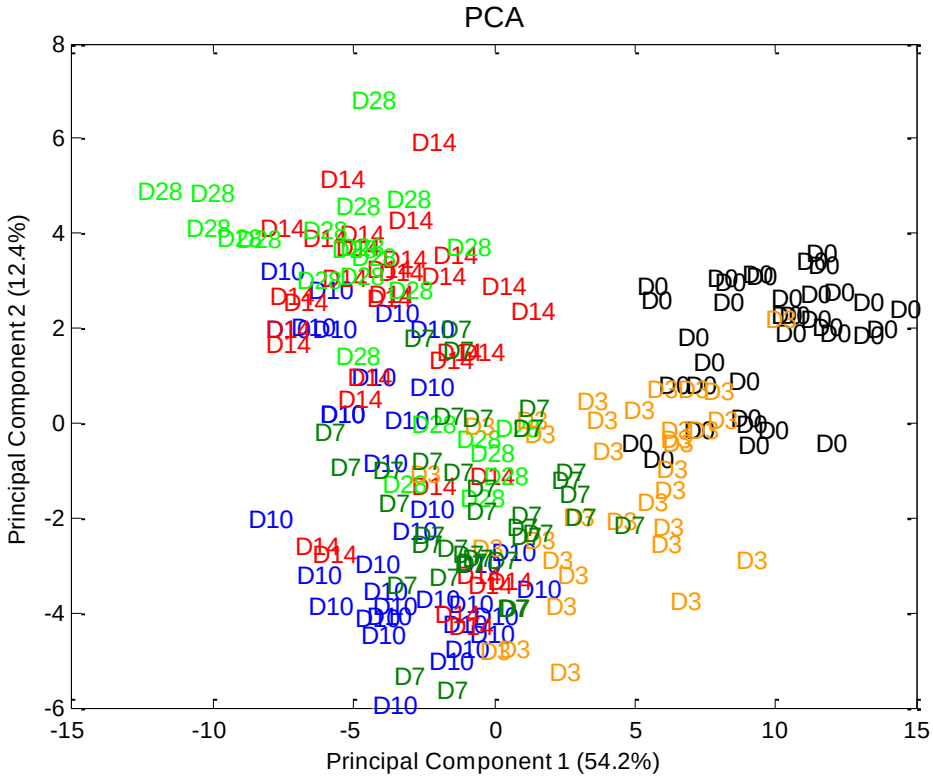

Figure 35. Principal component analysis of the osteogenic differentiation of DPSCs at days 0, 3, 7, 10, 14 and 28. 2D scatter plot for principal components 1 and 2. Each position displayed is the average of three spectra, one from each donor, for every time point. There is a clear trend in PC1 between days 0 and 10 and a further trend in PC2 between days 0 and 10 and days 10 and 28.

The PCA scores plot demonstrated a clustering of spectra at each time point, illustrating that the spectral collection was reproducible. As expected, there was overlapping of spectra between adjacent time points as there was a phenotypic shift that was continuous in nature during cellular differentiation. Despite the overlapping of time points a clear trend was observed from day 0 to day 10 along PC1 while a trend from day 10 to day 28 was observed along PC2. Loadings plots can be drawn for each PC to illustrate those spectral features that are responsible for the variance in that PC. Peaks on the same side of a loading plot will be behaving similarly, whilst peaks on opposite sides of a loading plot will be behaving differently with respect to their scores within a given PC. Figure 36 illustrates the loading plots for PC1 and PC2.

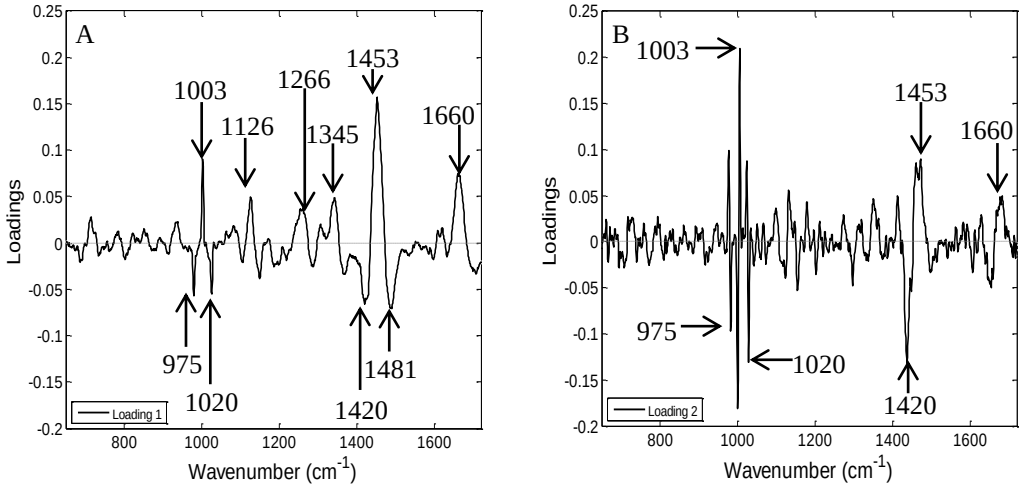

Figure 36. PCA loadings plot for A) PC1 and B) PC2 from the PCA of DPSCs that had been osteo-induced for 0, 3, 7, 10, 14 and 28 days. Significant positive and negative peaks are marked.

The loading plot for PC1 showed positive peaks for wavenumbers corresponding to amide bonds (1266 cm^{-1} and 1660 cm^{-1}), CH_3, CH_2 from collagen (1345 cm^{-1} and 1453 cm^{-1}), phenylalanine (1003 cm^{-1}) and lipids (1126 cm^{-1}) whilst wavenumbers corresponding to ribose (975 cm^{-1} and 1020 cm^{-1}), the nucleic acids guanine and adenine (1420 cm^{-1}) and DNA (1481 cm^{-1}) had negative peaks. Similarly the loading plot for PC2 had positive peaks at 1003 cm^{-1}, 1453 cm^{-1} and 1660 cm^{1} with negative peaks at 975 cm^{-1}, 1020 cm^{-1} and 1420 cm^{-1}. Putative peak assignments were based on Movasaghi *et al* 2007 (97). As the above individual PCs both use the same areas it may be hard to differentiate which are the important vibrations with respect to time, therefore PC1 was plotted against PC2 (Figure 37). In this instance the position of a given wavenumber on the plot when transposed on the original scores plot indicates where that wavenumber varies most greatly, as illustrated in section 1.4. This loadings plot showed that two protein associated peaks at 1453 cm^{-1} and 1660 cm^{-1} transpose along the trend in PC1 from days 0 to 10, whilst two DNA/RNA associated peaks 975 cm^{-1} and 1020 cm^{-1} transpose along the trend in PC2 from days 10 to 28 as did the phenylalanine peak at 1003 cm^{-1}.

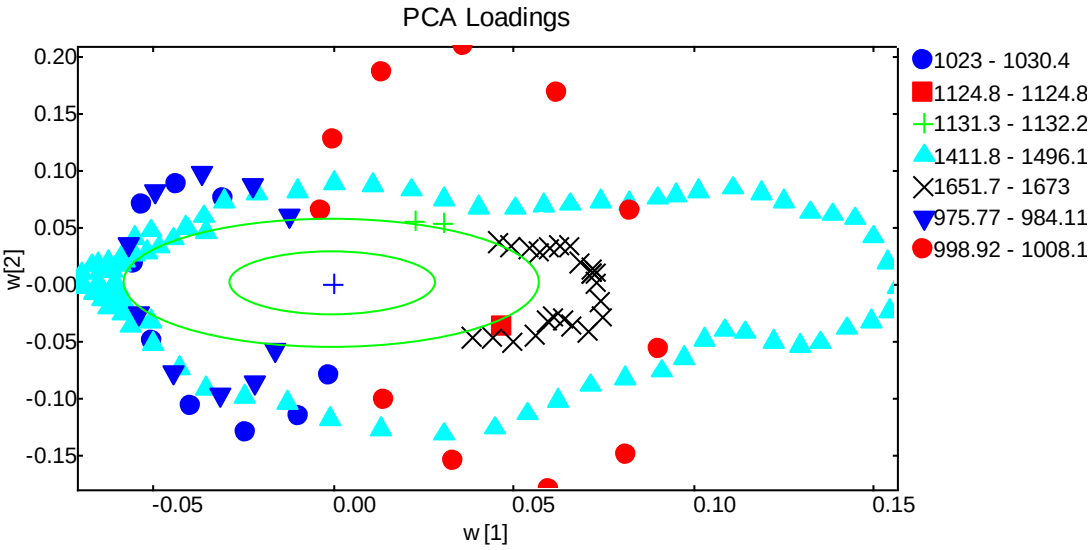

Figure 37. PCA loadings plot for PC1 *versus* PC2, the outer green circle indicates 95% confidence. In the key are groups of wavenumbers from peaks that vary significantly.

Finally, to confirm osteogenic differentiation of DPSCs at day 28 several Raman spectra were acquired from putative mineralised nodules, (Figure 38). The well characterised mineral associated region, 955-964 cm^{-1}, described in several previous studies (101, 133, 134), was clearly evident.

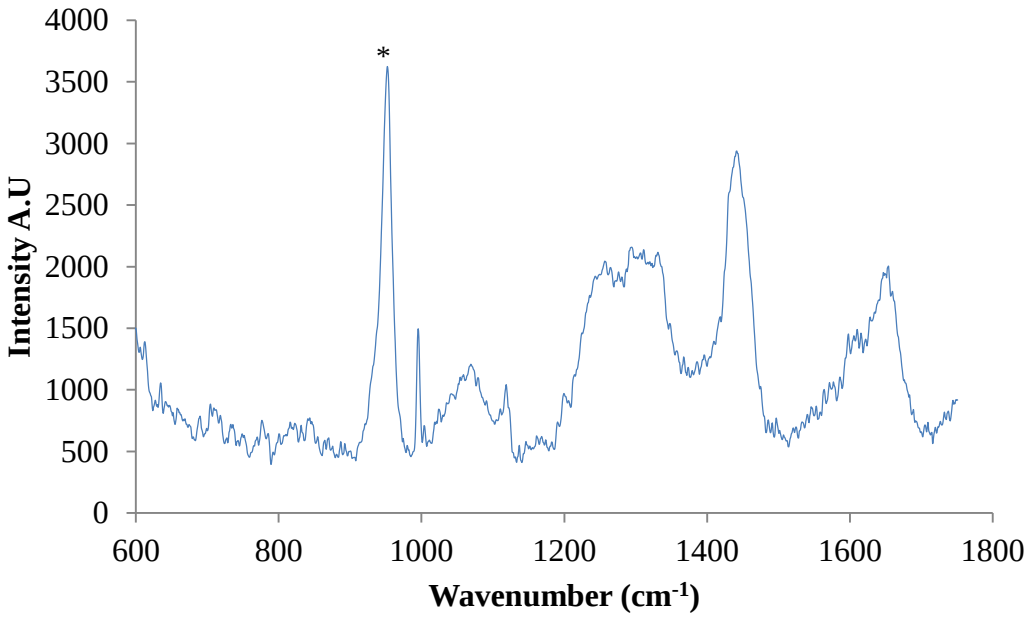

Figure 38. Average background subtracted spectra of osteo-induced DPSCs at day 28 acquired from sites of putative mineralised nodules, n=5. The well characterised mineral associated region at ~955-964 cm^{-1} is clearly evident, marked *.

5.3.2 Confirmation of Osteogenic Differentiation of DPSCs ± Analysis by Raman Spectroscopy using qRT-PCR and Alizarin Red Staining

qRT-PCR and Alizarin red staining were used to confirm osteogenic differentiation of DPSCs. Samples that had undergone Raman measurements and those grown in parallel without being subject to Raman were analysed to determine if the data acquisition process and the Raman spectroscopy itself had any effect on DPSC osteogenic differentiation. Significant increases in *ALP* and *OC* expression were observed between days 0 and 28 irrespective of whether or not the DPSCs had undergone Raman analysis ($p<0.001$ and $p<0.05$ respectively) (Figure 39). There was no significant difference in the expression of either gene between DPSCs which had/had not been analysed by Raman spectroscopy.

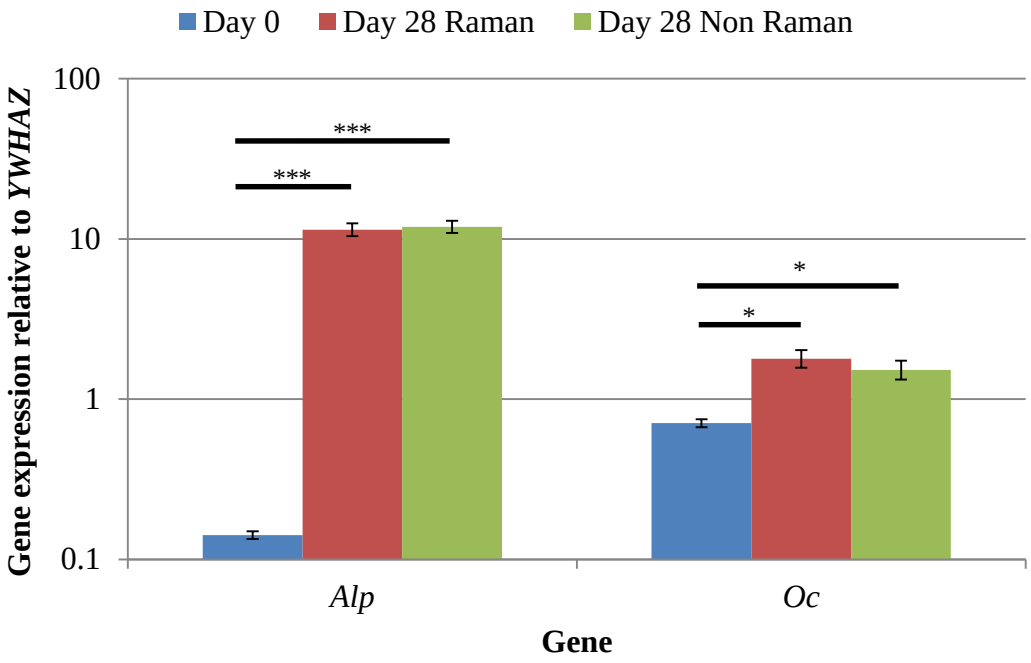

Figure 39. A comparison of DPSC osteogenic gene expression at day 0, and day 28 from cells that had/had not undergone Raman spectroscopy. Results show mean ±SE, n=3 (day 0), n=12 (day 28 + Raman), n=12 (day 28 – Raman). *** p<0.001, * p<0.05. Statistical significance was determined using a one-way ANOVA. Significant increases in the expression of both genes was found between days 0 and 28 and there was no difference in the expression between DPSCs that had and had not undergone Raman spectroscopy.

Alizarin red staining was used to demonstrate extracellular matrix calcification by DPSCs after 28 days of osteo-induction for samples that had been analysed by Raman spectroscopy and those that had not (Figure 40). Positive Alizarin red staining was observed in all samples, with no discernible differences between the Raman and non-Raman groups.

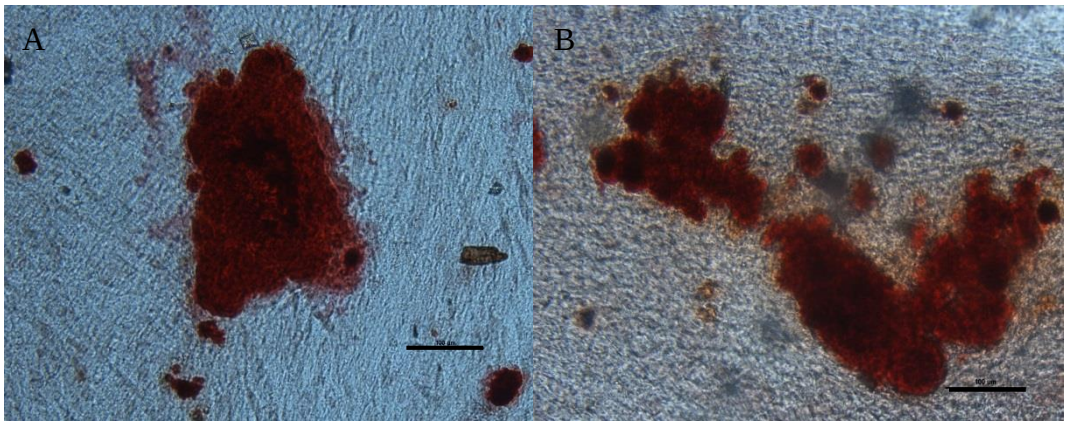

Figure 40. Alizarin red staining of DPSCs after 28 days of osteo-induction that A) had undergone Raman measurements and B) had not undergone Raman measurements. Scale bars = 100 µm. Positive staining of mineralised nodules was observed regardless of whether the DPSCs had undergone Raman spectroscopy or not.

5.3.3 Comparison of Cell Stress Marker Gene Expression Between DPSCs ± Analysis by Raman Spectroscopy using qRT-PCR

The data acquisition process when performing Raman spectroscopy has the potential to induce a cell stress response due to, for example, limited gas diffusion and exposure to ambient temperature and gas concentrations. In order to test for any cell stress response, the expression of three marker genes: heat shock transcription factor 1 (*HSF*), hypoxia inducible factor 1 (*HIF*) and lactate dehydrogenase (*LDH*) was determined by qRT-PCR from DPSCs at day 0 and day 28 ± Raman spectroscopy (Figure 41). No significant differences in the expression of all three genes was observed between the groups.

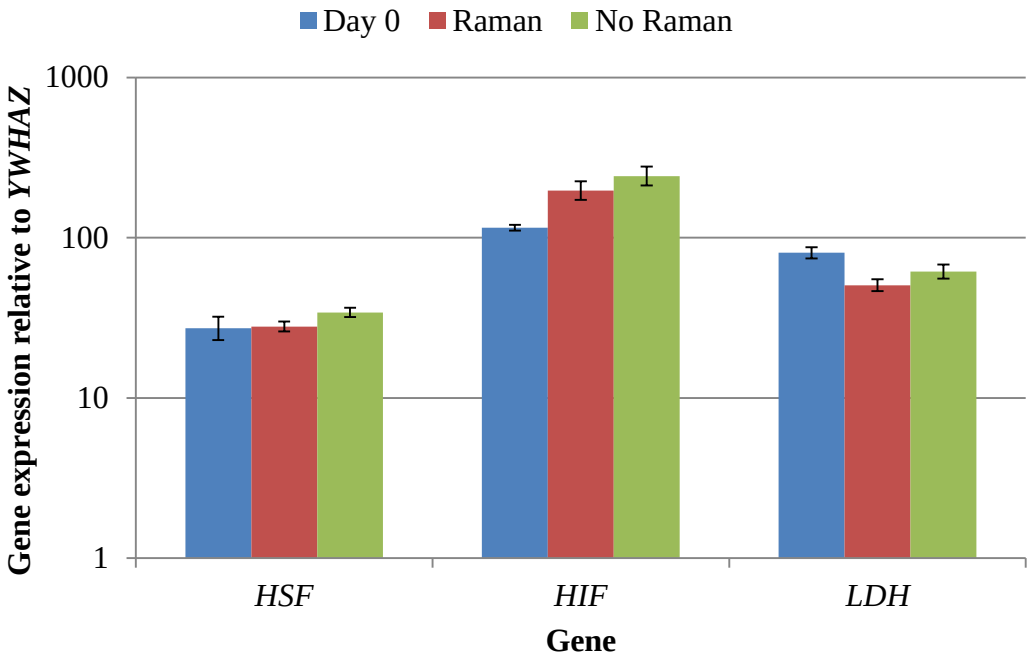

Figure 41. A comparison of DPSC cell stress marker expression at day 0 and day 28 from cells that had/had not undergone Raman spectroscopy. Results show mean ±SE, n=3 (day 0), 12 (day 28 + Raman), 12 (day 28 – Raman). Statistical significance was determine using a one-way ANOVA. No significant changes in gene expression were observed.

5.4 Discussion

The aim of this study was to validate the method developed and described in Chapter 4 by using Raman spectroscopy to investigate the well-characterised osteogenic differentiation of DPSCs, prior to the outcome becoming apparent by the emergence of mineralised nodules in the cultures. At this end point there is no need for a non-invasive method to determine cellular differentiation status as such nodules are clearly discernible under an ordinary microscope without staining. Therefore there was a focus on acquiring spectra in the first 14 days of osteo-induction with a view to identifying spectral features that may indicate/predict cell differentiation.

PCA was performed on spectra acquired throughout the DPSC osteo-inductive differentiation process. PCA is already widely used in the analysis of spectroscopic data (103, 123, 131, 193, 194) and is well suited to reducing the complexity of large multivariate data sets (121). The PCA scores plot of PC1 *versus* PC2 demonstrated two phases in the process hinged at approximately day 10, a relatively early stage in the osteogenic lineage for these cells (139). The loadings for PC1 and PC2 indicated that the pattern of those spectral features indicative of proteins and lipids was similar while features indicative of DNA and RNA had the opposite pattern to those of protein and lipids but were also similar to one another. When the loadings for PC1 and PC2 were plotted against each other, protein associated peaks were shown to vary the most in PC1 and therefore from days 0 to 10 while DNA/RNA associated peaks varied the most in PC2 and therefore from days 10 to 28. It is clear from the averaged spectra at each time point that the protein associated peaks at 1453 cm^{-1} and 1660 cm^{-1} were increasing in intensity. Taken together this suggests that in the early stages of DPSC osteogenic differentiation, increasing protein content is the main spectroscopic marker. This is in agreement with the findings of many others (101, 104, 134) and is the first instance where this has been demonstrated using the same cell cultures. However, a firm conclusion is more difficult to draw in the case of the DNA/RNA associated peaks contributing to the trend in PC2 due to their relatively low signal intensity in the original spectra and the lower contribution of PC2 (12.4%) to the variation within the data set. Schulze *et al* 2010 (104) found that one of the major indicators of differentiation in embryonic stem cells was the ratio

of spectral peaks related to proteins and DNA/RNA, concluding that the intensity of protein associated peaks increased in intensity whilst DNA/RNA peaks decreased in intensity with differentiation. Whilst it is clear from the data here that the intensity of protein associated peaks increases with time, the trend was less clear with regards to DNA/RNA. Finally, the method was clearly able to detect late stage osteogenic differentiation when directed toward mineralised nodules as evidenced by the prominent mineral associated region at 955-964 cm^{-1}.

In order for Raman spectroscopy to be truly non-invasive, Raman spectra were acquired repeatedly over time from the same cell cultures under aseptic conditions, using the method developed and described in Chapter 4. This allowed DPSCs to be cultured and analysed over time in the same culture vessel. However, a lack of optimised environmental control during the acquisition of spectra had the potential to induce a cell stress response. In order to investigate any cell stress the expression of heat shock transcription factor 1 (*HSF*), hypoxia inducible factor 1 (*HIF1*) and lactate dehydrogenase (*LDH*) was determined by qRT-PCR. *HSF* is a transcription factor regulating the expression of several important heat shock factor proteins including HSP70 and HSP90 (195) and whilst it is primarily induced by hyperthermia it has been shown to be activated in response to increasing temperature following hypothermia (196). *HIF1* is expressed in response to hypoxia which at physiological levels (2-9% O_2) is beneficial and a key regulatory mechanism in several biological processes including embryogenesis and stem cell function, however overexpression at pathological levels (<1% O_2) is associated with several conditions including ischemia and cancer (197-199). *LDH* expression is known to be stimulated by *HIF1* expression and is associated with cancer through increased anaerobic glycolysis by a process termed the Warburg effect (200, 201). No significant differences in the expression of all three markers genes were found in DPSCs associated with the Raman sampling process and relative to the start of the experiment. Whilst this is not an exhaustive interrogation of the effects of performing Raman spectroscopy on DPSCs in ambient conditions for approximately 3 h at a time, it does indicate that any effects were negligible as far as these key stress markers are concerned. Previous studies have also demonstrated that Raman spectroscopy and in particular exposure of cells to near infra-red lasers with a power on the sample of up to 115 mW does not induce cell damage (102). Finally, the

method had no effect, detrimental or otherwise, on the osteogenic differentiation process as evidenced by no differences in the expression of osteogenic marker genes or in Alizarin red staining between DPSCs that had or had not undergone analysis by Raman spectroscopy.

Chapter 6
Assessment of the Adipogenic Differentiation of ADSCs by Raman Spectroscopy

In Chapter 4 an aseptic method capable of acquiring longitudinal Raman measurements from cells in culture during their sequential differentiation was developed; in Chapter 5 this method was validated through the characterisation of the osteogenic differentiation of DPSCs. In this final study, a less well characterised differentiation lineage was studied by Raman spectroscopy. Adipogenic differentiation was chosen to illustrate the potential of the methodology because there is a very clear end point to the process evidenced by, the accumulation of lipid-rich vacuoles within the cells. Adipose derived stem cells (ADSCs) were therefore selected as the cell source for the study.

6.1 Introduction

There have been several studies using Raman spectroscopy to characterise the osteogenic differentiation process as described previously in section 1.5.4 and Chapter 5. This is perhaps unsurprising given that the end point of osteogenesis is the formation of mineralised nodules which are easily detected by Raman spectroscopy and possess a chemistry very different to that of the surrounding cells. However, there has also been a small number of studies that have illustrated the possible use of Raman spectroscopy to characterise cardiac (103, 202) and neural cell differentiation (203).

Adipogenic differentiation, one of the archetypal lineages along which MSCs differentiate (55), is accompanied by very clear biochemical/intracellular events. During the initial stages of adipogenic differentiation, stem cells undergo a period of growth arrest and mitotic clonal expansion which triggers the expression of two key pro-adipogenic transcription factors: peroxisome proliferator-activated receptor γ (PPARγ) and CCAAT/enhancer binding protein α (C/EBPα) (204-206). The

induction of PPARγ and C/EBPα and subsequent maintenance of their expression is required to produce a mature adipocyte phenotype and leads to the expression of several genes indicative of a mature adipocyte phenotype including fatty acid synthase, fatty acid binding protein, leptin and adiponectin (139, 207). The action of these genes results in increased glucose uptake, fat accumulation and insulin sensitivity, producing the characteristic adipocyte phenotype of large spherical cells containing many lipid-rich vacuoles. This is therefore a longitudinal process with clear chemical changes that Raman spectroscopy should be well suited to characterising.

Two studies have previously used Raman spectroscopy to attempt to characterise adipogenic differentiation. However, these studies used the derivative Raman methods, outlined in section 1.3.2, surface enhanced Raman spectroscopy (SERS) and coherent anti-stokes Raman spectroscopy (CARS). Both of these methods have their drawbacks. SERS is not non-invasive as the sample has to be treated with gold nanoparticles and CARS can only provide excitation at one vibrational frequency at a time, increasing the total time required for analysis. Moody *et al* 2010 (208) used the SERS approach to characterise the adipogenic differentiation of ADSCs over 22 days. The authors also took spectra from uninduced cells to determine which spectral features were unique to differentiating cells. It was found that peaks in the regions 1200-1275 cm^{-1} and 1390-1610 cm^{-1} were the most useful for describing differentiation. However, due to the small laser spot size used (2 μm), many of the peaks in these regions varied greatly in intensity due to differences in the loci from which they were acquired. Further, the authors admitted that the use of gold nanoparticles produced spectra of higher intensity near the endosomes where the particles aggregated and also resulted in weaker spectra over time as the nanoparticles were exocytosed, making their spectra difficult to compare. Finally, no mathematical analysis of the spectra was undertaken to explore the relationship of specific spectral features with one another over time. Mouras *et al* 2012 (209) used CARS amongst other methods to characterise the adipogenic differentiation of ADSCs over 14 days. CARS only provides excitation at a single vibrational frequency at a time and the authors use of CARS in their study was restricted to measuring the intensity of the CH_2 stretch frequency, which is associated with lipids, at 2845 cm^{-1}.

There is very little spectroscopic data on the adipogenic differentiation of stem cells in the literature. However, the adipogenic differentiation process itself is rich in clear chemical transitions that should be well suited to Raman analysis. In this study, adipogenic differentiation was induced in ADSCs over 14 days taking spectra at regular time intervals. As with the previous chapter, the aim was to ascertain if there were any features in the spectra that could be used to predict differentiation, particularly in the early stages of process before the presence of fat droplets became evident by eye.

6.2 Materials and Methods

6.2.1 Analysis of ADSC Adipogenic Differentiation using Raman Spectroscopy

6.2.1.1 Cell Culture

Adipose derived stem cells where purchased from Zen-Bio (Zen-Bio, Research Triangle Park, CA, USA). Each batch was comprised of cells from multiple donors (see Table 8 for details). ADSCs had tested positive for tri-lineage differentiation and the cell surface markers CD44 and CD105 and negative for the cell surface markers CD31 and CD45 prior to purchase. Informed ethical consent was obtained by Zen-Bio prior to isolation and sale. ADSCs from each batch were expanded and prepared separately for Raman spectroscopy as described in the general methods (sections 2.1, 2.2 and 2.5.3). Cells were left 48 hours to adhere then either adipo-induced using adipogenic induction medium supplied by Zen-Bio (DMEM / Ham's F-12 (1:1, v/v), HEPES pH 7.4, foetal bovine serum, biotin, pantothenate, human insulin, dexamethasone, isobutylmethylxanthine, PPARγ agonist, penicillin, streptomycin, amphotericin B (concentrations not supplied)) or cultured in basal medium. This time point was designated as day 0. At day 7, half the adipogenic induction medium was aspirated and replaced with adipogenic maintenance medium, also supplied by Zen-Bio (DMEM / Ham's F-12 (1:1, v/v), HEPES pH 7.4, fetal bovine serum, Biotin, pantothenate, human insulin, dexamethasone, penicillin, streptomycin, amphotericin B (concentrations not supplied)). To assess the effects of Raman spectroscopy and the Raman sampling process itself on ADSCs, an equal number of cultures were maintained in adipogenic or basal medium but did not undergo Raman analysis. Each individual batch of ADSCs was analysed once.

Table 8. List of ADSC multi-donor batches used in the study including the average age of the donors across each batch sample.

Batch	Number of donors	Average age
1	6	51
2	8	44
3	7	44
4	7	32
5	9	48

6.2.1.2 Raman Spectroscopy

Raman spectroscopy was performed using a Renishaw RM series 1000 microscope as described in the general methods (section 2.5.3). Spectra were acquired at days 0, 3, 7, 10 and 14 in both basal and adipogenic culture. The number of spectra acquired and the parameters used are described in section 5.2.1.2.

6.2.1.3 Processing and Analysis of Spectra

Descriptions of the processing and analysis of spectra can be found in section 5.2.1.3 and Appendix A. Outlier removal was not required in the processing of spectra acquired from ADSCs.

6.2.2 The Effect of Raman Spectroscopy on Adipogenic and Cell Stress Marker Gene Expression

RNA isolation and reverse transcription were performed as previously described in the general methods (section 2.3). qRT-PCR was performed using TaqMan gene expression assays (Applied Biosystems, Carlsbad, USA) for peroxisome proliferator-activated receptor gamma (*PPARγ*) and adiponectin (*ADIPOQ*): assay numbers Hs01115513_m1 and Hs00605917_m1 respectively, to determine adipogenic marker gene expression, and *HSF1*, *HIF1* and *LDH* (assay numbers listed in section 5.2.2), to determine cell stress marker gene expression. Gene expression analysis was carried out on ADSC batches 1, 3, and 5 ± testing by Raman spectroscopy at day 0 and at day 14 of basal and adipogenic cultures. Gene

expression was analysed using the same ADSC batches cultured in adipogenic or basal medium. Reactions and analysis were carried out as described in section 5.2.2.

6.2.3 The Effect of Raman Spectroscopy on Lipid Accumulation using Oil Red O Staining

To test for the presence of lipid droplet accumulation within the ADSCs following their differentiation, Oil red O staining was performed on adipo-induced and basal cultured samples ± sampling by Raman spectroscopy after 14 days. Oil red O staining was performed on ADSC batches 2 and 4 cultured in either adipogenic or basal medium. Prior to staining, a 0.5% stock solution of Oil red O was prepared in 100% isopropanol (Sigma-Aldrich, Gillingham, UK). A working solution was created by diluting the stock 3:2 in de-ionised water and filtered prior to use. ADSCs were first washed with PBS then fixed in NBF for 1 hour at room temperature. ADSCs were then washed with de-ionised water, followed by 60% isopropanol and then stained with Oil red O solution for 15 minutes at room temperature. Excess Oil red O stain was washed away with 60% isopropanol. Finally, to stain cell nuclei, samples were stained with Haematoxylin (Sigma-Aldrich, Gillingham, UK) for 30 seconds and the excess stain washed away with de-ionised water. ADSCs were imaged on a Leica DMI6000b microscope (Leica Microsystems, Milton Keynes, UK).

6.3 Results

6.3.1 Characterisation of Adipogenic Differentiation of DPSCs by Raman Spectroscopy

In Chapter 5, the osteogenic differentiation of DPSCs was characterised by Raman spectroscopy and compared with data from previous studies to assess the validity of the newly developed methodology described in Chapter 4. In this study, a less well described differentiation lineage (adipogenesis) was characterised using Raman spectroscopy. Figure 42 depicts the average spectra for each time point (days 0 , 3, 7, 10 and 14 of culture) for ADSCs cultured under adipogenic conditions and in basal culture. There was a clear increase in the intensity of many peaks, including the characteristic CH_3, CH_2 group in lipids at 1302 cm^{-1}, CH_2 in fatty acids at 1441 cm^{-1} and C=C in lipids at 1654 cm^{-1} in spectra from adipo-induced ADSCs after 7 days of induction compared with similar spectra obtained from cells in basal culture.

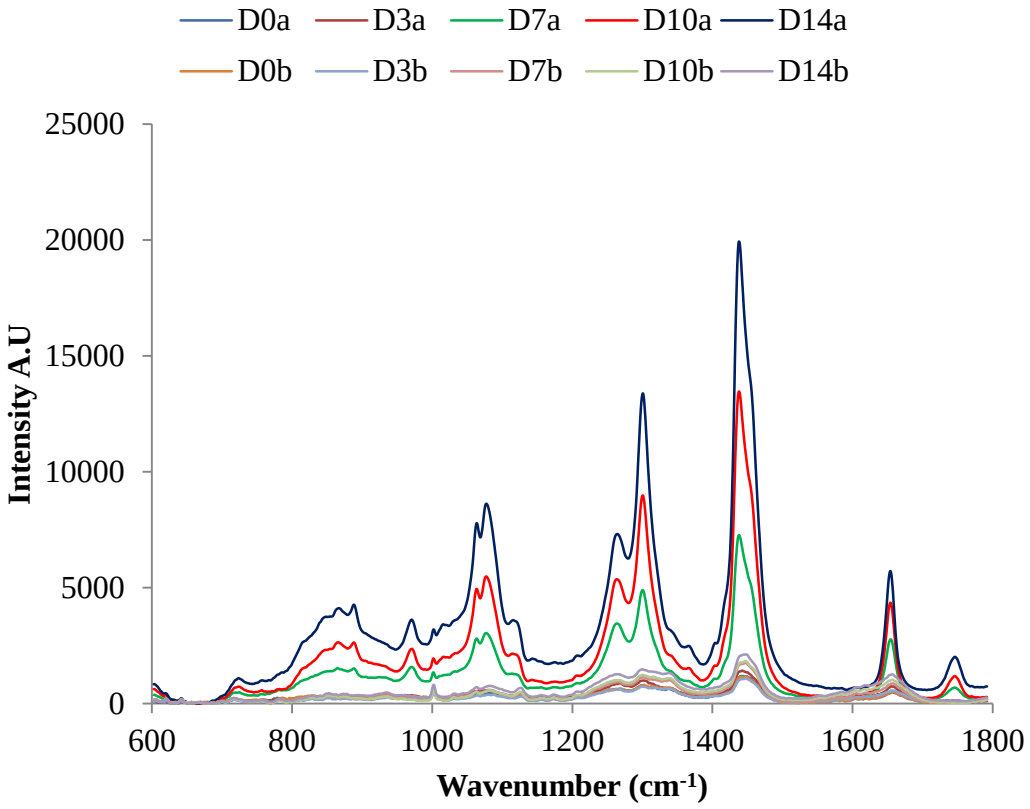

Figure 42. Average background subtracted spectra from adipo-induced (a) and basal cultured (b) ADSCs taken at days 0, 3, 7, 10 and 14, n=75 spectra per time point from 5 multi-donor batches. A pronounced change in spectra from adipo-induced ADSCs can be seen from day 7 onwards whilst spectra from basal cultured ADSCs varied little.

PCA was performed on spectra obtained from 5 ADSC multi-donor batches which had been averaged, *n*=75 spectra at each time point. Figure 43 is a 2D scatter plot of PC1 and PC2 scores accounting for 99.3% and 0.3% of the variation in the data set respectively. There was a clustering of all the spectra from basal cultured ADSCs and the majority of the spectra at days 0 and 3 from the adipo-induced ADSCs (circled in the figure). However, spectra from adipo-induced ADSCs at days 7, 10 and 14 clearly cluster away from this and from one another. This resulted in two trends firstly in PC1 from day 0 to 14, secondly in PC2 from day 0 to 7 and then day 7 to 14.

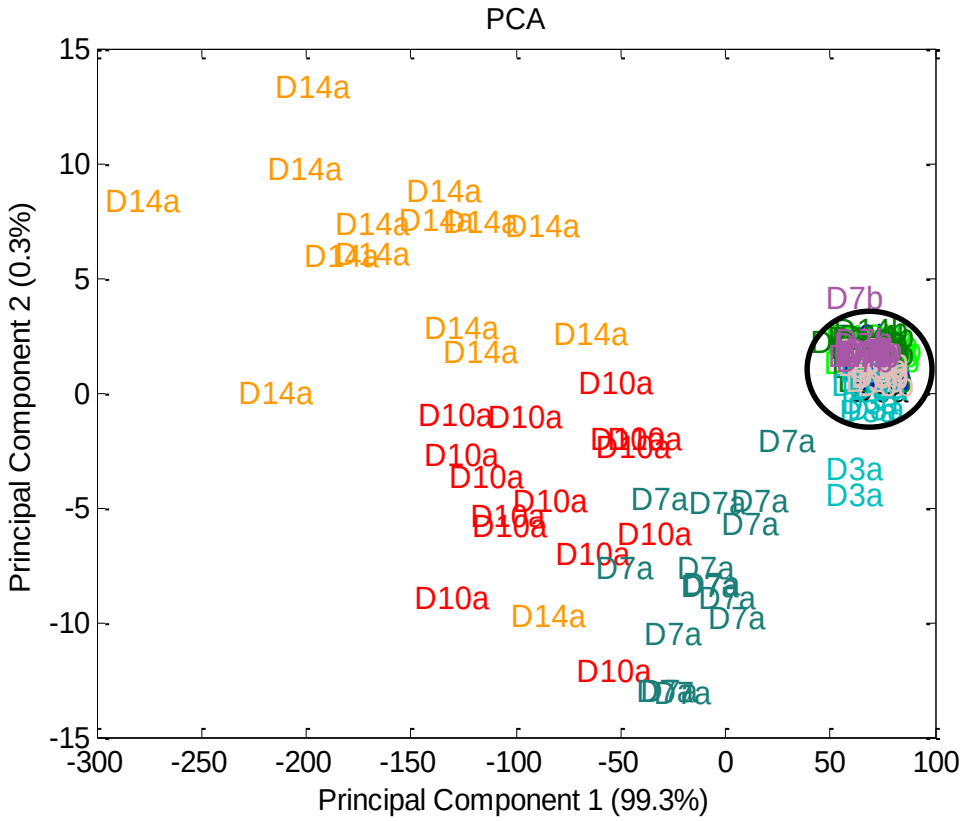

Figure 43. Principal component analysis of spectra acquired from (a) adipo-induced and (b) basal cultured ADSCs at days 0, 3, 7, 10 and 14 of culture. Each point is the average of 5 spectra, one from each multi-donor batch. Circled are all the spectra from the basal cultured ADSCs, indicating no trends in the data with time. Trends can be observed in the spectra from adipo-induced ADSCs in both PC1 and PC2 with increasing time in culture.

In order to ascertain which peaks were responsible for the variation within the principal components, the loadings for each PC were plotted (Figure 44). The loadings for PC1 showed positive peaks for wavenumbers corresponding to C-N

bonds in proteins and lipids (1082 cm^{-1}), CH_3, CH_2 in lipids (1302 cm^{-1}), CH_2 in fatty acids (1441 cm^{-1}) and C=C bonds in lipids (1654 cm^{-1}) whilst wavenumbers corresponding to the nucleic acids guanine and adenine (1417 cm^{-1}) and DNA (1481 cm^{-1}) had negative peaks. Similarly, the loadings plot for PC2 had positive peaks corresponding to C-C bonds in collagen (971.5 cm^{-1}), and amide bonds (1266 cm^{-1} and 1660 cm^{-1}). The assignment of the negative peaks in PC2 is less certain. Putative peak assignments based on Movasaghi *et al* 2007 (97).

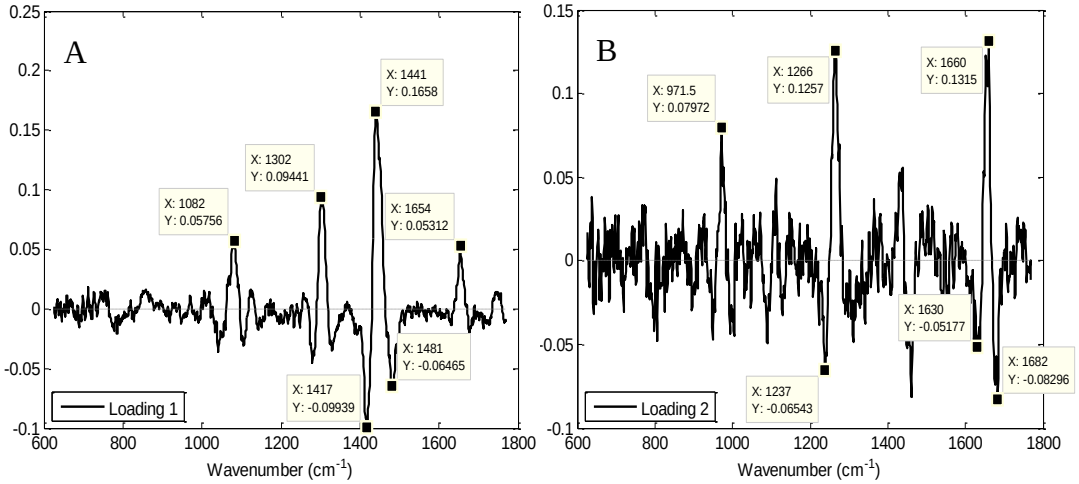

Figure 44. Loadings from the principal component analysis of ADSCs in adipogenic and basal culture, (A) principal component 1, (B) principal component 2. Significant peaks of interest are indicated.

In order to identify the time point at which each peak varied most, the loadings for PC1 and PC2 were plotted against one another (Figure 45). As previously described in Chapter 5, the position of a given wavenumber on the loadings plot when transposed to the original scores plot indicates the samples in which a particular wavenumber varied the most. This demonstrated that the lipid associated peaks in the lower right quadrant of the loadings plot varied the most between days 3 and 7 in spectra from adipo-induced ADSCs found in the same quadrant of the scores plot. Similarly, it was also observed that the protein and nucleic acid associated peaks varied between days 10 and 14 in spectra from adipo-induced ADSCs.

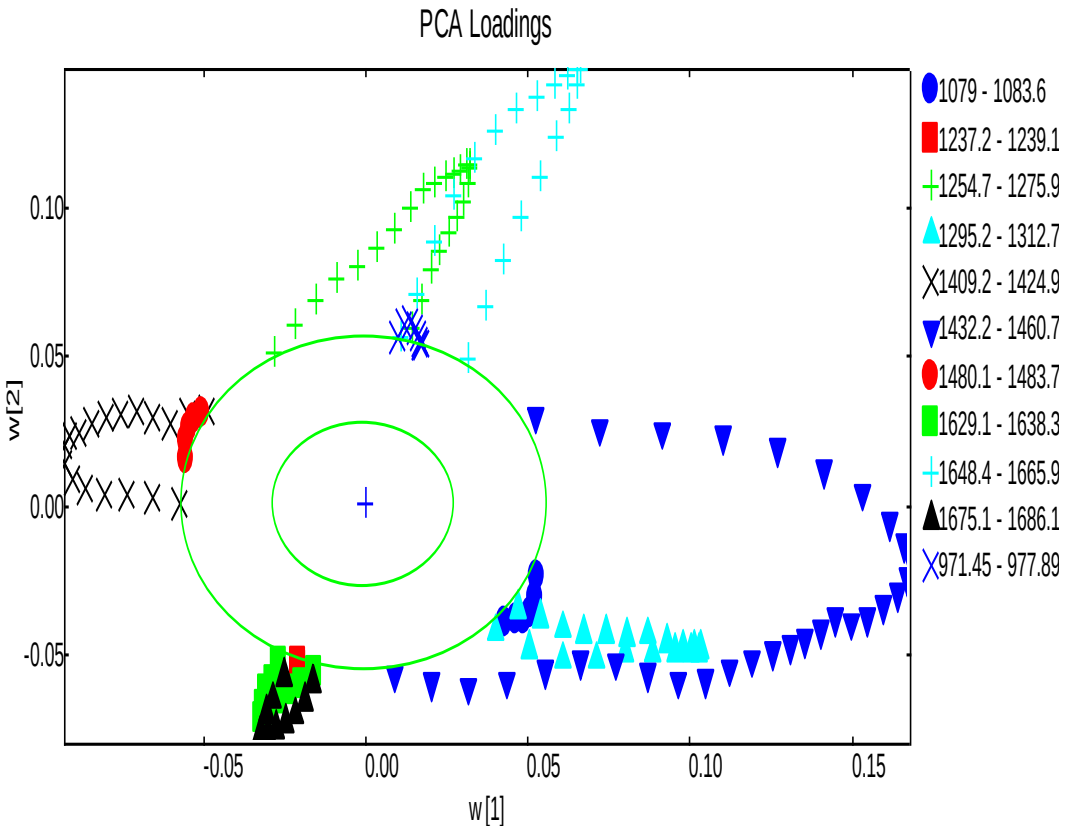

Figure 45. PCA loadings plot for PC1 *versus* PC2, the outer green circle indicates 95% confidence. In the legend are groups of wavenumbers from peaks that vary significantly.

In order to determine if any spectral features were indicative of the early differentiation process, PCA was performed on spectra from ADSCs cultured in adipogenic or basal medium at day 3 (Figure 46). Principal components 1 and 3 were plotted accounting for 44.6% and 5.6% of the variation respectively. All of the spectra from the ADSCs cultured in basal medium and a majority of those from the adipo-induced ADSCs were clustered together. However, a small number of spectra were removed from the main cluster based on contributions from both PC1 and PC3 in the adipogenic culture group.

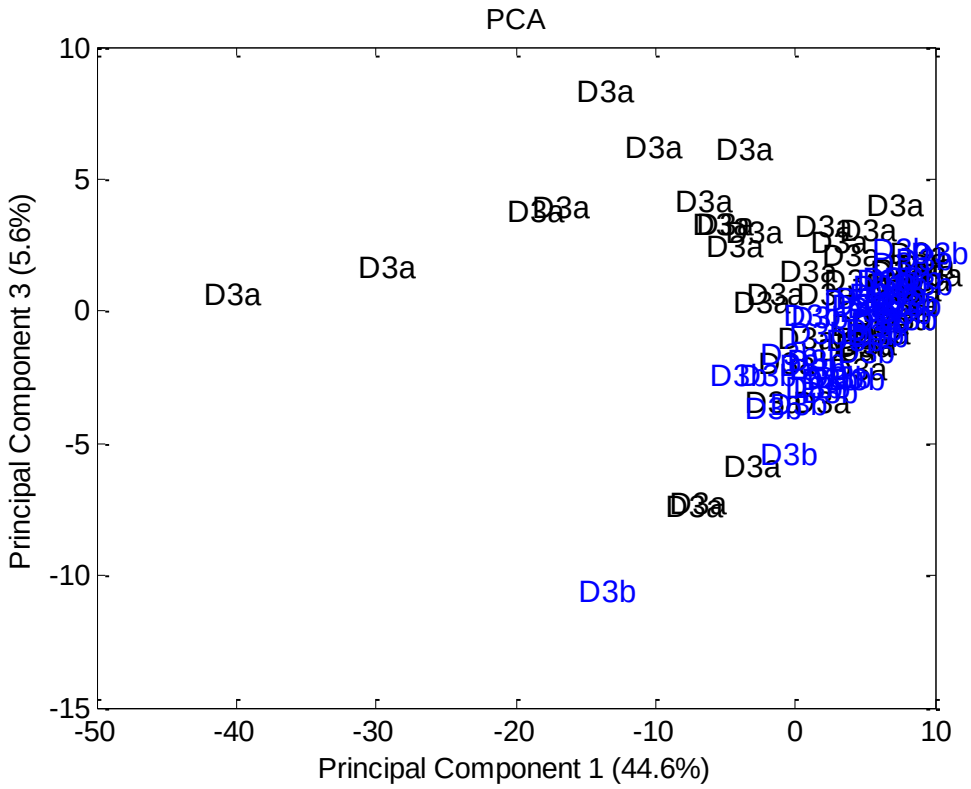

Figure 46. Principal component analysis of spectra from (a) adipo-induced and (b) basal cultured ADSCs after 3 days. It can be seen that even at this very early stage of adipogenic culture, spectra from adipo-induced ADSCs are beginning to cluster away from spectra obtained from cells in basal medium.

The loadings for PC1 and PC3 (Figure 47) highlighted that there were two potential molecular species in the prominent 1430-1460 cm^{-1} region, the first in PC1 at 1452 cm^{-1} and the second in PC3 at 1438 cm^{1}. Based on the review by Movasaghi *et al* 2007 (97) these may represent CH_3, CH_2 in collagen and CH_2 in fatty acids respectively. The remaining peaks in PC1 correspond to phenylalanine (1006 cm^{-1}) and amide bonds (1655 cm^{-1}).

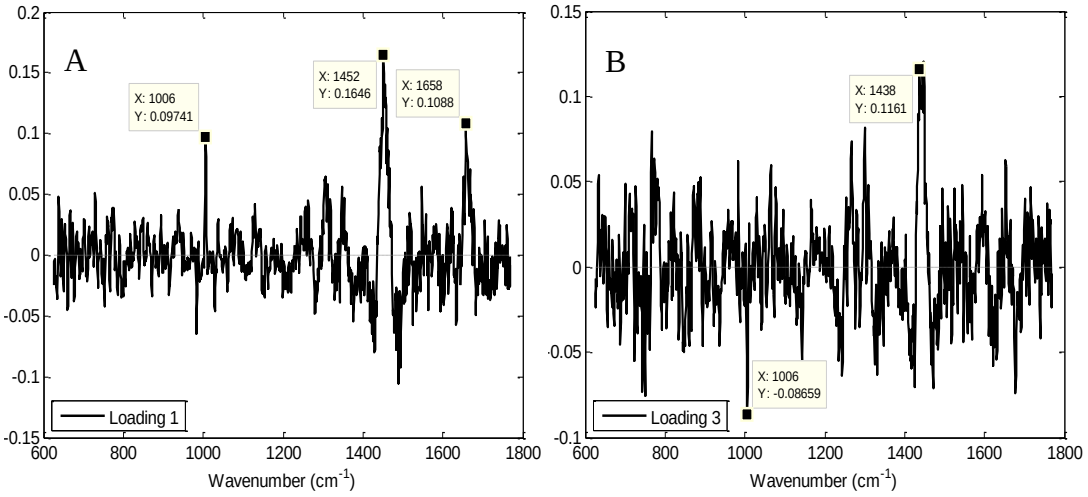

Figure 47. Loadings from the principal component analysis of ADSCs in adipogenic culture and basal medium, (A) principal component 1, (B) principal component 3. Marked are significant peaks of interest.

Finally, three spectra from 14 day, adipo-induced ADSCs were plotted (Figure 48). There was a clear shoulder on the latter portion of the peak in the 1430-1460 cm^{-1} region which further indicated the presence of two separate molecular species in this area.

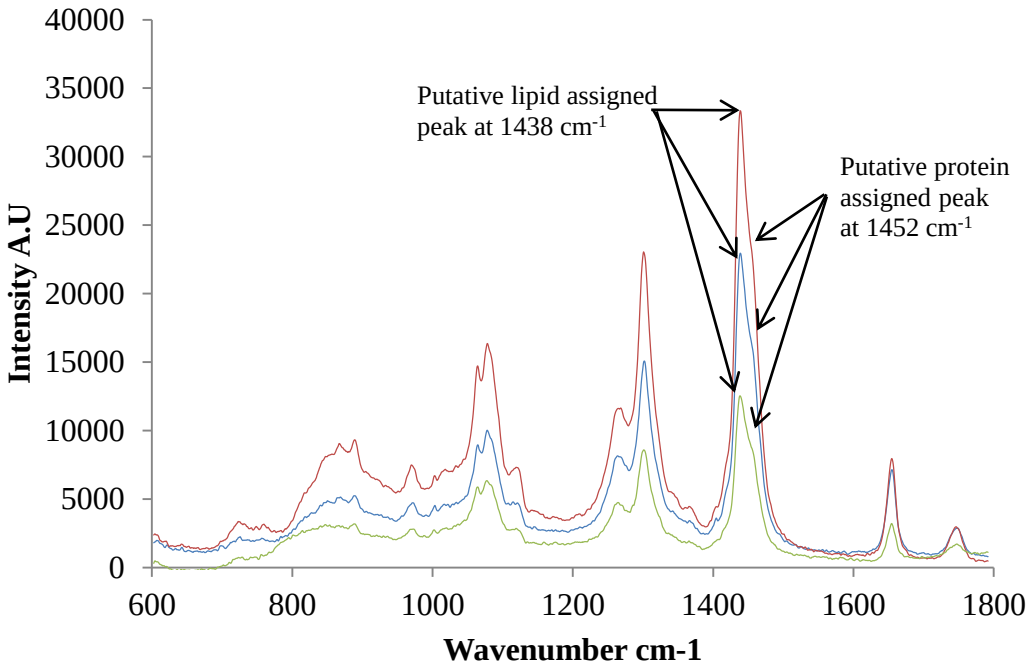

Figure 48. Graph of three background subtracted spectra from adipo-induced ADSCs after 14 days of induction. Indicated are the two putative peaks in the 1430-1460 cm^{-1} region as shown by the shoulder in the latter portion of the region.

6.3.2 Adipogenic Differentiation of ADSCs ± Analysis by Raman Spectroscopy using qRT-PCR and Oil Red O Staining

In order to confirm the adipogenic differentiation of ADSCs the expression of two adipogenic marker genes *PPARγ* and *ADIPOQ* were measured and Oil red O staining used to detect lipid droplet accumulation. Both were also used to determine if the Raman acquisition process had any effect on adipogenesis. Significant increases in *PPARγ* and *ADIPOQ* expression were observed during the culture period irrespective of the Raman acquisition process ($p<0.001$ for *PPARγ*, *ADIPOQ* was undetectable at day 0). However, there was significantly less expression of *PPARγ* and *ADIPOQ* in ADSCs that had been subjected to Raman analysis compared with those that had not been analysed by Raman ($p<0.01$ and $p<0.001$ respectively).

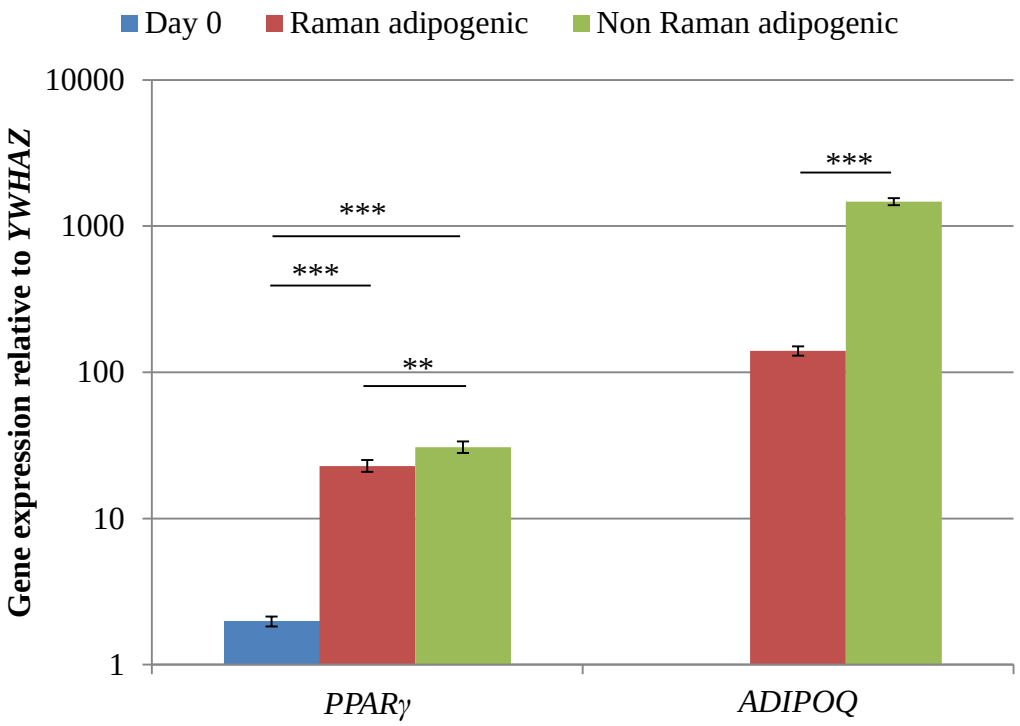

Figure 49. A comparison of ADSC adipogenic marker gene expression at day 0 and day 14 from ADSCs in adipogenic culture that had/had not undergone Raman spectroscopy. Results show mean ± SE (n=9). *** p<0.001, ** p<0.01. Statistical significance was determined using a one-way ANOVA. Significant increases in the expression of both genes was found between days 0 and 14, however, there was also a significant difference in the expression of both genes between cells that had undergone Raman spectroscopy compared with those that had not.

The expression of both marker genes was also analysed in ADSCs cultured in basal medium. A significant decrease in the expression of *PPARγ* was observed after 14 days irrespective of the Raman acquisition process ($p<0.001$). However, no significant differences in the expression of either gene were observed between ADSCs that had/had not undergone Raman analysis.

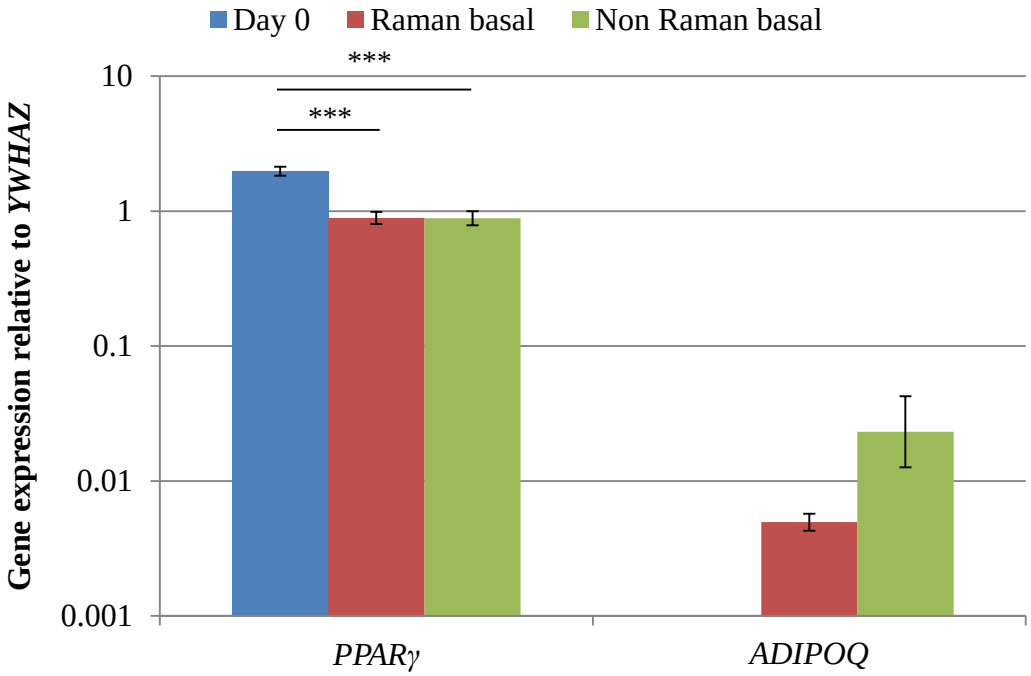

Figure 50. A comparison of ADSC adipogenic marker gene expression at day 0 and day 14 from cells cultured in basal medium that had/had not undergone Raman spectroscopy. Results show mean ± SE (n=9). *** p<0.001. Statistical significance was determined using a one-way ANOVA. No significant differences in the expression of either marker gene was detected between cells that had undergone Raman spectroscopy compared with those that /had not.

Oil red O staining confirmed the presence of lipid droplets in adipo-induced ADSC cultures after 14 days regardless of whether the cells had undergone Raman analysis or not (Figure 51). No lipid droplets were detected in the basal cultured ADSCs (Figure 52).

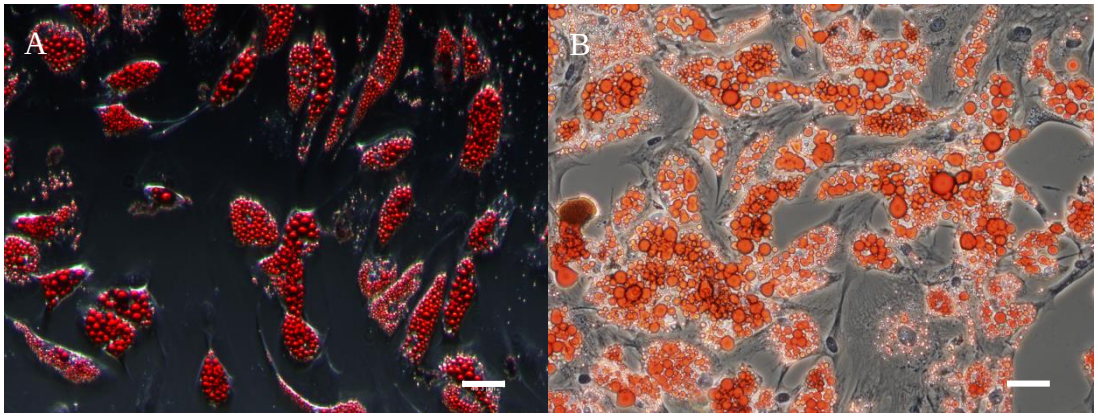

Figure 51. Oil red O staining of ADSCs after 14 days of adipo-induction for cells that A) had undergone Raman measurements and B) had not undergone Raman measurements. Scale bars = 50 µm. Positive staining of lipid droplets was observed regardless of whether ADSCs had undergone Raman spectroscopy or not.

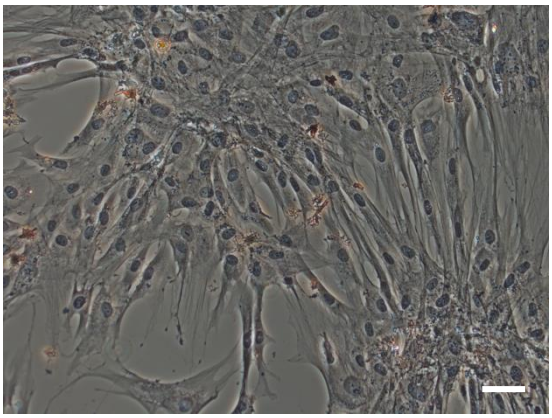

Figure 52. Oil red O staining of ADSCs after 14 days of culture in basal medium. Scale bar = 50 µm. No lipid droplet accumulation was observed.

6.3.3 Comparison of Cell Stress Marker Gene Expression Between ADSCs ± Analysis by Raman Spectroscopy using qRT-PCR

The expression of the three cell stress markers *HIF*, *LDH* and *HSF* was determined to test if the Raman sampling process had induced any cell stress response as described in section 5.3.3. The expression of all three markers was significantly increased for ADSCs cultured under adipogenic conditions for 14 days regardless of Raman sampling, $p<0.001$, with the exception of *HIF* in ADSCs that had not undergone Raman analysis (Figure 53). However, there were conflicting differences in the expression of the three markers between ADSCs from the Raman and non-Raman groups. There was a significant increase in the expression of *HIF*, $p<0.001$, in ADSCs that had undergone Raman, a significant decrease in the expression of *LDH*, $p<0.001$ and no difference was observed in the expression of *HSF*.

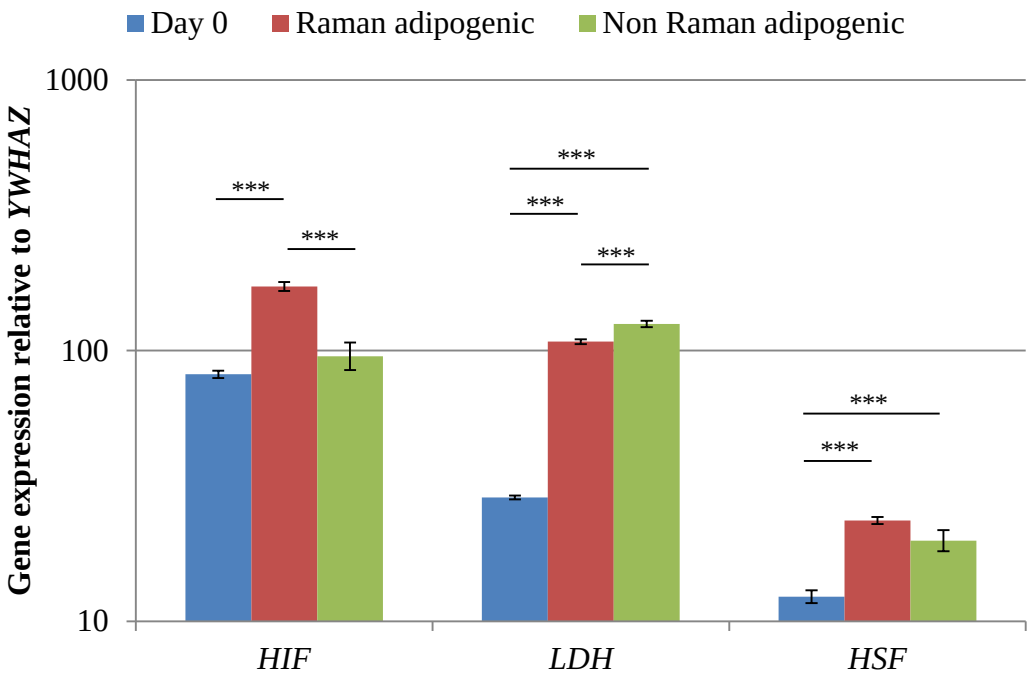

Figure 53. A comparison of ADSC cell stress marker gene expression for cells cultured under adipogenic conditions at day 0 and day 14 ± Raman analysis. Results show mean ± SE (n=9). *** p<0.001. Statistical significance was determined using a one-way ANOVA. Significant up-regulation of all stress marker genes was observed after 14 days in adipogenic culture regardless of whether the cells had undergone Raman spectroscopy (with the exception of *HIF*). Significant differences in the expression of *HIF* and *LDH* were also observed between the Raman and non-Raman groups.

6.4 Discussion

The aim of this study was to characterise the adipogenic differentiation of ADSCs by Raman spectroscopy using the aseptic methodology developed and described in Chapter 4. In Chapter 5 it was shown that this methodology was capable of generating data in agreement with the published data using Raman spectroscopy in characterising osteogenic differentiation. In this study, adipogenesis was selected for characterisation as spectroscopic data in the literature is sparse for this differentiation lineage.

PCA was performed on spectra acquired from ADSCs throughout the adipogenic differentiation process during 14 days of adipogenic culture. The PCA scores plot for PC1 *versus* PC2 demonstrated a continuous trend in PC1 from day 0 to day 14 and a trend in PC2 from day 0 to day 7 followed by a trend from day 7 to day 14. PC1 encompassed the vast majority of the variation in the data set (99.3%). When the loadings for PC1 were plotted, it was found that several peaks indicative of lipids and fatty acids were behaving in a similar fashion whilst peaks indicative of nucleic acids were behaving in an opposing manner. PC2, whilst only accounting for 0.3% of the variation in the data set, was found to be comprised of peaks relating to protein content. When the loadings for PC1 and PC2 were plotted against one another, it was demonstrated that lipid associated features were most variable early on in the differentiation process, between days 3 and 7. Features associated with nucleic acid and protein varied most at the end of the process, at day 14. This is broadly in agreement with the study by Moody *et al* 2010 (208) who also determined that peaks in the region 1390-1610 cm^{-1} varied most during the adipogenic differentiation process, many of which were also found to vary in this study. The spectra from ADSCs cultured in basal medium varied little over the course of 14 days and those spectra formed a tight cluster upon PCA analysis underlining the lack of variation in these cells in the absence of inductive cues. Finally, to ascertain if any spectral features may have been predictive of the differentiation process, PCA was performed on spectra from ADSCs cultured under adipogenic and basal conditions after 3 days of culture. The results indicated that spectra from the adipo-induced cells were beginning to cluster away from spectra obtained from cells cultured in basal medium. The loadings indicated that this was

due to a single lipid associated peak at 1438 cm^{-1}. This analysis also indicated a novel finding that there is likely two closely related molecular species in the region 1430-1460 cm^{-1}, a region that is often taken to be a single peak indicative of proteins. Confirmation of MSC adipogenic differentiation using conventional techniques such Oil red O staining or qRT-PCR usually occurs between 7 and 21 days (52, 55, 139), the Raman spectra in this study indicate that adipogenesis can be detected several days earlier and in a non-invasive manner.

As previously described for osteo-differentiation in Chapter 5, qRT-PCR and histological staining were used to confirm that adipogenic differentiation had occurred over the culture period and to determine if the process had been perturbed by the Raman sampling method. There was a significant increase in the expression of both *PPARγ* and *ADIPOQ* following 14 days of adipogenic induction and Oil red O staining confirmed that adipo-induced ADSCs had produced lipid-rich vacuoles. A mature adipocyte phenotype was therefore observed in adipo-induced ADSCs irrespective of whether or not they had undergone Raman analysis but the expression levels of adipogenic marker genes was significantly reduced in ADSCs that had undergone Raman analysis. This was most prominent in an approximately 10 fold reduction in the expression of *ADIPOQ*, however, it is difficult to ascertain if this reduction in gene expression was biologically significant as a mature adipocyte phenotype (the presence of lipid-rich vacuoles) was observed. It is widely accepted that there is a dysregulation of adipogenesis and the associated marker genes in obesity as a result of hypoxia (210). Indeed, several studies have demonstrated that *ADIPOQ* expression is reduced under both persistent or intermittent hypoxia (211-213) such as might be anticipated during prolonged Raman sampling. Furthermore, the increased expression of *HIF1* as a result of hypoxia has been shown to directly reduce the expression of *ADIPOQ* by adipocytes (214) whilst inhibition of *HIF1* has been shown to increase *ADIPOQ* expression (215). In this study *HIF1* expression was significantly increased in ADSCs that had undergone Raman analysis compared with those that had not. Therefore the increased expression of *HIF1* in ADSCs that had undergone Raman analysis may have caused the observed decrease in the expression of *ADIPOQ* and may also have been further exacerbated directly by hypoxic conditions.

LDH and *HSF* were the other two cell stress markers assessed in this study and both were up-regulated in ADSCs after 14 days of induction regardless of whether the cells had undergone Raman analysis. *LDH* expression is known to be stimulated by the expression of *HIF1* (201). However, this does not explain the observed increase expression of *LDH* in ADSCs that had not undergone Raman sampling where *HIF1* expression was not up-regulated, indicating that some other factor must have been responsible for this observation. Glucose is required for fatty acid synthesis by adipocytes. However, glucose metabolism can also result in the production of lactate and it has been shown that in older adipocytes with high fat content that there is a shift toward producing more lactate from glucose as opposed to fatty acids (216, 217). In order to metabolise any excess lactate there would need to be a concomitant increase in lactate dehydrogenase production and this may explain the observed increase in its expression and may also indicate that the ADSCs may have been overstimulated. Finally, given that adipocytes are a key cell type in energy metabolism and that *LDH* is also involved in energy metabolism, with hindsight, *LDH* is likely a poor choice of cell stress marker for this study. There is little data in the literature indicating a role for *HSF* in adipocytes or adipose tissue, healthy or otherwise, so the reason for the up-regulation of *HSF* observed after 14 days of induction is unclear. However, it can be concluded that this was not due to the Raman sampling process as there was no significant difference in the expression of *HSF* between ADSCs that had/had not undergone Raman analysis.

Chapter 7

Discussion

The field of tissue engineering and regenerative medicine has evolved rapidly in the last two decades. The core aim of the field is to enhance the body's innate healing capacity using a combination of bioactive scaffolds, cells and chemical and physical cues to achieve improved clinical outcomes for patients. To this end there are numerous active clinical trials for the treatment of a plethora of conditions using what could be described as tissue engineering/regenerative medicine based approaches. Of these clinical trials 411 are listed as MSC based therapies on clinicaltrials.gov (as of July 2014). Despite this, there is a shortage of techniques that are capable of characterising cells in a non-invasive manner. Development of such a technique would offer the following benefits for cell based therapies:

1. Improved safety, as the cells used would be those that were characterised. This would add a layer of quality control in the development of cell based therapies.
2. Easier passage through EU regulatory approval as the use of a non-invasive cellular characterisation methodology on those cells to be implemented in a cell based therapy could be considered minimally manipulated.
3. Reduced costs to implement as current techniques rely on expensive reagents such as antibodies conjugated with fluorophores and DNA primers/probes.
4. Reduced quantity of cells (which can be a scarce resource) required due to the fewer number of experiments required.
5. Reduced time required to carry out characterisation saving both time and money.

There are many techniques currently being investigated that would permit the non-invasive characterisation of cells, many of which are spectroscopic approaches (82, 83, 218-220). Spectroscopy itself is simply the study of the interaction between electromagnetic radiation (light) and matter. Different forms of spectroscopy utilise almost every aspect of the electromagnetic spectrum. Raman spectroscopy typically operates in the near infra-red region of the spectrum, at least when used in cellular characterisation and is capable of providing a "chemical fingerprint" of a sample

based on the molecular bonds contained within (135). As such Raman spectroscopy is well suited to detecting differences between cell cultures or differences over time within the same cell culture. There have been many studies that have used Raman spectroscopy to characterise cell viability, differences in cell type and cell differentiation (99, 101, 102, 104, 128-134) as described in section 1.5. However, to date, there have been very few studies where the sterility of the cell cultures used was not compromised. Maintaining cell sterility throughout analysis using Raman spectroscopy is required for the technique to be considered truly non-invasive otherwise the cells analysed could not subsequently be used. The aim of this project was to develop a method that would permit the acquisition of repeated Raman measurements from the same cell cultures over time and to validate this method by using it to characterise stem cell differentiation compared with conventional methodologies.

7.1 Development of an Aseptic Method for Longitudinal Stem Cell Characterisation by Raman Spectroscopy

The objective addressed in Chapters 3 and 4 was the development of a novel method for the acquisition of Raman spectra that was aseptic and non-invasive. Specifically in Chapter 3 a material that was suitable for Raman spectroscopy and did not interfere with the osteogenic differentiation of DPSCs was assessed. In Chapter 4 an enclosed cell culture system that remained aseptic throughout Raman measurements was developed.

Previous studies have used a range of materials as substrates for cell culture in order to perform Raman spectroscopy. These include quartz, MgF_2 and CaF_2 as discussed (100, 101, 128) in section 3.1. The rationale for the use of these materials is two-fold; firstly, they are inorganic in nature and so possess minimal Raman signal in the region of interest for cells and secondly they cause little background fluorescence as they contain few impurities. However, there is little data in the literature regarding the effects on stem cells associated with their culture on these substrates as most cell culture is routinely performed on treated polystyrene surfaces. In Chapter 3 the proliferation, viability and osteogenic differentiation of DPSCs cultured on quartz or MgF_2 was compared with DPSCs cultured on tissue

culture plastic. It was found that proliferation and viability of DPSCs was unaffected by culturing on quartz or MgF_2. However, gene expression analysis and Alizarin red staining demonstrated that the osteogenic differentiation of DPSCs was reduced on both quartz and MgF_2, though this effect was far greater in DPSCs cultured on MgF_2. This effect could not be attributed to the dissolution of ions into the cell culture medium but may have been due to differences in the surface chemistry and nano-topography of quartz and MgF_2 compared with tissue culture plastic. Nevertheless, tissue culture plastic is unsuitable for Raman spectroscopy applications so quartz was selected as the substrate of choice for the remainder of the project.

There are many studies in the literature where Raman spectroscopy has been used to characterise cells (99, 101, 102, 104, 128-134). However, almost all of these studies compromised the sterility of their cells in acquiring spectra. There are advantages to working in a non-sterile manner, such as reducing the working distance between the microscope objective and sample therefore increasing the amount of Raman signal collected. Smaller working distances also mean that a very high magnification microscope objective can be used, permitting the study of intracellular organelles. However, if cells are to be used after analysis by Raman spectroscopy they must remain sterile. The objective in Chapter 4 was to design a novel cell culture method that would permit this. Three different approaches were investigated.

The first approach attempted was to culture cells on a quartz disc mounted on a quartz platform within a petri dish. This was unsuccessful as a Raman signal from the plastic petri dish could still be detected. The second approach was to culture cells on the inside of a quartz cuvette and this failed due to too long a working distance reducing the intensity of the Raman signal collected. This was likely due to the thickness of the quartz cuvette. Baldwin and Batchelder (189) showed that when acquiring spectra through an interface as the interface gets thicker, then a lower magnification and numerical aperture microscope objective must be used, however, this increases the working distance and therefore reduces the amount of Raman signal collected. Finally, cell culture flasks that had been modified with quartz windows were investigated and found to allow the collection of the greatest amount

of Raman signal from the cells compared with the previous two methods. This approach then went through several rounds of optimisation to select the microscope objective and exposure parameters that resulted in the best possible Raman signal being acquired. There is little data in the literature where high quality spectra have been acquired from cells under sterile conditions, most likely due to the difficulties in satisfying both criteria. It is unclear whether the method described here in Chapter 4 permits the acquisition of the best possible Raman spectra from cells. However, the spectra acquired were comparable to those in the literature acquired from cells under non-sterile conditions as evidenced by the detection of many commonly detected biologically associated features in the spectra (Figure 54).

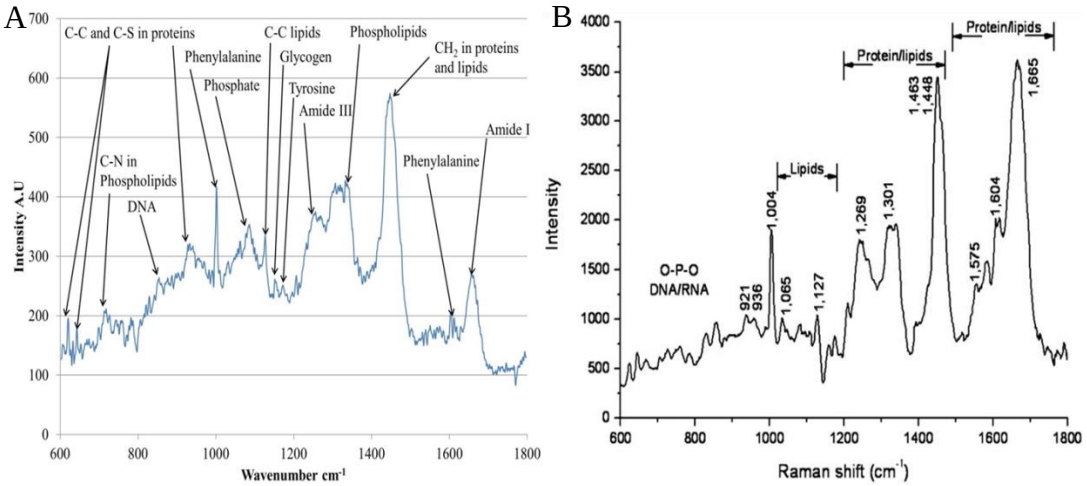

Figure 54. A comparison of spectra from A) undifferentiated DPSCs cultured using the aseptic methodology developed and described in Chapter 4, B) undifferentiated bone marrow-derived MSCs reproduced from (134). Whilst there are differences between the two spectra there are also similarities including many peaks typical of spectra acquired from biological samples such as phenylalanine at ~1000 cm^{-1}, CH_2 in proteins at ~1450 cm^{-1} and amide I at ~1660 cm^{-1}.

7.2 Validation of the Aseptic Method using Raman Spectroscopy to Characterise Stem Cell Differentiation

The objective in Chapters 5 and 6 was to validate the novel cell culture method developed in the previous chapters by using Raman spectroscopy to characterise the differentiation of a well-studied lineage, osteogenic differentiation followed by its use to study a less well studied lineage, adipogenic differentiation.

The characterisation of the osteogenic differentiation process using Raman spectroscopy was carried out in Chapter 5. Several published studies using a non-sterile method provided a guide as to the spectral features to expect to detect (101, 104, 129, 132-134). However, the presence/absence of particular peaks might be considered to be only the most basic indicator. The data sets in this thesis contain ~800 spectra from various time points during differentiation and each spectrum contains ~1200 variables (the wavenumbers which relate to particular molecular species). In order to derive meaningful information from such a large multivariate data set its dimensionality must be reduced, decreasing the number of variables whilst retaining as much information as possible. PCA is ideal for this task as it combines variables into principal components according to how much their variation affects the data set as a whole. PCA was used here to better describe the changes in the cell spectra as the differentiation process progressed. It was found that the early stages of osteo-differentiation were characterised by changes in two peaks associated with molecular species commonly found in proteins and more specifically in fibrillar collagen. It is known that stem cells undergoing osteogenic differentiation first produce a collagen rich extracellular matrix prior to mineralisation. It is possible that this is what was detected and that this feature could be used as an early indicator of osteo-differentiation before the result becomes evident by the emergence of mineralised nodules. In Chapter 6 the adipogenic differentiation process was characterised. As with the previous chapter, PCA was again used to describe changes in the spectra over time. It was found that spectral features that related to molecular bonds found in lipids and fatty acids varied throughout the 14 days of adipo-induction. However, a single peak in the day 3 spectra associated with fatty acids was found to distinguish a number of the spectra acquired from adipo-induced ADSCs from the spectra acquired from the ADSCs cultured under basal conditions. As such the emergence of this peak may serve as an early indicator of adipogenic differentiation prior to the later emergence of readily observed large lipid-rich vacuoles.

The main objective of Chapters 5 and 6 was to demonstrate that Raman spectroscopy could be used to characterise the osteogenic and adipogenic differentiation of stem cells in an aseptic culture environment. In addition, qRT-PCR and histochemical staining were used to confirm that differentiation had occurred

and if the sampling process had had any effect on differentiation. Significant up-regulation in the expression of both osteogenic and adipogenic marker genes was observed at the end of their respective induction and Alizarin red and Oil red O staining were both positive regardless of whether the cells had undergone analysis by Raman spectroscopy. There was no difference in osteogenic marker gene expression between DPSCs that had/had not undergone Raman analysis indicating that neither Raman spectroscopy or the sampling protocol had apparently affected osteogenic differentiation. However, the expression of adipogenic markers genes was *significantly* reduced in ADSCs that had undergone Raman spectroscopy compared with those that had not. Potential reasons for this were discussed in section 6.4, however, the reduction in gene expression was unlikely to be *biologically* significant as evidenced by the prominent Oil red O staining observed in ADSCs that had undergone Raman analysis. A recent review by Vogel and Marcotte 2012 (221) explored the relationship between mRNA and protein production and reported that only 40% of the variation in protein levels can be attributed to mRNA levels the rest resulting from post-transcriptional regulation, indicating that changes in mRNA levels may not result in altered cellular phenotype. The expression of a panel of cell stress marker genes was also measured by qRT-PCR in both studies. There was no significant variation in marker gene expression in DPSCs undergoing osteogenic differentiation and expression was not affected by Raman sampling. However, statistically significant variations were observed in ADSCs undergoing adipogenic differentiation potential reasons for which were discussed in section 6.4. This indicates that differences in either the source of the MSCs used or in the differentiation lineage/differentiated phenotype may have influenced a cell stress response.

In this study, characterisation of osteogenic differentiation was carried out using DPSCs. Characterisation of adipogenic differentiation was carried out using ADSCs. Both cell types have a known propensity towards to their respective osteo and adipogenic lineages (192, 222). It is well known that MSCs derived from different sources such a bone marrow, adipose, or dental pulp possess slightly different properties (223-225). Aside from the noted differences in differentiation capacity toward a given lineage, MSCs from different sources can also vary in their cell surface antigen profile and immunosuppressive capabilities (225-227). It has

recently been shown that hypoxic culture conditions can improve the proliferation and differentiation of MSCs (228) and more recently that the response to hypoxia varies between MSCs derived from different sources (229). This indicates that the difference in MSCs used between the osteogenic and adipogenic studies in Chapters 5 and 6 may have influenced the observed difference in cell stress response. There are also differences in phenotype between osteoblasts and adipocytes. Although closely related lineages, differentiation towards an osteoblast phenotype usually occurs at the expense of the adipocyte phenotype and vice versa (230). This is thought to be due to the up-regulation and activity of the two transcription factors *PPARγ* and *RUNX2* which up-regulate adipogenesis and osteogenesis respectively whilst suppressing the expression of the other transcription factor (231-233). This highlights the divergence between the two phenotypes which is further increased upon terminal differentiation.

7.3 Future Work

This project was a proof of principle study, testing the hypothesis that stem cell differentiation could be characterised over time using Raman spectroscopy in an aseptic cell culture environment. Stem cells were cultured and differentiated in monolayer culture as this represented the simplest most predictable/reproducible cell culture modality. As discussed in section 1.1 tissue engineering approaches use one or more of cells, scaffold materials, physical and chemical cues in formulating potential treatment strategies. Therefore an interesting future study would be to characterise stem cell differentiation on a range of scaffold materials using Raman spectroscopy where differentiation was guided either by the scaffold itself or the cell culture medium. However, this would present some challenges:

1. The cell culture system would need to be redesigned to accommodate the scaffold material.
2. The Raman signal from the scaffold may obscure the Raman signal of the cells.

The design of a new cell culture vessel would depend entirely on the scaffold material being used, something that works for a solid glass ceramic is unlikely to be suitable for a hydrogel. Figure 55 depicts a potential method for acquiring Raman spectra from cells cultured on a glass ceramic scaffold. In this instance the scaffold

would be placed on an O-ring within the vessel. The reasons for this are two-fold, first to allow perfusion of the medium to all parts of the scaffold so reducing the likelihood of cell death and second to position the scaffold as close as possible to the microscope objective. The struts of the O-ring would need to be reasonably tall and the vessel itself reasonably thin as the working distance to the scaffold would need to be as small as possible to permit the use of higher magnification microscope objectives. The lid of the vessel would need to be removable or the vessel itself modified to permit changing of the cell culture medium. Whether removable or not, the lid would need to be thin so that Raman spectra could be taken through it. Finally the vessel should be fabricated from quartz or another material the generates minimal Raman signal.

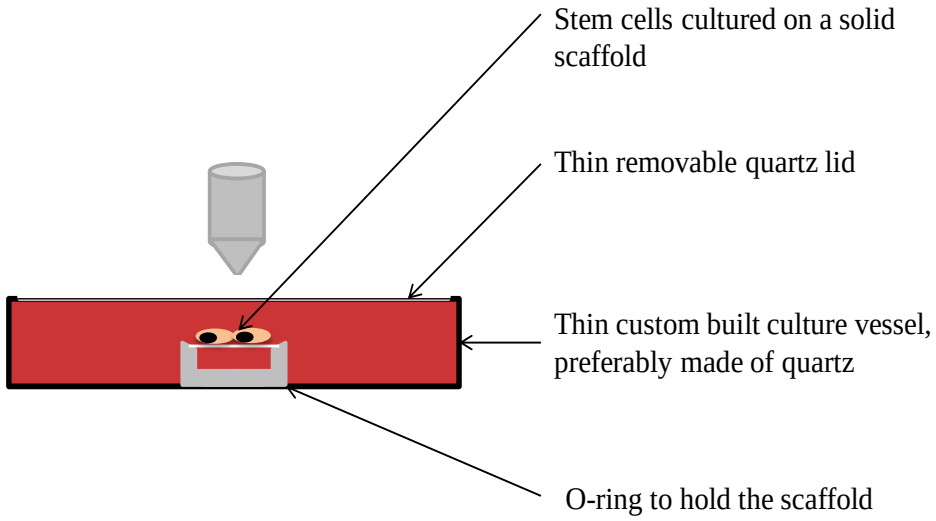

Figure 55. A schematic of a potential aseptic cell culture system for acquiring Raman spectra from cells cultured on a solid scaffold.

Clearly the system just described or the one developed and described in this thesis would not work for cells encapsulated in an amorphous hydrogel. In the case of cell/hydrogel constructs it would be possible to pass them through a quartz capillary (Figure 56). Again the walls of the capillary would need to be thin so that spectra could be acquired through them. Additionally the capillary would need to be sealed at the ends which means they would be single use, the constructs being transferred into a fresh capillary each time they are analysed.

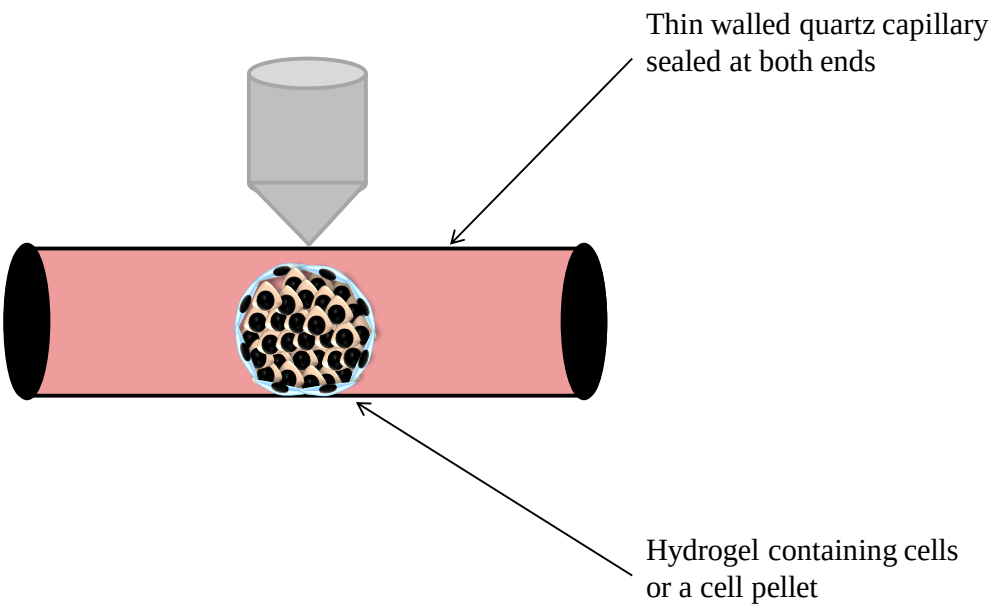

Figure 56. A schematic for a potential method to acquire Raman spectra from a cell pellet or cells encapsulated in a hydrogel.

The other major issue when acquiring Raman spectra from cells cultured on scaffolds is accounting for the Raman signal generated by the scaffold itself and delineating this from the signal generated by the cells and their ECM. The first point to consider is whether the scaffold produces Raman peaks in regions that will most likely be used to characterise the cells. For example bioactive glass ceramic scaffolds can contain hydroxyapatite to facilitate stem cell differentiation down the osteogenic lineage (234). MSCs following osteo-induction will produce far less hydroxyapatite in the form of mineralised nodules than would be contained within the scaffold and it would therefore be difficult to attribute any hydroxyapatite associated peaks in the spectra as being the result of cellular differentiation. This leads to the second point, that of the processing of spectra from cell/scaffold constructs. Processing of Raman spectra generally requires a subtraction of the background signal. In the case of a cell/scaffold construct spectra of an unseeded scaffold within the sampling vessel would serve as the background. However, due to sampling geometry and localised differences in the chemical composition of the scaffold between sampling loci there would likely be small differences in each background spectrum obtained. This could in part be ameliorated by using an average of the background spectra, however, the sample chemistry of the scaffold beneath each cell from which a spectrum is acquired will still vary and contribute to the cell spectrum.

An approach that would help tackle both the problems discussed would be the incorporation of a completely sterile enclosure around the entire microscope. Such chambers are readily available from several manufacturers and permit control over temperature, oxygenation and humidity similar to an incubator. Control over these factors could help mitigate any cell stress response. However, if the chamber was also a glove box with an airlock (Figure 57) samples could be worked on directly with higher magnification microscope objectives without compromising sterility, removing the need for *de novo* culture vessels. As higher magnification/numerical aperture microscope objective produce a smaller focal volume contributions to spectra from a scaffold could be reduced. In order for this to be implemented as a quality control method for the production and characterisation of stem cells for patient use the equipment and method would have to be designed with adherence to good manufacturing practice (GMP) in mind.

Figure 57. Image of a glove box that could be placed around a Raman microscope the direct acquisition of Raman spectra from sterile cells. Image from http://www.laboratory-supply.net/gloveboxes/isolation_glovebox.html

7.4 Implications of Aseptic, Non-invasive Stem Cell Characterisation using Raman Spectroscopy

Raman spectroscopy already has proven utility in discriminating between different cell types and the characterisation of cells as discussed in section 1.5. Methods such as immunofluorescence and qRT-PCR are currently widely used in this regard. Raman spectroscopy however is non-invasive and non-destructive, so cells remain alive and no labels are added. The capacity to do this under aseptic conditions is a key advance in promoting Raman spectroscopy as an alternative to conventional methods in cellular characterisation as this means that cells are not only analysed but can be retained for further use. This project has demonstrated that despite the limitations of working with an aseptic culture environment (reduced Raman signal from increasing the working distance between sample and microscope as well as acquiring spectra through a quartz interface) the spectra produced are still of comparable quality to those taken in a non-sterile environment. This may encourage future investigators not to forsake culture sterility in favour of maximising Raman signal.

As part of a separate project under the supervision of Avacta Group plc, the industry CASE sponsor of this project, a hypothetical business plan concerning the application of Raman spectroscopy to cellular characterisation was developed. The full report can be found in Appendix B, herein lies a summary. The plan was not intended as a formal business plan but an aspirational outline for a Raman spectroscopy based product including all its potential applications, target market, risk factors and costings. Two target markets were identified, the research community and the health care sector. This was based on the product's ability to monitor cellular phenotype and differentiate between cells of different phenotypes. Such abilities would permit the live monitoring of stem cell differentiation status, something that would be of great use to the research community and the detection of cancerous cells which differ in phenotype to the surrounding cells within a biopsy, which would be of use to the health care sector. In order to achieve this several technologies would need to be developed. This includes software that can reliably and reproducibly conduct pre-processing and analysis of Raman spectra, automation of the system such that it can acquire spectra from the desired area of the cell/sample

and development of an aseptic environmentally contained sampling area such as that described in section 7.3. It was shown that such a product could also offer significant savings in time and money when compared with current techniques used to achieve the same ends. However one of the greatest risks to the development of a Raman spectroscopy based product would be convincing the target market to adopt the technology, particularly as it is an unfamiliar technique to the end users.

7.5 Conclusion

The development of techniques capable of non-invasive and non-destructive cellular characterisation is a key target in tissue engineering and regenerative medicine. Building on previous work, this thesis has shown that Raman spectroscopy can be used in such a capacity whilst also maintaining the sterility of the cell cultures analysed. It was shown that high quality reproducible spectra could be acquired from cells in order to characterise their differentiation down the adipogenic and osteogenic lineages. The spectra acquired were of a comparable quality to those reported in the literature from studies where the sterility of samples was sacrificed in favour of reducing the working distance to the samples increasing the intensity of the Raman signal collected. This highlights that whilst the Raman effect may be weak it is still possible to work at longer distances, maintain the sterility of samples and still detect changes in cellular phenotype. This work could lead to greater acceptance of Raman spectroscopy as a viable technique for cellular characterisation and lead to further refinements of the method.

List of Abbreviations

- ΔCT – Comparative cycle threshold
- ± – Plus or minus
- 2D – Two dimensional
- 3D – Three dimensional
- *ADIPOQ* – Adiponectin
- ADSC – Adipose-derived stem cell
- AlGaAs diode – Aluminium gallium arsenide diode
- *ALP* – Alkaline phosphatase
- α-MEM – Alpha modified essential medium
- ANN – Artificial neural network
- ANOVA – Analysis of variance
- CARS – Coherent anti-stokes Raman spectroscopy
- CCD – Charge coupled device
- CD31 – Cluster of differentiation 31/Platelet endothelial cell adhesion molecule
- CD44 – Cluster of differentiation 44/Homing cell adhesion molecule
- CD45 – Cluster of differentiation 45/Protein tyrosine phosphatase, receptor type, C
- CD105 – Cluster of differentiation 105/Endoglin
- CD146 – Cluster of differentiation 146/Melanoma cell adhesion molecule
- cDNA – Complementary deoxyribonucleic acid
- *C/EBPα* – CCAAT/enhancer binding protein α
- CHO – Chinese hamster ovary cells
- cm – Centimetre
- c-MYC - V-myc avian myelocytomatosis viral oncogene homolog
- *COL1A1/COL1* – Alpha-1 type 1 collagen
- DMEM – Dulbecco's modified Eagle's medium
- DNA – Deoxyribonucleic acid
- DNase – Deoxyribonuclease
- DPSC – Dental pulp stem/stromal cell
- ECM – Extracellular matrix
- EDTA – Ethylenediaminetetraacetic acid
- EDX – Energy dispersive X-ray spectroscopy
- ELISA – Enzyme linked immunosorbent assay
- EM – Electromagnetic
- ESC – Embryonic stem cell

- ESR – Electron spin resonance
- EU – European Union
- FACS – Fluorescence activated cell sorting
- FAD – Fatty acid desaturase
- FCS – Foetal calf serum
- FDA – Food and drug administration
- FTIR – Fourier transform infrared spectroscopy
- g – Gram
- GA – Genetic algorithm
- GAG – Glycosaminoglycan
- *GAPDH* – Glyceraldehyde 3-phosphate dehydrogenase
- GMP – Good manufacturing practice
- HBSS – Hanks balanced salt solution
- HeNe laser – Helium neon laser
- HEPES – 4-(2-hydroxyethyl)-1-piperazineethanesulfonic acid
- *HIF* – Hypoxia inducible factor 1
- HSC – Haematopoietic stem cell
- *HSF* – Heat shock transcription factor 1
- iPS – Induced pluripotent stem cell
- KLF4 – Kruppel-like factor 4
- kPa – Kilopascal
- L – Litre
- *LDH* – Lactate dehydrogenase
- m – Metre
- MDCK – Madin-Darby canine kidney cells
- MEPE – Matrix extracellular phosphoglycoprotein
- mg – Milligram
- mL – Millilitre
- MLR – Multiple linear regression
- mm – Millimetre
- mM – Millimolar
- MRI – Magnetic resonance imaging
- MSC – Mesenchymal stem/stromal cell
- MTT – 3-(4,5-dimethylthiazol-2-yl)2,5-diphenyltetrazolium
- mW – Milliwatt
- NA – Numerical aperture
- NADH – Nicotinamide adenine dinucleotide (reduced)
- NBF – Neutral buffered formalin
- ng – Nanogram

- NHS – National health service
- nm – Nanometre
- nM – Nanomolar
- NMR – Nuclear magnetic resonance
- *OC* – Osteocalcin
- OCT3/4 – Octamer-binding transcription factor 3/4
- PBS – Phosphate buffered saline
- PC – Principal component
- PCA – Principal component analysis
- PCR – Polymerase chain reaction
- PE – Processing element
- PLGA – Ploy(lactic-co-glycolic acid)
- PLLA – Poly-L-lactide
- PLS – Partial least squares
- pO_2 – Partial pressure of oxygen
- *PPARγ* – Peroxisome proliferator-activated receptor γ
- qRT-PCR – Quantitative real-time polymerase chain reaction
- Qz – Quartz
- R&D – Research and development
- RBC – Red blood cell
- RGD – Arginylglycylaspartic acid
- ROS – Reactive oxygen species
- rpm – Revolution per minute
- RRS – Resonance Raman spectroscopy
- *RUNX2* – Runt related transcription factor 2
- S:N – Signal to noise ratio
- SD – Standard deviation
- SE – Standard error
- SEM – Scanning electron microscopy
- SERS – Surface enhanced Raman spectroscopy
- siRNA – Small interfering ribonucleic acid
- SOX2 – SRY (sex determining region Y)-box2
- SOX9 – SRY (sex determining region Y)-box9
- SSEA4 – Stage specific embryonic antigen 4
- SV40 – Simian vacuolating virus 40
- TEM – Transmission electron microscopy
- TERS – Tip enhanced Raman spectroscopy
- µg – Microgram
- UK – United Kingdom

- µL – Microliter
- µM – Micrometre
- US – United States of America
- UV – Ultraviolet
- *YWHAZ* – Tyrosine 3-monooxygenase/tryptophan 5-monooxygenase activation protein, zeta

Appendix A

Step by Step Pre-processing and Analysis of Raman Spectra

Contained in this appendix is a complete step by step description of the pre-processing and analysis of Raman spectra acquired from osteo-induced DPSCs.

A.1 Pre-processing of Spectra in Grams

The following pre-processing steps were applied to each individual spectrum in Grams/32. First the average of 12 cell-free background spectra ("background spectrum") were subtracted from every raw spectrum obtained from the cells ("cell spectrum"). The following figures are a worked example of the entire pre-processing using a raw cell spectrum from DPSCs following 28 days of osteo-induction.

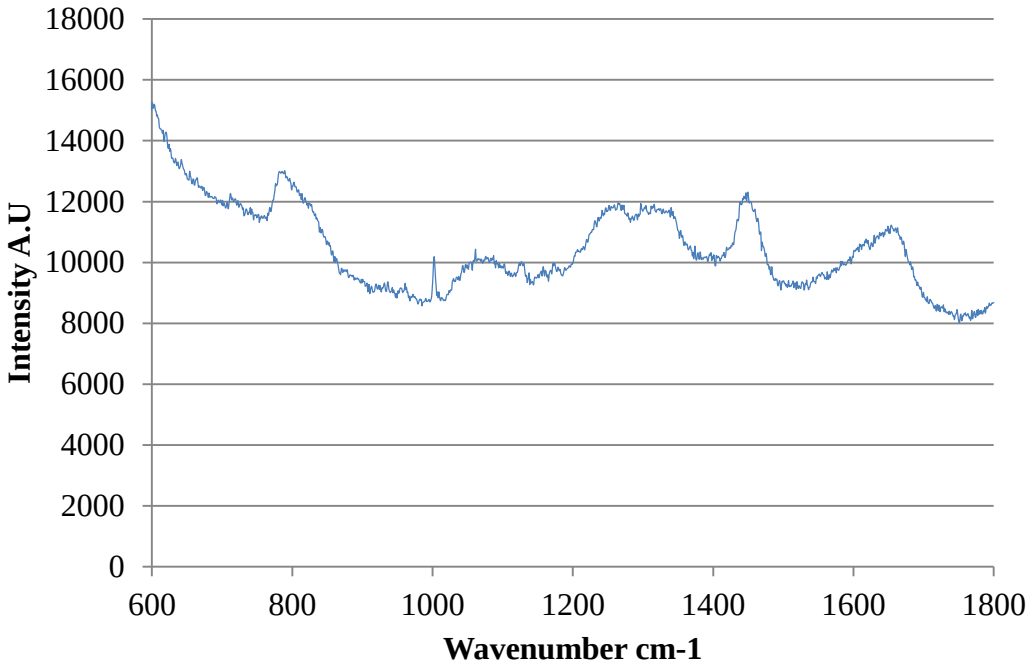

Figure 58. Representative raw cell spectrum obtained from DPSCs following 28 days of osteo-induction with a 120 second exposure.

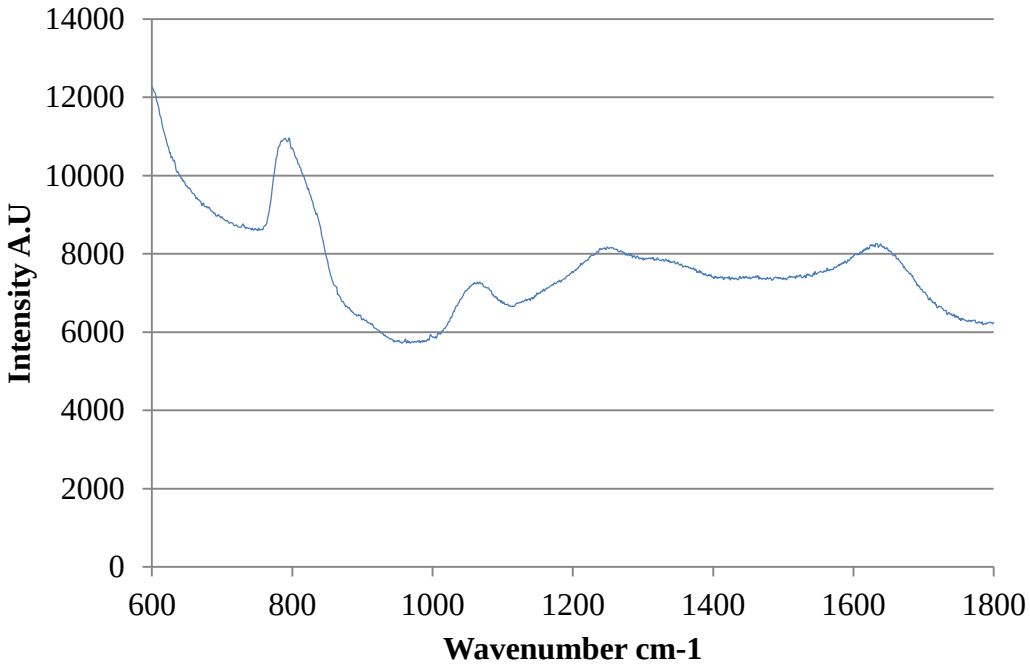

Figure 59. Average of 12 cell-free background spectra acquired with a 120 second exposure.

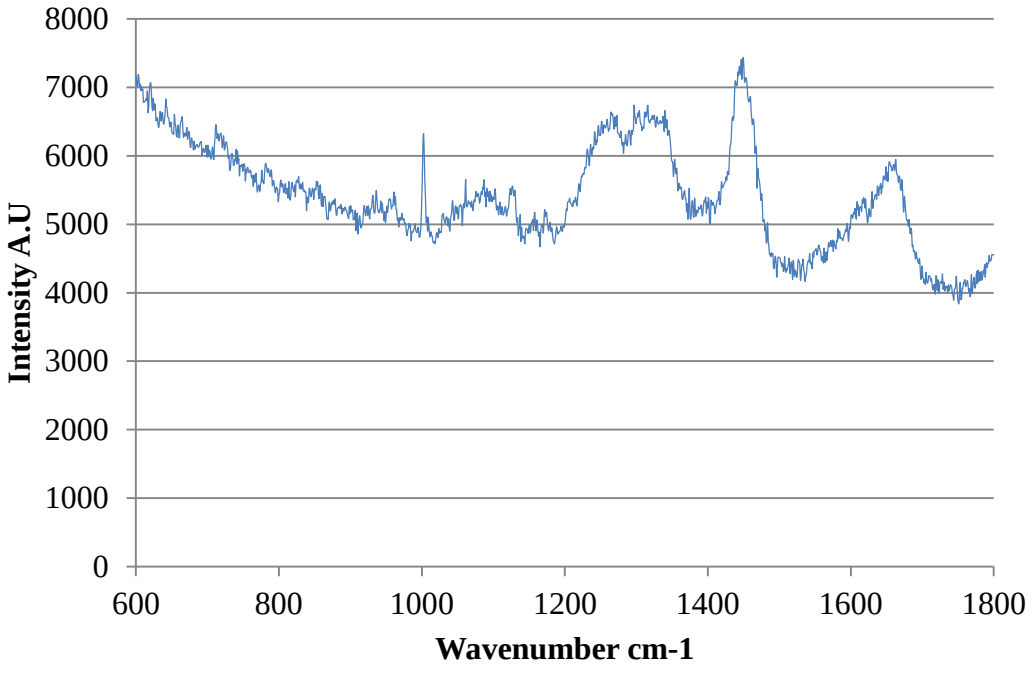

Figure 60. Cell spectrum (Figure 58) following subtraction of the background spectrum (Figure 59).

Due to variation in the microscope stage height from differences in cell layer thickness and from the thickness of the glue used to adhere the quartz discs to their flasks, the proportion of the background spectrum subtracted varied from one spectrum to another. This could result in “over” or “under” subtraction. Below are examples of over and under subtraction.

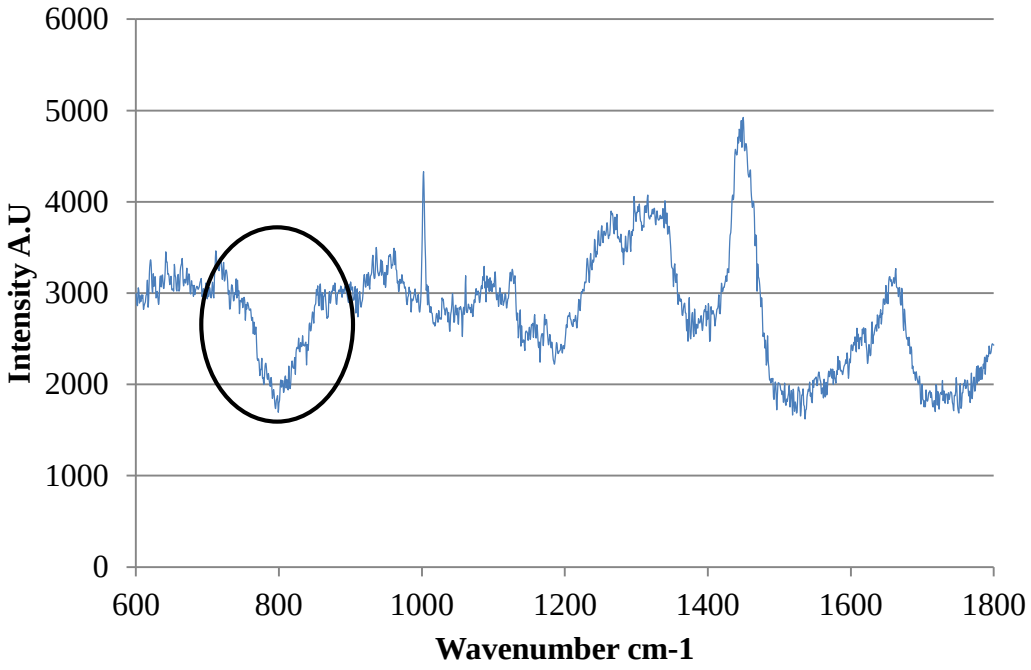

Figure 61. Example of an over subtraction of a background spectrum (Figure 59) from a cell spectrum (Figure 58). The circled trough is the result of an over subtraction of the contribution of the quartz to the background spectrum.

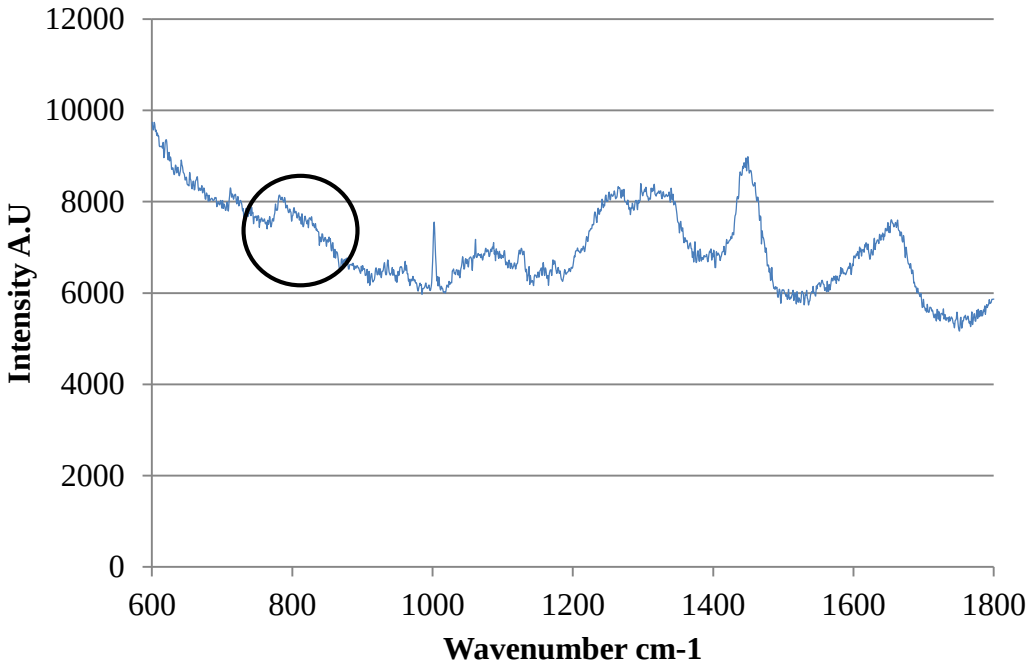

Figure 62. Example of an under subtraction of a background spectrum (Figure 59) from a cell spectrum (Figure 58). The circled peak is the result of an under subtraction of the contribution of the quartz to the background spectrum.

Circled is a peak/trough contributed by the quartz if that background has not been subtracted properly.

Following this, the baseline was flattened using four fixed points based on high/low points in the spectrum, marked, and the spectra smoothed using a seven point Savitzky-Golay filter.

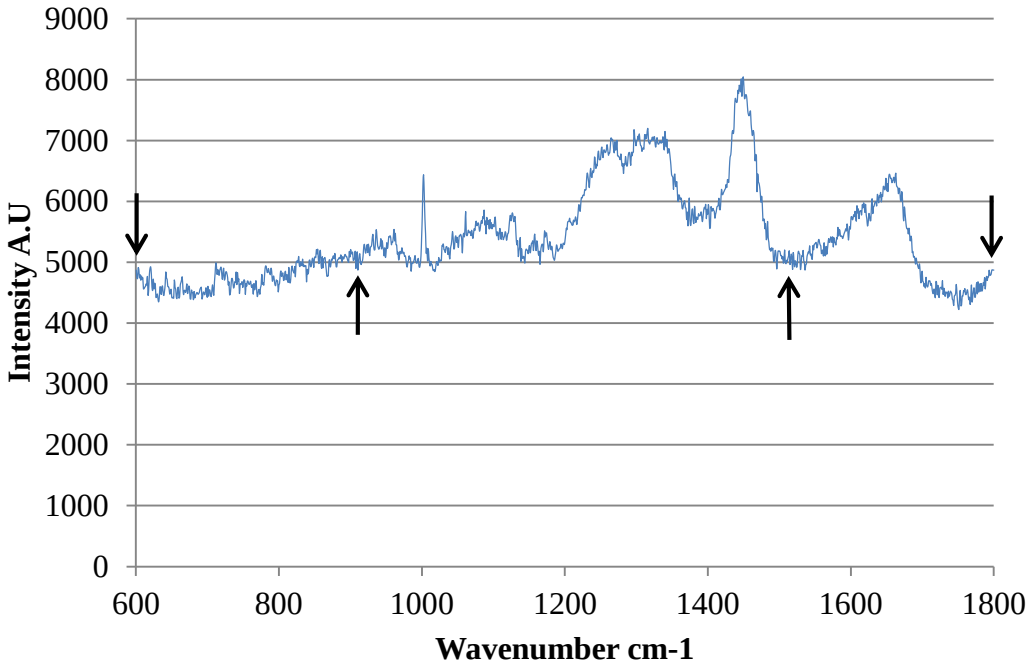

Figure 63. Baseline flattening of a spectrum, the four points used are marked.

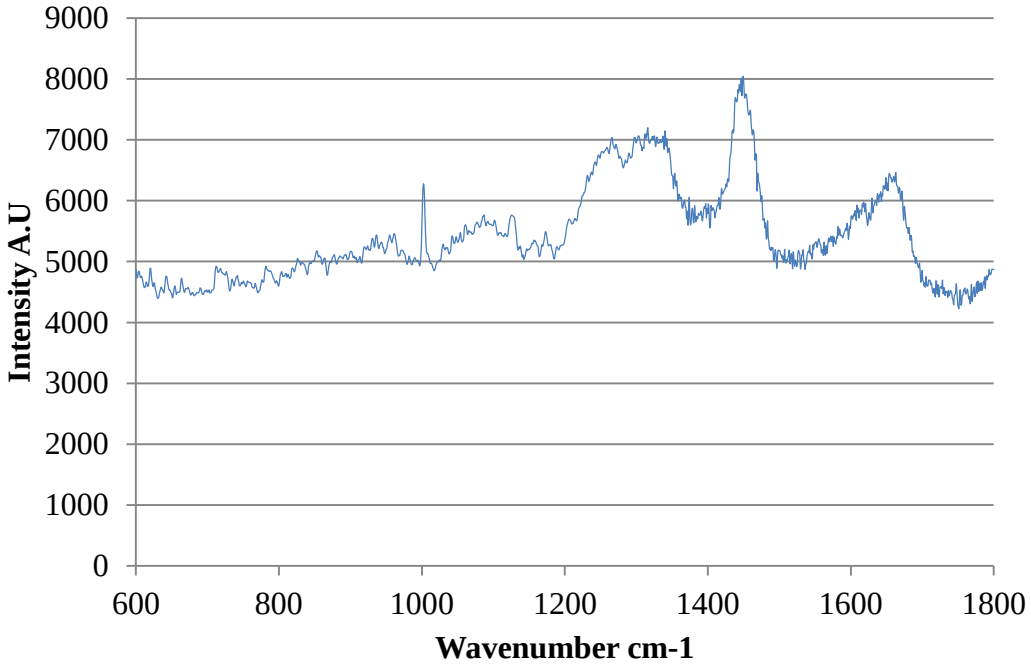

Figure 64. Smoothing of a spectrum using a 7 point Savitzky-Golay filter.

Finally the two axes were standardised. The x-axis was normalised to the peak at 1000 cm^{-1} to correct for minor variation from the instrumentation over the course of the experiment and the lowest point of the spectrum reduced to a y-axis value of 0.

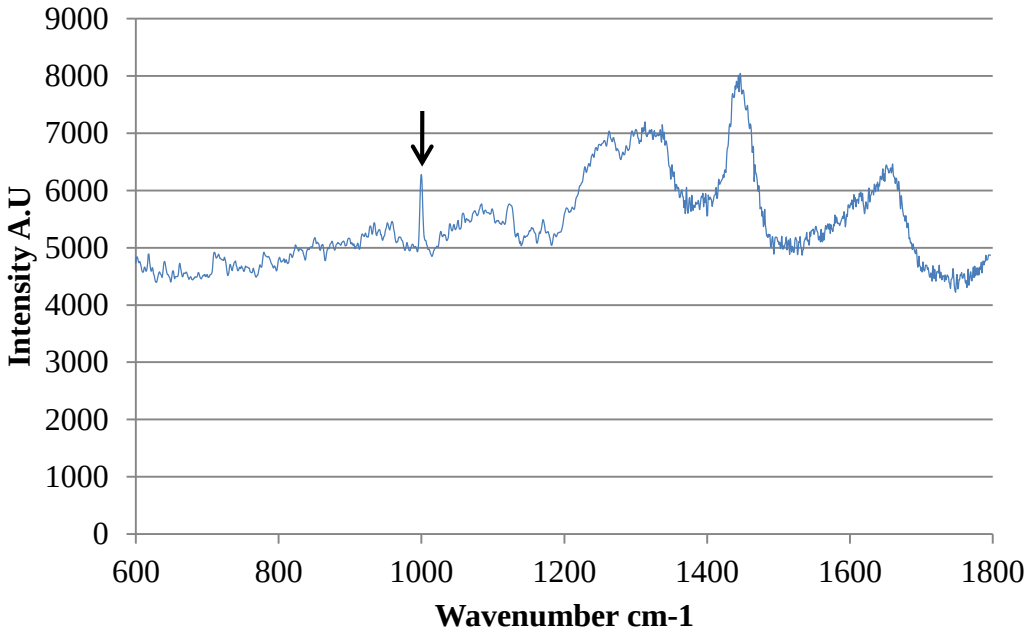

Figure 65. X-axis adjusted so the marked peak equalled 1000 cm^{-1}

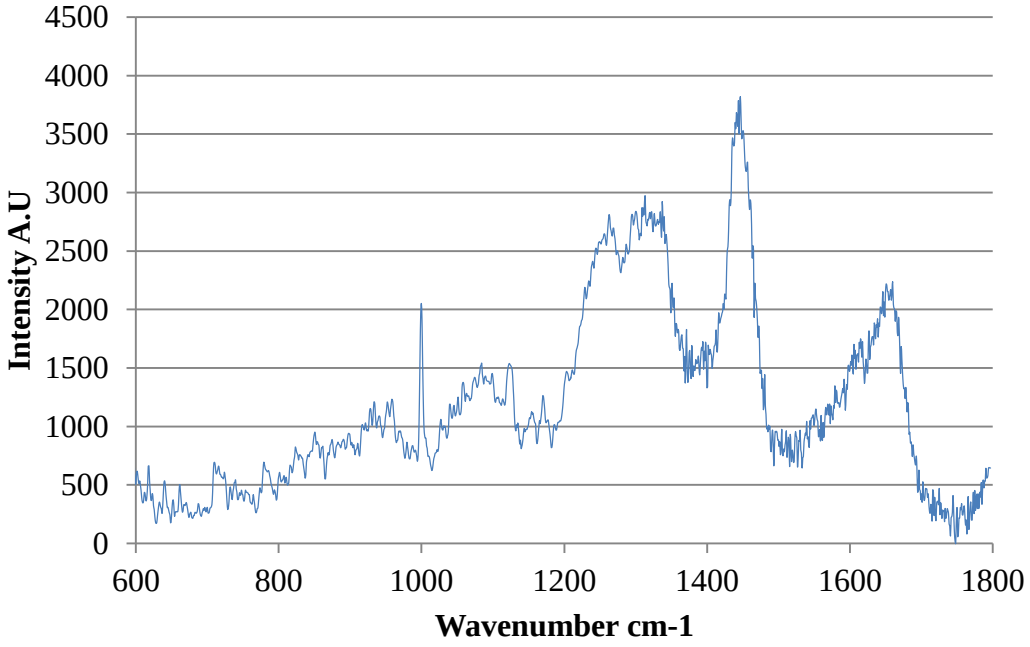

Figure 66. Y-axis adjusted so the lowest point of the spectrum equalled 0.

All spectra were then exported and copied into Microsoft Excel.

A.2 Further Processing in Matlab and Principal Component Analysis

Following pre-processing in Grams all the spectra from each individual donor sample were collated and imported into Matlab. The following figures illustrate the entire data handling and analysis process for all the spectra acquired from osteo-induced DPSCs the data from which is described in Chapter 5. Figure 67-Figure 76 illustrate the removal of outlying spectra from the same single donor, this process was repeated for the spectra acquired from every other donor.

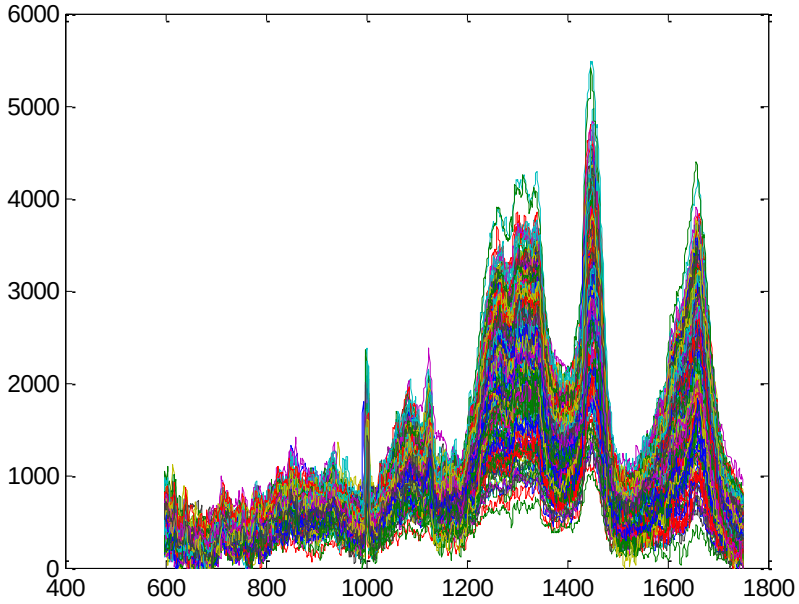

Figure 67. All the spectra acquired at all time points during osteo-induction from one donor following pre-processing in Grams.

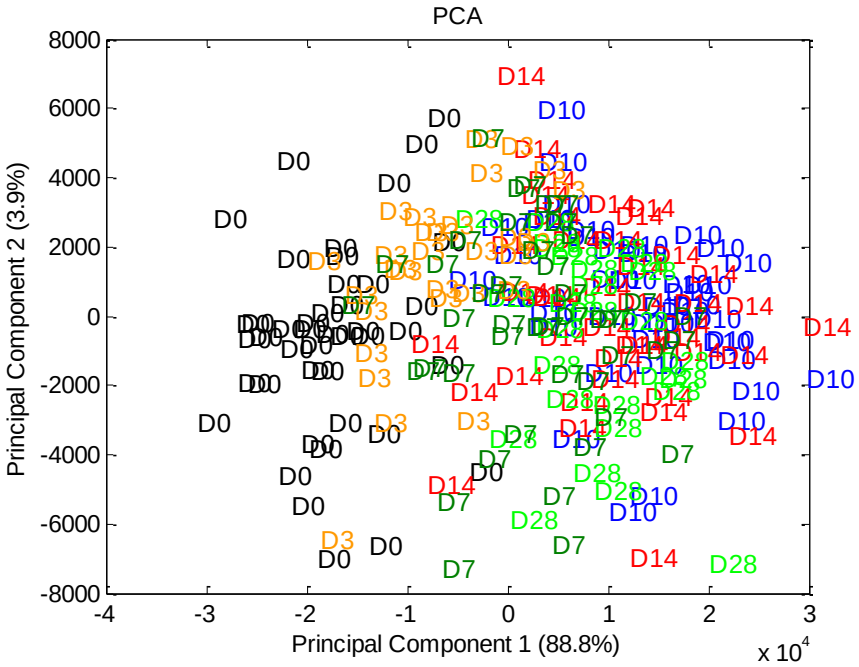

Figure 68. PCA for principal components 1 and 2 of all the spectra from one donor following pre-processing in Grams.

Whilst there appears to be a trend in the data there are clearly outlying spectra, based on contributions from PC1, in every time point which need to be removed. Outliers were determined based on extremes in principal component one as this was responsible for the vast majority of the variation in each data set. Approximately 10% of the spectra in each time point were removed. The next 6 figures outline this removal process for each time point from one donor, boxed are those spectra that were removed.

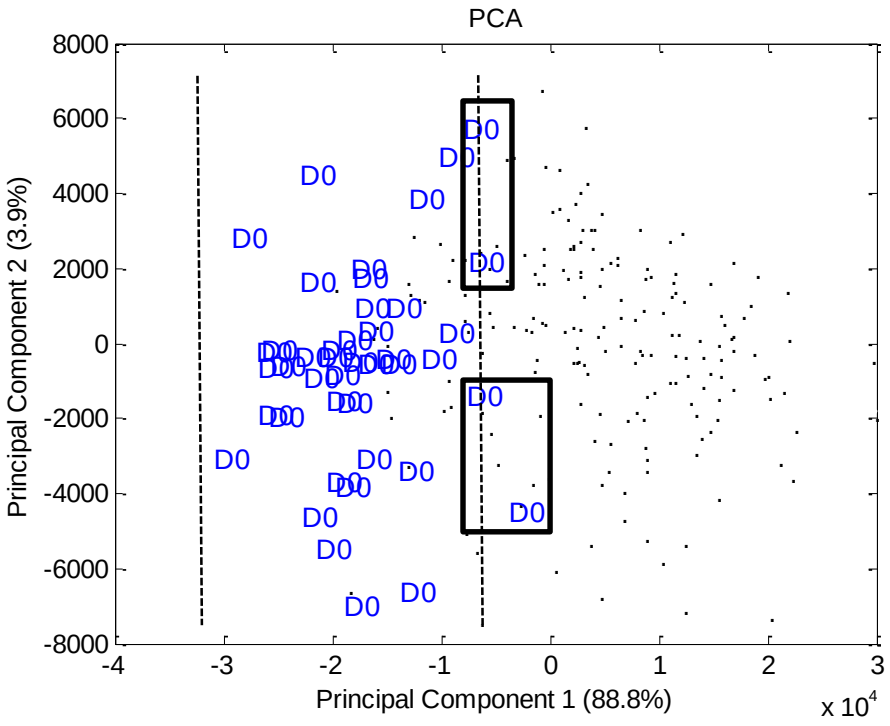

Figure 69. Outlier removal for day 0. The removed outliers are boxed, everything within the dashed lines was retained.

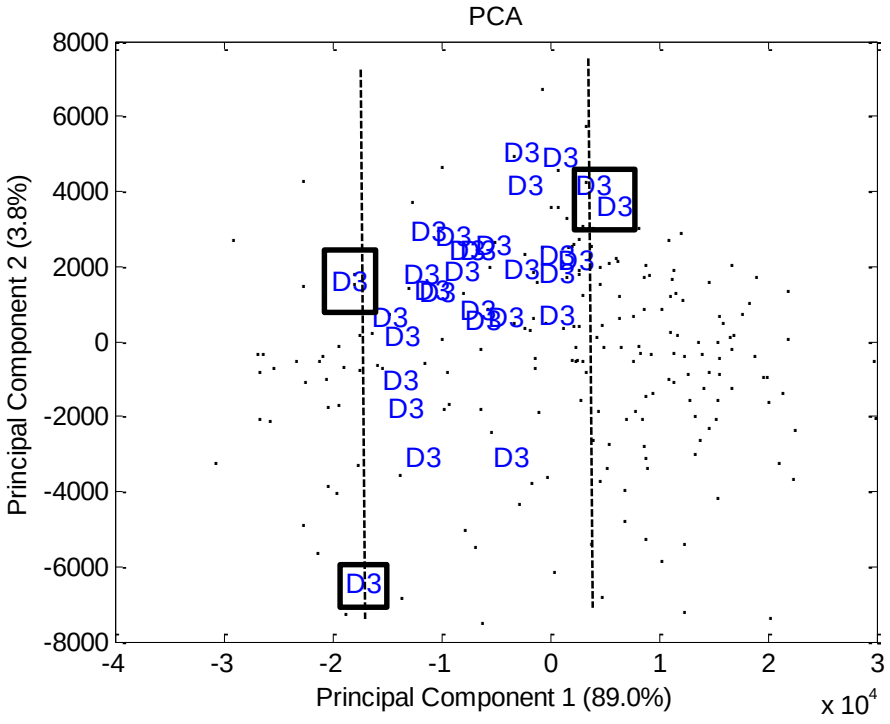

Figure 70. Outlier removal for day 3. The removed outliers are boxed, everything within the dashed lines was retained.

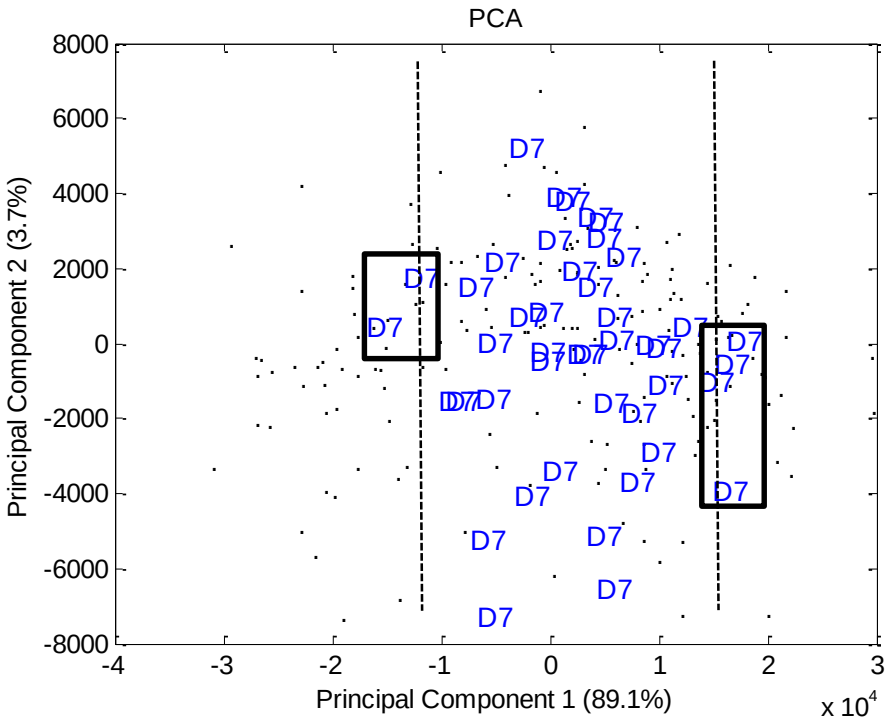

Figure 71. Outlier removal for day 7. The removed outliers are boxed, everything within the dashed lines was retained.

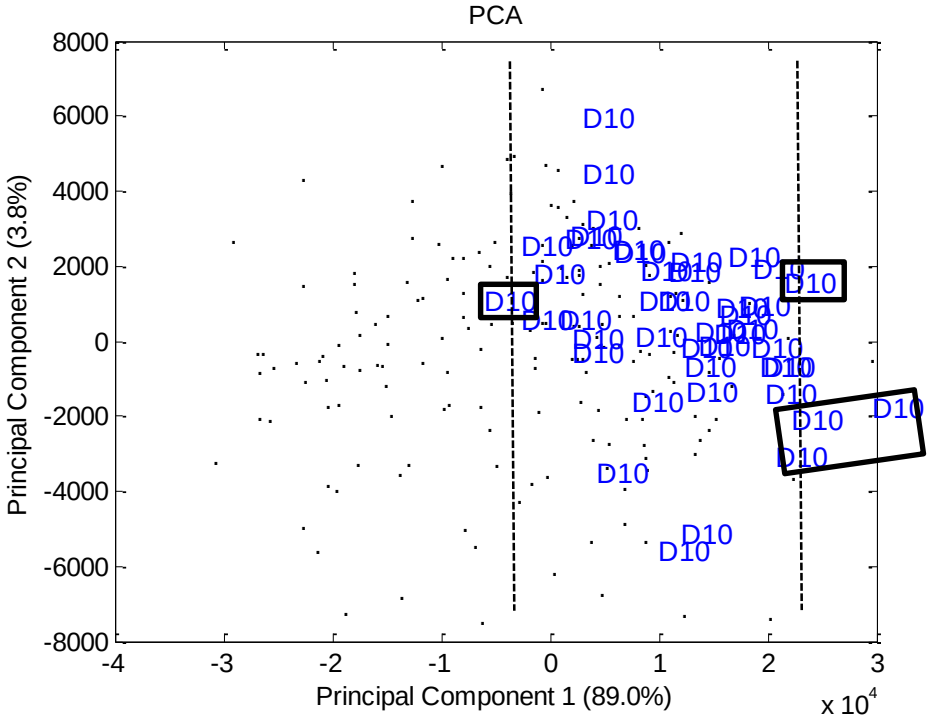

Figure 72. Outlier removal for day 10. The removed outliers are boxed, everything within the dashed lines was retained.

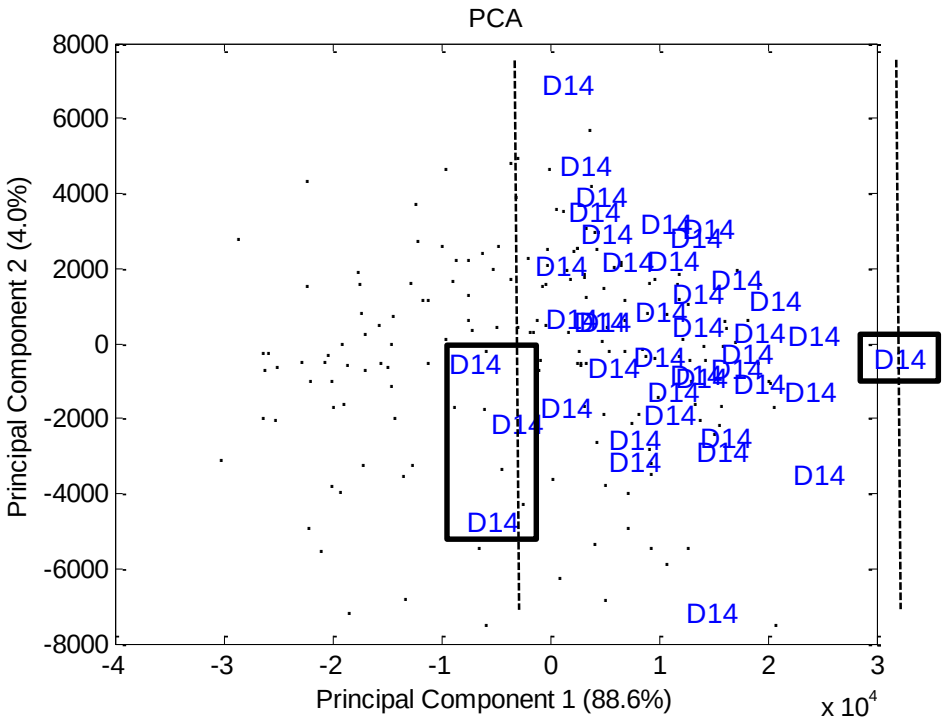

Figure 73. Outlier removal for day 14. The removed outliers are boxed, everything within the dashed lines was retained.

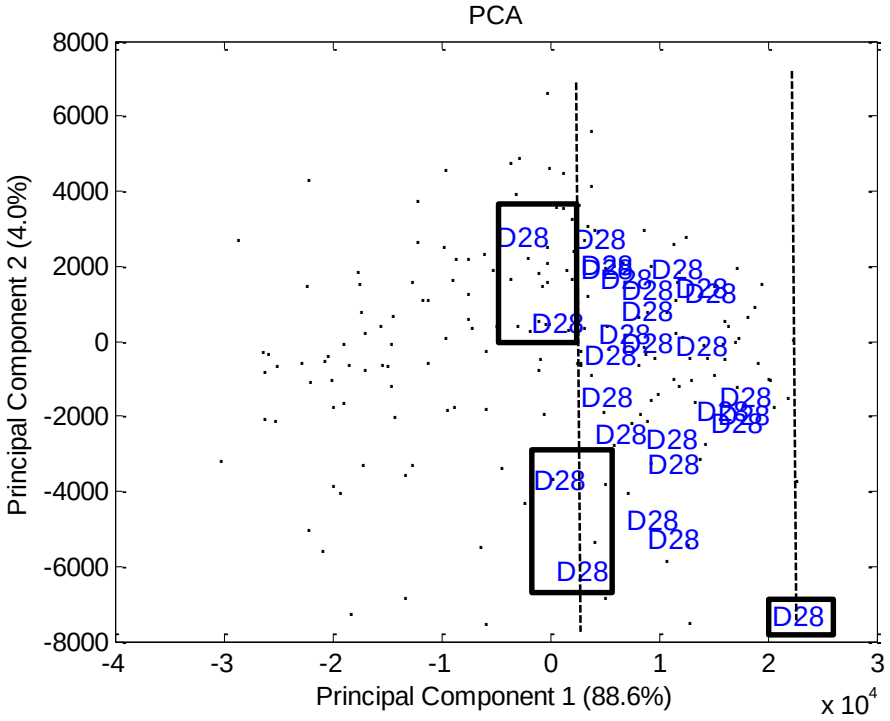

Figure 74. Outlier removal for day 28. The removed outliers are boxed, everything within the dashed lines was retained.

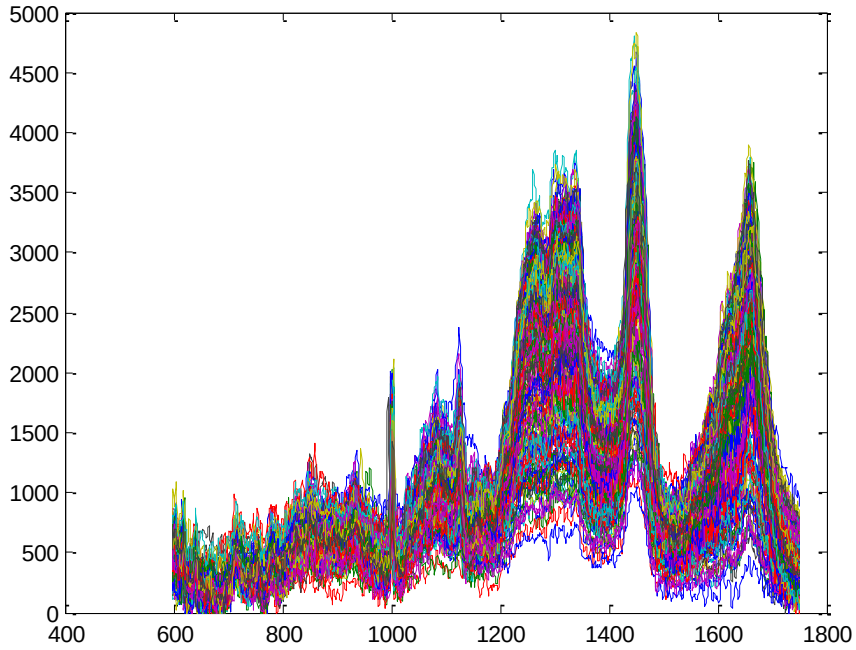

Figure 75. All the spectra acquired at all the time points during osteo-induction from one donor following outlier removal.

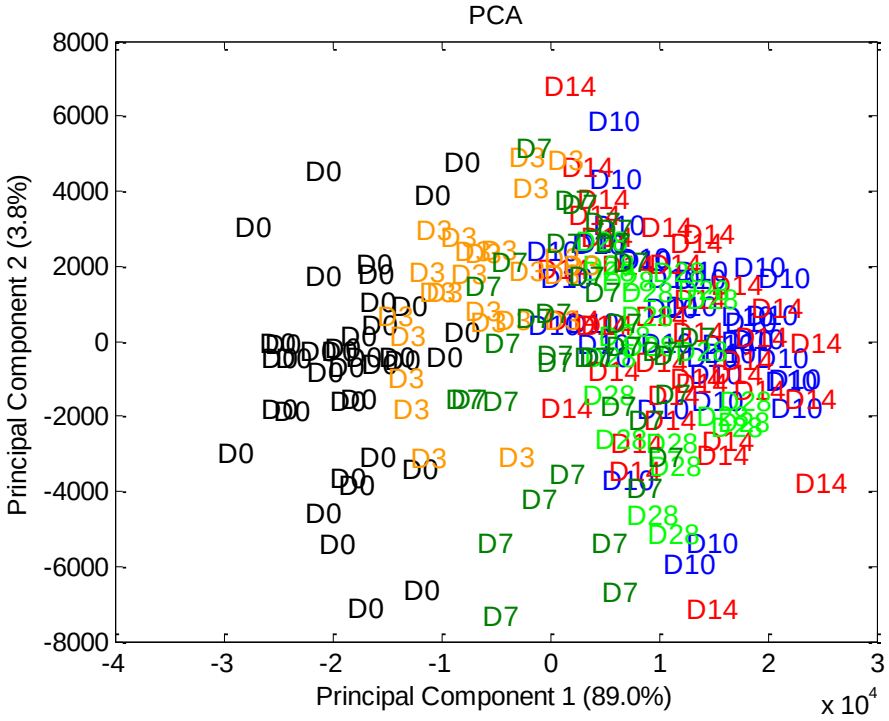

Figure 76. PCA for principal components 1 and 2 of all the spectra acquired from osteo-induced DPSCs from a single donor following outlier removal.

Following outlier removal for all three patient samples the data was combined by taking one spectrum from each donor per time point and averaging.

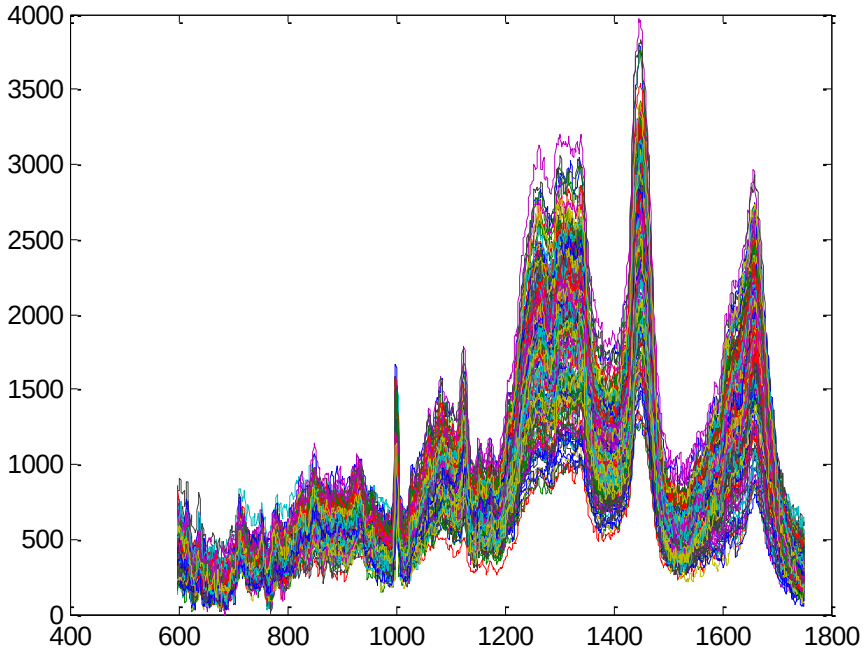

Figure 77. The entire data set of spectra acquired from osteo-induced DPSCs plotted after averaging across the three donors.

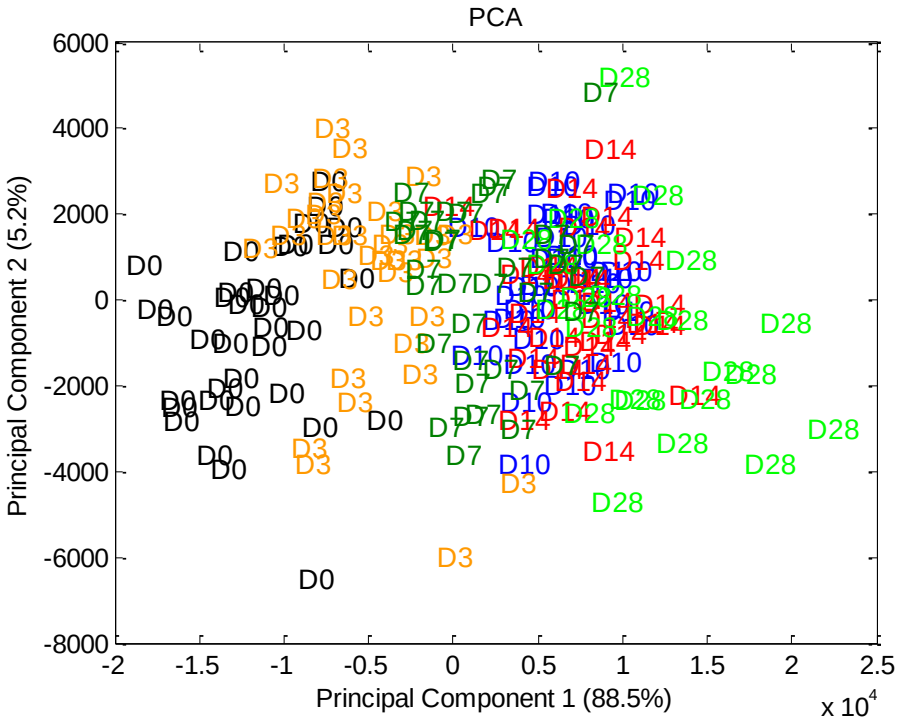

Figure 78. PCA for principal components 1 and 2 of the entire data set acquired from osteo-induced DPSCs after averaging across the three donors.

Following this, second derivative spectra were calculated and further smoothing performed, second derivative spectra are very noisy and therefore require extensive smoothing (114). Other processing methods such as baseline corrections or calculating the standard normal variate were also assessed to find the optimal processing methodology but are not presented as they were not used.

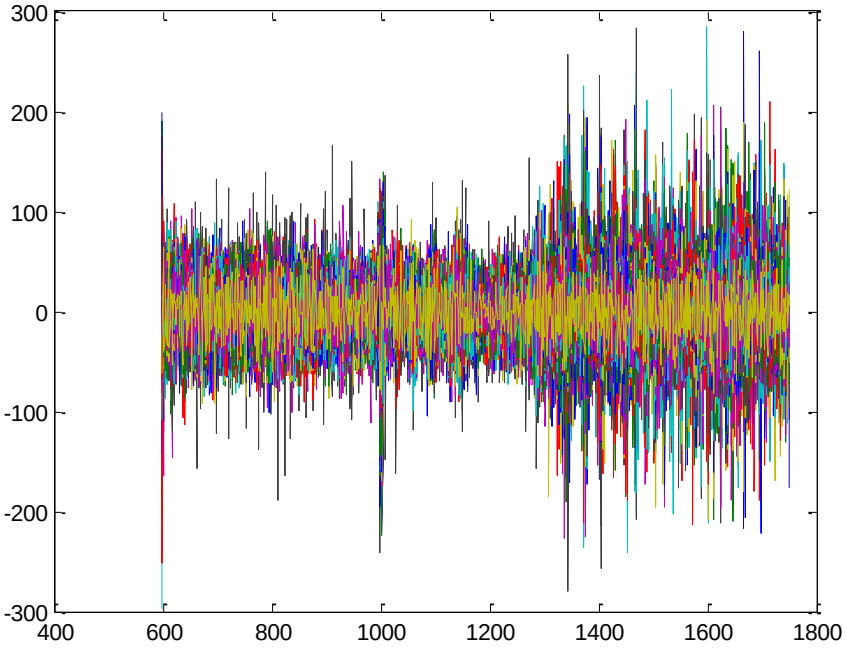

Figure 79. 2nd derivative spectra calculated from the average spectra across the three osteo-induced DPSC donor samples.

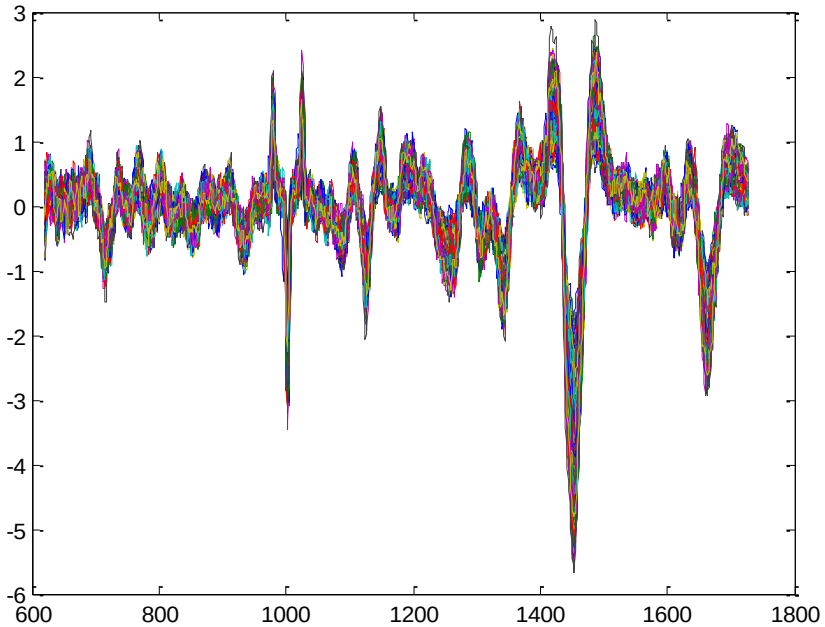

Figure 80. 2nd derivative spectra calculated from the average spectra across the three osteo-induced DPSC donor samples following smoothing with a 25 point filter.

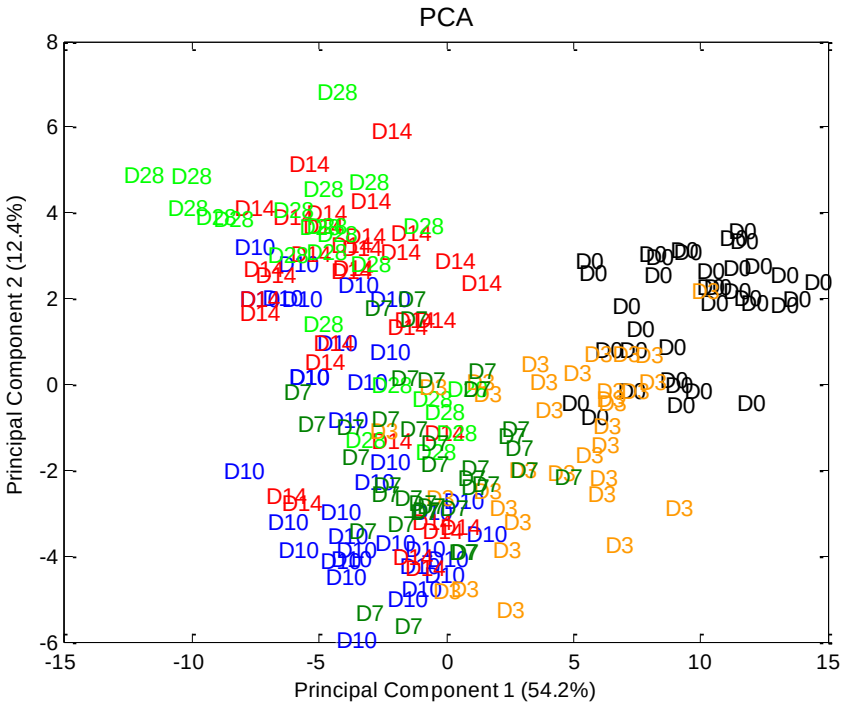

Figure 81. PCA for principal components 1 and 2 of the fully processed spectra acquired from three osteo-induced DPSC donor samples.

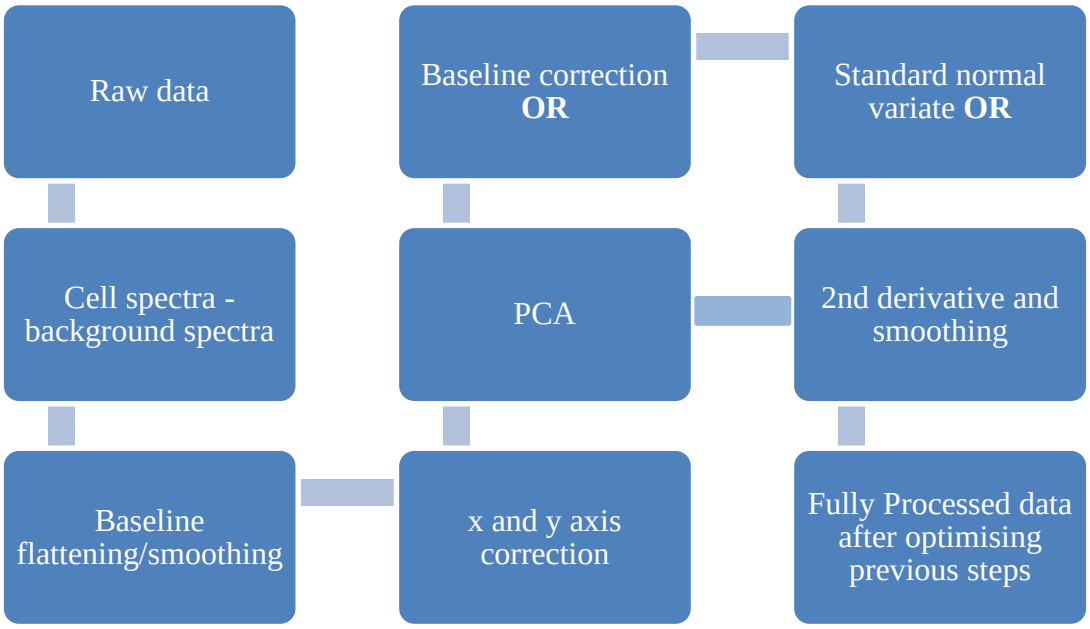

Figure 82. Summary work flow for processing raw DPSC spectra.

Appendix B

The Commercialisation of a "Raman Cell Analyser"

This document was produced as part of an ancillary project under the supervision of Avacta Group. This is intended to mirror aspects of the "stage 0" product development phase. This is not intended to be a realistic business plan but is an aspirational outline to a product whose contents would be refined through interaction with the target market and by technical feasibility testing.

Raman Cell Analyser

This document outlines a product that utilises Raman spectroscopy to determine cellular differentiation status and/or differentiate between cellular populations. The initial product release is intended as an R&D tool only; with subsequent releases finding clinical applications should the product meet regulatory requirements. The envisioned product possesses several key advantages over current gold standards. Chief amongst these is the non-invasive and non-destructive manner of the technique permitting *in situ* analysis and subsequent re-use/implantation of samples. The product will be competitively priced with regards to the equipment whose function it is intended to replace and its running costs significantly lower. Experiments using the Raman Cell Analyser will require the use of specialised *de novo* consumables which will generate a continuous revenue stream.

B.1 Product Vision

B.1.1 Product Outline

The Raman Cell Analyser will possess two core capabilities, the monitoring of cellular differentiation status and the discrimination of different cell types. This will position the Raman Cell Analyser to access markets in both research and clinical laboratories. In order to achieve this, an optical system capable of producing spot sizes from 1 μm to 10's of μm will be required allowing users to study intracellular organelles, individual cells or clusters of cells. The system must also be capable of working with either adherent or suspended cell samples. Finally the Raman Cell Analyser will possess a software package capable of performing all the spectral data processing for the removal of noise etc and possess a feature for the logging of 'training data' that can be used to classify subsequent samples.

B.1.2 Product Development Road Map

The first product release will be under the manual control of the researcher, they would have to locate the regions they wish to analyse. The accompanying software will be easy to use and capable of processing and classifying spectra (based on previous 'training' data). Subsequent product releases will allow automation of the system and increase the length of time that samples may be analysed. This will be achieved by incorporation of software similar to Nikon's CL-quant which allows users to specify a nucleus, for example, based on its size/morphology. Such automation will generate interest within clinical pathology laboratories providing rapid automated diagnoses. For established users improvements to the software such as the incorporation of user generated cellular profiles will offer a library of data with which to reference. Automation will also save significant amounts of time for the user. Finally, the incorporation of temperature, gas and humidity control systems would allow samples to remain within the system indefinitely permitting continuous analysis. This would save further time for current users and permit experiments to be run on long timescales with a minimum of effort. Such improvements could also generate interest within the pharmaceutical industry as they would allow high throughput screening of cells in toxicology assays. A summary of information can be found in Table 9.

Table 9. A summary of the product development road map.

Product Release	Target Market	Product Features	Barriers
1	R&D labs (academic)	Hardware, manual spectral acquisition. Software, automatic spectral processing, capable of spectral classification	Reliable predication of many cell phenotypes, capacity to work with 3D samples
2	Users of version 1, late uptake R&D users, clinical labs	Hardware, morphology based automated spectral acquisition. Software, user generated library of pre-loaded cellular phenotype classifications	Regulatory approval (high fidelity prediction of malignancy)
3	Previous users, pharmaceutical labs	Hardware, gas, temperature and humidity control of the microscope stage	Detection of subtle changes in cell phenotype related to toxicology

B.2 Customer Specification

B.2.1 Research and Development Users

Research and development scientists currently analyse cellular differentiation status by invasive and/or destructive methods. There is recognition within this group that non-invasive methods will be required for the high throughput translation of regenerative medicine therapies. The Raman Cell Analyser is intended to occupy this niche. In order to achieve this, the Raman Cell Analyser needs to reliably predict the phenotype of a cell/group of cells and be able to distinguish this from any solution the cells are in or material they are adhered to. Therefore a broad range of samples must be accommodated from suspended cells, to monolayers and 3D constructs, this however presents the opportunity for multiple consumable types. As a key advantage the Raman Cell Analyser will work with live samples in a minimal medium. Whilst alone, the Raman Cell Analyser will not be able to provide detailed biochemical data, for example the expression of a key gene of interest, it will be able to provide real-time *in situ* assessments of cellular differentiation status.

B.2.2 Clinical Users

The NHS pathology service performs much of the diagnostic work for the organisation. A recent review of the service indicated a need for more cost effective and efficient technologies to reduce the time for diagnosis, streamline the service and reduce costs. One use of the Raman Cell Analyser will be the discrimination of different cell types within a mixed sample, such as the presence of malignant cells within a biopsy. In order to achieve this, the cells would be suspended in solution and analysed by passing through a quartz capillary. Whilst this test would not yield the exact nature of a cancer, for example the presence of a particular genetic mutation, it would provide a quick, general diagnosis which could then be followed up by a more thorough analysis. This would provide a more targeted approach both in the time of the pathologists and in the costs of further experiments.

B.3 Target Market

Clinical laboratories such as those in the NHS would be most interested in the ability of the Raman Cell Analyser to discriminate between different cell types such as in the detection of cancer. Research laboratories such as those found in Universities would be most interested in the capacity for non-invasive, live, monitoring of cellular status. However, these applications are not mutually exclusive to their target markets.

B.3.1 Research and Development Laboratories

One of the functions of the Raman Cell Analyser will be the *in situ* monitoring of cellular differentiation status. A literature search for stem cell differentiation shows the following publication trend, a quadrupling of publications in a ten year period with year on year increases. The number of publications where the UK was indicated as the country of origin is also included. It should be noted that ~25% of publications do not identify a country of origin Table 10.

Table 10. Stem cell differentiation publication between 2002-2011

Year of publication	Number of publications	UK publications
2011	22902	591
2010	22199	605
2009	18916	511
2008	17103	425
2007	14056	411
2006	12953	336
2005	10303	255
2004	8971	249
2003	7596	194
2002	6091	158

There are 113 universities in the UK. Some of these such as the London School of Economics would clearly have no use for the Raman Cell Analyser. The number of potential sales of the Raman Cell Analyser to the remainder will largely depend on the price point. If the price is seen as too high then it would likely be funded out of a universities capital expenditure budget, greatly reducing potential unit sales. Therefore a price needs to be set that would permit funding at faculty (a university may have several faculties, such as medicine or biological sciences where a Raman Cell Analyser may find use) or even individual research group level to increase unit sales. It is unlikely that too many research groups within a university would share a Raman Cell Analyser as potentially long sampling times, the logistics of moving samples around a campus and competing busy schedules would make too much sharing prohibitive. This coupled with a competitive price could further increase unit sales. Research in stem cell differentiation can mean researchers handling cells in many conformations including in suspension, monolayers and 3D constructs. This presents the opportunity for the *de novo* design of cell culture vessels specialised for each application that would need to be purchased for each individual experiment/sample.

In summary, there is increasing research output both globally and nationally concerning the use of stem cells and their potential in regenerative medicine therapies. However, one barrier in the advancement of such therapies to a clinical setting is the lack of suitable methods for their non-invasive and non-destructive characterisation. The Raman Cell Analyser seeks to bridge this gap and if priced competitively provide an alternative to those current methods that require extrinsic labelling or destruction of samples.

B.3.2 Clinical Laboratories

The main clinical laboratory target would be the pathology departments within the NHS that perform much of their laboratory based diagnostic testing. The NHS has 151 primary care trusts containing 353 hospitals. The aim would be to supply one Raman Cell Analyser into each pathology department. One application of the Raman Cell Analyser will be the detection of cancerous cells in a biopsy. In the UK alone

270000 cases of cancer are diagnosed per annum. Cancer is seldom diagnosed by one method alone; the Raman Cell Analyser would not claim to be able to do this. Instead it would be marketed as a quick test (hours in timescale) that could detect the presence of cancer allowing pathologists to better allocate their time and money with subsequent tests such histopathological screening of tissue (up to a week in timescale). Each test performed by the Raman Cell Analyser would require a single use quartz capillary to prevent cross contamination of samples, current prices on quartz capillaries range from £75-100 for 25 units.

B.3.3 End User Specification

There will likely be a range from students, technicians, postdoctoral researchers and professionally trained biomedical scientists and pathologists. A recurrent theme amongst these groups will be their training in biological disciplines. Therefore their understanding of, and desire to use, a spectroscopic technique will likely be low. As such the Raman Cell Analyser will need to be simple to use. Samples must be easily loaded into the machine and software provided that guides the user through the acquisition of the spectra, processing of the data and providing a concise report at the end.

B.4 Competitive Strengths and Weaknesses

B.4.1 Research and Development Laboratories

Core, gold standard techniques used for stem cell characterisation include quantitative real time polymerase chain reaction (qRT-PCR), fluorescence activated cell sorting (FACS) and immunohistochemistry. A common theme amongst these techniques is their targeting of molecular or genetic markers essential for a given differentiation pathway/phenotype. Such specificity is their main strength as they reveal key biochemical data on cellular differentiation status. Many such markers are well characterised for a given differentiation lineage and their detection is considered essential to demonstrate. However such techniques are either invasive (they use exogenous labels) or destructive (they require the complete destruction of the sample) and therefore don't lend themselves toward clinical applications. Ideally researchers would like to perform *in situ* analysis of a sample prior to its implantation in a patient for increased safety. The Raman Cell Analyser would cater for this need.

Comparison between established techniques and the Raman Cell Analyser are difficult. Established techniques are highly specific, targeting known proteins or genes of interest and therefore yield very specific data on the status of the sample. However, such detail isn't always necessary, if the question posed is, "have these stem cells differentiated and if so to what degree" then changes seen in their spectra may provide a sufficient answer. Such changes have already been observed using Raman spectroscopy albeit under non sterile conditions. If such findings can be confirmed in a *de novo* sterile system then cells analysed in this manner could subsequently be used in further applications. Therefore if the aim is simply to demonstrate differentiation then the Raman Cell Analyser would possess a key advantage over established techniques. It is, however, unlikely that the Raman Cell Analyser would be able to compete, if information on key cell signalling events, for example, were the object of a study.

There are several techniques currently being investigated that also seek to cater for the non-invasive characterisation of stem cells. These include but are not limited to

two photon excited fluorescence microscopy, nuclear magnetic resonance (NMR) spectroscopy and impedance spectroscopy. Two photon excited fluorescence microscopy utilises the endogenous fluorescence of common biological molecules. It has demonstrated good 3D depth resolution an advantage it possesses over other technologies. However, the only significant fluorescence detected by this method thus far is from NADH and FAD which means the technique is currently only sensitive to changes in redox status. NMR spectroscopy is capable of detecting many small molecules such as metabolites and can be used for both absolute and relative quantification. However, detection of larger molecules such as proteins is not possible. Further, analysis of live cells requires immersion in aqueous solutions. In NMR techniques must be used to supress the effect of such solutions which can lead to problems detecting resonances near the solution. Impedance spectroscopy differentiates between cell populations based on their electrical resistance. As a technology for the non-invasive characterisation of cells impedance spectroscopy is in its infancy compared with other techniques. Impedance spectroscopy involves the culturing of cells on platinum electrodes. Platinum is a known mutagen and its potential effect on cell cultures is yet to be delineated.

B.4.2 Clinical Laboratories

Cancer diagnosis generally requires a multi-faceted approach from imaging techniques such magnetic resonance imaging (MRI) to histopathology techniques such as tissue histology and screening of molecular markers through techniques such as enzyme linked immunosorbent assays (ELISA). The pathological methods for cancer diagnosis are highly specific and used to detect molecular markers indicative of a malignant phenotype. However, this specificity makes the reagent costs of such techniques expensive and they are time consuming to perform. The Raman Cell Analyser would not aim to replace any of these techniques but would be another tool available to be used in synergistic manner to speed up the diagnosis and reduce the cost of cancer detection. For example, a cell suspension from a tissue biopsy could be rapidly analysed by the Raman Cell Analyser to detect the presence of malignant cells. This information could then better inform on those patients who require more detailed follow up using more time consuming and costly techniques such as MRI.

B.5 Business Model

B.5.1 Pricing, Usage and Sales Projections

The first release of the Raman Cell Analyser into research and development laboratories should be priced no greater than £30000. A price at this level would be in a range that individual research groups could purchase. This would be competitive with the latest qRT-PCR machines and significantly lower than the price of a good confocal microscope.

Monitoring of cellular differentiation status can take up to several weeks and a good study will test several patient samples to account for individual variability. Many researchers demonstrate differentiation by changes occurring over several time points and this would be replicated when using the Raman Cell Analyser so equipment usage would be high. Accounting for optimisation, the provision of training data and true experimental samples a good study will require 10-20 individual consumables for the culturing of samples.

A conservative estimate of potential customers within UK university research and development labs indicates there may be approximately 300 just at faculty level. If 10% of this market can be reached that would generate sales of £900,000. At current publication levels there are 600 publications per year that could involve the use of a Raman Cell Analyser if 10% of these were reached this would generate consumable sales of 600-1200 a year generating revenue of £60,000-£120,000.

Providing the Raman Cell Analyser can meet the regulatory requirements for its use in cancer diagnosis the aim would be to sell a unit to each NHS pathology laboratory. This could generate unit sales of £105,900,000, assuming sales to each NHS hospital, though it is unlikely that each unit would be sold at list price for such a bulk order. It is difficult to ascertain the number of the 270000 cancer diagnoses per year where the Raman Cell Analyser would be applicable however, the upper consumables sales this could generate are approximately £1,080,000 per annum based on a price of £100 for 25 quartz capillaries.

B.5.2 Competitor Cost Analysis

For research and development laboratories:

The following listed are the equipment costs associated with the core techniques required for publication for tissue engineering applications. There can be further costs but these would be associated with techniques specialised for a particular application.

Basic qRT-PCR machine ~£5000 up to ~£20000 for the best with analysis software etc. Consumables, RNA purification ~ £200 (50 preps), reverse transcription ~ £80 (50 preps), PCR probes ~£120 per gene (200 preps), PCR reaction mix ~£200 (200 preps)

Basic fluorescence microscope, ~£5000 up to £50k+ for a confocal microscope. Consumables, primary antibodies ~£250 per marker, secondary antibodies ~£125 per fluorophore.

Phase contrast microscope £1000-2000 basic up to ~£10000, additional imaging camera and software, tissue processor £10000-150000 and microtome £5000-10000, histology primary antibodies ~£250 per marker, primary antibody conjugates such as horseradish peroxide ~£170 (25 preps).

For clinical labs:

A review of NHS pathology criticised the service for the lack of financial data available so a cost analysis is difficult. However, the cost of a single experiment using the Raman Cell Analyser could be as little as £3, to cover the cost of a single use quartz capillary and an appropriate solution to suspend the sample in. In contrast a single ELISA test for cancer biomarkers costs ~£5 and a histology test ~£15. However, the Raman Cell Analyser would not be marketed as a replacement for these tests but as a quick and cheap guide as to whether to perform them.

B.6 Risk analysis

Each of the following sections highlights the risks and potential barriers to market and release of the three products outlined in the product development timeline.

B.6.1 Product Version One

The first release of the Raman Cell Analyser is solely intended as a research and development tool intended to reliably monitor the progress of stem cell differentiation without destroying or damaging the sample. Listed are the main issues that could hinder product development at this stage.

1. Acquiring a strong and well resolved signal in a closed system
    a. Design of sample holders that maximise this signal.
2. Detecting differentiation before it is possible by eye:
    a. Are there differences in spectra early in the differentiation process?
    b. If the differences are small, will there be sufficient resolution in the system to detect them?
3. Development of sufficiently sensitive software to analyse spectra
4. Demonstrating depth penetration in 3D samples.
5. Demonstrating an ability to isolate the signal of a cell from that of a scaffold that will likely possess a stronger Raman signal.
6. Convincing the research community to change engrained habits.

B.6.2 Product Version Two

The second release of the Raman Cell Analyser will still function as a research and development tool. However, improved features that permit automation of the system will allow users to generate greater amounts of data with less ‘hands on’ time. Such features will also allow the Raman Cell Analyser to reach additional markets in clinical pathology where it will be able to differentiate between different cell types in mixed samples. Listed are the main challenges for this product release.

1. Convincing existing users to purchase again, this may be overcome by designing version 1 in such a way that it may be retrofitted or by only adding

improved software to version 2 such that existing users need only purchase the additional software.

2. Developing or licensing software that can accurately identify cells or their features in many different settings.
3. Regulatory approval for clinical setting, would need to demonstrate very high detection for malignancy even in samples where there is very little. This is will likely involve clinical trials and therefore be costly.
4. Driving the participation in the uploading of user generated profiles, which would greatly increase the products value and usability but will likely be resisted by the research community wishing to protect their work.

B.6.3 Product Version Three

The third release of the Raman Cell Analyser will build on the previous releases by providing a fully controllable environment for cell samples including temperature, humidity and gas concentrations. This will allow one machine to accommodate many samples and analysis may automatically switch between them. Such high throughput screening may open further markets in toxicity screening of new pharmaceuticals for example. Listed are the main challenges for this product release.

1. Such additional hardware will likely require a redesign of the product.
2. The additional features will add value for existing users but the cost of the new design must not become prohibitive.
3. Previous versions will fit on a bench top, this version should be similarly small so as not to require too much lab space.

B.7 Summary

- The Raman Cell Analyser will have two core capabilities, monitoring of cellular status and distinguishing between different cell types.
- The technique will be entirely non-invasive and non-destructive.
- Phased product releases will accommodate greater system automation.
- Two core target markets, initially stem cell and regenerative medicine researchers within higher education research institutions. Later product releases targeted at clinical pathology diagnostics chiefly within the NHS.
- The Raman Cell Analyser could replace existing techniques for the routine assessment of cellular differentiation but will be incapable of more specific biological analysis.
- There is broad pricing potential as existing techniques are expensive so the Raman Cell Analyser could be priced competitively to meet the needs of the customer.
- Proof of concept for the Raman Cell Analyser's core capabilities are already reported in the scientific literature. However, technical challenges remain that must be addressed during product development.

Appendix C

Research Publications

Research Papers

Raman Spectroscopy using an Aseptic Method can Detect Changes Associated with Osteogenic Differentiation in Dental Pulp Stromal Cells. Adam Mitchell, Lorna Ashton, Xuebin B. Yang, Royston Goodacre, Alistair Smith, Jennifer Kirkham, PLOS one (under revision)

Abstract

There is an unmet need for the non-invasive characterisation of stem cells to facilitate the translation of cell-based therapies. Raman spectroscopy has proven utility in stem cell characterisation but as yet no method has been reported capable of taking repeated aseptic measurements of living cells. The aim of this study was to determine if Raman spectroscopy could be used to characterise human dental pulp stromal cell (DPSC) differentiation down the osteogenic lineage by taking repeated measurements from the same cell cultures over time. DPSCs were isolated from extracted premolar teeth from 3 consenting donors. Following *in vitro* expansion, DPSCs were maintained for 28 days in osteo-inductive medium. Raman spectra were acquired from the cells at days 0, 3, 7, 10, 14 and 28. Principal component analysis (PCA) was carried out to assess if there was any temporal spectral variation. At day 28, differentiation was confirmed using alizarin red staining and qRT-PCR for alkaline phosphatase and osteocalcin. Alizarin red staining was positive in all samples at day 28 and significant increases in alkaline phosphatase ($p<0.001$) and osteocalcin ($p<0.05$) gene expression were also observed. PCA of the Raman data demonstrated trends in PC1 from days 0-10, influenced by protein associated features and PC2 from days 10-28, influenced by DNA/RNA associated features. Raman spectroscopy can non-invasively detect changes in osteogenic cell cultures that are commensurate with cell differentiation. The data suggest that prediction and monitoring of DPSC differentiation using aseptic technique prior to their use in further applications might therefore be possible.

Introduction

The field of tissue engineering and regenerative medicine has advanced rapidly since its inception by Langer and Vacanti in 1993 (1), with clinical trials for the treatment of numerous conditions underway (80). Stem cells are an important component of the tissue engineering toolkit, from pluripotent embryonic stem cells and induced pluripotent stem cells to multipotent somatic stem cells including mesenchymal stem cells (MSCs) and haematopoietic stem cells (HSCs). The use of MSCs avoids the ethical concerns associated with embryonic stem cell research and whilst MSCs cannot differentiate along as many cell lineages they still possess demonstrable capacity for differentiation into osteoblasts, chondrocytes, adipocytes (55), tenocytes (235), hepatocytes (236) and neural cells (237). Such directed differentiation of MSCs and validation of their resulting phenotype requires significant expansion of stem cell cultures and testing with invasive and/or destructive methods that preclude their subsequent use in clinical application. Non-invasive methods that can reliably monitor stem cell differentiation could reduce the need for *in vitro* expansion and save researchers a great deal of time and resources when conducting their experiments. Raman spectroscopy is one such potential methodology for *in situ* analysis.

Raman spectroscopy has the capacity to be both non-invasive and non-destructive and utilises a monochromatic light source to determine sample chemistry. Upon interaction with the sample a small fraction of the light, approximately 1 in 10^6 to 10^8 photons (108), is shifted in wavelength with respect to the incident laser. Many chemical bonds in the sample cause unique Raman shifts such that the resultant spectrum can be considered to be a ‘molecular fingerprint’ that is unique to the sample under analysis. Several recent publications have described the use of Raman spectroscopy to determine cell viability (99, 128, 129), to identify general markers of cell differentiation (104, 128), to track differentiation to an osteoblastic phenotype (132) and to elucidate changes in extracellular matrix calcification and/or mineralisation concomitant with osteoblastic differentiation (101, 133, 134). These studies have identified a signature profile for the differentiation of stem cells down the osteogenic lineage based on the emergence and relative ratios of peaks in their Raman spectra illustrated in Figure 83. Whilst these data have highlighted the potential usefulness of Raman spectroscopy in stem cell phenotyping, to date

multiple longitudinal measurements of the *same* cell population have been precluded due to the need to maintain sterility of the cell cultures. Raman scattering efficiency is very poor and the distance between the sample and the microscope objective needs to be as small as possible. In order to maximise the potential of Raman spectroscopy as a tool for *non-invasive* stem cell characterisation, studies need to be conducted under aseptic conditions while maintaining the strength of the Raman signal. This would then ultimately permit early/predictive identification of differentiation such that stem cells may be used in further downstream applications.

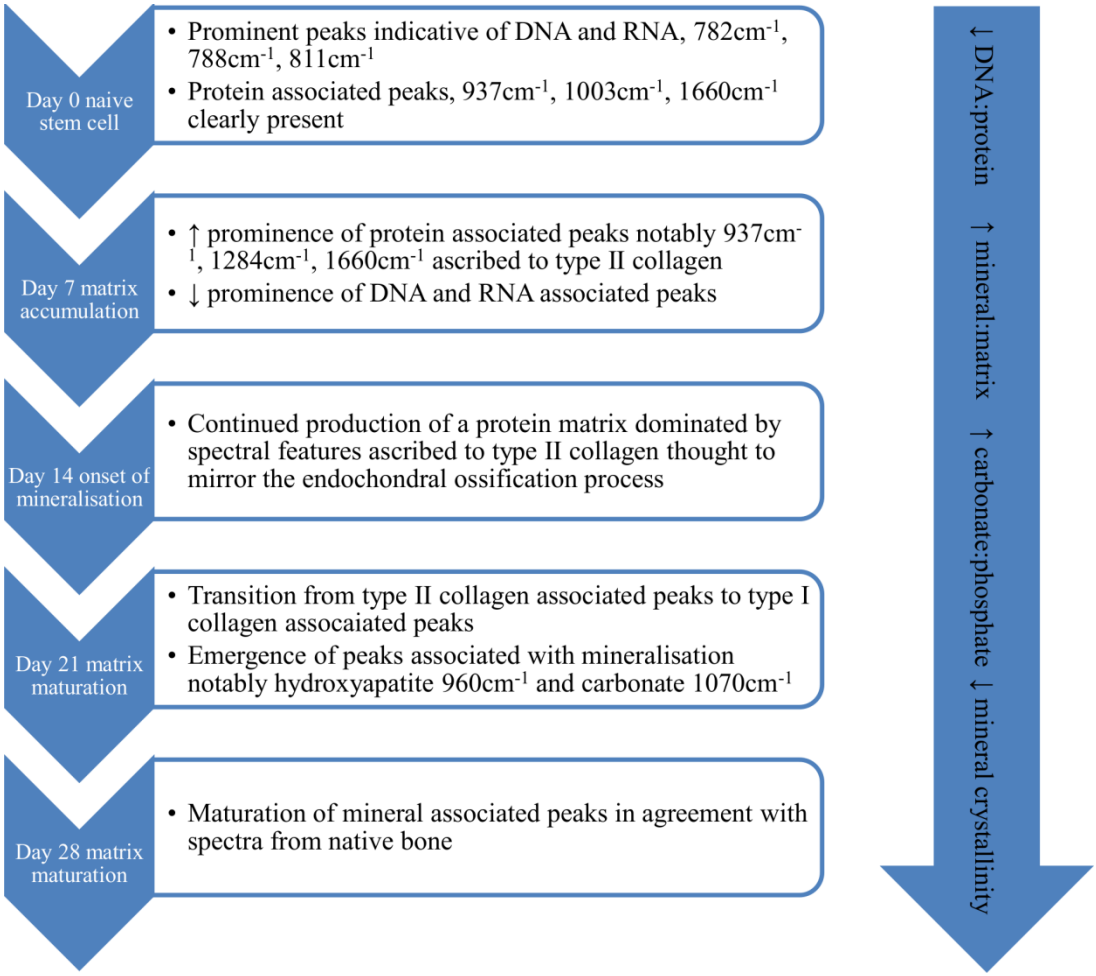

Figure 83. Proposed timeline of events outlining the osteogenic differentiation process of stem cells using Raman spectroscopy, based on data from (9, 11-15)

In this study, our aim was to develop a novel methodology that permits both the long term aseptic culture of human dental pulp stromal cells (DPSCs) and the repeated acquisition of Raman spectra in the same cell cultures. DPSCs are one of several sources that are more broadly classed as MSCs and were first isolated by Gronthos

et al 2000 (53). They have since been shown to differentiate down multiple lineages including osteogenic, dentinogenic, adipogenic, chondrogenic, myogenic and neurogenic and express many of the cell surface markers used to characterise bone marrow derived MSCs (225, 238-241). However, it should be noted that the propensity for differentiation along a specific lineage can vary amongst MSCs derived from different sources (241, 242). DPSCs were chosen specifically for this study as they have a proven predisposition toward the osteogenic/dentinogenic lineage (192), presenting a reliable and well documented sample for evaluating our new method. We envisage that Raman spectroscopy would be used as part of a minimally invasive approach to tissue engineering as such we used unsorted stromal cells from the dental pulp as opposed to a fluorescence activated cell-sorted (FACS) enriched stem cell population. We induced DPSC osteogenic differentiation and acquired Raman spectra at regular time intervals throughout the osteogenic pathway to determine both technical feasibility and identify whether changes in the Raman spectra might be indicative/predictive of the differentiation process.

Materials and Methods

Characterisation of Dental Pulp Stromal Cell (DPSC) Osteogenic Differentiation using Raman Spectroscopy

DPSC Isolation and Culture

Human molars were obtained from one male and two female donors, aged 9, 22 and 35y, by informed written consent (in the case of minors, consent was obtained through the parent/guardian) through the Leeds School of Dentistry Research Tissue Bank as authorised by the Dental Research Ethics Committee (DREC 07/H1306/93+5). DPSCs were isolated by the collagenase/dispase digestion method previously described by Gronthos *et al* (129) and maintained in basal medium, α-MEM containing 10% foetal calf serum (FCS) (Biosera, Ringmer, UK), 1% 10000 units/10 mg/mL penicillin /streptomycin solution (Sigma-Aldrich, Gillingham, UK) and 1% 200 mM L-glutamine (Sigma-Aldrich). Cultures were incubated at 37°C, 5% CO_2 and routinely passaged. DPSCs at passage 3 were used in all subsequent experiments.

Quartz Customised Flask Preparation

Customised cell culture flasks with quartz windows (Figure 84), suitable for Raman spectroscopy, were prepared by drilling 1 cm diameter holes in 25cm^2 cell culture flasks. Flasks were washed several times with sterile pure water to remove debris and finally sterilised with 70% ethanol. Heat sterilised quartz discs (Global Optics, Bournemouth, UK), 14 mm diameter x 0.15 mm thickness, were glued to the outside of the flasks using a UV cured methacrylate glue (Loctite, Hempstead, UK) and cured for 5 min under UV light. To ensure complete sterilisation, flasks were placed under a UV lamp for a further 90 min and periodically rotated to ensure penetration to all surfaces.

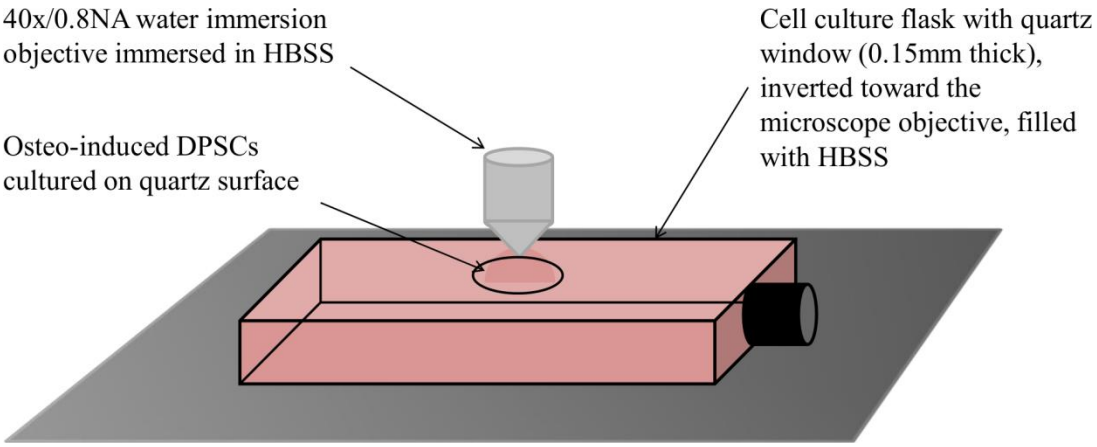

Figure 84. Schematic of a quartz window customised flask prepared for Raman spectroscopy. The microscope used to acquire Raman spectra uses an upright turret, therefore flasks had to be inverted toward the microscope objective. This necessitated the filling of the flask with HBSS to prevent the cells from desiccating during analysis.

DPSC Sample Preparation and Raman Spectroscopy

Sterile poly-L-lysine (0.1 mg/mL, molecular weight, 70,000-150,000 (Sigma-Aldrich)) was used to coat the quartz surface of the customised flasks to enhance cell adhesion, as poly-L-lysine coatings have little/no effect on Raman spectra (140). The solution was then aspirated and the flask dried in an incubator at 37°C overnight. DPSCs suspended in basal medium were pipetted directly on to the quartz surface at 1×10^5 cells/cm^2 (n=3) and incubated overnight at 37°C to adhere. The following day flasks were topped up with osteoinductive medium, (basal medium supplemented with 0.25 mM ascorbic acid, 10 mM β-glycerophosphate and 100 nM dexamethasone (all Sigma-Aldrich)). This was designated day 0. Each of the donor samples was cultured and analysed in triplicate. An equal number of samples were maintained in osteogenic conditions but did not undergo Raman analysis. These were used as controls for the sampling process. At no point during the cell culture period was there any evidence of bacterial or fungal contamination.

Prior to analysis the cell culture medium was aspirated and flasks filled with Hanks balanced salt solution (HBSS) with glucose added to a final level of 0.45%. Flasks were placed on the stage of a Leica DMLM microscope attached to a Renishaw RM series Raman spectrometer and inverted toward the objective. A 40×/0.8NA water immersion objective was immersed in a small drop of HBSS placed on the quartz

surface. DPSCs were first brought into focus under transmitted white light then over-focused by 5 µm and switched to 785 nm light for spectrum acquisition. Spectra were acquired at days 0, 3, 7, 10, 14 and 28. At each time point 15 spectra were acquired over the wavenumber range 600-1800 cm^{-1} with an exposure time of 120 s and the power on the sample from the 785 nm laser was 66 mW. With 9 samples (three donors in triplicate) this produced a total of 135 spectra at each time point. All spectra were acquired from the DPSC monolayer even at later time points, despite the emergence of mineralised nodules, for consistency. Cell free sections of quartz were used to acquire the background spectrum. Following analysis the HBSS was aspirated and replaced with osteoinductive medium and the flasks returned to the incubator.

Data Analysis

Pre-processing of spectra was performed in Grams/32 (Thermo Scientific, Waltham, USA) with further processing and validation by principal component analysis (PCA) performed in Matlab version R2013b. In Grams each individual spectrum was background subtracted using cell free areas of HBSS filled quartz customised flasks, y-axis normalised to the peak at 1003 cm^{-1} to correct for any minor unavoidable instrumental drift due to sampling over a long period of time, and smoothed using a 7 point Savitzky-Golay filter. All spectra were then exported to Microsoft Excel for further processing in Matlab. PCA was performed on all spectra from each individual donor and used to remove outlying spectra from each time point. The data were then averaged using one spectrum from each donor per time point. Finally second derivative spectra were calculated and further smoothing performed. PCA was then carried out to visualise the fully processed data. Such pre-processing was required to overcome intrinsic experimental constraints such as the longer working distance and the need to acquire spectra through an interface presented by working aseptically with quartz windowed flasks.

Osteogenic and Cell Stress Marker Gene Expression of DPSCs ± Analysis by Raman Spectroscopy Determined by qRT-PCR

To determine the stage of osteogenic differentiation and any effects of Raman spectroscopy on the osteoinductive process, qRT-PCR was used to determine

marker gene expression, RNA isolation and reverse transcription was performed on DPSCs following osteoinductive culture ± Raman spectroscopy analysis. Briefly, DPSCs were lysed by incubation with Trizol® (Invitrogen, Paisley, UK) for 20 min at room temperature. RNA was extracted from cell lysates using an RNeasy mini kit with additional DNase digestion (Qiagen, Crawley, UK) following the manufacturers recommendations. RNA concentrations were quantified using a NanoDrop spectrophotometer (Thermo Scientific). A High Capacity RNA-to-cDNA Kit (Applied Biosystems, Carlsbad, USA) was used to prepare 200 ng of cDNA in 20 μL reaction volumes as per the manufacturer's instructions. Reactions were run on a MJ Research PTC-100 Thermo Cycler, at 37°C for 1 h and 95°C for 5 min. qRT-PCR was performed using TaqMan gene expression assays (Applied Biosystems) for alkaline phosphatase (*ALP*) and osteocalcin (*OC*): assay numbers Hs01029144-m1 and Hs00609452-g1 respectively, to determine osteogenic marker expression and for heat shock transcription factor 1 (*HSF1*), hypoxia inducible factor 1 (*HIF1A*) and lactate dehydrogenase (*LDH*): assay numbers Hs00232134-m1, Hs00153153-m1 and Hs00929956-m1 respectively, to investigate cell stress marker expression. Reactions were carried out in 96 well plates on a Roche LightCycler® 480 system. Optimal cDNA concentration was determined to be 5 ng/reaction by plotting standard curves with known cDNA concentrations. Data were normalised to *YWHAZ* assay number Hs00237047-m1, and analysed using the comparative cycle threshold method (ΔCT). *YWHAZ* was selected as it has been shown to be a far more reliable housekeeping gene compared with some of the more traditional housekeeping genes such as *GAPDH* and *ACTB* (157). Three patient samples, one in duplicate, were analysed using both DPSCs that had undergone analysis by Raman spectroscopy and DPSCs cultured in parallel under the same conditions but without subjection to Raman spectroscopy after 28 days of osteoinductive culture. Samples were analysed in triplicate for a total n=12 for each group. Samples from day 0 were used to provide a baseline. Graphs of the mean ΔCT ± SE were plotted in Microsoft Excel and statistical significance was determined by one-way ANOVA using GraphPad Instat 3 software.

Extracellular Matrix Calcification of DPSC cultures ± Analysis by Raman Spectroscopy using Alizarin Red Staining

Alizarin red staining was performed on day 28 DPSC cultures that had been analysed by Raman spectroscopy and those that had not (n=2). In both cases, DPSCs had been cultured in osteoinductive medium as described above. Cell monolayers were washed twice with PBS and fixed in 10% neutral buffered formalin for 1 h at room temperature. Cell monolayers were incubated with 1% Alizarin red solution (Sigma-Aldrich) (pH 4.2), for 20 min at room temperature. The Alizarin red solution was then removed and excess stain washed away with repeated washes with de-ionised water. Cultures were then imaged using an Olympus BX50 microscope with accompanying Nikon DS-Fi1 camera.

Results

Osteogenic Differentiation of DPSCs Characterised by Raman Spectroscopy

Raman spectroscopy has previously been used to demonstrate late stage osteogenic differentiation of stem cells by analysing putative mineralised nodules (101, 134). In this study DPSCs were analysed by Raman spectroscopy with a focus on earlier time points, prior to the emergence of mineralised nodules, to ascertain if the spectra were indicative/predictive of the osteogenic differentiation process. Figure 34 depicts the average spectra for each time point (day 0 to day 28) following subtraction of the signal from the (quartz) background. Many peaks typical of biological samples were clearly evident such as phenylalanine at 1003cm^{-1}, CH_3, CH_2 found in collagen at 1453cm^{-1} and amide I at 1660cm^{-1}.

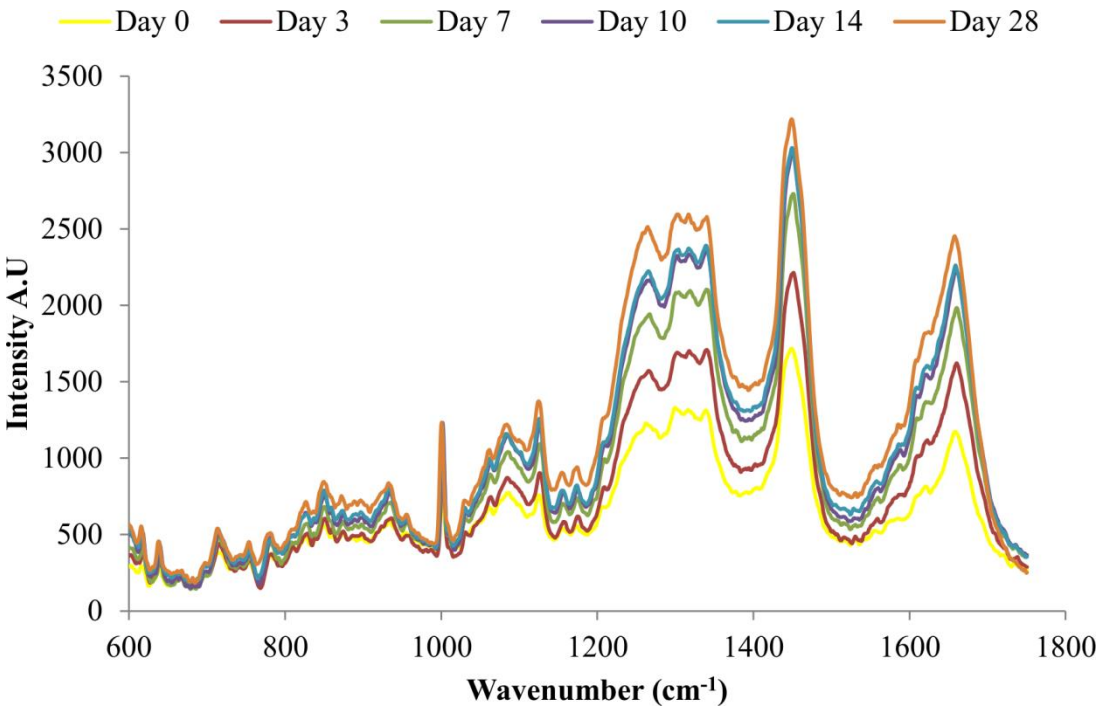

Figure 85. Average background subtracted spectra of osteo-induced DPSCs at days 0, 3, 7, 10, 14 and 28, n=135 spectra per time point from three separate donors.

Principal component analysis (PCA) was performed on spectra obtained from DPSCs from three donor samples, analysed in triplicate, which had been averaged, *n*=135 spectra at each time point. PCA is a method of reducing the dimensionality of multivariate data into groups of potentially correlated variables called principal

components (PCs). PC1 represents the group of variables responsible for the greatest amount of variation in the data and PC2 the group of variables responsible for the second greatest variation in the data and so on. In the case of Raman spectra such as those presented here the variables are the wavenumbers which in turn correspond to particular molecular species within the cells. Figure 86A is a 2D scatter plot of PC1 and PC2 scores accounting for 54.2% and 12.4% of the variation in the data set respectively, this indicates that the wavenumbers contained within PC1 and concomitantly the molecular species they are associated with accounted for 54.2% of the variation in the data set and so on. The PCA scores plot demonstrated a clustering of spectra at each time point, illustrating that the spectral collection was reproducible. As expected, there was overlapping of spectra between adjacent time points as there was a phenotypic shift that was continuous in nature during cellular differentiation. Despite the overlapping of time points a clear trend was observed from day 0 to day 10 along PC1 while a trend from day 7 to day 28 was observed along PC2. Loadings plots can be drawn for each PC to illustrate those spectral features that are responsible for the variance in that PC. Peaks on the same side of a loading plot will be behaving similarly, whilst peaks on opposite sides of a loading plot will be behaving differently with respect to their scores within a given PC. Figure 86B+C illustrate the loading plots for PC1 and PC2.The loading plot for PC1 showed positive peaks for wavenumbers corresponding to amide bonds (1260 cm^{-1} and 1660 cm^{-1}), CH_3, CH_2 from collagen (1345 cm^{-1} and 1453 cm^{-1}), phenylalanine (1003 cm^{-1}) and lipids (1126 cm^{-1}) whilst wavenumbers corresponding to ribose (975 cm^{-1} and 1020 cm^{-1}), the nucleic acids guanine and adenine (1420 cm^{-1}) and DNA (1490 cm^{-1}) had negative peaks. Similarly the loading plot for PC2 had positive peaks at 1003 cm^{-1}, 1453 cm^{-1} and 1660 cm^{1} with negative peaks at 975 cm^{-1}, 1020 cm^{-1} and 1490 cm^{-1}. Putative peak assignments were based on Movasaghi *et al* (97). As the above individual PCs both use the same areas it may be hard to differentiate which are the important vibrations with respect to time, therefore PC1 was plotted against PC2 (Figure 86D). In this instance the position of a given wavenumber on the plot when transposed on the original scores plot indicates where that wavenumber varies most greatly. This loadings plot showed that two protein associated peaks at 1453 cm^{-1} and 1660 cm^{-1} transpose along the trend in PC1 from days 0 to 10, whilst two DNA/RNA associated peaks 975 cm^{-1} and 1020 cm^{-1}

transpose along the trend in PC2 from days 10 to 28 as did the phenylalanine peak at 1003 cm^{-1}.

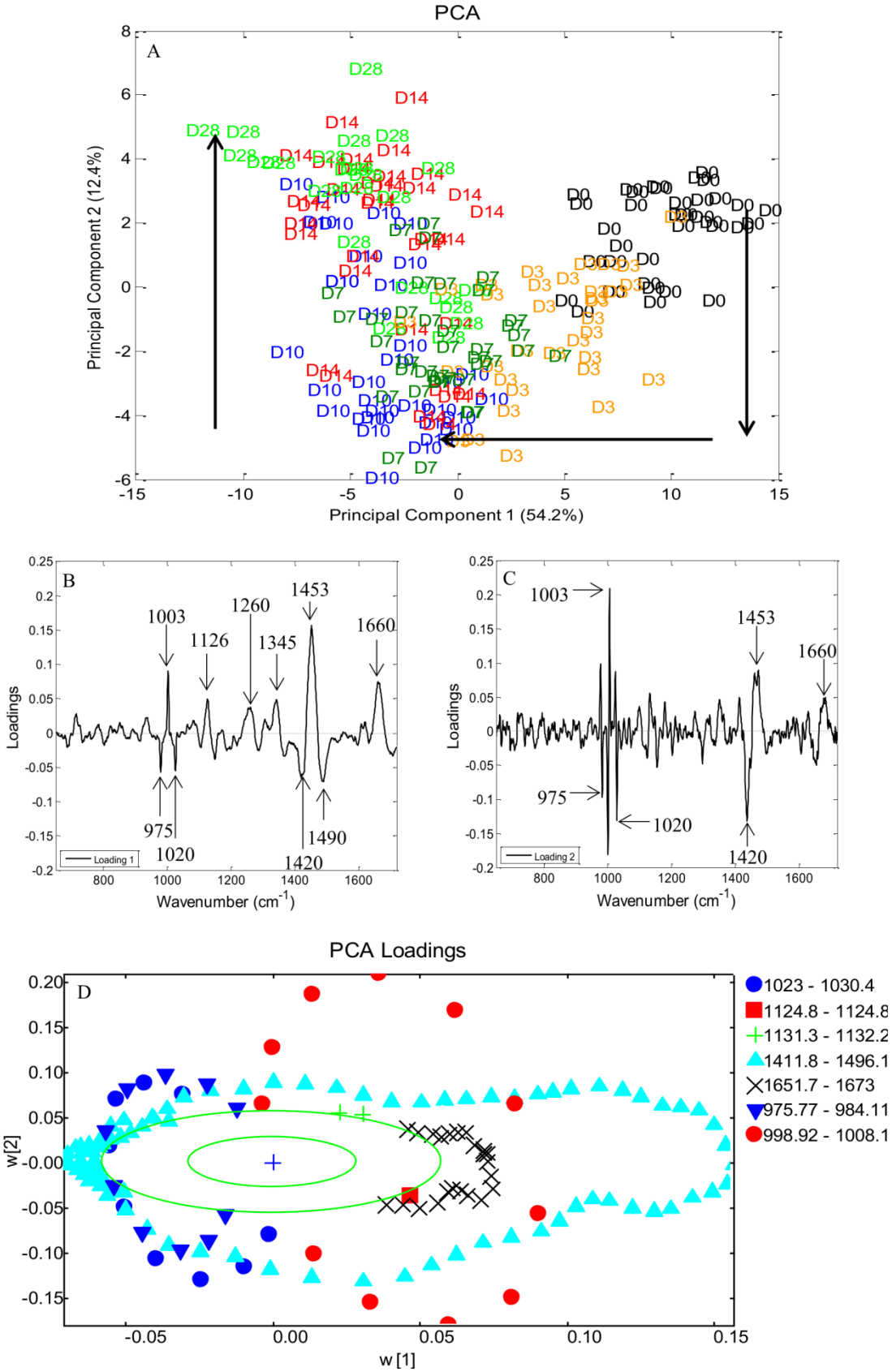

Figure 86. A) Principal component analysis of the osteogenic differentiation of DPSCs at days 0, 3, 7, 10, 14 and 28. 2D scatter plot for principal components 1 and 2. Each position displayed is the average of three spectra, one from each donor, for every time point. There is a clear trend in PC1 between days 0 and 10 and a further trend in PC2 between days 0 and 10 and days 10 and 28, marked with arrows. B + C) PCA loadings plot for PC1 and PC2 respectively, from the PCA of DPSCs that had been osteo-induced for 0, 3, 7, 10, 14 and 28 days. Significant positive and negative peaks are marked. D) PCA loadings plot for PC1 *versus* PC2, the outer green circle indicates 95% confidence. In the legend are groups of wavenumbers from peaks that vary significantly.

Finally, to confirm osteogenic differentiation of DPSCs at day 28 several Raman spectra were acquired from putative mineralised nodules, (Figure 87). The well characterised mineral associated region, 955 cm^{-1}-964 cm^{-1}, described in several previous studies (101, 133, 134), was clearly evident.

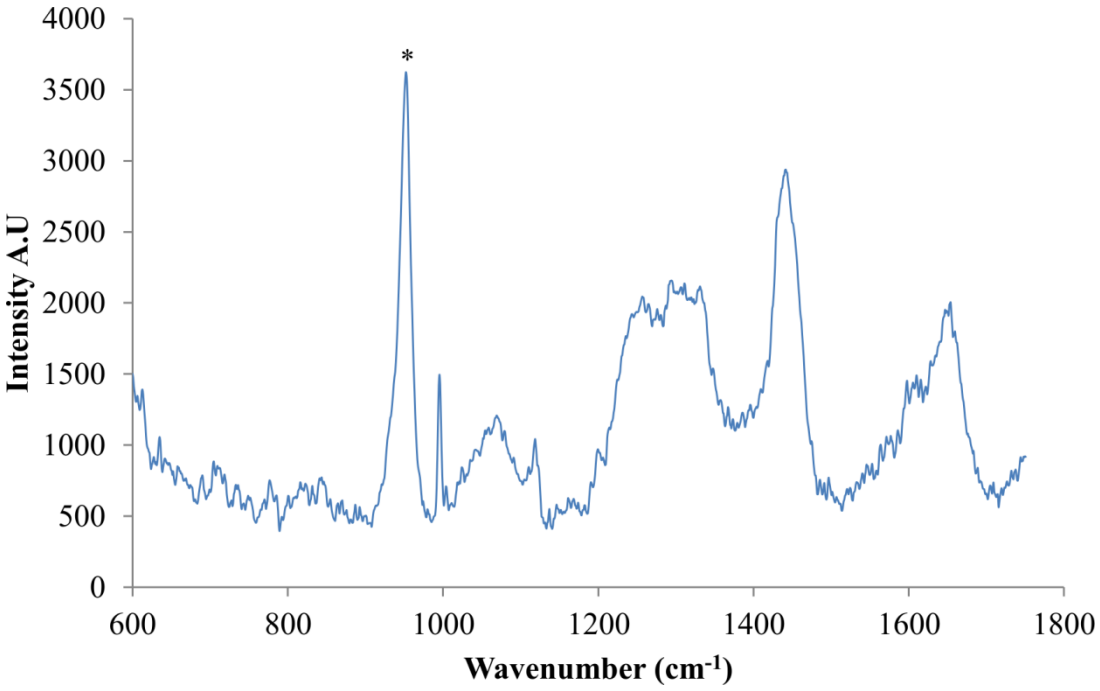

Figure 87. Average background subtracted spectra of osteo-induced DPSCs at day 28 acquired from putative mineralised nodules, n=5. The well characterised mineral associated region at ~955cm^{-1}-964cm^{-1} is clearly evident, marked *.

Osteogenic Differentiation of DPSCs ± Analysis by Raman Spectroscopy using qRT-PCR and Alizarin Red Staining

qRT-PCR and Alizarin red staining were used to confirm osteogenic differentiation of DPSCs after 28 days in osteoinductive medium. Samples that had undergone Raman measurements, and those grown in parallel without being subject to Raman, were analysed to determine if the data acquisition process and the Raman spectroscopy itself had any effect on DPSC osteogenic differentiation. qRT-PCR showed significant increases in *ALP* and *OC* expression between days 0 and 28 of osteo-inductive culture irrespective of whether or not the DPSCs had undergone Raman analysis ($p<0.001$ and $p<0.05$ respectively) (Figure 88A). There was no significant difference in the expression of either gene between DPSCs which had been analysed by Raman spectroscopy and those that had not.

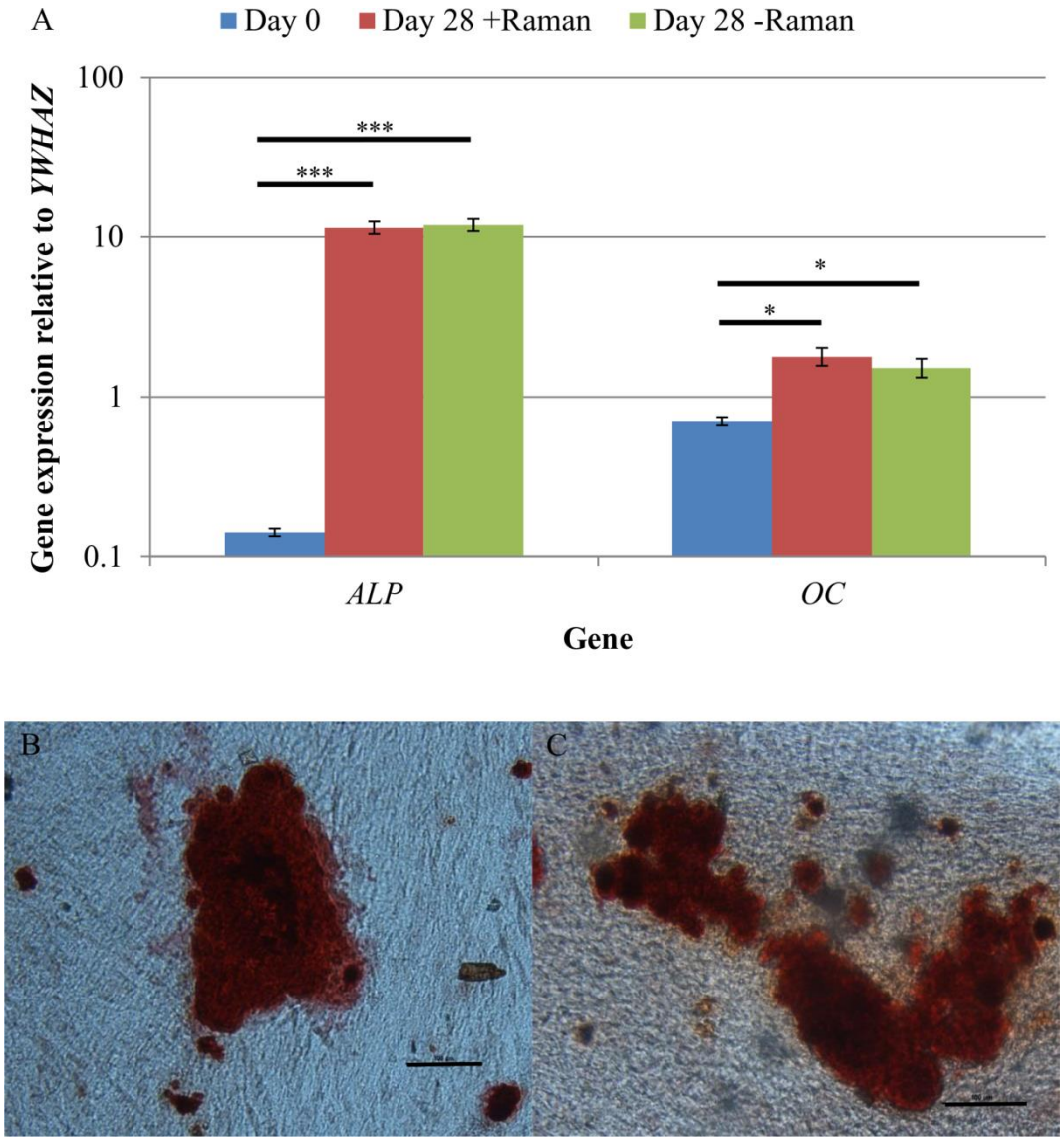

Figure 88. A) A comparison of DPSC osteogenic gene expression at day 0, and day 28 from cells that had/had not undergone Raman spectroscopy. Results show mean ±SE, n=3 (day 0), n=12 (day 28 + Raman), n=12 (day 28 – Raman). *** p<0.001, * p<0.05. Significant increases in the expression of both genes was found between days 0 and 28 and there was no difference in the expression between DPSCs that had and had not undergone Raman spectroscopy. Alizarin red staining of DPSCs after 28 days of osteo-induction that B) had undergone Raman measurements and C) had not undergone Raman measurements. Scale bars = 100 µm. Positive staining of bone nodules was observed regardless of whether the DPSCs had undergone Raman spectroscopy or not.

Alizarin red staining was used to demonstrate extracellular matrix calcification in DPSC cultures after 28 days of osteo-induction for samples that had been analysed by Raman spectroscopy (Figure 88B) and those that had not (Figure 88C). Positive

Alizarin red staining was observed in all samples, with no discernible differences between the Raman and non-Raman groups, however this was not quantified.

Comparison of DPSCs Cell Stress Marker Gene Expression ± Analysis by Raman Spectroscopy using qRT-PCR

The data acquisition process during Raman spectroscopy used in this study was entirely aseptic and non-invasive permitting the same cell cultures to be analysed repeatedly throughout the differentiation process. However, this method had the potential to induce a cell stress response, due to, for example, limited gas diffusion, exposure to ambient temperature and atmospheric gas concentrations, as well as the laser on the sample. In order to test for any cell stress response, the expression of three marker genes, heat shock transcription factor 1 (*HSF*), hypoxia inducible factor 1 (*HIF*) and lactate dehydrogenase (*LDH*) was determined by qRT-PCR for DPSCs at day 0 and day 28 ± Raman spectroscopy (Figure 89). No significant differences in the expression of all three genes were observed between the groups ($p>0.05$) showing that the Raman and the new culturing approach had not affected the cells.

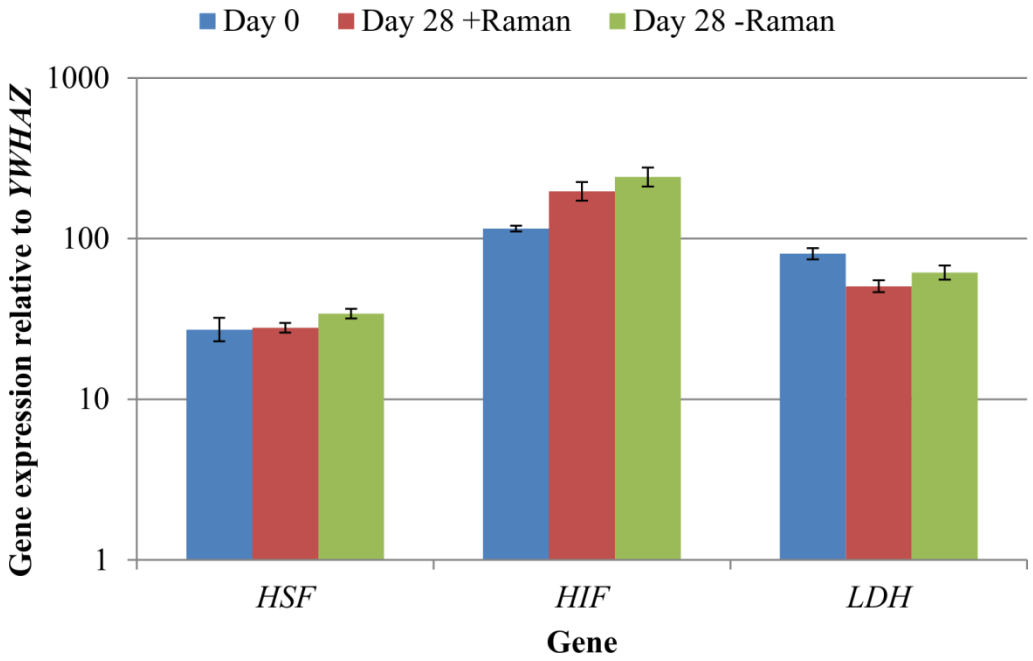

Figure 89. A comparison of DPSC cell stress marker expression at day 0, and day 28 from cells that had/had not undergone Raman spectroscopy. Results show mean ±SE, n=3 (day 0), 12 (day 28 + Raman), 12 (day 28 – Raman). No significant changes in gene expression were observed.

Discussion

This study had two aims, to develop a method for the aseptic acquisition of Raman spectra from the same cell cultures over a period of time that did not perturb the cells during Raman analysis and to validate this approach by characterising the osteogenic differentiation of DPSCs, prior to the outcome becoming apparent by the emergence of mineralised nodules. At this end point there is no need for a non-invasive method to determine cellular differentiation status as such nodules are clearly discernible under an ordinary microscope without staining. Therefore we focused on acquiring spectra in the first 14 days of osteo-induction with a view to identifying spectral features that may indicate/predict cell differentiation.

The first aim of this study, to acquire Raman spectra repeatedly over time from the same cell cultures under aseptic conditions, was achieved by customising standard tissue culture flasks with quartz windows. This allowed DPSCs to be cultured and analysed in the same vessel making the method truly non-invasive. There was no evidence of any bacterial or fungal contamination of our cultures at any point. However, in future experiments towards the clinical application of our research an extensive demonstration that the technique used is aseptic would be conducted. A lack of optimised environmental control during spectra acquisition had the potential to induce a cell stress response. In order to investigate any cell stress the expression of heat shock transcription factor 1 (*HSF*), hypoxia inducible factor 1 (*HIF1*) and lactate dehydrogenase (*LDH*) was determined by qRT-PCR. *HSF* is a transcription factor regulating the expression of several important heat shock factor proteins including HSP70 and HSP90 (195) and whilst it is primarily induced by hyperthermia it has been shown to be activated in response to increasing temperature following hypothermia (196). *HIF1* is expressed in response to hypoxia which at physiological levels (2-9% O_2) is beneficial and a key regulatory mechanism in several biological processes including embryogenesis and stem cell function, however overexpression at pathological levels (<1% O_2) is associated with several conditions including ischemia and cancer (197-199). *LDH* expression is known to be stimulated by *HIF1* expression and is associated with cancer through increased anaerobic glycolysis by a process termed the Warburg effect (200, 201). No significant differences in the expression of all three markers genes were found in

DPSCs regardless of the Raman sampling process and relative to the start of the experiment. Whilst this is not an exhaustive interrogation of the effects of performing Raman spectroscopy on DPSCs in ambient conditions for approximately 3 h at a time, it does indicate that any effects were negligible. Previous studies have also demonstrated that Raman spectroscopy and in particular exposure of cells to near infra-red lasers with a power on the sample of up to 115 mW does not induce cell damage (102). Finally, we determined that our method had no effect, detrimental or otherwise, on the osteogenic differentiation process as evidenced by no differences in the expression of osteogenic marker genes or in Alizarin red staining between DPSCs that had or had not undergone analysis by Raman spectroscopy.

The second aim of the study, to validate our aseptic method for cell phenotyping, was achieved using repeated Raman measurements to characterise the osteogenic differentiation of DPSCs. PCA was performed on spectra acquired throughout the osteoinductive differentiation process. The PCA scores plot of PC1 *versus* PC2 demonstrated two phases in the process hinged at approximately day 10. The loadings for PC1 and PC2 indicated that the pattern of those spectral features indicative of proteins and lipids was similar while features indicative of DNA and RNA had the opposite pattern but were also similar to one another. When the loadings for PC1 and PC2 were plotted against each other, protein associated peaks were shown to vary the most in PC1 and therefore from days 0 to 10 while DNA/RNA associated peaks varied the most in PC2 and therefore from days 10 to 28. It is clear from the averaged spectra at each time point that the protein associated peaks at 1453 cm^{-1} and 1660 cm^{-1} were increasing in intensity. Taken together this suggests that in the early stages of DPSC osteogenic differentiation increasing protein content is the main marker. This is in agreement with the findings of many others (101, 104, 134) and is the first instance where this has been demonstrated using the same cell cultures. However, a firm conclusion is more difficult to draw in the case of the DNA/RNA associated peaks contributing to the trend in PC2 due to their relatively low signal intensity in the original spectra and the lower contribution of PC2 (12.4%) to the variation within the data set. Schulze *et al* 2010 (104) found that one of the major indicators of differentiation in embryonic stem cells was the ratio of spectral peaks related to proteins and DNA/RNA, concluding that the

intensity of protein associated peaks increased in intensity whilst DNA/RNA peaks decreased in intensity with differentiation. Whilst it is clear from our data that the intensity of protein associated peaks increases with time the trend is less clear with regards to DNA/RNA. Our method however, was clearly able to detect late stage osteogenic differentiation, when directed toward mineralised nodules as evidenced by the prominent mineral associated region at 955-964cm^{-1}.

In order to enhance the translation of stem cell based therapies into the clinic, methods that permit the non-invasive characterisation of stem cell cultures prior to their end point are required. Our method, involving the use of standard cell culture flasks customised with quartz windows to permit analysis by Raman spectroscopy is simple, easily reproducible and capable of detecting events that are commensurate with the osteogenic differentiation process of DPSCs. This approach is easily scaled and capable of producing large numbers of Raman-characterised clinically relevant cells. As a research tool this method can greatly reduce the time and cost associated with producing and validating osteo-induced stem cells for use in further research such as the production of cell seeded tissue engineered constructs.

Oral Presentations

Raman Spectroscopy in the Non-invasive Phenotyping of Human Dental Pulp Stem Cells (hDPSCs) – Identification of a Suitable Substrate for Cell Culture. Adam Mitchell, Xuebin B. Yang, Alistair Smith, Jennifer Kirkham, Leeds School of Dentistry postgraduate research day, July 2012

Non-destructive phenotyping of stem cells is increasingly important in both research and clinical settings. Current methods render samples unusable for further applications. Using Raman spectroscopy, which has previously been employed to discriminate between naïve and differentiated stem cells, would permit subsequent sample re-use. However, on-going monitoring of stem cell differentiation in a single sample is lacking. To achieve this, a Raman appropriate substrate material must be identified as tissue culture plastic is unsuitable.

hDPSCs were isolated from healthy teeth donated with full consent. Following expansion hDPSCs were seeded on magnesium fluoride (MgF_2), quartz, or tissue culture plastic, cultured to confluence and osteo-induced. Differentiation was assessed at 7 and 28 days using qRT-PCR for osteogenic gene markers, and alizarin red staining.

After 28 days there were no significant differences in gene expression between hDPSCs cultured on quartz and tissue culture plastic, those cultured on MgF_2 exhibited significantly lower levels of *COL1A* expression, and the late osteogenic marker osteocalcin. Alizarin red staining of hDPSCs grown on quartz and tissue culture plastic was comparable but weaker on MgF_2.

hDPSCs osteo-induced on quartz substrates possess a comparable phenotype to those cultured on tissue culture plastic in contrast to those grown on MgF_2. The presence of Mg^{++} in culture medium has been demonstrated to inhibit calcification and this may explain the weaker induction of hDPSCs grown on MgF_2 if Mg^{++} from the substrate is leeching into the medium. We conclude that quartz will be a useful substrate for non-invasive stem cell phenotyping using Raman spectroscopy.

Raman spectroscopy can be used to non-invasively and aseptically characterise stem cell differentiation. Adam Mitchell, Lorna Ashton, Xuebin B. Yang, Royston Goodacre, Alistair Smith, Jennifer Kirkham, Leeds School of Dentistry postgraduate research day, July 2014 (1st place – oral presentation)

There is an unmet need for the non-invasive characterisation of stem cells to facilitate the translation of cell-based therapies. Raman spectroscopy has proven utility in stem cell characterisation but as yet no method has been reported capable of taking repeated aseptic measurements of living cells, such that the cells remain suitable for clinical use. The aim of this study was to develop such a method and validate it through the characterisation of stem cell osteogenic and adipogenic differentiation. Human dental pulp stromal cells (DPSCs) and adipose derived stem cells (ADSCs) were osteo and adipo-induced respectively in custom made cell culture flasks with quartz windows appropriate for Raman spectroscopy. Raman spectra were acquired at regular time intervals during the culture periods and principal component analysis (PCA) used to analyse the data. qRT-PCR measured the expression of osteogenic, adipogenic and cell stress markers. PCA of spectra obtained from osteo-induced DPSCs indicated that protein-associated features varied significantly early in the differentiation process (days 0-10) whilst DNA/RNA-associated features varied significantly later on (days 10-28). qRT-PCR showed that osteogenic marker gene expression was significantly increased after 28 days. Cell stress marker expression was unaffected the Raman process. PCA of spectra obtained from adipo-induced ADSCs indicated that lipid-associated features varied significantly throughout adipogenesis (days 0-14) whilst protein and DNA/RNA-associated features varied significantly later on (days 7-14). Adipogenic marker gene expression was significantly increased after 14 days. The Raman spectra acquired in this study and the important spectral features revealed through PCA are broadly in agreement with the findings of previous studies using fixed (non-living) cells and/or non-sterile methods that preclude repeated measurements over time. In contrast, this study has demonstrated that repeated Raman measurements of living cells can be obtained under aseptic conditions, providing a potential method for non-invasive stem cell characterisation for subsequent clinical use.

Raman spectroscopy can be used to non-invasively and aseptically characterise stem cell differentiation. Adam Mitchell, Lorna Ashton, Xuebin B. Yang, Royston Goodacre, Alistair Smith, Jennifer Kirkham, Joint Doctoral Training Centre in Tissue Engineering and Regenerative Medicine conference, July 2014

There is an unmet need for the non-invasive characterisation of stem cells to facilitate the translation of cell-based therapies. Raman spectroscopy has proven utility in stem cell characterisation but as yet no method has been reported capable of taking repeated aseptic measurements of living cells, such that the cells remain suitable for clinical use. The aim of this study was to develop such a method and validate it through the characterisation of stem cell osteogenic and adipogenic differentiation. Human dental pulp stromal cells (DPSCs) and adipose derived stem cells (ADSCs) were osteo and adipo-induced respectively in custom made cell culture flasks with quartz windows appropriate for Raman spectroscopy. Raman spectra were acquired at regular time intervals during the culture periods and principal component analysis (PCA) used to analyse the data. qRT-PCR measured the expression of osteogenic, adipogenic and cell stress markers. PCA of spectra obtained from osteo-induced DPSCs indicated that protein-associated features varied significantly early in the differentiation process (days 0-10) whilst DNA/RNA-associated features varied significantly later on (days 10-28). qRT-PCR showed that osteogenic marker gene expression was significantly increased after 28 days. Cell stress marker expression was unaffected the Raman process. PCA of spectra obtained from adipo-induced ADSCs indicated that lipid-associated features varied significantly throughout adipogenesis (days 0-14) whilst protein and DNA/RNA-associated features varied significantly later on (days 7-14). Adipogenic marker gene expression was significantly increased after 14 days. The Raman spectra acquired in this study and the important spectral features revealed through PCA are broadly in agreement with the findings of previous studies using fixed (non-living) cells and/or non-sterile methods that preclude repeated measurements over time. In contrast, this study has demonstrated that repeated Raman measurements of living cells can be obtained under aseptic conditions, providing a potential method for non-invasive stem cell characterisation for subsequent clinical use.

Poster Presentations

Raman Spectroscopy in the Non-invasive Phenotyping of Human Dental Pulp Stem Cells (hDPSCs) – Identification of a Suitable Substrate for Cell Culture. Adam Mitchell, Xuebin B. Yang, Alistair Smith, Jennifer Kirkham, Joint Doctoral Training Centre in Tissue Engineering and Regenerative Medicine conference, July 2012

Introduction:

Non-destructive phenotypic characterisation of stem cells is becoming increasingly important in both research and clinical settings. Current methods such as immunohistology, qRT-PCR and western blotting render samples unusable for further applications. One of several methods that would permit the subsequent re-use of samples is Raman spectroscopy. Raman spectroscopy has already been used to discriminate between cancerous and non-cancerous cells (1), and naïve and differentiated stem cells (2). However, an on-going assessment of stem cell differentiation of a single sample is yet to be demonstrated. In order to achieve this, a suitable substrate material that does not interfere with the differentiation process must be identified as tissue culture plastic is unsuitable for Raman spectroscopy applications

Materials and Methods:

hDPSCs were isolated from healthy teeth donated with appropriate ethical consent. Following population expansion hDPSCs were seeded on to magnesium fluoride (MgF_2), quartz, or tissue culture plastic, cultured to confluence and osteo-induced. Differentiation was assessed at 7 and 28 days using alizarin red staining, and qRT-PCR for osteogenic gene markers.

Results:

After 28 days there were no significant differences in gene expression between hDPSCs grown on quartz and tissue culture plastic. However, those cultured on MgF_2 exhibited significantly lower levels of expression of type 1 collagen, and the late osteogenic marker osteocalcin (fig 1). Alizarin red staining of hDPSCs grown on quartz and tissue culture plastic after 28 days was comparable, but weaker for those cultured on MgF_2.

Discussion:

hDPSCs osteo-induced on quartz substrates possess a comparable phenotype to those cultured on tissue culture plastic, whilst those grown on MgF_2 do not. The presence of Mg^{++} in culture media has been demonstrated to inhibit calcification in a dose dependant manner (3). This may explain the weaker induction of hDPSCs grown on MgF_2 if Mg^{++} from the substrate is leeching into the media.

Conclusion:

Raman spectroscopy of hDPSCs cultured on quartz substrates will provide a mechanism for non-invasive phenotyping of stem cell differentiation along the osteogenic pathway.

Development of a method for the non-invasive and non-destructive characterisation of human dental pulp stem cells. Adam Mitchell, Xuebin B. Yang, Alistair Smith, Jennifer Kirkham, Leeds School of Dentistry postgraduate research day, July 2013

There is need for characterisation of stem cell differentiation using non-invasive and non-destructive methods for both research applications and prior to their use in cell-based regenerative therapies. Raman spectroscopy, which uses near infra-red light to determine sample chemistry, has been used to characterise stem cells but its application has been limited due to an inability to maintain sterility. The aim of this study was to design a system to permit repeated application of Raman spectroscopy to living stem cells in long term culture. This required 1) identification of a Raman appropriate substrate, 2) development of a system to maintain culture sterility and 3) selection of an optical configuration to maximise the Raman signal. Quartz and MgF_2 were investigated as potential cell culture substrates. Dental pulp stem cells (DPSCs) were osteo-induced and their stage of differentiation assessed by qRT-PCR and alizarin red staining. Quartz cuvettes and cell culture flasks, customised to accommodate quartz coverslips were tested for culture sterility. A variety of microscope lenses were tested for optimal Raman signal acquisition and average spectra produced from 50 individual loci for each cell culture. Results demonstrated that DPSCs cultured on quartz but not MgF_2 had similar osteogenic differentiation to those cultured on tissue culture plastic. DPSCs cultured in quartz cuvettes and in customised culture flasks were successfully maintained in sterile conditions for up to 28 days. Customised culture flasks were selected as the thickness of the cuvette quartz precluded successful acquisition of Raman spectra. A 40x 0.8NA water immersion lens demonstrated reproducible spectra and the best signal intensity to noise ratio. Sterility can be maintained and Raman spectra successfully acquired using cell culture flasks customised with quartz windows and a water immersion lens. This offers a non-invasive system by which Raman spectroscopy may be used to characterise the differentiation status of stem cells.

Development of a method for the non-invasive and non-destructive characterisation of human dental pulp stem cells. Adam Mitchell, Xuebin B. Yang, Alistair Smith, Jennifer Kirkham, Joint Doctoral Training Centre in Tissue Engineering and Regenerative Medicine conference, July 2013

There is need for characterisation of stem cell differentiation using non-invasive and non-destructive methods for both research applications and prior to their use in cell-based regenerative therapies. Raman spectroscopy, which uses near infra-red light to determine sample chemistry, has been used to characterise stem cells but its application has been limited due to an inability to maintain sterility. The aim of this study was to design a system to permit repeated application of Raman spectroscopy to living stem cells in long term culture. This required 1) identification of a Raman appropriate substrate, 2) development of a system to maintain culture sterility and 3) selection of an optical configuration to maximise the Raman signal. Quartz and MgF_2 were investigated as potential cell culture substrates. Dental pulp stem cells (DPSCs) were osteo-induced and their stage of differentiation assessed by qRT-PCR and alizarin red staining. Quartz cuvettes and cell culture flasks, customised to accommodate quartz coverslips were tested for culture sterility. A variety of microscope lenses were tested for optimal Raman signal acquisition and average spectra produced from 50 individual loci for each cell culture. Results demonstrated that DPSCs cultured on quartz but not MgF_2 had similar osteogenic differentiation to those cultured on tissue culture plastic. DPSCs cultured in quartz cuvettes and in customised culture flasks were successfully maintained in sterile conditions for up to 28 days. Customised culture flasks were selected as the thickness of the cuvette quartz precluded successful acquisition of Raman spectra. A 40x 0.8NA water immersion lens demonstrated reproducible spectra and the best signal intensity to noise ratio. Sterility can be maintained and Raman spectra successfully acquired using cell culture flasks customised with quartz windows and a water immersion lens. This offers a non-invasive system by which Raman spectroscopy may be used to characterise the differentiation status of stem cells.

Development of a method for the non-invasive and non-destructive characterisation of human dental pulp stem cells. Adam Mitchell, Xuebin B. Yang, Alistair Smith, Jennifer Kirkham, Regener8 conference, Leeds, October 2013

There is need for characterisation of stem cell differentiation using non-invasive and non-destructive methods for both research applications and prior to their use in cell-based regenerative therapies. Raman spectroscopy, which uses near infra-red light to determine sample chemistry, has been used to characterise stem cells but its application has been limited due to an inability to maintain sterility. The aim of this study was to design a system to permit repeated application of Raman spectroscopy to living stem cells in long term culture. This required 1) identification of a Raman appropriate substrate, 2) development of a system to maintain culture sterility and 3) selection of an optical configuration to maximise the Raman signal. Quartz and MgF_2 were investigated as potential cell culture substrates. Dental pulp stem cells (DPSCs) were osteo-induced and their stage of differentiation assessed by qRT-PCR and alizarin red staining. Quartz cuvettes and cell culture flasks, customised to accommodate quartz coverslips were tested for culture sterility. A variety of microscope lenses were tested for optimal Raman signal acquisition and average spectra produced from 50 individual loci for each cell culture. Results demonstrated that DPSCs cultured on quartz but not MgF_2 had similar osteogenic differentiation to those cultured on tissue culture plastic. DPSCs cultured in quartz cuvettes and in customised culture flasks were successfully maintained in sterile conditions for up to 28 days. Customised culture flasks were selected as the thickness of the cuvette quartz precluded successful acquisition of Raman spectra. A 40x 0.8NA water immersion lens demonstrated reproducible spectra and the best signal intensity to noise ratio. Sterility can be maintained and Raman spectra successfully acquired using cell culture flasks customised with quartz windows and a water immersion lens. This offers a non-invasive system by which Raman spectroscopy may be used to characterise the differentiation status of stem cells.

Raman Spectroscopy Using an Aseptic Method can Characterise Osteo-induction in Dental Pulp Stromal Cells. Adam Mitchell, Lorna Ashton, Xuebin B. Yang, Royston Goodacre, Alistair Smith, Jennifer Kirkham, Termis EU, Genoa, Italy, June 2014

Introduction

Stem cell based therapies are becoming increasingly prominent with many now in clinical trials (1). Non-invasive and non-destructive characterisation of stem cells prior to their use in downstream applications is important both for safety reasons and in reducing material, time and monetary costs. Raman spectroscopy has been used previously in live cell analysis (2). However, a methodology for repeated live cell measurements under sterile conditions has yet to be demonstrated. The aim of this study was to develop such a method utilising osteoinduced human dental pulp stromal cells (hDPSC).

Materials and Methods

hDPSCs were isolated and maintained for 28 days in osteo-inductive medium in cell culture flasks customised with quartz windows suitable for Raman analysis. Raman spectra were acquired from the cells at days 0, 3, 7, 10, 14 and 28 n=135 per time point. Principle Component Analysis (PCA) assessed spectral variation with time. At day 28, osteogenic differentiation was assessed using alizarin red staining and qRT-PCR for *ALP* and *OC.* qRT-PCR was also used to assess the expression of the cell stress markers *HIF-1*, *HSF-1* and *LDH* at day 0 and at day 28 on hDPSCs that had undergone Raman spectroscopy and those that had not. Statistical significance was determined by one-way ANOVA.

Results

PCA demonstrated trends in PC1 and PC2, Figure 1. Loadings for PC1 showed a positive effect in peaks indicative of proteins (1003cm^{-1}, 1260cm^{-1}, 1345cm^{-1}, 1453cm^{-1} and 1660cm^{-1}) and a negative effect of peaks indicative of DNA and RNA (975cm^{-1}, 1020cm^{-1}, 1420cm^{-1} and 1490cm^{-1}). PC2 was positive for peaks at 1003cm^{-1}, 1453cm^{-1} and 1660cm^{-1} and negative for peaks at 975cm^{-1}, 1020cm^{-1} and

1490cm^{-1}. Alizarin red staining was positive in all samples at day 28 and significant increases in *ALP* ($p<0.001$) and *OC* ($p<0.05$) gene expression were observed. No significant variation in the expression of the three cell stress markers was detected ± Raman spectroscopy.

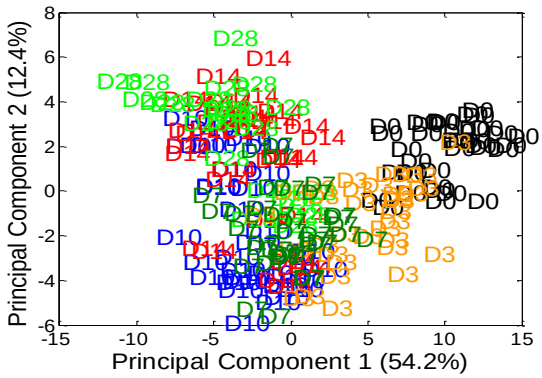

Figure 1. PCA of osteo-induced DPSCs

Discussion and Conclusions

Raman spectroscopy can detect changes in hDPSCs under osteo-inductive culture that are commensurate with cell differentiation, particularly in the first two weeks, prior to any phenotypic changes observed using other invasive methodologies. The novel methodology used was able to maintain sterility for the course of the experiment, permitted repeated measurements of the same cultures and did not induce a cell stress response. The data suggest that prediction and monitoring of hDPSCs differentiation prior to their use in further applications might therefore be possible.

Raman Spectroscopy Using an Aseptic Method can Characterise Osteo-induction in Dental Pulp Stromal Cells. Adam Mitchell, Lorna Ashton, Xuebin B. Yang, Royston Goodacre, Alistair Smith, Jennifer Kirkham, International Association of Dental Research world congress, Cape Town, South Africa, June 2014

Objectives:

Traditional methods for characterising stem cell differentiation are often destructive and/or invasive. To facilitate scale up and clinical translation of cell-based therapies, non-invasive methods are therefore required. Raman spectroscopy has previously been used in cell analysis but there are no methodologies available capable of making repeated Raman measurements on the same living cells in long term culture while maintaining sterility. The aim of this study was to determine if Raman spectroscopy could be used to assess human dental pulp stromal cell (hDPSC) differentiation down the osteogenic lineage by taking repeated measurements from the same cell cultures.

Methods:

hDPSCs were isolated from extracted premolar teeth from 3 consenting donors. Following *in vitro* expansion, hDPSCs were maintained for 28 days in osteo-inductive medium. Raman spectra were acquired from the cells at days 0 (n=108), 3 (n=102), 7 (n=114), 10 (n=105), 14 (n=105) and 28 (n=72). Principle Component Analysis (PCA) was carried out to assess spectral variation with time using MatLab. At day 28, differentiation was assessed using alizarin red staining and qRT-PCR for alkaline phosphatase and osteocalcin.

Results:

PCA demonstrated a trend in PC1, responsible for ~90% of the variation in the data set, which increased between days 0 and 10, plateauing afterwards. Loadings for PC1 showed an increase in spectral peaks indicative of proteins ($1000cm^{-1}$, $1320cm^{-1}$ and $1650cm^{-1}$). Peaks indicative of lipids ($1450cm^{-1}$ and $1300cm^{-1}$) and DNA, ($1080cm^{-1}$) decreased. Alizarin red staining was positive in all samples at day 28 and significant increases in alkaline phosphatase ($p<0.001$) and osteocalcin ($p<0.05$) gene expression were observed.

Conclusion:

Raman spectroscopy can non-invasively detect changes in osteogenic cell cultures that are commensurate with cell differentiation, particularly in the first two weeks. The data suggest that prediction and monitoring of hDPSCs differentiation prior to their use in further applications might therefore be possible.

References

1. R. Langer and J. P. Vacanti, "Tissue engineering," *Science* 260(5110), 920-926 (1993)
2. A. Atala, F. K. Kasper and A. G. Mikos, "Engineering Complex Tissues," *Science Translational Medicine* 4(160), (2012)
3. L.-C. Gerhardt and A. R. Boccaccini, "Bioactive Glass and Glass-Ceramic Scaffolds for Bone Tissue Engineering," *Materials* 3(7), 3867-3910 (2010)
4. R. E. McMahon, L. Wang, R. Skoracki and A. B. Mathur, "Development of nanomaterials for bone repair and regeneration," *Journal of Biomedical Materials Research Part B-Applied Biomaterials* 101B(2), 387-397 (2013)
5. B. R. Whatley and X. Wen, "Intervertebral disc (IVD): Structure, degeneration, repair and regeneration," *Materials Science & Engineering C-Materials for Biological Applications* 32(2), 61-77 (2012)
6. S. MacNeil, "Biomaterials for tissue engineering of skin," *Materials Today* 11(5), 26-35 (2008)
7. G. Lu and S. Huang, "Bioengineered skin substitutes: key elements and novel design for biomedical applications," *International Wound Journal* 10(4), 365-371 (2013)
8. S. J. Kew, J. H. Gwynne, D. Enea, M. Abu-Rub, A. Pandit, D. Zeugolis, R. A. Brooks, N. Rushton, S. M. Best and R. E. Cameron, "Regeneration and repair of tendon and ligament tissue using collagen fibre biomaterials," *Acta Biomaterialia* 7(9), 3237-3247 (2011)
9. M. T. Rodrigues, R. L. Reis and M. E. Gomes, "Engineering tendon and ligament tissues: present developments towards successful clinical products," *Journal of Tissue Engineering and Regenerative Medicine* 7(9), 673-686 (2013)
10. A. Abruzzo, C. Fiorica, V. D. Palumbo, R. Altomare, G. Damiano, M. C. Gioviale, G. Tomasello, M. Licciardi, F. S. Palumbo, G. Giammona and A. I. Lo Monte, "Using Polymeric Scaffolds for Vascular Tissue Engineering," *International Journal of Polymer Science* (2014)
11. A. H. Huang and L. E. Niklason, "Engineering of arteries in vitro," *Cellular and Molecular Life Sciences* 71(11), 2103-2118 (2014)
12. L. L. Hench, "The story of Bioglass (R)," *J. Mater. Sci.-Mater. Med.* 17(11), 967-978 (2006)
13. X. H. Liu, J. M. Holzwarth and P. X. Ma, "Functionalized Synthetic Biodegradable Polymer Scaffolds for Tissue Engineering," *Macromolecular Bioscience* 12(7), 911-919 (2012)
14. E. T. Pashuck and M. M. Stevens, "Designing Regenerative Biomaterial Therapies for the Clinic," *Science Translational Medicine* 4(160), (2012)
15. Z. Pan and J. D. Ding, "Poly(lactide-co-glycolide) porous scaffolds for tissue engineering and regenerative medicine," *Interface Focus* 2(3), 366-377 (2012)
16. C. M. Agrawal and R. B. Ray, "Biodegradable polymeric scaffolds for musculoskeletal tissue engineering," *Journal of Biomedical Materials Research* 55(2), 141-150 (2001)
17. X. K. Li, S. X. Cai, B. Liu, Z. L. Xu, X. Z. Dai, K. W. Ma, S. Q. Li, L. Yang, K. L. P. Sung and X. B. Fu, "Characteristics of PLGA-gelatin complex as potential artificial nerve scaffold," *Colloids and Surfaces B-Biointerfaces* 57(2), 198-203 (2007)

18. N. Diban, S. Haimi, L. Bolhuis-Versteeg, S. Teixeira, S. Miettinen, A. Poot, D. Grijpma and D. Stamatialis, "Hollow fibers of poly(lactide-co-glycolide) and poly(epsilon-caprolactone) blends for vascular tissue engineering applications," *Acta Biomaterialia* 9(5), 6450-6458 (2013)
19. A. D. Cook, J. S. Hrkach, N. N. Gao, I. M. Johnson, U. B. Pajvani, S. M. Cannizzaro and R. Langer, "Characterization and development of RGD-peptide-modified poly(lactic acid-co-lysine) as an interactive, resorbable biomaterial," *Journal of Biomedical Materials Research* 35(4), 513-523 (1997)
20. N. H. Dormer, V. Gupta, A. M. Scurto, C. J. Berkland and M. S. Detamore, "Effect of different sintering methods on bioactivity and release of proteins from PLGA microspheres," *Materials Science & Engineering C-Materials for Biological Applications* 33(7), 4343-4351 (2013)
21. B. M. Holzapfel, J. C. Reichert, J. T. Schantz, U. Gbureck, L. Rackwitz, U. Noth, F. Jakob, M. Rudert, J. Groll and D. W. Hutmacher, "How smart do biomaterials need to be? A translational science and clinical point of view," *Advanced Drug Delivery Reviews* 65(4), 581-603 (2013)
22. M. Steinwachs, "New Technique for Cell-Seeded Collagen Matrix-Supported Autologous Chondrocyte Transplantation," *Arthroscopy-the Journal of Arthroscopic and Related Surgery* 25(2), 208-211 (2009)
23. T. Fujisato, T. Sajiki, Q. Liu and Y. Ikada, "Effect of basic fibroblast growth factor on cartilage regeneration in chondrocyte-seeded collagen sponge scaffold," *Biomaterials* 17(2), 155-162 (1996)
24. U. Noth, L. Rackwitz, A. Heymer, M. Weber, B. Baumann, A. Steinert, N. Schutze, F. Jakob and J. Eulert, "Chondrogenic differentiation of human mesenchymal stem cells in collagen type I hydrogels," *J. Biomed. Mater. Res. Part A* 83A(3), 626-635 (2007)
25. L. A. Pfister, M. Papaloizos, H. P. Merkle and B. Gander, "Nerve conduits and growth factor delivery in peripheral nerve repair," *Journal of the Peripheral Nervous System* 12(2), 65-82 (2007)
26. P. Caione, R. Boldrini, A. Salerno and S. G. Nappo, "Bladder augmentation using acellular collagen biomatrix: a pilot experience in exstrophic patients," *Pediatric Surgery International* 28(4), 421-428 (2012)
27. J. Still, P. Glat, P. Silverstein, J. Griswold and D. Mozingo, "The use of a collagen sponge/living cell composite material to treat donor sites in burn patients," *Burns* 29(8), 837-841 (2003)
28. C. J. Little, N. K. Bawolin and X. B. Chen, "Mechanical Properties of Natural Cartilage and Tissue-Engineered Constructs," *Tissue Eng. Part B-Rev.* 17(4), 213-227 (2011)
29. J. E. Arenas-Herrera, I. K. Ko, A. Atala and J. J. Yoo, "Decellularization for whole organ bioengineering," *Biomedical Materials* 8(1), (2013)
30. N. S. Greaves, B. Benatar, M. Baguneid and A. Bayat, "Single-stage application of a novel decellularized dermis for treatment-resistant lower limb ulcers: Positive outcomes assessed by SIAscopy, laser perfusion, and 3D imaging, with sequential timed histological analysis," *Wound Repair and Regeneration* 21(6), 813-822 (2013)
31. K. I. Lee, J. S. Lee, J. G. Kim, K. T. Kang, J. W. Jang, Y. B. Shim and S. H. Moon, "Mechanical properties of decellularized tendon cultured by cyclic straining bioreactor," *J. Biomed. Mater. Res. Part A* 101(11), 3152-3158 (2013)
32. L. C. Gerhardt, K. L. Widdows, M. M. Erol, A. Nandakumar, I. S. Roqan, T. Ansari and A. R. Boccaccini, "Neocellularization and neovascularization of

nanosized bioactive glass-coated decellularized trabecular bone scaffolds," *J. Biomed. Mater. Res. Part A* 101A(3), 827-841 (2013)
33. J. E. Nichols, J. Niles, M. Riddle, G. Vargas, T. Schilagard, L. Ma, K. Edward, S. La Francesca, J. Sakamoto, S. Vega, M. Ogadegbe, R. Mlcak, D. Deyo, L. Woodson, C. McQuitty, S. Lick, D. Beckles, E. Melo and J. Cortiella, "Production and Assessment of Decellularized Pig and Human Lung Scaffolds," *Tissue Engineering Part A* 19(17-18), 2045-2062 (2013)
34. A. M. Kajbafzadeh, N. Javan-Farazmand, M. Monajemzadeh and A. Baghayee, "Determining the Optimal Decellularization and Sterilization Protocol for Preparing a Tissue Scaffold of a Human-Sized Liver Tissue," *Tissue Engineering Part C-Methods* 19(8), 642-651 (2013)
35. C.-x. Liu, S.-r. Liu, A. b. Xu, Y.-z. Kang, S.-b. Zheng and H.-l. Li, "Preparation of whole-kidney acellular matrix in rats by perfusion," *Nan fang yi ke da xue xue bao = Journal of Southern Medical University* 29(5), 979-982 (2009)
36. A. A. Maximow, "Relation of blood cells to connective tissues and endothelium," *Physiol. Rev.* 4(4), 533-563 (1924)
37. H. J. Zhang and Z. Z. Wang, "Mechanisms that mediate stem cell self-renewal and differentiation," *J. Cell. Biochem.* 103(3), 709-718 (2008)
38. G. M. Kruger, J. T. Mosher, S. Bixby, N. Joseph, T. Iwashita and S. J. Morrison, "Neural crest stem cells persist in the adult gut but undergo changes in self-renewal, neuronal subtype potential, and factor responsiveness," *Neuron* 35(4), 657-669 (2002)
39. A. Foudi, K. Hochedlinger, D. Van Buren, J. W. Schindler, R. Jaenisch, V. Carey and H. Hock, "Analysis of histone 2B-GFP retention reveals slowly cycling hematopoietic stem cells," *Nat. Biotechnol.* 27(1), 84-90 (2009)
40. A. Wilson, E. Laurenti, G. Oser, R. C. van der Wath, W. Blanco-Bose, M. Jaworski, S. Offner, C. F. Dunant, L. Eshkind, E. Bockamp, P. Lio, H. R. MacDonald and A. Trumpp, "Hematopoietic Stem Cells Reversibly Switch from Dormancy to Self-Renewal during Homeostasis and Repair," *Cell* 135(6), 1118-1129 (2008)
41. S. H. He, D. Nakada and S. J. Morrison, "Mechanisms of Stem Cell Self-Renewal," *Annu. Rev. Cell Dev. Biol.* 25(377-406 (2009)
42. S. M. Mitalipov, R. R. Yeoman, H. C. Kuo and D. P. Wolf, "Monozygotic twinning in rhesus monkeys by manipulation of in vitro-derived embryos," *Biology of Reproduction* 66(5), 1449-1455 (2002)
43. M. J. Evans and M. H. Kaufman, "ESTABLISHMENT IN CULTURE OF PLURIPOTENTIAL CELLS FROM MOUSE EMBRYOS," *Nature* 292(5819), 154-156 (1981)
44. J. A. Thomson, J. Itskovitz-Eldor, S. S. Shapiro, M. A. Waknitz, J. J. Swiergiel, V. S. Marshall and J. M. Jones, "Embryonic stem cell lines derived from human blastocysts," *Science* 282(5391), 1145-1147 (1998)
45. M. R. Kuehn, A. Bradley, E. J. Robertson and M. J. Evans, "A POTENTIAL ANIMAL-MODEL FOR LESCH-NYHAN SYNDROME THROUGH INTRODUCTION OF HPRT MUTATIONS INTO MICE," *Nature* 326(6110), 295-298 (1987)
46. D. Q. Pei, "Regulation of Pluripotency and Reprogramming by Transcription Factors," *Journal of Biological Chemistry* 284(6), 3365-3369 (2009)
47. C. B. Cohen, "Ethical and Policy Issues Surrounding the Donation of Cryopreserved and Fresh Embryos for Human Embryonic Stem Cell Research," *Stem Cell Reviews and Reports* 5(2), 116-122 (2009)

48. I. Hyun, "The bioethics of stem cell research and therapy," *Journal of Clinical Investigation* 120(1), 71-75 (2010)
49. A. Zarzeczny and T. Caulfield, "Emerging Ethical, Legal and Social Issues Associated with Stem Cell Research & and the Current Role of the Moral Status of the Embryo," *Stem Cell Reviews and Reports* 5(2), 96-101 (2009)
50. K. Takahashi and S. Yamanaka, "Induction of pluripotent stem cells from mouse embryonic and adult fibroblast cultures by defined factors," *Cell* 126(4), 663-676 (2006)
51. Friedens.Aj, Chailakh.Rk and K. S. Lalykina, "Development of fibroblast colonies in monolayer cultures of guinea-pig bone marrow and spleen cells," *Cell Tissue Kinet* 3(4), 393 (1970)
52. P. A. Zuk, M. Zhu, H. Mizuno, J. Huang, J. W. Futrell, A. J. Katz, P. Benhaim, H. P. Lorenz and M. H. Hedrick, "Multilineage cells from human adipose tissue: Implications for cell-based therapies," *Tissue Engineering* 7(2), 211-228 (2001)
53. S. Gronthos, M. Mankani, J. Brahim, P. G. Robey and S. Shi, "Postnatal human dental pulp stem cells (DPSCs) in vitro and in vivo," *Proceedings of the National Academy of Sciences of the United States of America* 97(25), 13625-13630 (2000)
54. P. Levitt, M. L. Cooper and P. Rakic, "Coexistence of neuronal and glial precursor cells in the cerebral ventricular zone of the fetal monkey - an ultrastructural immunoperoxidase analysis," *J Neurosci* 1(1), 27-39 (1981)
55. M. F. Pittenger, A. M. Mackay, S. C. Beck, R. K. Jaiswal, R. Douglas, J. D. Mosca, M. A. Moorman, D. W. Simonetti, S. Craig and D. R. Marshak, "Multilineage potential of adult human mesenchymal stem cells," *Science* 284(5411), 143-147 (1999)
56. S. Snykers, De Kock, J., Tamara, V. and Rogiers, V. , "Hepatic differentiation of mesenchymal stem cells: in vitro strategies.," *Methods in Molecular Biology* 698(305-314 (2011)
57. W. S. N. Shim, S. Jiang, P. Wong, J. Tan, Y. L. Chua, Y. S. Tan, Y. K. Sin, C. H. Lim, T. Chua, M. Teh, T. C. Liu and E. Simr, "Ex vivo differentiation of human adult bone marrow stem cells into cardiomyocyte-like cells," *Biochemical and Biophysical Research Communications* 324(2), 481-488 (2004)
58. H. Tanaka, C. L. Murphy, C. Murphy, M. Kimura, S. Kawai and J. M. Polak, "Chondrogenic differentiation of murine embryonic stem cells: Effects of culture conditions and dexamethasone," *J. Cell. Biochem.* 93(3), 454-462 (2004)
59. K. D. Lee, T. K. C. Kuo, J. Whang-Peng, Y. F. Chung, C. T. Lin, S. H. Chou, J. R. Chen, Y. P. Chen and O. K. S. Lee, "In vitro hepatic differentiation of human mesenchymal stem cells," *Hepatology* 40(6), 1275-1284 (2004)
60. V. W. Wong, M. Sorkin and G. C. Gurtner, "Enabling stem cell therapies for tissue repair: Current and future challenges," *Biotechnology Advances* 31(5), 744-751 (2013)
61. D. J. Prockop, "[ldquo]Stemness[rdquo] Does Not Explain the Repair of Many Tissues by Mesenchymal Stem//Multipotent Stromal Cells (MSCs)," *Clin Pharmacol Ther* 82(3), 241-243 (0000)
62. D. G. Phinney, G. Kopen, R. L. Isaacson and D. J. Prockop, "Plastic adherent stromal cells from the bone marrow of commonly used strains of inbred mice: Variations in yield, growth, and differentiation," *J. Cell. Biochem.* 72(4), 570-585 (1999)
63. T. Graf and M. Stadtfeld, "Heterogeneity of Embryonic and Adult Stem Cells," *Cell Stem Cell* 3(5), 480-483 (2008)

64. J. Voog and D. L. Jones, "Stem Cells and the Niche: A Dynamic Duo," *Cell Stem Cell* 6(2), 103-115 (2010)
65. F. J. Lv, R. S. Tuan, K. M. C. Cheung and V. Y. L. Leung, "Concise Review: The Surface Markers and Identity of Human Mesenchymal Stem Cells," *Stem Cells* 32(6), 1408-1419 (2014)
66. B. Levi, D. C. Wan, J. P. Glotzbach, J. Hyun, M. Januszyk, D. Montoro, M. Sorkin, A. W. James, E. R. Nelson, S. L. Li, N. Quarto, M. Lee, G. C. Gurtner and M. T. Longaker, "CD105 Protein Depletion Enhances Human Adipose-derived Stromal Cell Osteogenesis through Reduction of Transforming Growth Factor beta 1 (TGF-beta 1) Signaling," *Journal of Biological Chemistry* 286(45), 39497-39509 (2011)
67. S. M. Dellatore, A. S. Garcia and W. M. Miller, "Mimicking stem cell niches to increase stem cell expansion," *Curr. Opin. Biotechnol.* 19(5), 534-540 (2008)
68. E. Fuchs, T. Tumbar and G. Guasch, "Socializing with the neighbors: Stem cells and their niche," *Cell* 116(6), 769-778 (2004)
69. S. J. Morrison and A. C. Spradling, "Stem cells and niches: Mechanisms that promote stem cell maintenance throughout life," *Cell* 132(4), 598-611 (2008)
70. K. G. Battiston, J. W. C. Cheung, D. Jain and J. P. Santerre, "Biomaterials in co-culture systems: Towards optimizing tissue integration and cell signaling within scaffolds," *Biomaterials* 35(15), 4465-4476 (2014)
71. M. C. Simon and B. Keith, "The role of oxygen availability in embryonic development and stem cell function," *Nat Rev Mol Cell Biol* 9(4), 285-296 (2008)
72. P. J. Emans, L. W. van Rhijn, T. J. M. Welting, A. Cremers, N. Wijnands, F. Spaapen, J. W. Voncken and V. P. Shastri, "Autologous engineering of cartilage," *Proceedings of the National Academy of Sciences* 107(8), 3418-3423 (2010)
73. M. A. A. van Vlimmeren, A. Driessen-Mol, M. v. d. Broek, C. V. C. Bouten and F. P. T. Baaijens, *Controlling matrix formation and cross-linking by hypoxia in cardiovascular tissue engineering* (2010).
74. P. Godara, C. D. McFarland and R. E. Nordon, "Design of bioreactors for mesenchymal stem cell tissue engineering," *Journal of Chemical Technology and Biotechnology* 83(4), 408-420 (2008)
75. J. A. King and W. M. Miller, "Bioreactor development for stem cell expansion and controlled differentiation," *Current Opinion in Chemical Biology* 11(4), 394-398 (2007)
76. M. Schroeder, S. Niebruegge, A. Werner, E. Willbold, M. Burg, M. Ruediger, L. J. Field, J. Lehmann and R. Zweigerdt, "Differentiation and lineage selection of mouse embryonic stem cells in a stirred bench scale bioreactor with automated process control," *Biotechnology and Bioengineering* 92(7), 920-933 (2005)
77. C. J. Kirkpatrick, S. Fuchs and R. E. Unger, "Co-culture systems for vascularization - Learning from nature," *Advanced Drug Delivery Reviews* 63(4-5), 291-299 (2011)
78. D. Cigognini, A. Lomas, P. Kumar, A. Satyam, A. English, A. Azeem, A. Pandit and D. Zeugolis, "Engineering in vitro microenvironment for cell bases therapies and drug discovery," *Drug Discovery Today* 18(21-22), 1099-1108 (2013)
79. K. C. Wu, C. L. Tseng, C. C. Wu, F. C. Kao, Y. K. Tu, E. C. So and Y. K. Wang, "Nanotechnology in the regulation of stem cell behavior," *Science and Technology of Advanced Materials* 14(5), (2013)
80. A. Trounson, R. G. Thakar, G. Lomax and D. Gibbons, "Clinical trials for stem cell therapies," *Bmc Medicine* 9((2011)

81. K. C. Cheung, M. Di Berardino, G. Schade-Kampmann, M. Hebeisen, A. Pierzchalski, J. Bocsi, A. Mittag and A. Tárnok, "Microfluidic impedance-based flow cytometry," *Cytometry Part A* 77A(7), 648-666 (2010)
82. K. Heileman, J. Daoud and M. Tabrizian, "Dielectric spectroscopy as a viable biosensing tool for cell and tissue characterization and analysis," *Biosensors & Bioelectronics* 49(348-359 (2013)
83. V. Turzhitsky, L. Qiu, I. Itzkan, A. A. Novikov, M. S. Kotelev, M. Getmanskiy, V. A. Vinokurov, A. V. Muradov and L. T. Perelman, "Spectroscopy of Scattered Light for the Characterization of Micro and Nanoscale Objects in Biology and Medicine," *Appl. Spectrosc.* 68(2), 133-154 (2014)
84. X. Liang, B. W. Graf and S. A. Boppart, "Imaging engineered tissues using structural and functional optical coherence tomography," *J. Biophotonics* 2(11), 643-655 (2009)
85. A. A. Appel, M. A. Anastasio, J. C. Larson and E. M. Brey, "Imaging challenges in biomaterials and tissue engineering," *Biomaterials* 34(28), 6615-6630 (2013)
86. D. W. Ball, *The Basics of Spectroscopy*, SPIE, Bellingham (2001).
87. Antonine Education, "Antonine Education Website," (2011).
88. M. Malet-Martino and U. Holzgrabe, "NMR techniques in biomedical and pharmaceutical analysis," *Journal of Pharmaceutical and Biomedical Analysis* 55(1), 1-15 (2011)
89. M. van der Graaf, "In vivo magnetic resonance spectroscopy: basic methodology and clinical applications," *European Biophysics Journal* 39(4), 527-540 (2010)
90. R. Ahmad and P. Kuppusamy, "Theory, Instrumentation, and Applications of Electron Paramagnetic Resonance Oximetry," *Chemical Reviews* 110(5), 3212-3236 (2010)
91. M. Kohno, "Applications of Electron Spin Resonance Spectrometry for Reactive Oxygen Species and Reactive Nitrogen Species Research," *Journal of Clinical Biochemistry and Nutrition* 47(1), 1-11 (2010)
92. A. Downes, R. Mouras and A. Elfick, "Optical Spectroscopy for Noninvasive Monitoring of Stem Cell Differentiation," *J. Biomed. Biotechnol.* (2010)
93. C. Kendall, M. Isabelle, F. Bazant-Hegemark, J. Hutchings, L. Orr, J. Babrah, R. Baker and N. Stone, "Vibrational spectroscopy: a clinical tool for cancer diagnostics," *Analyst* 134(6), 1029-1045 (2009)
94. L. M. Miller and P. Dumas, "From structure to cellular mechanism with infrared microspectroscopy," *Current Opinion in Structural Biology* 20(5), 649-656 (2010)
95. J. Q. Brown, K. Vishwanath, G. M. Palmer and N. Ramanujam, "Advances in quantitative UV-visible spectroscopy for clinical and pre-clinical application in cancer," *Curr. Opin. Biotechnol.* 20(1), 119-131 (2009)
96. D. L. Andrews, and Demidov, A. A., *An Introduction to Laser Spectroscopy*, Plenum Press, New York (1995).
97. Z. Movasaghi, S. Rehman and I. U. Rehman, "Raman spectroscopy of biological tissues," *Appl. Spectrosc. Rev.* 42(5), 493-541 (2007)
98. A. Downes and A. Elfick, "Raman Spectroscopy and Related Techniques in Biomedicine," *Sensors* 10(3), 1871-1889 (2010)
99. H. Bai, P. Chen, H. Fang, L. Lin, G. Q. Tang, G. G. Mu, W. Gong, Z. P. Liu, H. Wu, H. Zhao and Z. C. Han, "Detecting viability transitions of umbilical cord

mesenchymal stem cells by Raman micro-spectroscopy," *Laser Phys. Lett.* 8(1), 78-84 (2011)
100. A. R. Boyd, G. A. Burke and B. J. Meenan, "Monitoring cellular behaviour using Raman spectroscopy for tissue engineering and regenerative medicine applications," *J. Mater. Sci.-Mater. Med.* 21(8), 2317-2324 (2010)
101. E. Gentleman, R. J. Swain, N. D. Evans, S. Boonrungsiman, G. Jell, M. D. Ball, T. A. V. Shean, M. L. Oyen, A. Porter and M. M. Stevens, "Comparative materials differences revealed in engineered bone as a function of cell-specific differentiation," *Nat. Mater.* 8(9), 763-770 (2009)
102. I. Notingher, G. Jell, U. Lohbauer, V. Salih and L. L. Hench, "In situ non-invasive spectral discrimination between bone cell phenotypes used in tissue engineering," *J. Cell. Biochem.* 92(6), 1180-1192 (2004)
103. F. C. Pascut, H. T. Goh, N. Welch, L. D. Buttery, C. Denning and I. Notingher, "Noninvasive Detection and Imaging of Molecular Markers in Live Cardiomyocytes Derived from Human Embryonic Stem Cells," *Biophys. J.* 100(1), 251-259 (2011)
104. H. G. Schulze, S. O. Konorov, N. J. Caron, J. M. Piret, M. W. Blades and R. F. B. Turner, "Assessing Differentiation Status of Human Embryonic Stem Cells Noninvasively Using Raman Microspectroscopy," *Anal. Chem.* 82(12), 5020-5027 (2010)
105. K. Hamada, K. Fujita, N. I. Smith, M. Kobayashi, Y. Inouye and S. Kawata, *Raman microscopy for dynamic molecular imaging of living cells*, SPIE (2008).
106. Y. Liu, G. J. Sonek, M. W. Berns and B. J. Tromberg, "Physiological monitoring of optically trapped cells: assessing the effects of confinement by 1064-nm laser tweezers using microfluorometry," *Biophys. J.* 71(4), 2158-2167 (1996)
107. R. J. Swain and M. M. Stevens, "Raman microspectroscopy for non-invasive biochemical analysis of single cells," *Biochem. Soc. Trans.* 35(544-549 (2007)
108. D. I. Ellis and R. Goodacre, "Metabolic fingerprinting in disease diagnosis: biomedical applications of infrared and Raman spectroscopy," *Analyst* 131(8), 875-885 (2006)
109. J. Conroy, A. G. Ryder, M. N. Leger, K. Hennessey and M. G. Madden, "Qualitative and quantitative analysis of chlorinated solvents using Raman spectroscopy and machine learning," in *Opto-Ireland 2005: Optical Sensing and Spectroscopy* H. J. Byrne, E. Lewis, B. D. MacCraith, E. McGlynn, J. A. McLaughlin, G. D. Osullivan, A. G. Ryder and J. E. Walsh, Eds., pp. 131-142, Spie-Int Soc Optical Engineering, Bellingham (2005).
110. E. B. Hanlon, R. Manoharan, T. W. Koo, K. E. Shafer, J. T. Motz, M. Fitzmaurice, J. R. Kramer, I. Itzkan, R. R. Dasari and M. S. Feld, "Prospects for in vivo Raman spectroscopy," *Phys. Med. Biol.* 45(2), R1-R59 (2000)
111. R. E. Rasmussen, M. Hammerwilson and M. W. Berns, "Mutation and sister chromatid exchange induction in Chinese-hamster ovary (CHO) cells by pulsed excimer laser-radiation at 193 nm and 308 nm and continuous UV-radiation at 254 nm," *Photochem Photobiol* 49(4), 413-418 (1989)
112. A. Downes, R. Mouras, M. Mari and A. Elfick, "Optimising tip-enhanced optical microscopy," *J. Raman Spectrosc.* 40(10), 1355-1360 (2009)
113. T. Bocklitz, A. Walter, K. Hartmann, P. Roesch and J. Popp, "How to pre-process Raman spectra for reliable and stable models?," *Anal. Chim. Acta* 704(1-2), 47-56 (2011)
114. P. Lasch, "Spectral pre-processing for biomedical vibrational spectroscopy and microspectroscopic imaging," *Chemometrics Intell. Lab. Syst.* 117(100-114 (2012)

115. T. W. Randolph, "Scale-based normalization of spectral data," *Cancer Biomarkers* 2(3-4), 135-144 (2006)
116. P. Marchand and L. Marmet, "BINOMIAL SMOOTHING FILTER - A WAY TO AVOID SOME PITFALLS OF LEAST-SQUARES POLYNOMIAL SMOOTHING," *Rev. Sci. Instrum.* 54(8), 1034-1041 (1983)
117. C. A. Lieber and A. Mahadevan-Jansen, "Automated method for subtraction of fluorescence from biological Raman spectra," *Appl. Spectrosc.* 57(11), 1363-1367 (2003)
118. D. M. Zhang and D. Ben-Amotz, "Enhanced chemical classification of Raman images in the presence of strong fluorescence interference," *Appl. Spectrosc.* 54(9), 1379-1383 (2000)
119. A. Savitzky and M. J. E. Golay, "SMOOTHING + DIFFERENTIATION OF DATA BY SIMPLIFIED LEAST SQUARES PROCEDURES," *Anal. Chem.* 36(8), 1627-& (1964)
120. T. Rajalahti and O. M. Kvalheim, "Multivariate data analysis in pharmaceutics: A tutorial review," *International Journal of Pharmaceutics* 417(1-2), 280-290 (2011)
121. R. Bro and A. K. Smilde, "Principal component analysis," *Analytical Methods* 6(9), 2812-2831 (2014)
122. S. Wold, K. Esbensen and P. Geladi, "PRINCIPAL COMPONENT ANALYSIS," *Chemometrics Intell. Lab. Syst.* 2(1-3), 37-52 (1987)
123. H. Shinzawa, K. Awa, W. Kanematsu and Y. Ozaki, "Multivariate data analysis for Raman spectroscopic imaging," *J. Raman Spectrosc.* 40(12), 1720-1725 (2009)
124. S. Agatonovic-Kustrin and R. Beresford, "Basic concepts of artificial neural network (ANN) modeling and its application in pharmaceutical research," *Journal of Pharmaceutical and Biomedical Analysis* 22(5), 717-727 (2000)
125. M. Paliwal and U. A. Kumar, "Neural networks and statistical techniques: A review of applications," *Expert Systems with Applications* 36(1), 2-17 (2009)
126. W. P. Worzel, J. Yu, A. A. Almal and A. M. Chinnaiyan, "Applications of genetic programming in cancer research," *International Journal of Biochemistry & Cell Biology* 41(2), 405-413 (2009)
127. M. E. Street, M. Buscema, A. Smerieri, L. Montanini and E. Grossi, "Artificial Neural Networks, and Evolutionary Algorithms as a systems biology approach to a data-base on fetal growth restriction," *Progress in Biophysics & Molecular Biology* 113(3), 433-438 (2013)
128. V. V. Pully, A. Lenferink, H. J. van Manen, V. Subramaniam, C. A. van Blitterswijk and C. Otto, "Microbioreactors for Raman Microscopy of Stromal Cell Differentiation," *Anal. Chem.* 82(5), 1844-1850 (2010)
129. V. V. Pully and C. Otto, "The intensity of the 1602 cm(-1) band in human cells is related to mitochondrial activity," *J. Raman Spectrosc.* 40(5), 473-475 (2009)
130. Y. Ilin and M. L. Kraft, "Identifying the lineages of individual cells in cocultures by multivariate analysis of Raman spectra," *Analyst* 139(9), 2177-2185 (2014)
131. T. Ichimura, L.-d. Chiu, K. Fujita, S. Kawata, T. M. Watanabe, T. Yanagida and H. Fujita, "Visualizing Cell State Transition Using Raman Spectroscopy," *Plos One* 9(1), (2014)
132. H. K. Chiang, F. Y. Peng, S. C. Hung and Y. C. Feng, "In situ Raman spectroscopic monitoring of hydroxyapatite as human mesenchymal stem cells differentiate into osteoblasts," *J. Raman Spectrosc.* 40(5), 546-549 (2009)

133. H. Liu, W. Li, S. T. Shi, S. Habelitz, C. Gao and P. DenBesten, "MEPE is downregulated as dental pulp stem cells differentiate," *Archives of Oral Biology* 50(11), 923-928 (2005)
134. L. L. McManus, G. A. Burke, M. M. McCafferty, P. O'Hare, M. Modreanu, A. R. Boyd and B. J. Meenan, "Raman spectroscopic monitoring of the osteogenic differentiation of human mesenchymal stem cells," *Analyst* 136(12), 2471-2481 (2011)
135. I. Notingher, S. Verrier, H. Romanska, A. E. Bishop, J. M. Polak and L. L. Hench, "In situ characterisation of living cells by Raman spectroscopy," *Spectr.-Int. J.* 16(2), 43-51 (2002)
136. Z. A. Nima, A. Biswas, I. S. Bayer, F. D. Hardcastle, D. Perry, A. Ghosh, E. Dervishi and A. S. Biris, "Applications of surface-enhanced Raman scattering in advanced bio-medical technologies and diagnostics," *Drug Metabolism Reviews* 46(2), 155-175 (2014)
137. A. Samanta, S. Jana, R. K. Das and Y. T. Chang, "Biocompatible surface-enhanced Raman scattering nanotags for in vivo cancer detection," *Nanomedicine* 9(3), 523-535 (2014)
138. S. Ye, Y. Mao, Y. Guo and S. Zhang, "Enzyme-based signal amplification of surface-enhanced Raman scattering in cancer-biomarker detection," *Trac-Trends in Analytical Chemistry* 55(43-54 (2014)
139. C. Vater, P. Kasten and M. Stiehler, "Culture media for the differentiation of mesenchymal stromal cells," *Acta Biomaterialia* 7(2), 463-477 (2011)
140. A. K. Kniggendorf, T. W. Gaul and M. Meinhardt-Wollweber, "Effects of Ethanol, Formaldehyde, and Gentle Heat Fixation in Confocal Resonance Raman Microscopy of Purple NonSulfur Bacteria," *Microscopy Research and Technique* 74(2), 177-183 (2011)
141. E. Karaoz, B. N. Dogan, A. Aksoy, G. Gacar, S. Akyuz, S. Ayhan, Z. S. Genc, S. Yuruker, G. Duruksu, P. C. Demircan and A. E. Sariboyaci, "Isolation and in vitro characterisation of dental pulp stem cells from natal teeth," *Histochemistry and Cell Biology* 133(1), 95-112 (2010)
142. E. Kaivosoja, G. Barreto, K. Levon, S. Virtanen, M. Ainola and Y. T. Konttinen, "Chemical and physical properties of regenerative medicine materials controlling stem cell fate," *Annals of Medicine* 44(7), 635-650 (2012)
143. A. Obata and T. Kasuga, "Stimulation of human mesenchymal stem cells and osteoblasts activities in vitro on silicon-releasable scaffolds," *J. Biomed. Mater. Res. Part A* 91A(1), 11-17 (2009)
144. J. K. Pijanka, D. Kumar, T. Dale, I. Yousef, G. Parkes, V. Untereiner, Y. Yang, P. Dumas, D. Collins, M. Manfait, G. D. Sockalingum, N. R. Forsyth and J. Sule-Suso, "Vibrational spectroscopy differentiates between multipotent and pluripotent stem cells," *Analyst* 135(12), 3126-3132 (2010)
145. D. Bosnakovski, M. Mizuno, G. Kim, S. Takagi, M. Okumura and T. Fujinaga, "Isolation and multilineage differentiation of bovine bone marrow mesenchymal stem cells," *Cell and Tissue Research* 319(2), 243-253 (2005)
146. D. C. Colter, I. Sekiya and D. J. Prockop, "Identification of a subpopulation of rapidly self-renewing and multipotential adult stem cells in colonies of human marrow stromal cells," *Proceedings of the National Academy of Sciences of the United States of America* 98(14), 7841-7845 (2001)
147. E. J. Gang, S. H. Hong, J. A. Jeong, S. H. Hwang, S. W. Kim, I. H. Yang, C. Y. Ahn, H. Han and H. Kim, "In vitro mesengenic potential of human umbilical cord blood-derived mesenchymal stem cells," *Biochemical and Biophysical Research Communications* 321(1), 102-108 (2004)

148. J. M. Seong, B. C. Kim, J. H. Park, I. K. Kwon, A. Mantalaris and Y. S. Hwang, "Stem cells in bone tissue engineering," *Biomedical Materials* 5(6), (2010)
149. J. M. Curran, R. Chen and J. A. Hunt, "The guidance of human mesenchymal stem cell differentiation in vitro by controlled modifications to the cell substrate," *Biomaterials* 27(27), 4783-4793 (2006)
150. J. E. Phillips, T. A. Petrie, F. P. Creighton and A. J. García, "Human mesenchymal stem cell differentiation on self-assembled monolayers presenting different surface chemistries," *Acta Biomaterialia* 6(1), 12-20 (2010)
151. S. H. Oh, T. H. Kim, G. I. Im and J. H. Lee, "Investigation of Pore Size Effect on Chondrogenic Differentiation of Adipose Stem Cells Using a Pore Size Gradient Scaffold," *Biomacromolecules* 11(8), 1948-1955 (2010)
152. Y. Zhang, W. Fan, Z. Ma, C. Wu, W. Fang, G. Liu and Y. Xiao, "The effects of pore architecture in silk fibroin scaffolds on the growth and differentiation of mesenchymal stem cells expressing BMP7," *Acta Biomaterialia* 6(8), 3021-3028 (2010)
153. M. J. Dalby, N. Gadegaard, R. Tare, A. Andar, M. O. Riehle, P. Herzyk, C. D. W. Wilkinson and R. O. C. Oreffo, "The control of human mesenchymal cell differentiation using nanoscale symmetry and disorder," *Nat. Mater.* 6(12), 997-1003 (2007)
154. T. Sjöström, M. J. Dalby, A. Hart, R. Tare, R. O. C. Oreffo and B. Su, "Fabrication of pillar-like titania nanostructures on titanium and their interactions with human skeletal stem cells," *Acta Biomaterialia* 5(5), 1433-1441 (2009)
155. A. J. Engler, S. Sen, H. L. Sweeney and D. E. Discher, "Matrix Elasticity Directs Stem Cell Lineage Specification," *Cell* 126(4), 677-689 (2006)
156. M. Nii, J. H. Lai, M. Keeney, L.-H. Han, A. Behn, G. Imanbayev and F. Yang, "The effects of interactive mechanical and biochemical niche signaling on osteogenic differentiation of adipose-derived stem cells using combinatorial hydrogels," *Acta Biomaterialia* 9(3), 5475-5483 (2013)
157. E. Ragni, M. Vigano, P. Rebulla, R. Giordano and L. Lazzari, "What is beyond a qRT-PCR study on mesenchymal stem cell differentiation properties: how to choose the most reliable housekeeping genes," *Journal of Cellular and Molecular Medicine* 17(1), 168-180 (2013)
158. O. Frank, M. Heim, M. Jakob, A. Barbero, D. Schafer, I. Bendik, W. Dick, M. Heberer and I. Martin, "Real-time quantitative RT-PCR analysis of human bone marrow stromal cells during osteogenic differentiation in vitro," *J. Cell. Biochem.* 85(4), 737-746 (2002)
159. F. Djouad, C. Bony, T. Haupl, G. Uze, N. Lahlou, P. Louis-Plence, F. Apparailly, F. Canovas, T. Reme, J. Sany, C. Jorgensen and D. Noel, "Transcriptional profiles discriminate bone marrow-derived and synovium-derived mesenchymal stem cells," *Arthritis Research & Therapy* 7(6), R1304-R1315 (2005)
160. B. W. Park, Y. S. Hah, D. R. Kim, J. R. Kim and J. H. Byun, "Osteogenic phenotypes and mineralization of cultured human periosteal-derived cells," *Archives of Oral Biology* 52(10), 983-989 (2007)
161. B. W. Park, Y. S. Hah, M. J. Choi, Y. M. Ryu, S. G. Lee, D. R. Kim, J. R. Kim and J. H. Byun, "In Vitro Osteogenic Differentiation of Cultured Human Dental Papilla-Derived Cells," *Journal of Oral and Maxillofacial Surgery* 67(3), 507-514 (2009)
162. J. Y. Ma, X. Z. He and E. Jabbari, "Osteogenic Differentiation of Marrow Stromal Cells on Random and Aligned Electrospun Poly(L-lactide) Nanofibers," *Annals of Biomedical Engineering* 39(1), 14-25 (2011)

163. IHCWORLD Life Science Information Network, "Alizarin red s staining protocol for calcium," (2011).
164. O. Barbier, L. Arreola-Mendoza and L. M. Del Razo, "Molecular mechanisms of fluoride toxicity," *Chem.-Biol. Interact.* 188(2), 319-333 (2010)
165. J. H. Jeng, C. C. Hsieh, W. H. Lan, M. C. Chang, S. K. Lin, L. J. Hahn and M. Y. P. Kuo, "Cytotoxicity of sodium fluoride on human oral mucosal fibroblasts and its mechanisms," *Cell Biology and Toxicology* 14(6), 383-389 (1998)
166. K. L. Koss and R. D. Grubbs, "ELEVATED EXTRACELLULAR MG2+ INCREASES MG2+ BUFFERING THROUGH A CA-DEPENDENT MECHANISM IN CARDIOMYOCYTES," *American Journal of Physiology* 267(2), C633-C641 (1994)
167. F. Kircelli, M. E. Peter, E. S. Ok, F. G. Celenk, M. Yilmaz, S. Steppan, G. Asci, E. Ok and J. Passlick-Deetjen, "Magnesium reduces calcification in bovine vascular smooth muscle cells in a dose-dependent manner," *Nephrol. Dial. Transplant.* 27(2), 514-521 (2012)
168. G. Weder, N. Blondiaux, M. Giazzon, N. Matthey, M. Klein, R. Pugin, H. Heinzelmann and M. Liley, "Use of Force Spectroscopy to Investigate the Adhesion of Living Adherent Cells," *Langmuir* 26(11), 8180-8186 (2010)
169. D. J. Kim, G. S. Kim, J. H. Hyung, W. Y. Lee, C. H. Hong and S. K. Lee, "Direct observation of CD4 T cell morphologies and their cross-sectional traction force derivation on quartz nanopillar substrates using focused ion beam technique," *Nanoscale Research Letters* 8((2013)
170. O. Koehler, C. Mueller, A. Hermsdoerfery, H. Roehl and C. Ziegler, "Initial bioadhesion on medical glass packaging materials investigated by dynamic contact angle measurements," *Physica Status Solidi a-Applications and Materials Science* 210(5), 983-987 (2013)
171. K. P. Fears, D. Y. Petrovykh, S. J. Photiadis and T. D. Clark, "Circular Dichroism Analysis of Cyclic beta-Helical Peptides Adsorbed on Planar Fused Quartz," *Langmuir* 29(32), 10095-10101 (2013)
172. F. Draux, P. Jeannesson, A. Beljebbar, A. Tfayli, N. Fourre, M. Manfait, J. Sule-Suso and G. D. Sockalingum, "Raman spectral imaging of single living cancer cells: a preliminary study," *Analyst* 134(3), 542-548 (2009)
173. I. Georgakoudi, W. L. Rice, M. Hronik-Tupaj and D. L. Kaplan, "Optical Spectroscopy and Imaging for the Noninvasive Evaluation of Engineered Tissues," *Tissue Eng. Part B-Rev.* 14(4), 321-340 (2008)
174. K. Hamada, K. Fujita, N. I. Smith, M. Kobayashi, Y. Inouye and S. Kawata, "Raman microscopy for dynamic molecular imaging of living cells," *Journal of Biomedical Optics* 13(4), (2008)
175. G. J. Puppels, J. H. F. Olminkhof, G. M. J. Segersnolten, C. Otto, F. F. M. Demul and J. Greve, "LASER IRRADIATION AND RAMAN-SPECTROSCOPY OF SINGLE LIVING CELLS AND CHROMOSOMES - SAMPLE DEGRADATION OCCURS WITH 514.5NM BUT NOT WITH 660NM LASER-LIGHT," *Experimental Cell Research* 195(2), 361-367 (1991)
176. E. Wisse, F. Braet, H. Duimel, C. Vreuls, G. Koek, S. Damink, M. A. J. van den Broek, B. De Geest, C. H. C. Dejong, C. Tateno and P. Frederik, "Fixation methods for electron microscopy of human and other liver," *World Journal of Gastroenterology* 16(23), 2851-2866 (2010)
177. C. H. Fox, F. B. Johnson, J. Whiting and P. P. Roller, "FORMALDEHYDE FIXATION," *Journal of Histochemistry & Cytochemistry* 33(8), 845-853 (1985)

178. F. D'Amico, E. Skarmoutsou and F. Stivala, "State of the art in antigen retrieval for immunohistochemistry," *Journal of Immunological Methods* 341(1-2), 1-18 (2009)
179. C. S. Foster, C. M. Gosden and Y. Q. Q. Ke, "Primer: tissue fixation and preservation for optimal molecular analysis of urologic tissues," *Nature Clinical Practice Urology* 3(5), 268-278 (2006)
180. J. D. McGhee and P. H. Vonhippel, "FORMALDEHYDE AS A PROBE OF DNA-STRUCTURE .4. MECHANISM OF INITIAL REACTION OF FORMALDEHYDE WITH DNA," *Biochemistry* 16(15), 3276-3293 (1977)
181. S. P. Denyer, "Mechanisms of action of antibacterial biocides," *International Biodeterioration & Biodegradation* 36(3-4), 227-245 (1995)
182. S. M. Ali, F. Bonnier, A. Tfayli, H. Lambkin, K. Flynn, V. McDonagh, C. Healy, T. C. Lee, F. M. Lyng and H. J. Byrne, "Raman spectroscopic analysis of human skin tissue sections ex-vivo: evaluation of the effects of tissue processing and dewaxing," *Journal of Biomedical Optics* 18(6), (2013)
183. S. M. Ali, F. Bonnier, H. Lambkin, K. Flynn, V. McDonagh, C. Healy, T. C. Lee, F. M. Lyng and H. J. Byrne, "A comparison of Raman, FTIR and ATR-FTIR micro spectroscopy for imaging human skin tissue sections," *Analytical Methods* 5(9), 2281-2291 (2013)
184. A. D. Meade, C. Clarke, F. Draux, G. D. Sockalingum, M. Manfait, F. M. Lyng and H. J. Byrne, "Studies of chemical fixation effects in human cell lines using Raman microspectroscopy," *Analytical and Bioanalytical Chemistry* 396(5), 1781-1791 (2010)
185. F. C. Pascut, H. T. Goh, V. George, C. Denning and I. Notingher, "Toward label-free Raman-activated cell sorting of cardiomyocytes derived from human embryonic stem cells," *Journal of Biomedical Optics* 16(4), (2011)
186. K. W. Short, S. Carpenter, J. P. Freyer and J. R. Mourant, "Raman spectroscopy detects biochemical changes due to proliferation in mammalian cell cultures," *Biophys. J.* 88(6), 4274-4288 (2005)
187. M. Pudlas, D. A. C. Berrio, M. Votteler, S. Koch, S. Thude, H. Walles and K. Schenke-Layland, "Non-contact discrimination of human bone marrow-derived mesenchymal stem cells and fibroblasts using Raman spectroscopy," *Medical Laser Application* 26(3), 119-125 (2011)
188. S. Al-Nasiry, N. Geusens, M. Hanssens, C. Luyten and R. Pijnenborg, "The use of Alamar Blue assay for quantitative analysis of viability, migration and invasion of choriocarcinoma cells," *Human Reproduction* 22(5), 1304-1309 (2007)
189. K. J. Baldwin and D. N. Batchelder, "Confocal Raman microspectroscopy through a planar interface," *Appl. Spectrosc.* 55(5), 517-524 (2001)
190. J. Haseloff, E.-L. Dormand and A. Brand, "Live Imaging with Green Fluorescent Protein," in *Confocal Microscopy Methods and Protocols* S. Paddock, Ed., pp. 241-259, Humana Press (1999).
191. A. Ghita, F. C. Pascut, V. Sottile and I. Notingher, "Monitoring the mineralisation of bone nodules in vitro by space- and time-resolved Raman micro-spectroscopy," *Analyst* 139(1), 55-58 (2014)
192. A. B. Vasandan, S. R. Shankar, P. Prasad, V. S. Jahnavi, R. R. Bhonde and S. J. Prasanna, "Functional differences in mesenchymal stromal cells from human dental pulp and periodontal ligament," *Journal of Cellular and Molecular Medicine* 18(2), 344-354 (2014)
193. L. Notingher, G. Jell, P. L. Notingher, I. Bisson, O. Tsigkou, J. M. Polak, M. M. Stevens and L. L. Hench, "Multivariate analysis of Raman spectra for in vitro

non-invasive studies of living cells," *Journal of Molecular Structure* 744(179-185 (2005)
194. E. Brauchle and K. Schenke-Layland, "Raman spectroscopy in biomedicine - non-invasive in vitro analysis of cells and extracellular matrix components in tissues," *Biotechnology Journal* 8(3), 288-297 (2013)
195. A. K. Velichko, E. N. Markova, N. V. Petrova, S. V. Razin and O. L. Kantidze, "Mechanisms of heat shock response in mammals," *Cellular and Molecular Life Sciences* 70(22), 4229-4241 (2013)
196. K. D. Sarge, "Regulation of HSF1 Activation and Hsp Expression in Mouse Tissues under Physiological Stress Conditions," *Annals of the New York Academy of Sciences* 851(1), 112-116 (1998)
197. S. L. Dunwoodie, "The Role of Hypoxia in Development of the Mammalian Embryo," *Developmental Cell* 17(6), 755-773 (2009)
198. M. C. Simon and B. Keith, "The role of oxygen availability in embryonic development and stem cell function," *Nat. Rev. Mol. Cell Biol.* 9(4), 285-296 (2008)
199. P. Imanirad and E. Dzierzak, "Hypoxia and HIFs in regulating the development of the hematopoietic system," *Blood Cells Molecules and Diseases* 51(4), 256-263 (2013)
200. V. R. Fantin, J. St-Pierre and P. Leder, "Attenuation of LDH-A expression uncovers a link between glycolysis, mitochondrial physiology, and tumor maintenance," *Cancer Cell* 9(6), 425-434 (2006)
201. P. Miao, S. L. Sheng, X. G. Sun, J. J. Liu and G. Huang, "Lactate Dehydrogenase A in Cancer: A Promising Target for Diagnosis and Therapy," *Iubmb Life* 65(11), 904-910 (2013)
202. F. C. Pascut, S. Kalra, V. George, N. Welch, C. Denning and I. Notingher, "Non-invasive label-free monitoring the cardiac differentiation of human embryonic stem cells in-vitro by Raman spectroscopy," *Biochimica Et Biophysica Acta-General Subjects* 1830(6), 3517-3524 (2013)
203. T. H. Kim, K. B. Lee and J. W. Choi, "3D graphene oxide-encapsulated gold nanoparticles to detect neural stem cell differentiation," *Biomaterials* 34(34), 8660-8670 (2013)
204. Q. Q. Tang, T. C. Otto and M. D. Lane, "CCAAT/enhancer-binding protein beta is required for mitotic clonal expansion during adipogenesis," *Proceedings of the National Academy of Sciences of the United States of America* 100(3), 850-855 (2003)
205. Q. Q. Tang, T. C. Otto and M. D. Lane, "Mitotic clonal expansion: A synchronous process required for adipogenesis," *Proceedings of the National Academy of Sciences of the United States of America* 100(1), 44-49 (2003)
206. B. Feve, "Adipogenesis: cellular and molecular aspects," *Best Practice & Research Clinical Endocrinology & Metabolism* 19(4), 483-499 (2005)
207. L. Chen, J. Song, J. Cui, J. Hou, X. Zheng, C. Li and L. Liu, "microRNAs regulate adipocyte differentiation," *Cell Biology International* 37(6), 533-546 (2013)
208. B. Moody, C. M. Haslauer, E. Kirk, A. Kannan, E. G. Loboa and G. S. McCarty, "In Situ Monitoring of Adipogenesis with Human-Adipose-Derived Stem Cells Using Surface-Enhanced Raman Spectroscopy," *Appl. Spectrosc.* 64(11), 1227-1233 (2010)
209. R. Mouras, P. O. Bagnaninchi, A. R. Downes and A. P. D. Elfick, "Label-free assessment of adipose-derived stem cell differentiation using coherent anti-Stokes Raman scattering and multiphoton microscopy," *Journal of Biomedical Optics* 17(11), (2012)

210. P. Trayhurn, "Hypoxia and adipocyte physiology: implications for adipose tissue dysfunction in obesity," *Annual review of nutrition* 34(207-236 (2014)
211. Y. Ishihara, K. Ohmori, A. U. Hasan, N. Ishihara, T. Noma and M. Kohno, "Intermittent Hypoxia Deteriorates Mesenchymal Cells Differentiating to Adipocytes: An in vitro Demonstration of Vicious Link of Obesity, Sleep Apnea and Increased Cardiovascular Risk," *Circulation* 126(21), (2012)
212. D. Mazzatti, F. L. Lim, A. O'Hara, I. S. Wood and P. Trayhurn, "A microarray analysis of the hypoxia-induced modulation of gene expression in human adipocytes," *Archives of Physiology and Biochemistry* 118(3), 112-120 (2012)
213. A. Wree, A. Mayer, S. Westphal, A. Beilfuss, A. Canbay, R. R. Schick, G. Gerken and P. Vaupel, "Adipokine expression in brown and white adipocytes in response to hypoxia," *Journal of Endocrinological Investigation* 35(5), 522-527 (2012)
214. C. Jiang, J.-H. Kim, F. Li, A. Qu, O. Gavrilova, Y. M. Shah and F. J. Gonzalez, "Hypoxia-inducible Factor 1 alpha Regulates a SOCS3-STAT3-Adiponectin Signal Transduction Pathway in Adipocytes," *Journal of Biological Chemistry* 288(6), 3844-3857 (2013)
215. Y. Kihira, M. Miyake, M. Hirata, Y. Hoshina, K. Kato, H. Shirakawa, H. Sakaue, N. Yamano, Y. Izawa-Ishizawa, K. Ishizawa, Y. Ikeda, K. Tsuchiya, T. Tamaki and S. Tomita, "Deletion of Hypoxia-Inducible Factor-1 alpha in Adipocytes Enhances Glucagon-Like Peptide-1 Secretion and Reduces Adipose Tissue Inflammation," *Plos One* 9(4), (2014)
216. G. van Hall, "Lactate kinetics in human tissues at rest and during exercise," *Acta Physiologica* 199(4), 499-508 (2010)
217. M. Digirolamo, F. D. Newby and J. Lovejoy, "LACTATE PRODUCTION IN ADIPOSE-TISSUE - A REGULATED FUNCTION WITH EXTRA-ADIPOSE IMPLICATIONS," *Faseb Journal* 6(7), 2405-2412 (1992)
218. C. Kallaway, L. M. Almond, H. Barr, J. Wood, J. Hutchings, C. Kendall and N. Stone, "Advances in the clinical application of Raman spectroscopy for cancer diagnostics," *Photodiagnosis and Photodynamic Therapy* 10(3), 207-219 (2013)
219. M. Namboodiri, T. Khan, K. Karki, M. M. Kazemi, S. Bom, G. Flachenecker, V. Namboodiri and A. Materny, "Nonlinear spectroscopy in the near-field: time resolved spectroscopy and subwavelength resolution non-invasive imaging," *Nanophotonics* 3(1-2), 61-73 (2014)
220. D. Simonova and I. Karamancheva, "APPLICATION OF FOURIER TRANSFORM INFRARED SPECTROSCOPY FOR TUMOR DIAGNOSIS," *Biotechnology & Biotechnological Equipment* 27(6), 4200-4207 (2013)
221. C. Vogel and E. M. Marcotte, "Insights into the regulation of protein abundance from proteomic and transcriptomic analyses," *Nature Reviews Genetics* 13(4), 227-232 (2012)
222. M. Konno, A. Hamabe, S. Hasegawa, H. Ogawa, T. Fukusumi, S. Nishikawa, K. Ohta, Y. Kano, M. Ozaki, Y. Noguchi, D. Sakai, T. Kudoh, K. Kawamoto, H. Eguchi, T. Satoh, M. Tanemura, H. Nagano, Y. Doki, M. Mori and H. Ishii, "Adipose-derived mesenchymal stem cells and regenerative medicine," *Development Growth & Differentiation* 55(3), 309-318 (2013)
223. Y.-J. Chang, D. T.-B. Shih, C.-P. Tseng, T.-B. Hsieh, D.-C. Lee and S.-M. Hwang, "Disparate mesenchyme-lineage tendencies in mesenchymal stem cells from human bone marrow and umbilical cord blood," *Stem Cells* 24(3), 679-685 (2006)
224. C. K. Rebelatto, A. M. Aguiar, M. P. Moretao, A. C. Senegaglia, P. Hansen, F. Barchiki, J. Oliveira, J. Martins, C. Kuligovski, F. Mansur, A. Christofis, V. F. Amaral, P. S. Brofman, S. Goldenberg, L. S. Nakao and A. Correa, "Dissimilar

differentiation of mesenchymal stem cells from bone marrow, umbilical cord blood, and adipose tissue," *Experimental Biology and Medicine* 233(7), 901-913 (2008)
225. F.-J. Lv, R. S. Tuan, K. M. C. Cheung and V. Y. L. Leung, "Concise Review: The Surface Markers and Identity of Human Mesenchymal Stem Cells," *Stem Cells* 32(6), 1408-1419 (2014)
226. C. Menard and K. Tarte, "Immunoregulatory properties of clinical grade mesenchymal stromal cells: evidence, uncertainties, and clinical application," *Stem Cell Research & Therapy* 4((2013)
227. A. Tarnok, H. Ulrich and J. Bocsi, "Phenotypes of Stem Cells from Diverse Origin," *Cytometry Part A* 77A(1), 6-10 (2010)
228. N. Haque, M. T. Rahman, N. H. Abu Kasim and A. M. Alabsi, "Hypoxic Culture Conditions as a Solution for Mesenchymal Stem Cell Based Regenerative Therapy," *Scientific World Journal* (2013)
229. B. Dionigi, A. Ahmed, E. C. Pennington, D. Zurakowski and D. O. Fauza, "A comparative analysis of human mesenchymal stem cell response to hypoxia in vitro: Implications to translational strategies," *Journal of Pediatric Surgery* 49(6), 915-918 (2014)
230. A. W. James, "Review of Signaling Pathways Governing MSC Osteogenic and Adipogenic Differentiation," *Scientifica* 2013(684736-684736 (2013)
231. M. T. Valenti, U. Garbin, A. Pasini, M. Zanatta, C. Stranieri, S. Manfro, C. Zucal and L. D. Carbonare, "Role of Ox-PAPCs in the Differentiation of Mesenchymal Stem Cells (MSCs) and Runx2 and PPAR gamma 2 Expression in MSCs-Like of Osteoporotic Patients," *Plos One* 6(6), (2011)
232. L. Zhang, P. Su, C. Xu, C. Chen, A. Liang, K. Du, Y. Peng and D. Huang, "Melatonin inhibits adipogenesis and enhances osteogenesis of human mesenchymal stem cells by suppressing PPAR gamma expression and enhancing Runx2 expression," *Journal of Pineal Research* 49(4), 364-372 (2010)
233. X. D. Li, Q. J. Cui, C. H. Kao, G. J. Wang and G. Balian, "Lovastatin inhibits adipogenic and stimulates osteogenic differentiation by suppressing PPAR gamma 2 and increasing Cbfa1/Runx2 expression in bone marrow mesenchymal cell cultures," *Bone* 33(4), 652-659 (2003)
234. J. Venkatesan and S.-K. Kim, "Nano-Hydroxyapatite Composite Biomaterials for Bone Tissue Engineering-A Review," *Journal of Biomedical Nanotechnology* 10(10), 3124-3140 (2014)
235. W. Y. Tong, W. Shen, C. W. F. Yeung, Y. Zhao, S. H. Cheng, P. K. Chu, D. Chan, G. C. F. Chan, K. M. C. Cheung, K. W. K. Yeung and Y. W. Lam, "Functional replication of the tendon tissue microenvironment by a bioimprinted substrate and the support of tenocytic differentiation of mesenchymal stem cells," *Biomaterials* 33(31), 7686-7698 (2012)
236. D. K. Bishi, S. Mathapati, J. R. Venugopal, S. Guhathakurta, K. M. Cherian, S. Ramakrishna and R. S. Verma, "Trans-differentiation of human mesenchymal stem cells generates functional hepatospheres on poly(L-lactic acid)-co-poly(epsilon-caprolactone)/collagen nanofibrous scaffolds," *Journal of Materials Chemistry B* 1(32), 3972-3984 (2013)
237. J. S. Heo, S. M. Choi, H. O. Kim, E. H. Kim, J. You, T. Park, E. Kim and H. S. Kim, "Neural tiransdiffernetiation of human bone marrow mesenchymal stem cells on hydrophobic polymer-modified surface and therapeutic effects in an animal model of ischemic stroke," *Neuroscience* 238(305-318 (2013)
238. G. Laino, R. d'Aquino, A. Graziano, V. Lanza, F. Carinci, F. Naro, G. Pirozzi and G. Papaccio, "A new population of human adult dental pulp stem cells:

A useful source of living autologous fibrous bone tissue (LAB)," *Journal of Bone and Mineral Research* 20(8), 1394-1402 (2005)
239. W. Zhang, X. F. Walboomers, S. Shi, M. Fan and J. A. Jansen, "Multilineage differentiation potential of stem cells derived from human dental pulp after cryopreservation," *Tissue Engineering* 12(10), 2813-2823 (2006)
240. R. d'Aquino, A. Graziano, M. Sampaolesi, G. Laino, G. Pirozzi, A. De Rosa and G. Papaccio, "Human postnatal dental pulp cells co-differentiate into osteoblasts and endotheliocytes: a pivotal synergy leading to adult bone tissue formation," *Cell Death and Differentiation* 14(6), 1162-1171 (2007)
241. G. T.-J. Huang, S. Gronthos and S. Shi, "Mesenchymal Stem Cells Derived from Dental Tissues vs. Those from Other Sources: Their Biology and Role in Regenerative Medicine," *Journal of Dental Research* 88(9), 792-806 (2009)
242. R. Hass, C. Kasper, S. Boehm and R. Jacobs, "Different populations and sources of human mesenchymal stem cells (MSC): A comparison of adult and neonatal tissue-derived MSC," *Cell Communication and Signaling* 9((2011)